NON-CONVENTIONAL BUILDING BLOCKS FOR ORGANIC ELECTRONICS

by

Panikki Bandaralage Chandima Dhanuka Bandara Bulumulla

APPROVED BY SUPERVISORY COMMITTEE:

_____

Dr. Mihaela C. Stefan, Chair

_____

Dr. Michael C. Biewer

_____

Dr. Yves J. Chabal

_____

Dr. John P. Ferraris

This dissertation and all my academic achievements are dedicated to my parents whose

unconditional love and support laid the foundation to complete this work

NON-CONVENTIONAL BUILDING BLOCKS FOR ORGANIC ELECTRONICS

by

PANIKKI BANDARALAGE CHANDIMA DHANUKA BANDARA BULUMULLA, BS

DISSERTATION

Presented to the Faculty of

The University of Texas at Dallas

in Partial Fulfillment

of the Requirements

for the Degree of

DOCTOR OF PHILOSOPHY IN

CHEMISTRY

THE UNIVERSITY OF TEXAS AT DALLAS

August 2018

ACKNOWLEDGMENTS

NON-CONVENTIONAL BUILDING BLOCKS FOR ORGANIC ELECTRONICS

Panikki Bandaralage Chandima Dhanuka Bandara Bulumulla, PhD
The University of Texas at Dallas, 2018

Supervising Professor: Dr. Mihaela C. Stefan

Organic semiconductors are potential candidates for replacing high-cost silicon electronics for low-end applications where high mobilities are not required. Owing to unique advantages such as solution processability, flexibility, lightweight, low cost with countless structural modifications, organic semiconductors can be realized for many applications using high throughput roll-to-roll fabrication techniques. Hence, a remarkable amount of scientific efforts have been dedicated to improving electronic and physical properties of these materials. Throughout the past two decades, many improvements in the field have been achieved by designing novel building blocks. Since efficiencies and mobilities in organic solar cells and transistors have stagnated, it is highly desirable to seek and develop non-conventional building blocks for organic electronics.

In this dissertation, the fundamentals and recent developments of non-conventional materials are covered in Chapter 1. Operation principles, charge transport of organic field effect transistors and organic photovoltaics are introduced. Compared to conventional thiophene-based π-electron donor materials, promising non-conventional pyrrole based donor materials employed in organic electronics are discussed and summarized. Similarly, non-conventional electron acceptors could be used to fabricate organic solar cells. By using inorganic semiconducting quantum dots (QDs),

organic-inorganic hybrid solar cells could be fabricated. Different systems with polymer: QD solar cells are also discussed and summarized in chapter 1.

Chapter 2 describes the effect on organic field effect transistor (OFET) properties of two novel small molecules containing terminal *N*-dodecylthieno[3,2-*b*]pyrrole (TP) donors and *N*-dodecylfuro[3,2-*b*]pyrrole (FP) donors with a central thiophene flanked 5,6-difluorobenzo[*c*][1,2,5]thiadiazole (FBT) acceptor. The influence on frontier molecular orbital energy levels, UV-vis absorption, electrochemical properties, OFET parameters and morphological effects were investigated.

In chapter 3, the effect of flanking group on banana shape small molecules is discussed by using terminal *N*-dodecylthieno[3,2-*b*]pyrrole (TP) donors, and thiophene or furan flanked benzo[*c*][1,2,5]thiadiazole (BT) central units. Upon changing similar flanking groups, the curvature of the small molecules was changed. Thiophene flanked small molecule showed high hole mobility of 0.08 cm^2 /V s while furan flanked small molecule performs poorly due to both heteroatom effect and the degree of curvature.

Chapter 4 describes the extension of thieno[3,2-*b*]pyrrole based small molecules to polymers. A Novel conjugated polymer is synthesized by copolymerizing *N*-methylthieno[3,2-*b*]pyrrole and 2,5-bis(2-octyldodecyl)-3,6-di(thiophen-2-yl)-2,5-dihydropyrrolo[3,4-*c*]pyrrole-1,4-dione (DPP) via Stille coupling polymerization. With an optimized molecular weight, the polymer exhibited high hole mobility of 0.12 cm^2 /V s in OFET devices. The high hole mobility reflects the potential of the thieno[3,2-*b*]pyrrole building block.

Inorganic QDs also can be employed as electron acceptors compared to conventional fullerene derivatives in bulk heterojunction (BHJ) solar cells. However, they do not outperform

conventional fullerene counterparts. Therefore in chapter 5, a facile method is described to generate thiol functionalized block copolymers to improve the interaction between photoactive polymers and QDs. By incorporating only 17 mol% of the thiol containing block a two-fold increase in power conversion efficiency was observed. The improved interaction was supported by atomic force microscopy and photoluminescence quenching studies.

TABLE OF CONTENTS

Curriculum vitae

LIST OF FIGURES

LIST OF TABLES

LIST OF SCHEMES

CHAPTER 1

NON-CONVENTIONAL DONOR AND ACCEPTOR MATERIALS FOR ORGANIC

PHOTOVOLTAICS AND ORGANIC FIELD EFFECT TRANSISTORS

Authors – Chandima Bulumulla,[a] Ruvanthi N. Kularatne,[a] Ruwan Gunawardhana,[a] Michael C.

Biewer[a] and Mihaela C. Stefan[a,b]

[a]Department of Chemistry and Biochemistry, BE26

The University of Texas at Dallas

800 West Campbell Road

Richardson, Texas 75080, USA

[b]Department of Bioengineering, BSB11

The University of Texas at Dallas

800 West Campbell Road

Richardson, Texas 75080, USA

1.1 Abstract

Organic semiconductors are very attractive materials as compared to inorganic counterparts due to solution processability, light weight, flexibility and low-cost fabrication procedures. A significant amount of research has been carried out, and lately, material performances have started to stagnate. This has made chemists shift their focus from building materials constituting of conventional building blocks to explore non-conventional materials. The design and synthesis of non-conventional semiconducting materials derived from pyrroles are first discussed as an alternative to popular thiophene-based materials for organic field effect transistors. Secondly, utilization of inorganic quantum dots instead of regular fullerene derivatives in organic: inorganic hybrid photovoltaics and necessary polymer modifications are discussed including recent advancements and challenges in the field.

1.2 Introduction to Organic Semiconductors

The field of conjugated small organic molecules or polymers that show desirable electronic properties is known as organic electronics. It all started as a result of the discovery of doped *trans*-polyacetylene by Heeger, Shirakawa, and MacDiarmid, where they were recognized with the year 2000 Nobel prize in chemistry.[1] These findings gave rise to a wide range of applications including organic light emitting diodes (OLEDs),[2-4] organic photovoltaics (OPVs),[5-7] and organic field effect transistors (OFETs) owing to the tremendous amount of research carried out in both academia and industry.[8-10] The main driving force behind the research in organic electronics is the unique advantages offered by organic semiconductors and their ability to modify structures to fine-tune physical and electronic properties.[11]

The first generation of conducting polymers discovered between the 1970s to 1990s were insoluble in common organic solvents to limit post-polymerization processing. Out of the many first generation organic semiconducting polymers, polypyrrole, polythiophene, and polyaniline were of particular interest due to the high conductivities (above 1 S cm^{-1}) obtained for doped films.[12-15] Since these materials had exceptionally high conductivities in the doped state, the second generation of conducting polymers was synthesized by attaching alkyl chains to impart solubility. Poly(3-alkyl thiophene)s are one of the most widely studied conjugated polymer system with excellent physical and electronic properties.[16-18] Bulk heterojunction solar cells fabricated from poly(3-hexylthiophene) and [6,6]-phenyl-C$_{61}$-butyric acid methyl ester (PC$_{61}$BM) have exceeded power conversion efficiencies (PCEs) over 4% while in OFETs, P3HT analogs have reached hole mobilities over 1 cm^2 /V s.[19, 20] However, relatively high highest occupied molecular orbital (HOMO ~ -5.0 3V) and narrow band gap (~ 2.0 eV) limits stability and tunability of poly(3-alkyl thiophene)s. Therefore, third generation semiconducting polymers were engineered to adopt a donor-acceptor architecture which lowers the band gaps via orbital mixing of HOMO and lowest unoccupied molecular orbital (LUMO) energy levels of electron-donor and electron-acceptor materials as shown in Figure 1.1.
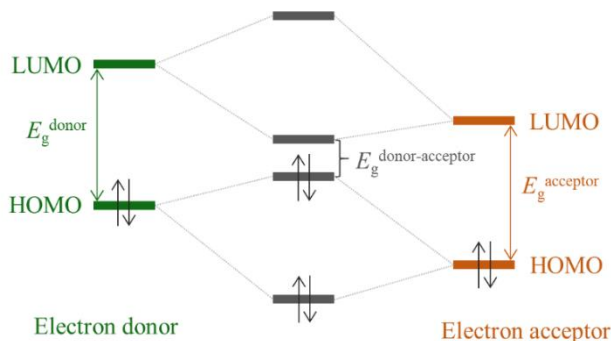
Figure 1.1 The molecular orbital mixing of electron donor and electron acceptor moieties

By polymerizing an electron-rich monomer with an electron deficient monomer, stable polymers were synthesized to alter frontier orbital energy levels and band gaps for OPVs and OFETs.[21] By creating alternating donor-acceptor type polymers, it is possible to tailor optical and electrochemical properties depending on the application. In addition, strong donor-acceptor interactions will keep polymer chains close to each other to facilitate better charge transport. Although polymers present higher conjugation lengths and excellent film-forming abilities, the control over molecular weight and polydispersity is minimal. Which results in higher batch-to-batch variations in polymeric systems since electronic performances often depend on molecular weights and polydispersities. To address this issue, small molecules or oligomers with precise molecular weights were synthesized. Interestingly, significant advancements have made in the last couple of years owing to dedicated research performed with small molecules reaching record-breaking PCEs of 9% in BHJ solar cells and hole mobilities over 10 cm^2 /V s in OFET devices.[8, 22, 23] Although OPVs have achieved significant advancements, they are still behind inorganic silicon solar cells (PCE > 20%) to consider for commercialization. On the other hand, organic small molecules employed for high performing OFETs (preferably acenes) require high-temperature processing conditions or vacuum evaporation methods which negates the unique advantages offered by organic materials. Therefore, solution processable small molecules were investigated over the past few years with different modifications on conventional building blocks. The discouraging results have drawn chemists attention to seek and explore potential non-conventional building blocks for OFETs. To come up with novel building blocks, it is important to first understand the charge transport mechanism of π-conjugated materials.

1.3 Charge Transport in π-Conjugated Materials

Organic semiconductors are made up of a backbone consisting of alternating single and double/triple bonds with sp^2/sp hybridized carbon or heteroatoms like sulfur, oxygen or nitrogen. While hybridized orbitals form σ-bonds, π-bonds are created by overlapping perpendicular P_z orbitals. Therefore, the electrons in the P_z orbitals (π-electrons) possess the ability to delocalize throughout the entire backbone. Since the overlap of P_z orbitals (or π-orbitals) are less compared to σ-orbitals, π-orbitals create frontier molecular orbitals. The molecular orbitals below HOMO level are filled with electrons consisting of antiparallel spin while molecular orbitals on or above LUMO levels are empty. To explain charge transport in organic semiconductors, many theories have developed depending on the crystallinity or structural disorders.[24-26] Different proposed microscopic charge transport mechanisms can be classified as; (1) classic band-like transport for single crystal materials and conducting polymers with extremely low dihedral angles (disorder free),[27-29] (2) mobility edge model for polycrystalline organic semiconductors,[26, 30-32] and (3) electron tunneling and hopping transport for highly disordered semiconductors.[26, 33] Since many organic semiconductors fall into the highly disordered category, tunneling and hopping model is considered as the preferred theoretical model to explain the charge transport. According to the aforementioned theory, the overall mobility is denoted as the collective mobility of electron tunneling and electron hopping. The contribution from electron tunneling dominates transport at relatively lower temperatures while at higher temperatures, hopping becomes more dominant. Since most organic semiconductors are processed at room temperature or higher, hopping mechanism is considered to be responsible for charge transport. When conjugated materials interact with charge carriers, polarons and bipolarons are generated as shown in Figure 1.2.
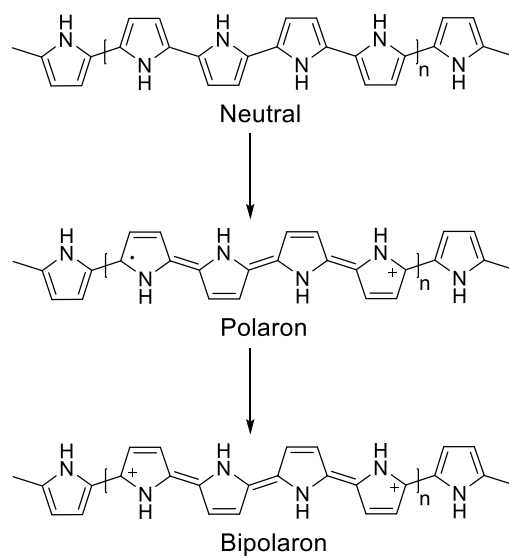
Figure 1.2 Formation of polaron and bipolaron in polypyrrole

Within an ordered conjugated backbone with minimal torsions, charge transport could be facilitated by hopping processes. Hence when designing novel non-conventional building blocks, it is important to select more electron-rich materials while maintaining minimum torsions along the backbones.

1.4 Working Principle of Organic Field Effect Transistors

A field effect transistor is a three-terminal electronic device that amplifies and switches electrical signals. The everyday life has been forever changed since the introduction of field effect transistors more than 50 years ago. With the emergence of flexible printed electronics, organic semiconductors are considered as favorite candidates if necessary requirements can be met. OFETs were initially fabricated by electropolymerization of 2,2′-bithiophene in 1986.[34] Until the 1990s, OFETs were employed as a tool to measure charge transport characteristics experimentally. Over

past two decades, significant progress have made in the field of printable OFETs reaching mobilities comparable to that of devices based on amorphous silicon.

OFETs have three terminals namely; gate, source (S), and drain (D). Organic semiconductor (OSC) of choice can be processed from solution deposition or vacuum sublimation. Since organic materials can be tailored to improve solubility, most of the materials are solution processed to highlight the added advantage compared to silicon technologies. Depending on the position of the three terminals there are 4 device configurations; (1) Bottom-gate/bottom-contact (BGBC), (2) Bottom-gate/top-contact (BGTC), (3) Top-gate/bottom-contact (TGBC), and (4) Top-gate/top-contact (TGTC) as shown in Figure 1.3.[32]
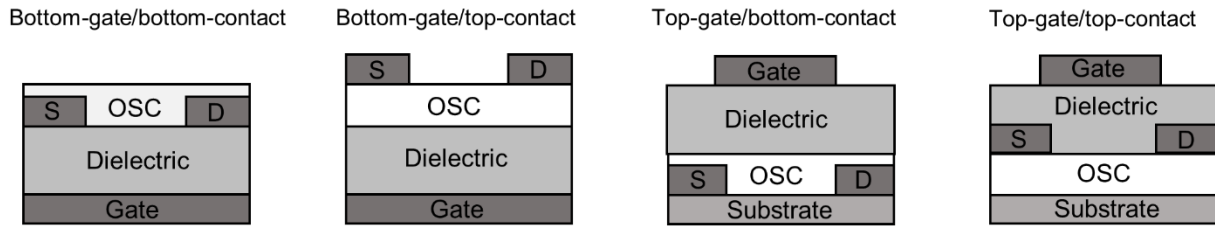
Figure 1.3 Device configurations of OFETs

Out of the above mentioned four device configurations, BGBC and BGTC device architectures are primarily used due to the ease of fabrication. Since holes are the major charge carriers in semiconducting organic materials, a negative voltage (larger than the threshold voltage (V_T)) is applied on the gate electrode to control the current flow between the source and drain terminals. This negative gate voltage causes positive charges to accumulate in the OSC near the dielectric layer interface. A second negative voltage is applied between the source and drain electrodes (V_{DS} or V_D) to create a flow of holes from source to drain. When the magnitude of V_D is increased, the

7

magnitude of the current between source and drain (I_{DS} or I_D) also increases until it reaches a saturation current. This is depicted in Figure 1.4 (b) and known as the output plot.
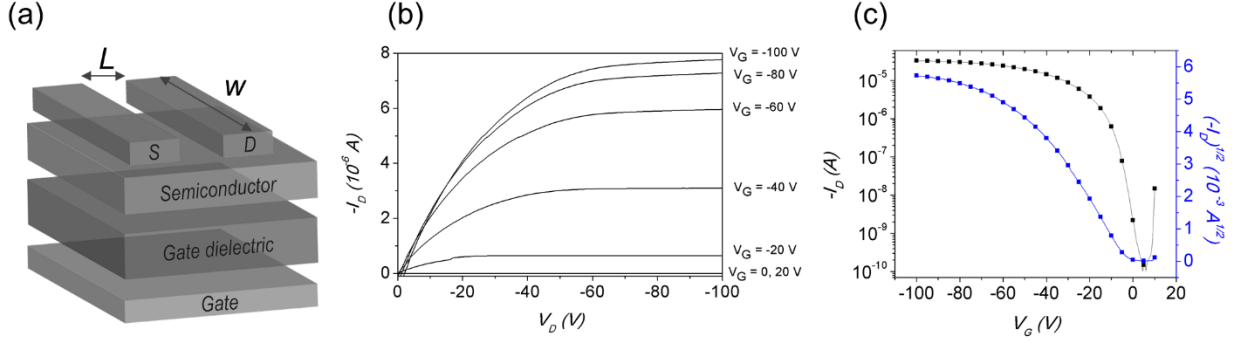
Figure 1.4 (a) The schematic diagram of BGTC OFET, (b) Output characteristics and, (c) Transfer curve of a typical OSC

The charge carrier mobility of an OFET can be calculated from the transfer curve (Figure 1.4 c), where gate voltage (V_G) is linearly increased, and the current between source and drain (I_D) is measured at a constant drain-source voltage (V_D). According to following equations, charge carrier mobilities are extracted from transfer curves in linear regions or saturation regimes depending on the curves obtained. If the curves show non-linear behavior in transfer plots, usually charger carrier mobilities in both regions.

$$I_D = \frac{W}{L}\mu C_i V_D(V_G - V_T) \qquad\qquad V_D < V_G - V_T \text{ (Linear Region)} \qquad\qquad (1.1)$$

$$I_D = \frac{W}{2L}\mu C_i(V_G - V_T)^2 \qquad\qquad V_D > V_G - V_T \text{ (Saturation Region)} \qquad\qquad (1.2)$$

Where, μ is charge carrier mobility, C_i is the capacitance per unit area, W and L are channel width and length (Figure 1.4(a)), respectively.

From OFET characterizations, three parameters are obtained to define the efficacy of the OSC; (1) charge carrier mobility, (2) current on-to-off ratio (I_{on}/I_{off}) and, (3) threshold voltage. The I_{on}/I_{off} is

defined as the ratio of I_D at higher gate voltages (on-state) and I_D at $V_G = 0$ V (leakage current). This parameter is used to calculate the conversion speed of a device. The threshold voltage is defined as the minimum V_G required to switch on an OFET. Ideal OFET would have a V_G close to 0 V.

1.5 Pyrrole Based Semiconductors for OFETs

The material selection criteria is an important aspect in organic semiconductors. In order to develop materials one must consider many factors including but not limited to π-electron richness, aromaticity, electrical conductivity, dipole moments, frontier energy levels, thermal and chemical stability, economics, etc. Among many suitable aromatic groups reported in the literature, the class of thiophene containing organic semiconductors is the most studied. Unfortunately, isoelectronic furan or pyrrole have received less attention in the field even though they have similar or even superior electronic properties. Out of the above mentioned 3 five-membered aromatic rings, the electron richness changes as pyrrole > furan > thiophene while stability trends in the opposite direction as shown in Figure 1.5. The DFT calculations predict comparatively a high HOMO level for pyrrole with respect to furan and thiophene indicating the instability toward atmospheric oxygen to yield oxidized materials upon exposure to air. Nonetheless, due to the electron-rich nature, polypyrrole (PPy) shows an extremely high electrical conductivity of 2×10^3 S cm^{-1} while polythiophenes range from 3.4×10^{-4} S cm^{-1} to 1.0×10^{-1} S cm^{-1} when doped with PF$_6^-$ and iodine respectively.[35, 36]

Although stability is an issue with pyrroles, it is an excellent building block for organic electronics due to the excessive π electron density that facilitates charge transfer. ,
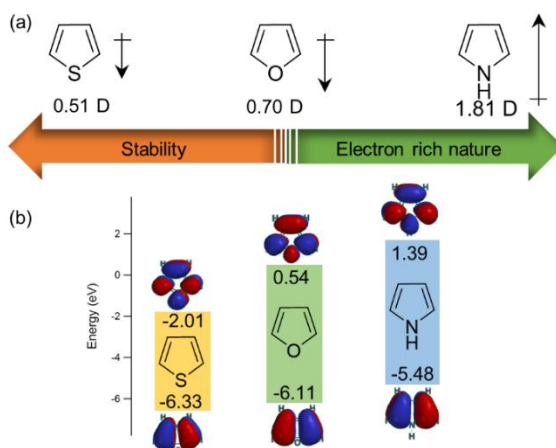
Figure 1.5 Comparison of isoelectronic thiophene, furan, and pyrrole (a) in terms of stability and electron richness and, (b) frontier energy levels estimated from DFT calculations with Spartan′16 (B3LYP 6/31 G* level of theory)

1.5.1   Oligopyrrole and Polypyrrole

The preparation of polypyrrole (PPy) can be achieved by either electrochemical or chemical oxidation. In both methods, the most accepted polymerization mechanism is the oxidation of the monomer to give rise to a radical cation. By coupling two of the generated pyrrole cations with subsequent deprotonation yield a bipyrrole. Andrieux et al. confirmed the formation of the bipyrrole.[37] Propagation step continues as the bipyrrole is followed by reoxidation, coupling, and deprotonation to form oligomers. Since oxidation potential of oligomeric pyrrole is lower than that of pyrrole monomer, radical coupling of oligomers are favored to produce a polymer.[38] The termination of the polymer is not understood completely but believed to either have a nucleophilic attack on the polymer chain,[39] or an attack from the radical cation to a neutral pyrrole monomer.[40] Highly conductive PPy films was first synthesized by Diaz et al. on a working electrode by using an electrolyte salt dissolved in 99% aqueous acetonitrile.[35, 41]

Scheme 1.1. Polymerization mechanism of pyrrole via radical cations
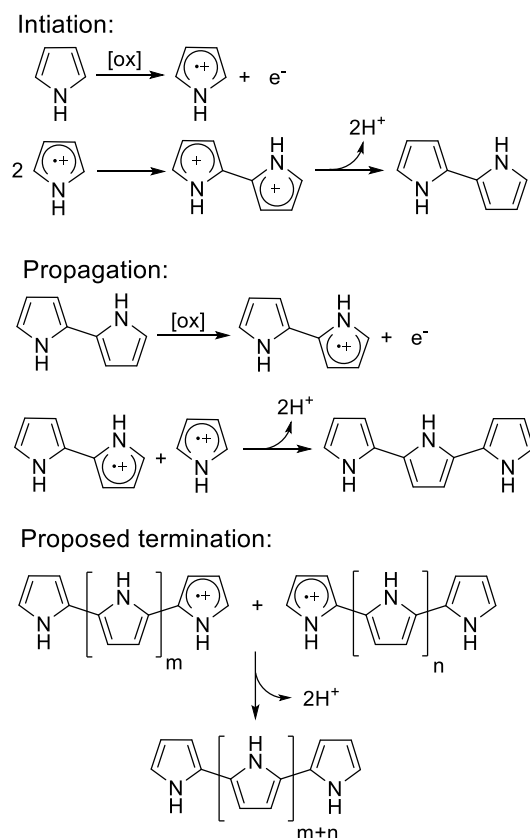
In contrast to electrochemical oxidation, chemical polymerization is suitable for mass production of PPy. Oxidizing agents such as ferric chloride,[42, 43] quinones,[44, 45] persulfates,[46] lead dioxide[47] is added to a solution of pyrrole and a dopant to precipitate the doped PPy. Usually, chemically prepared PPys exhibit lower electrical conductivities compared to PPys made electrochemically and various surfactants have used as additives to improve the conductivity.[48-50] Nonetheless, the chemical method provides more structure tunability via defined reaction conditions.[51] Another interesting approach has been taken by Yokozawa's group to develop poly(*N*-hexylpyrrole) by catalyst-transfer polycondensation (CTP) similar to that of regioregular poly(3-alkyl thiophene)s

by Grignard Metathesis Polymerization (GRIM).[52] This polymerization technique allows precision growth of monomer units unlike undesirable α-β and β-β coupling taking place in oxidative polymerizations. Authors claim that molecular weights up to 13,000 g mol^{-1} can be synthesized when Ni(dppe)Cl$_2$ is used as the catalyst. A year later, Stefan et al. showed that poly(*N*-dodecylpyrrole) could be synthesized by GRIM when *i*-PrMgCl.LiCl is used as the Grignard reagent in the magnesium halogen exchange step to generate polymers with M_n = 11, 900 g mol^{-1} and PDI = 1.4.[53] Block copolymers containing poly(N-alkyl pyrroles) have also synthesized separately by Yokozawa's and McNeil's group.[52, 54]

Compared to PPy, oligopyrroles has not generated much interest mainly due to the synthetic challenges of handling unstable material and performing multi-step synthesis with purifications at each step. However, oligopyrroles have synthesized by employing various synthetic routes including Paal-Knorr cyclization,[55] coupling of pyrrolinones with pyrroles,[56] Ullmann coupling,[57-59] and metal-catalyzed coupling reactions. To better understand the properties of PPy, oligopyrroles (Py)$_n$ have synthesized by Schluter and co-workers with n varying from 3, 5, 7 and 9. Authors have employed Stille coupling to synthesize well-defined oligomers via pyrrole monomers carrying *tert*-butoxycarbonyl (Boc) protecting groups at the nitrogen.[60, 61] The substituent effects on electrochemical properties were studied by Meijer and co-workers and found out that oxidation is easier with oligopyrrole compared to pyrrole monomers, contrary to the thiophene series .[62, 63] Same group have also synthesized a series of donor - oligopyrrole - acceptor type semiconductors to investigate the optical properties but unfortunately, none of the oligopyrroles have utilized in organic electronic applications.[64]

1.5.2 Pyrrole as a Co-Monomer/Unit

Due to the π-electron excessive nature of pyrroles, a single pyrrole unit can be installed to build semiconducting devices as an electron donor material. At the same time, to tune physicochemical properties such as solubility, different monomers containing alkyl chains could be inserted. In order to attach these pyrrole monomers to other aromatic units, different functionalizations are required at 2 or/and 5-positions of pyrrole depending on the C-C coupling technique. For the thiophene series, the most used derivative is the halogenated precursor since it can participate in Stille, Suzuki, Negishi and Grignard coupling reactions to generate semiconducting materials. For the halogenation of pyrroles, a significant amount of research has carried out especially with chlorine and bromine.[65-68] Halogenation reactions produced mixtures of compounds containing mono-, di-, tri- and tetra-substituted products.[65] Purification of the individual products is somewhat challenging due to oxidation in air. These compounds, however, can be stabilized by storing in ether/ hexane at cold temperatures with a soft base such as tributylamine or triethylamine. By changing the N-substituent to an electron withdrawing cleavable group such as Boc, stable halogenated derivatives can be synthesized.[69] After attaching strong electron withdrawing units, deprotection reactions can be performed to obtain stable units with pyrroles.[70, 71]

Another method to install pyrroles as single units is by using mono- or di-stannylated derivatives in Stille coupling reactions/ polymerizations. N-alkyl pyrroles can be easily converted to the stannylated derivatives by lithiation of the α- positions with n-BuLi at refluxing conditions in the presence of TMEDA as a ligand and hexane as the solvent.[69, 71-76] Boronic esters or acids could also be made from pyrrole to undergo Suzuki-Miyura/ Suzuki cross-coupling reactions.[77-79] Similarly, organozinc complexes could be prepared for pyrroles with lithiation and subsequent

quenching with $ZnCl_2$ to perform Kumada and Negishi coupling reactions.[80, 81] N-alkylated pyrroles can be converted to Grignard reagents to undergo coupling between halogenated aromatic groups.[82] Since pyrroles are extremely sensitive to air, all these reactions will require careful synthesis, purification, characterization, and storage. To mitigate this issue, direct arylation reactions can be employed as showed by Sadighi and co-workers.[83] Palladium or rhodium catalysts are used injunction with $ZnCl_2$ or cesium pivalate with the appropriate ligand respectively.[84] Possible functionalization routes are listed in Figure 1.6.
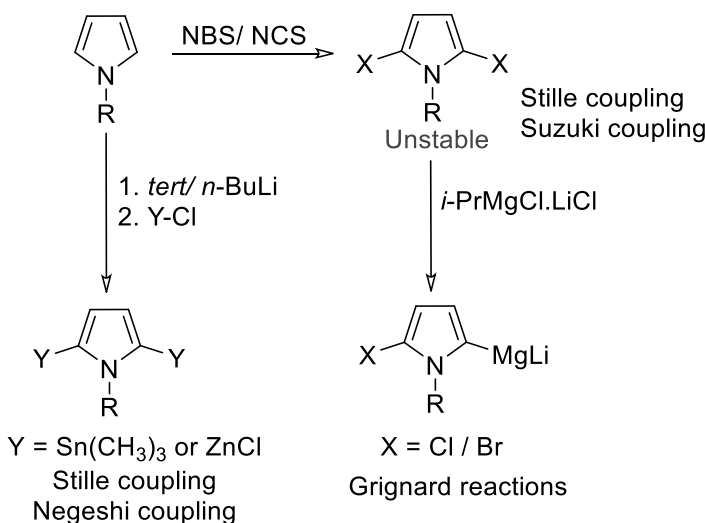
Figure 1.6 Routes to obtain functionalized N-alkylated pyrroles

Fujii et al. synthesized two oligomers (**SM1** and **SM2**) containing thiophene and a pyrrole backbone end capped with hexyl groups for field effect transistors (Figure 1.7).[85] **SM1** showed hole mobility of 0.008 cm^2 /V s and while **SM2** achieved 0.01 cm^2 /V s, on bare Si/SiO_2 substrates. After decorating the SiO_2 surface with an OTS self-assembled monolayer (SAM) hole mobilities improved to 0.009 cm^2 /V s and 0.05 cm^2 /V s respectively.
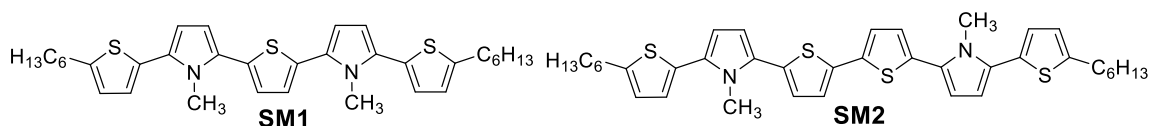
Figure 1.7 OSCs employed in OFETs by inserting pyrrole as a single unit

1.5.3 Fused Ring Systems Containing Pyrroles

1.5.3.1 Pyrrolo[3,2-*b*]pyrrole

Among the 10 π-electron family heterocycles, 1,4-dihydropyrrolo[3,2-*b*]pyrroles are the least studied system due to the π-electron excessive nature that leads to unstable material. These scaffolds were first discovered by Hemetsberger and Knittel in 1972, and until recently, multi-step syntheses with low overall yields were required to construct molecules containing pyrrolo[3,2-*b*]pyrrole moieties.[86-88] Recently, a one-pot synthesis (Figure 1.8) was discovered to synthesize 1,4-dihydropyrrolo[3,2-*b*]pyrroles starting with inexpensive, commercially available starting materials and no time-consuming column chromatography was required for purification.[89]
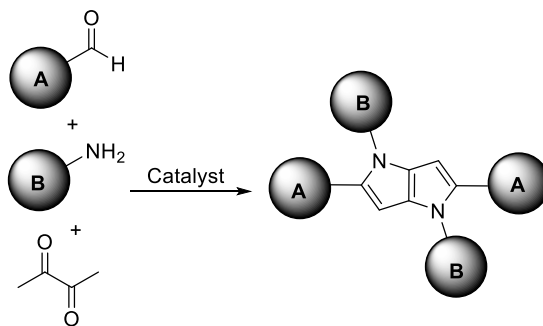
Figure 1.8 One-pot synthesis of pyrrolo[3,2-*b*]pyrrole small molecules

To date, no efforts have made to fabricate OFETs out of these materials despite the easy chemical synthesis.

1.5.3.2 Thieno[3,2-*b*]pyrrole

The synthesis of thieno[3,2-*b*]pyrrole was first developed in 1957 by Matteson and Snyder where they converted pyrrole to 3-thiocyanopyrrole, then cyclization followed by reduction using NaBH$_4$.[90] This method generated thieno[3,2-*b*]pyrrole monomer in relatively low yields. Another route to synthesize the same building block is via a Knoevenagel condensation reaction between thiophen-2-carboxyaldehyde and ethyl/methyl azidoacetate to generate the thienylacrylate, which could be cyclized by a Hemetsberger reaction. Later depending on the application, ester group at 5-position could be modified. Compared to the pyrrolo[3,2-*b*]pyrrole monomer, thieno[3,2-*b*]pyrrole has a low lying HOMO level which is beneficial for organic electronic device's long-term stability. Different synthetic routes to obtain thieno[3,2-*b*]pyrrole are presented in Figure 1.9.
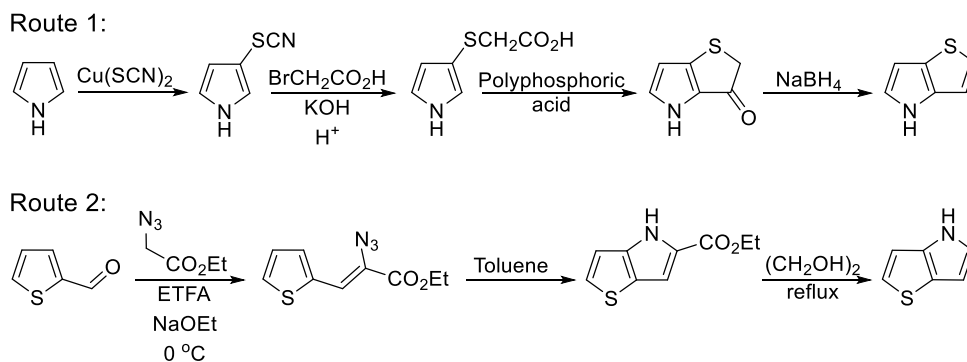
Figure 1.9 Different synthetic routes to obtain thieno[3,2-*b*]pyrrole

Comparatively, thieno[3,2-*b*]pyrrole is a stable monomer with a wider structure tunability for organic electronic applications via N-alkylation. Despite the synthetic advantages, this building block has been utilized in organic electronic applications in only one report. Jones et al. have employed bispyrrolothiophenes in a TP- Ar -TP sandwich configuration and hole mobilities in

OFETs have measured (Figure 1.10).[91] Authors have systematically varied the aromatic group (**SM3**-**SM8**) in the middle with none, bithiophene, phenyl, anthracene, 9,9-didodecylfluorene, and 2,1,3-benzothiadiazole while keeping the N-substituent constant (n-dodecane). Hole mobilities in top-gate/bottom-contact OFET devices varies 0.03 cm^2 /V s, 0.004 cm^2 /V s, 0.1 cm^2 /V s, 0.04 cm^2 /V s, 0.00003 cm^2 /V s and 0.28 cm^2 /V s when TFTs were annealed at 110 °C for only 5 mins in air. Interestingly, when n-dodecyl groups were replaced with methyl and phenyl groups containing electron donating and withdrawing groups (**SM9** to **SM12**), no field effect activity have observed highlighting the importance of the choice of N-substituents.
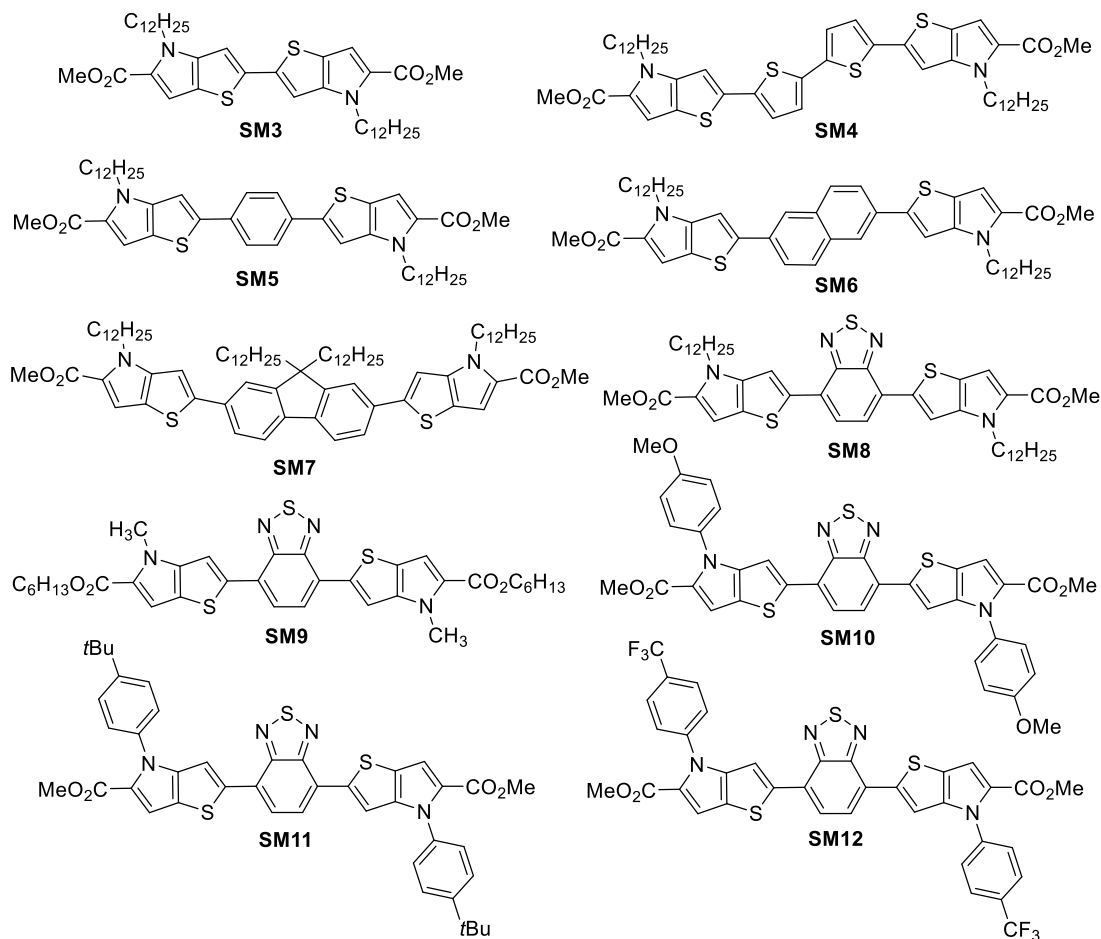
Figure 1.10 Chemical structures of thieno[3,2-*b*]pyrrole based OSCs used for OFETs

17

1.5.3.3 Dithieno[3,2-*b:2′,3′-d*]pyrrole

Out of all the pyrrole-containing building blocks, dithieno[3,2-*b*: 2′,3′-*d*]pyrrole (DTP) is the most used monomer to produce high charge carrier mobilities and semiconductors with reduced band gaps. Since the conductivity and redox potential measurements performed by Berlin et al. on poly(dithieno[3,2-*b*: 2′,3′-*d*]pyrrole), the interest for utilizing DTP as a monomer has progressively increased.[92] Compared to other pyrrole containing monomers DTP has low lying HOMO and allows solubility to impart from N-alkylation reactions. In addition, the monomer is symmetrical to generate regioregular structures, and minimal torsional effects are observed since solubilizing groups are installed in the middle ring. Since there are few dedicated reviews published on DTP earlier,[93-96] the most efficient synthetic route toward DTP (Figure 1.11) and promising small molecules and polymers employed for OFET are discussed.
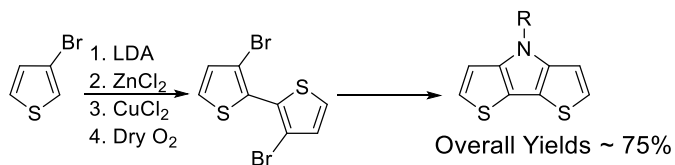
Figure 1.11 Most efficient synthetic route for *N*-functionalized dithieno[3,2-*b*:2′,3′-*d*]pyrrole

DTP unit has been extensively studied for OFET applications including both monomeric and polymeric materials (Figure 1.12 and Table 1.1). With the few small molecules and polymers containing DTP, a maximum hole mobility of 1.2 cm^2 /V s and a maximum electron mobility of 1.5 cm^2 /V s was achieved. The first report of N-alkylated DTP utilized for OFETs report by McCullough's group in 2008 where DTP was copolymerized with 2,5-dibromo-3-hexylthiophene (**P1**; M_n = 50.0 kDa, PDI = 1.7), 5,5′-dibromo-4,4′-didoceyl-2,2′-bithiophene (**P2**; M_n = 32.0 kDa,

PDI = 1.7) and 5,5′-dibromo-3,3′-dihexyl-2,2′-bithiophene (**P3**; M_n = 16.0 kDa, PDI = 1.9).[97] The three polymers showed average hole mobilities of 0.026 cm^2 /V s, 0.13 cm^2 /V s and 0.0035 cm^2 /V s for **P1**, **P2**, and **P3** respectively. These values were highly reproducible, but they suffered from low I_{on}/I_{off} ratios (4-120). Upon annealing, a reduction in the mobilities was recorded because polymer chains adapted a face-on orientation with respect to the substrate. Around the same time, Zhang et al. explored two polymers with a similar chemical structure to that of **P2**.[98] Instead of the *n*-octyl chain in DTP unit, methyl and n-dodecyl groups were attached to obtain **P4** (M_n = 17.4 kDa, PDI = 2.0) and **P5** (M_n = 29.7 kDa, PDI = 2.8), respectively. The mobility extracted in the saturated regime for **P4** was as high as 0.08 cm^2 /V s with I_{on}/I_{off} = 10^3. Devices made with similar processing conditions for **P5** showed even higher hole mobilities as 0.11 cm^2 /V s with I_{on}/I_{off} ratios close to 10^4. In 2009, Reynolds and co-workers exploited a DTP and benzobisthiadiazole copolymer (**P6**; M_n = 14.0 kDa, PDI = 3.6) for ambipolar OFETs.[99] The HOMO and LUMO energy levels of polymer **P6** were -5.1 eV and -4.3 eV indicating polymer would be appropriate for ambipolar OFETs. When devices were fabricated on top of octadecyltrichlorosilane treated SiO$_2$ surface, average p-channel and n-channel field effect mobilities were 1.2 × 10^{-3} cm^2 /V s and 5.8 × 10^{-4} cm^2 /V s. Same year Marder and co-workers published a polymer (**P7**) containing DTP and perylene diimide for n-type OFETs.[100] Authors claimed electron mobility of 1.2 × 10^{-3} cm^2 /V s for this polymer with a I_{on}/I_{off} = 10^3. A strong donor (DTP) – strong acceptor (diketopyrrolopyrrole) type polymer (**P8**; M_n = 11.7 kDa, PDI = 3.46) was synthesized by Nelson et al. where authors showed **P8** could achieve high hole mobility (0.41 cm^2 /V s) without thermal annealing treatments.[101] Jenekhe's group reported a copolymer (**P9**) synthesized from a benzobisthiazole acceptor and DTP donor moiety with two different molecular weights (**P9**$_{10}$; M_n

= 10.3 kDa, PDI = 3.12 and **P9**$_{52}$; M_n = 52.4 kDa, PDI = 2.82).[102] Despite the differences in the molecular weight, both polymers showed similar p-type OFET performances ($\mu_h \sim 5.0 \times 10^{-4}$ cm^2 /V s). The highest hole mobility recorded on a polymer consisting of DTP was reported recently by Hsu and co-workers for a dithienopyrrole vinylene donor and a diketopyrrolopyrrole acceptor.[103] Authors varied the length of the N-alkyl chain in the DPP unit to obtain **P10** (M_n = 38.0 kDa and PDI = 2.2) and **P11** (M_n = 16.0 kDa and PDI = 1.3). There are only a few reports published on DTP based small molecules utilized for OFETs. Marder's group first tested DTP containing small molecules for OFETs, where authors synthesized donor-acceptor-donor (D-A-D, **SM13**) and acceptor-donor-acceptor (A-D-A, **SM14**) type semiconductors in which donor was DTP and acceptor was benzothiadiazole.[104] The variation of the alkyl chains and chemical structure (D-A-D or A-D-A) was studied by OFET measurements. It was shown that D-A-D small molecules comprising of longer N-alkyl chains result in better field-effect characteristics. Moreover, the addition of terminal alkyl chains generated an almost ten-fold reduction in FET hole mobilities. Recently, two small molecules (**SM15** and **SM16**) composed of DTP dimer terminated with dicyanovinylene were synthesized by Zhu and co-workers.[105] The only difference between the two small molecules was the N-alkyl chains in the DTP unit; 2-hexyldecyl (**SM15**) and 2-ethylhexyl (**SM16**). **SM15** showed a high field effect mobility (0.11 cm^2 /V s) and I_{on}/I_{off} = 10^6, while **SM16** only gave 1.9×10^{-4} cm^2 /V s with I_{on}/I_{off} = 10^3. The drastic difference observed for the two small molecules was due to the morphological effects of the two semiconductor thin films. To date, there is only one high performing n-channel OFET made from DTP containing small molecules. Kippelen and co-workers synthesized a small molecule (**SM17**) with a central DTP

unit and terminal naphthalene diimide unit to generate high electron mobility (1.5 cm^2 /V s) with less batch-to-batch variation in OFET devices.[106]
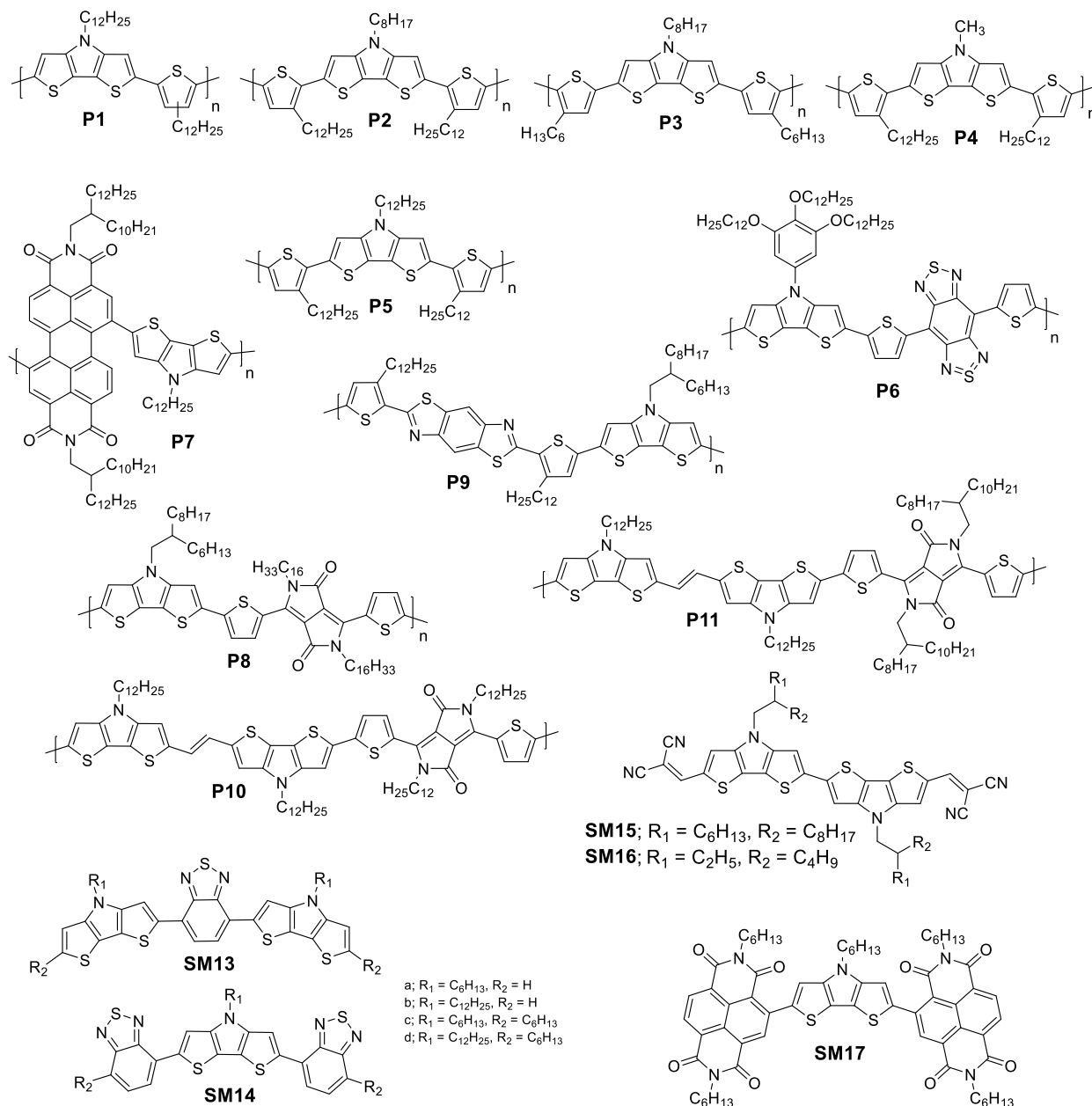
Figure 1.12 DTP based polymers and small molecules used for OFETs

Table 1.1 Electrochemical and OFET parameters of DTP based OSCs

	HOMO/LUMO (eV)	E_g (eV)	Device architecture	μ_h (cm^2/Vs)	μ_e (cm^2/Vs)	V_T (V)	I_{on}/I_{off}	Ref
P1	-4.68/ -2.94	1.74	BGBC	2.6×10^{-2}	-	60.0	4	[97]
P2	-4.88/ -3.02	1.86	BGBC	1.3×10^{-1}	-	-21.0	120	[97]
P3	-4.96/ -2.96	2.00	BGBC	3.5×10^{-3}	-	-23.0	140	[97]
P4	-4.92/ -2.43	2.49	BGBC	1.1×10^{-1}	-	-	10^3	[98]
P5	-4.93/ -2.40	2.53	BGBC	8.0×10^{-2}	-	-8.1	10^3	[98]
P6	-5.10/ -4.30	1.80	BGTC	1.2×10^{-3}	5.8×10^{-4}	-	-	[99]
P7	-5.50/ -3.90	1.60	BGTC	-	1.2×10^{-3}	-	10^3	[100]
P8	-5.20/ -4.05	1.15	BGBC	4.1×10^{-1}	-	-20.0	10^4	[101]
P9$_{10}$	-4.79/ -3.30	1.49	BGBC	2.2×10^{-4}	-	-28.6	10^4	[102]
P9$_{52}$	-4.79/ -3.30	”	BGBC	5.5×10^{-4}	-	-3.7	10^3	[102]
P10	-4.83/ -3.53	1.30	BGTC	6.9×10^{-1}	-	-27.0	10^2	[103]
P11	-4.97/ -3.58	1.39	BGTC	1.2×10^{0}	-	-19.0	10^2	[103]
SM13a	-4.9/ -3.1	1.9	BGTC	1.2×10^{-3}	-	7.9	10^2	[104]
SM13b	-4.9/ -3.1	1.9	BGTC	7.8×10^{-3}	-	9.5	10^3	[104]
SM13c	-4.8/ -3.0	1.8	BGTC	2.3×10^{-4}	-	0.2	10^3	[104]
SM13d	-4.8/ -3.0	1.8	BGTC	2.5×10^{-4}	-	-0.7	10^3	[104]
SM14	-5.2/ -2.9	2.2	BGTC	6.6×10^{-5}	-	-11.0	10^2	[104]
SM15	-5.31/ -3.38	1.93	BGTC	1.1×10^{-1}	-	-8.0	10^6	[105]
SM16	-5.30/ -3.37	1.93	BGTC	7.0×10^{-4}	-	-30.0	10^3	[105]
SM17	-	-	TGBC	-	1.5×10^{0}	13.0	10^3	[106]

1.5.3.4 Thieno[3,2-*b:2′*,3′-*d*]dipyrrole

The synthesis of the monomer thineo[3,2-*b*:2′,3′-*d*]dipyrrole (TDP) was first reported in 1976 by Fournari and co-workers.[107] This unstable monomer and has characteristics similar to pyrrole. The monomer TDP was first polymerized by Sannicolo and co-workers where authors claimed excellent air stability and resistivity to oxidative processes.[108] Later in 1990, Zotti and co-workers studied polypyrrole and poly(thienodipyrrole) using electrochemistry to investigate the oxidation

potentials of the monomer (bipyrrole vs. TDP) and redox potentials for the polymers.[109] The

incorporation of thiophene in between two pyrrole rings did not result in a significant change in

the electrochemical properties compared to that of PPy. Bipyrrole and TDP possessed oxidation

peak potentials of 0.55 V and 0.42 V, respectively and polymers made from both monomers gave

similar redox potentials (-0.20 V and -0.19 V). However, a drastic decrease in the conductivity for

TDP polymer (2 S cm^{-1}) was observed compared to PPy (100 S cm^{-1}). These experiments have

shown that the presence of the sulfur atom is noninfluential and oxidation is governed by pyrrole

rings to present a material which is similar to PPy.[109] The synthesis of the TDP unit is shown in

Figure 1.13.
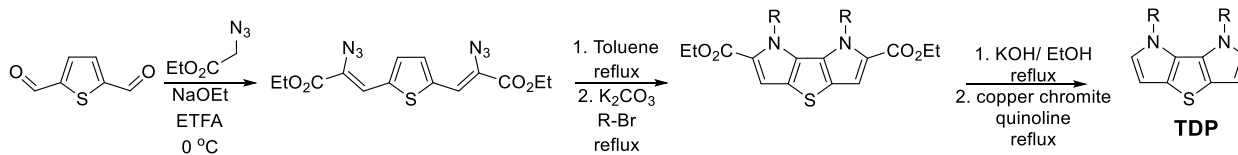
Figure 1.13 Synthetic route for N-alkylated TDP

Stefan and co-workers polymerized TDP using both metal catalyzed polymerization and oxidative

polymerization by FeCl$_3$.[73] Stille coupling polymerization generated oligomers instead of

polymers, but oxidative polymerization has led to molecular weights up to 6.5 kDa. It should be

noted that TDP unit is fairly unstable (similar to pyrrole monomer). Hence purification should be

performed with 1% tributylamine or triethylamine to prevent oxidation. Storage in hexane/pentane

at cold temperatures is advisable. Unfortunately, apart from conductivity measurements, no

organic electronic applications have pursued with this monomeric system yet.

1.5.3.5 *S,N*-Heteroacenes

Acenes are a popular class of high performing semiconductors for OFETs and OPVs in the organic electronics community. Among many examples, pentacene and its derivatives are widely studied for OFETs with outstanding charge carrier mobilities up to 40 cm^2 /V s.[8] Although these materials perform well in devices, practical applications are not amenable due to instability and limited solubility. Suga and co-workers first synthesized the 5 membered fused ring system containing alternating thiophene and pyrrole rings.[110] As shown in Figure 1.14, authors performed a retrosynthetic analysis first to find the precursors and synthesized the molecule via Negishi coupling and Tandem Buchwald-Hartwig coupling reactions.
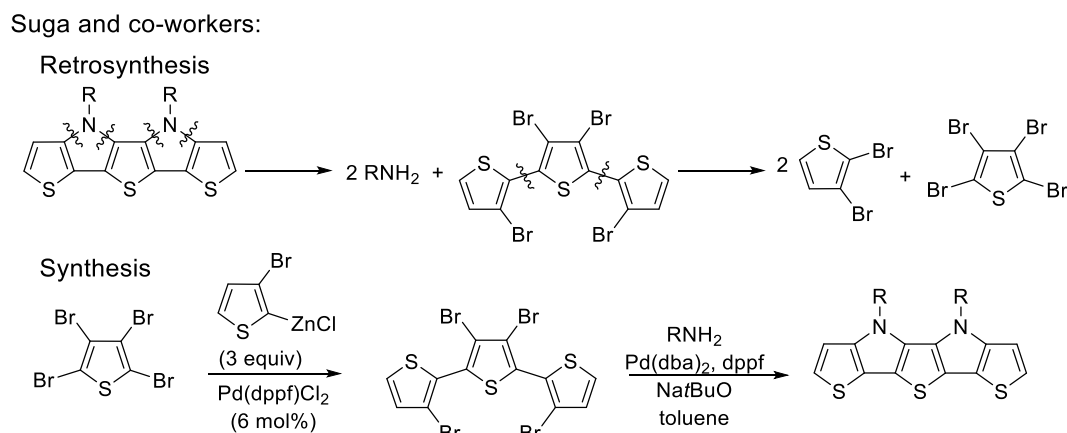
Figure 1.14 Synthesis of N-substituted dithieno[2,3-*d*:2′,3′-*d*′]thieno[3,2-*b*:3′,2′-*b*′]dipyrrole

To probe the effect of π-conjugation on fused ring systems authors performed DFT calculations on nitrogen-bridged oligothiophene skeletons up to 7 fused ring systems. With increasing number of fused rings, the band gap became smaller and similar to that found in relevant thienoacenes (Figure 1.15). However, an increase in the HOMO energy level was also observed through DFT calculations suggesting a higher number of fused rings could eventually destabilize the material.
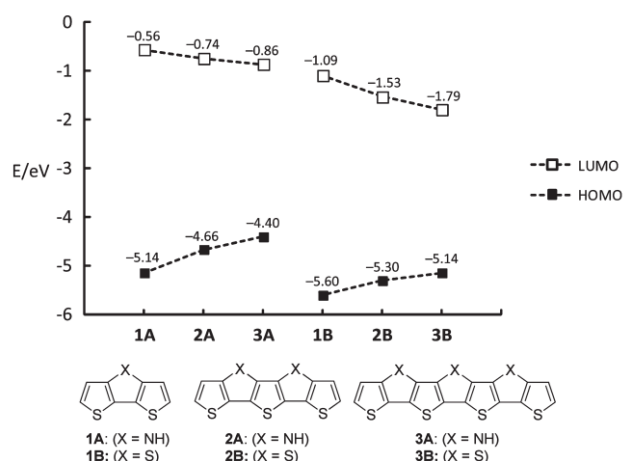
Figure 1.15 HOMO and LUMO energy level comparison of nitrogen-bridged oligothiophenes and thienoacenes. Figure adapted with permission from ref [109]. Copyright 2012 American Chemical Society

Bauerle's group in 2013 extended their work on DTP moieties to *S,N*-heteroacenes with a heterohexacene end-capped with a dicyanovinylene group (**SM18**).[111] Vacuum deposited **SM18** on the surface treated Si/SiO₂ substrates showed hole mobilities around 0.02 cm² /V s with large current on-to-off ratios (10⁵). Recently, Chung et al. reported a polymer (**P12**) consisting of *S,N*-heteroacene, and 5,6-difluorobenzotriazole where a maximum hole mobility of 0.093 cm² /V s was achieved in bottom-gate/top-contact devices.[112] The chemical structures, electrochemical and OFET performances are shown in Figure 1.16 and Table 1.2.
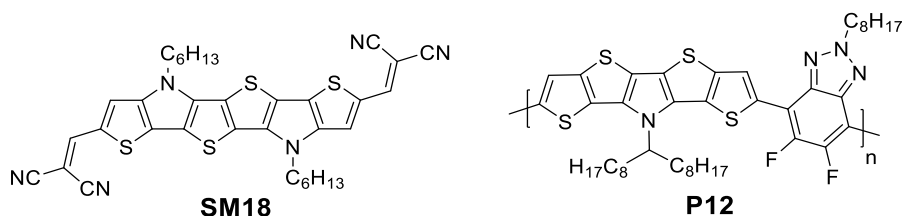
Figure 1.16 Chemical structures of *S,N*-heteroacenes employed for OFETs

Table 1.2 Electrochemical and OFET parameters of *S,N*-heteroacenes

	HOMO/LUMO (eV)	E_g (eV)	Device architecture	μ_h (cm^2/Vs)	μ_e (cm^2/Vs)	V_T (V)	I_{on}/I_{off}	Ref
SM18	-5.56/ -3.74	1.82	BGTC	2.1×10^{-2}	-	4.0	10^5	[110]
P12	-5.33/ -3.46	1.87	BGTC	9.3×10^{-2}	-	8.5	10^4	[111]

1.5.3.6 Indolo[3,2-*b*]indole

Another interesting class of fused ring systems including pyrroles are indolo[3,2-*b*]indoles. This building block was utilized in organic electronic applications in recent past and has been continuously using since then. This centrosymmetric building block was first introduced to OFETs by Park's group with a 20.7% overall yield (six steps).[113] Although this building block was reported previously, we have shown Park and co-workers route in Figure 1.17, due to the higher overall yield.
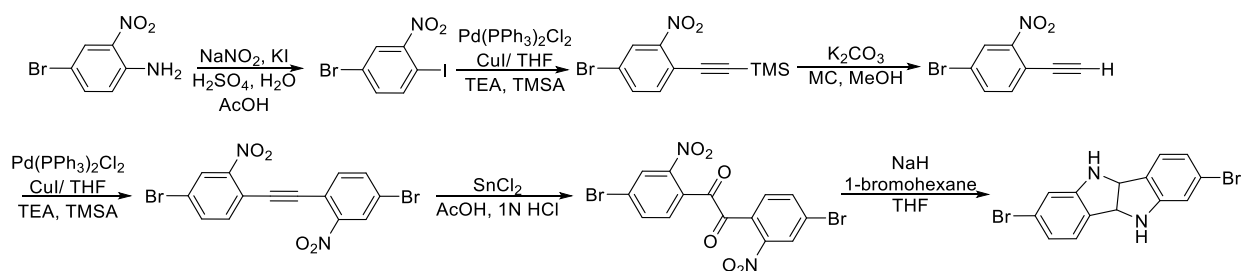
Figure 1.17 Synthetic route towards indolo[3,2-*b*]indoles

Four small molecules (**SM19**-**SM22**) were synthesized in the first report with a central IDID moiety and thiophene and bithiophene end caps with and without solubilizing alkyl chains to investigate OFET behavior. By vacuum depositing thin films of small molecules on the surface treated Si/SiO$_2$ substrates, high field-effect mobilities of 0.97 cm^2/V s was achieved for **SM22**

while other small molecules showed OFET performances in the range of 10^{-2} to 10^{-1} cm^2 /V s in bottom-gate/top-contact devices.
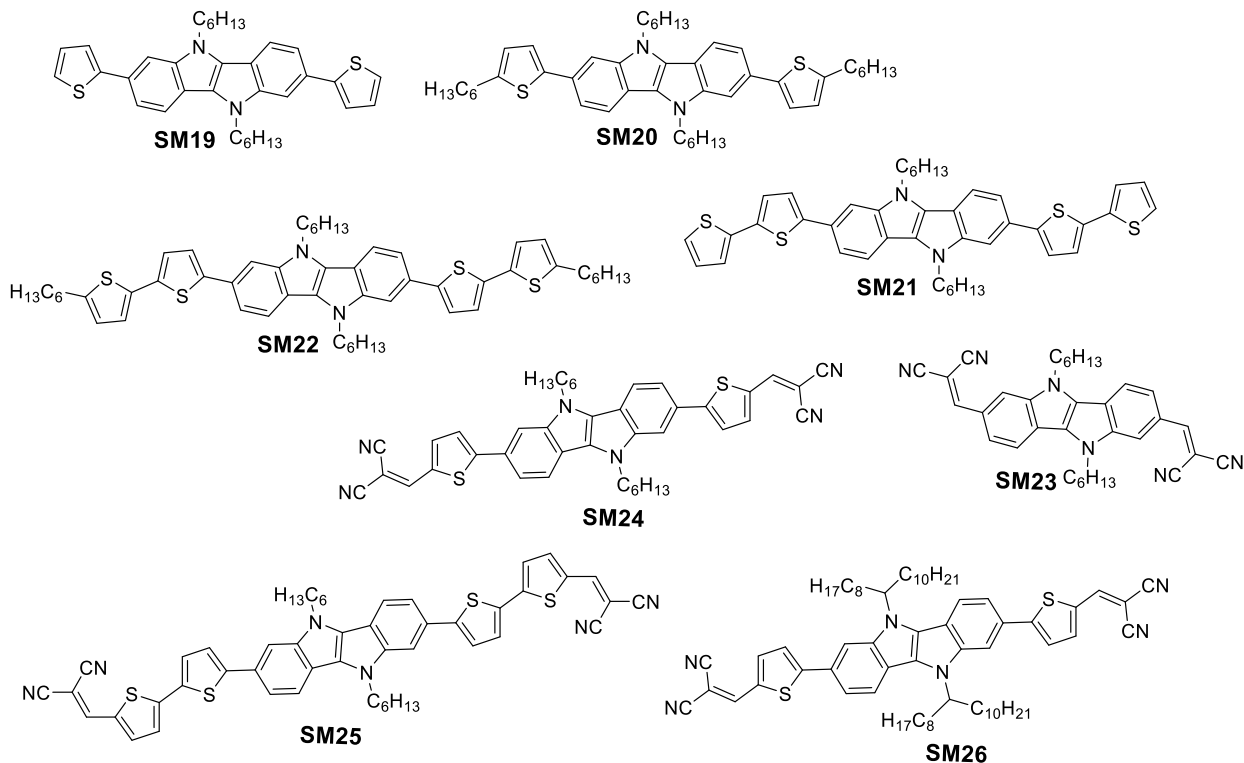
Figure 1.18 Indolo[3,2-*b*]indole based OSCs employed for OFETs

Solution-processed **SM22** devices exhibited hole mobilities up to 0.18 cm^2 /V s while showcasing similar threshold voltages and current on-to-off ratios. The same group synthesized a set of 4 small molecules (**SM23**-**SM26**) with dicyanovinylene end caps to obtain ambipolar OFETs.[114] However, based on the electrochemical properties and initial AFM measurements, authors did not evaluate ambipolar OFET characteristics of **SM23** and **SM25**. Meanwhile, **SM24** showed a balanced hole and electron mobility ($\mu_h/\mu_e = 0.84$) with a maximum hole mobility of 6.86×10^{-2} cm^2 /V s and electron mobility of 8.13×10^{-2} cm^2 /V s when substrates were heated to 120 °C for vacuum deposited thin films. By switching linear N-alkyl chains to branched chains (**SM26**), solubility was

improved and solution processed OFETs were built on **SM26**. An improvement in the hole mobility (9.67×10^{-2} cm^2/V s) was observed, but electron mobility dropped an order of magnitude (3.42×10^{-3} cm^2/V s) to show an imbalanced charge transport in ambipolar OFETs. All indolo[3,2-*b*]indole containing small molecules are shown in Figure 1.18, and their OFET performances are shown in Table 1.3.

Table 1.3 Electrochemical and OFET parameters of indolo[3,2-*b*]indole based semiconductors

	HOMO/LUMO (eV)	E_g (eV)	Device architecture	μ_h (cm^2/Vs)	μ_e (cm^2/Vs)	V_T (V)	I_{on}/I_{off}	Ref
SM19	-5.06/ -2.46	2.60	BGTC	3.2×10^{-2}	-	-11	10^4	113
SM20	-5.06/ -2.46	2.60	BGTC	5.1×10^{-2}	-	-5	10^5	113
SM21	-5.30/ -2.90	2.40	BGTC	3.4×10^{-1}	-	-10	10^5	113
SM22	-5.24/ -2.84	2.40	BGTC	9.7×10^{-1}	-	-12	10^5	113
SM23	-5.42/ -3.71	1.71	-	-	-	-	-	114
SM24	-5.09/ -3.86	1.23	BGTC	6.9×10^{-2}	8.1×10^{-2}	-13/61	10^3	114
SM25	-4.99/ -3.74	1.25	-	-	-		-	114
SM26	-	-	BGTC	9.7×10^{-2}	3.4×10^{-3}	-24/50	10^4	114

1.6 Working Principle of Organic Photovoltaics

The heavy dependence yet limited supply of fossil fuels poses an energy problem for the near future, presenting the need for a new renewable energy source. Solar energy is a unique solution to the energy crisis because of the clean, abundant supply. So far, different types of solar cells have been created to harness energy from sunlight, all known as photovoltaics (PV's). Among these PV's, OPVs have attracted heavy attention due to their structure tunability, flexibility, and solution processability. Although OPVs have not exceeded PCEs of inorganic solar cells, much progress has been made in the past two decades. First generation OPVs were made as single junction solar cells with PCEs less than 0.1% by sandwiching the OSC in between an anode (ITO) and cathode

(Ca/Al).[115] By inserting an electron acceptor layer C_{60} between the OSC and cathode, PCEs above 1% were obtained. Since the charge extraction only takes place at the interface of OSC and C_{60} in bilayer solar cells, BHJ solar cells were introduced to improve charge extraction and transport. Different device architectures are shown in Figure 1.19.
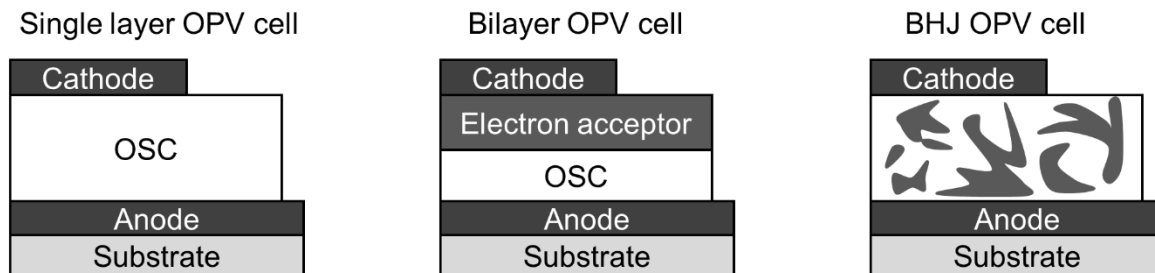
Figure 1.19 Device architectures for single layer, bilayer, and BHJ OPVs

Solar irradiance spectrum spans from 200 nm to 2000 nm in wavelength, while most of the solar energy lies in the range of 400 nm to 1250 nm. Therefore, materials that can efficiently absorb light up to near infrared region-I (NIR-I) are considered for OPV devices. To obtain materials with low band gaps, donor-acceptor type structures are usually employed. In a conventional OPV device, OSC is used as the photoactive material (donor), and fullerene derivatives ($PC_{61}BM$ or $PC_{71}BM$) are used as the electron acceptor. Upon absorbing solar energy, OSC will excite an electron from its HOMO level to the empty LUMO level creating an exciton or coulombically bound electron-hole pair. With the help of an electron accepting material, the excited electron in the LUMO level of the OSC can be transferred into the LUMO level of the fullerene derivative. Due to the ultra-fast lifetimes of excitons (< 1 ns) and smaller exciton diffusion lengths (< 20 nm), BHJ solar cells are found to be most effective among the three configurations mentioned above. It is also important to keep the HOMO level below -5.0 eV to extract holes from the anode. Usually,

a hole transporting layer, poly(3,4-ethylenedioxythiophene): polystyrene sulfonate (PEDOT:PSS) is used between the OSC and anode to facilitate the hole transport. The charge extraction is depicted in Figure 1.20.
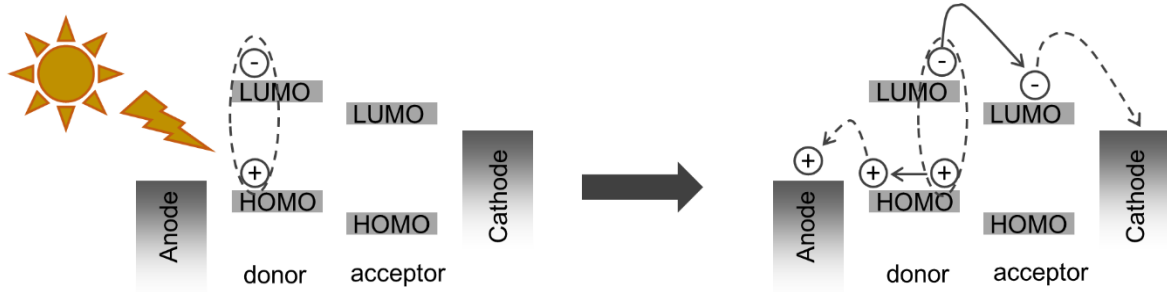
Figure 1.20 Generation and separation of excitons in BHJ solar cell

The efficacy of an OPV device is described by the ratio between output power and input power from the power source which mimics sunlight (Equation 1.3). The output power is defined as the product of open-circuit voltage (V_{oc}), short-circuit current density (J_{SC}) and fill factor (FF) (Equation 1.4). FF is defined as the ratio between the product of maximum current density (J_{max}) and maximum voltage (V_{max}) to the product of J_{SC} and V_{oc} (Equation 1.5). Following equations are employed to calculate PCE of a solar cell.

$$PCE(\eta) = \frac{P_{output}}{P_{input}} \tag{1.3}$$

$$P_{output} = V_{oc} \times J_{sc} \times FF \tag{1.4}$$

$$FF = \frac{V_{max} \times J_{max}}{V_{oc} \times J_{sc}} \tag{1.5}$$

A common OPV device architecture and a typical current density vs. voltage curve are shown in Figure 1.21 (a) and Figure 1.21 (b), respectively.
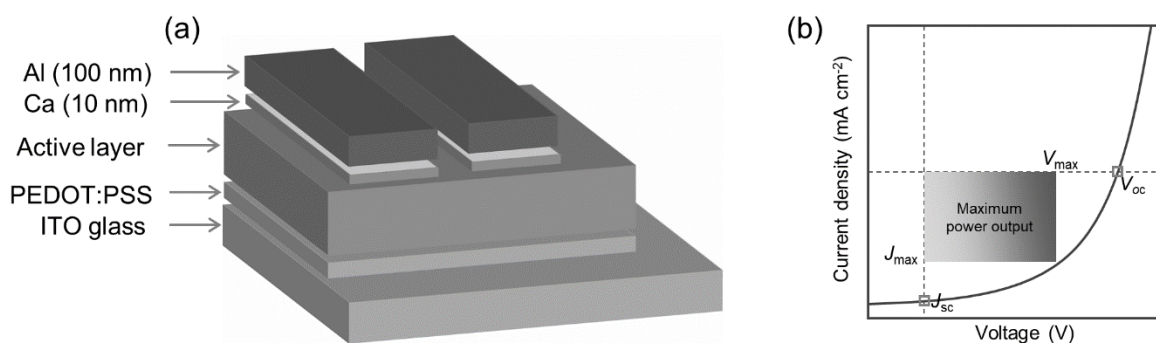
Figure 1.21 (a) Device architecture of an OPV, (b) a typical *J-V* curve for a OPV cell

Out of the three OPV cell parameters, V_{oc} can be predicted from the HOMO level of donor material (OSC) and LUMO level of the acceptor (fullerene derivative) according to equation (1.6).

$$V_{oc} = [1/e\ (E_{LUMO}^{acceptor} - E_{HOMO}^{donor}) - 0.3]\ V \qquad (1.6)$$

However, J_{sc} and *FF* cannot be predicted since these parameters depend on absorption of sun light, exciton dissociation, charge carrier recombination processes, series and shunt resistances and surface morphology. Due to the limitations of scalability, economic barriers and low electron mobilities associated with fullerene derivatives, non-conventional inorganic QDs were employed as electron acceptors due to tunable band gaps, higher electron mobilities and ease of synthesis.

1.7 Polymer Donor: Inorganic Nanoparticle Hybrid Solar Cells

The first report for hybrid solar cells was reported in 2002 by Alivisatos and co-workers where authors employed different shapes of CdSe nanoparticles with P3HT as the photo-absorber.[116] PCEs up to 1.7 % were reported for CdSe nanorods with an aspect ratio of 8.57 while nanorods with lower aspect ratios gave lower PCEs. Greenham, an co-workers, employed the conducting polymer poly(2-methoxy-5-(3′,7′-dimethyl-octyloxy)-*p*-phenylenevinylene) (OC$_1$C$_{10}$-PPV) with CdSe tetrapods to improve charge extraction three-dimensionally.[117] A significant amount of

research was then conducted to improve performances of hybrid solar cells, but irrespective of the donor material,[118, 119] shapes/ size of inorganic nanoparticles or type of semiconducting nanoparticles,[120-122] PCEs were not improved.

It was hypothesized that one of the limiting factors for lower PCEs was the uncontrollable phase separation in polymer nanocrystal blends. To address this issue, functional groups were introduced as end groups for polymer donors to improve the interaction with inorganic nanoparticles. Thiols, amines, carboxylic acids, phosphonic groups were used to directly attach or make favorable interactions. Liu et al. demonstrated amine end-functionalized P3HT could generate PCEs up to 1.6% with only half of the CdSe nanocrystal amount required for H/Br end-functionalized P3HT.[123] In our group we demonstrated that allyl end-capped P3HT could outperform thiol end-capped P3HT when CdSe QDs are employed as electron acceptors.[124] Different end-functionalized P3HT polymer are shown in Figure 1.22.
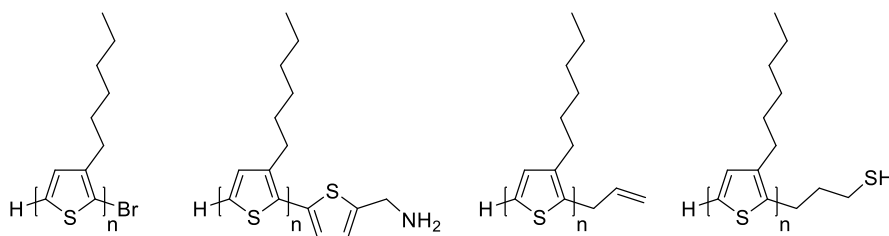
Figure 1.22 End-functionalized polythiophenes employed for hybrid solar cells

Another approach was to control the phase separation via ligand exchange reactions on nanoparticle surfaces. The process could be further categorized into pre-deposition and post-deposition ligand exchange reactions. Pre-deposition ligand exchange reactions are typically performed in solution-state by replacing native ligands on nanoparticles which were used in the original synthesis. Usually, long fatty acids are employed in the synthesis to passivate the

nanocrystal surface. The insulating nature of these long alkyl chains deteriorate the performances of solar cell devices. By replacing them with shorter aromatic ligands such as pyridine, better charge transport can be realized.[125] The inability to replace native ligands in a quantitative manner results in irreproducible PCEs which are dependent on the extent of the ligand exchange.[125] In order to have a reliable method for ligand exchange reactions, post-deposition ligand exchange reactions were developed by using monothiols and dithiols after depositing the active layer. Although thiols are considered as midgap hole traps for semiconducting nanocrystals, significant improvements were observed, especially for J_{sc}. Seo et al. showed that oleic acid ligands could be replaced with ethanedithiol ligands in a post-deposition ligand exchange.[126] Later, Zhou et al. reported ethanedithiol treatment for two polymer donors with significant improvements in J_{sc} (up to 50%) without degrading V_{oc} or FF.[127] It was shown that not only dithiols, monothiols could also improve performances in hybrid solar cells by post-deposition ligand exchange reactions.[128] In a combination of grafting with post-deposition ligand exchange reactions, Ren et al. showed enhancements in PCEs of P3HT:CdS hybrid solar cells up to 4.1%.[122]

Although these non-conventional inorganic semiconducting nanocrystals have the potential to surpass the performances of OPVs composed of conventional fullerene derivatives, they are not studied well enough due to the discouraging preliminary PCEs. However, if favorable phase separations can be achieved in thin films, more improvements could be made in this field.

1.8 Conclusions

While there is a promise and opportunities in the field of organic electronics, in order to improve electronic performances, novel materials have to be synthesized and tested. After screening for

potential non-conventional materials, as chemists many modifications could be performed with non-conventional building block tailored to specific applications.

1.9 References

1. Shirakawa, H.; Louis, E. J.; MacDiarmid, A. G.; Chiang, C. K.; Heeger, A. J., Synthesis of electrically conducting organic polymers: halogen derivatives of polyacetylene, (CH). *Journal of the Chemical Society, Chemical Communications* **1977**, (16), 578-580.

2. Jou, J.-H.; Kumar, S.; Agrawal, A.; Li, T.-H.; Sahoo, S., Approaches for fabricating high efficiency organic light emitting diodes. *Journal of Materials Chemistry C* **2015,** 3, (13), 2974-3002.

3. Scholz, S.; Kondakov, D.; Lüssem, B.; Leo, K., Degradation Mechanisms and Reactions in Organic Light-Emitting Devices. *Chemical Reviews* **2015,** 115, (16), 8449-8503.

4. Xu, R.-P.; Li, Y.-Q.; Tang, J.-X., Recent advances in flexible organic light-emitting diodes. *Journal of Materials Chemistry C* **2016,** 4, (39), 9116-9142.

5. Lu, L.; Zheng, T.; Wu, Q.; Schneider, A. M.; Zhao, D.; Yu, L., Recent Advances in Bulk Heterojunction Polymer Solar Cells. *Chemical Reviews* **2015,** 115, (23), 12666-12731.

6. Cheng, P.; Zhan, X., Stability of organic solar cells: challenges and strategies. *Chemical Society Reviews* **2016,** 45, (9), 2544-2582.

7.Günes, S.; Neugebauer, H.; Sariciftci, N. S., Conjugated Polymer-Based Organic Solar Cells. *Chemical Reviews* **2007,** 107, (4), 1324-1338.

8. Mei, J.; Diao, Y.; Appleton, A. L.; Fang, L.; Bao, Z., Integrated Materials Design of Organic Semiconductors for Field-Effect Transistors. *Journal of the American Chemical Society* **2013,** 135, (18), 6724-6746.

9. Muccini, M., A bright future for organic field-effect transistors. *Nature Materials* **2006,** 5, 605.

10. Sirringhaus, H., 25th Anniversary Article: Organic Field-Effect Transistors: The Path Beyond Amorphous Silicon. *Advanced Materials* **2014,** 26, (9), 1319-1335.

11. Jacob, V. M., Organic Semiconductors: Past, Present, and Future. *Electronics* **2014,** 3, (4).

12. Carrasco, P. M.; Grande, H. J.; Cortazar, M.; Alberdi, J. M.; Areizaga, J.; Pomposo, J. A., Structure–conductivity relationships in chemical polypyrroles of low, medium and high conductivity. *Synthetic Metals* **2006,** 156, (5), 420-425.

13. Salzner, U.; Lagowski, J. B.; Pickup, P. G.; Poirier, R. A., Comparison of geometries and electronic structures of polyacetylene, polyborole, polycyclopentadiene, polypyrrole, polyfuran, polysilole, polyphosphole, polythiophene, polyselenophene and polytellurophene. *Synthetic Metals* **1998,** 96, (3), 177-189.

14. Bhadra, S.; Khastgir, D.; Singha, N. K.; Lee, J. H., Progress in preparation, processing and applications of polyaniline. *Progress in Polymer Science* **2009,** 34, (8), 783-810.

15. Huang, J.; Virji, S.; Weiller, B. H.; Kaner, R. B., Polyaniline Nanofibers: Facile Synthesis and Chemical Sensors. *Journal of the American Chemical Society* **2003,** 125, (2), 314-315.

16. Zhang, R.; Li, B.; Iovu, M. C.; Jeffries-El, M.; Sauvé, G.; Cooper, J.; Jia, S.; Tristram-Nagle, S.; Smilgies, D. M.; Lambeth, D. N.; McCullough, R. D.; Kowalewski, T., Nanostructure Dependence of Field-Effect Mobility in Regioregular Poly(3-hexylthiophene) Thin Film Field Effect Transistors. *Journal of the American Chemical Society* **2006,** 128, (11), 3480-3481.

17. Iovu, M. C.; Sheina, E. E.; Gil, R. R.; McCullough, R. D., Experimental Evidence for the Quasi-"Living" Nature of the Grignard Metathesis Method for the Synthesis of Regioregular Poly(3-alkylthiophenes). *Macromolecules* **2005,** 38, (21), 8649-8656.

18. Iovu, M. C.; Jeffries-El, M.; Sheina, E. E.; Cooper, J. R.; McCullough, R. D., Regioregular poly(3-alkylthiophene) conducting block copolymers. *Polymer* **2005,** 46, (19), 8582-8586.

19. Chi, D.; Qu, S.; Wang, Z.; Wang, J., High efficiency P3HT:PCBM solar cells with an inserted PCBM layer. *Journal of Materials Chemistry C* **2014,** 2, (22), 4383-4387.

20. Holliday, S.; Ashraf, R. S.; Wadsworth, A.; Baran, D.; Yousaf, S. A.; Nielsen, C. B.; Tan, C.-H.; Dimitrov, S. D.; Shang, Z.; Gasparini, N.; Alamoudi, M.; Laquai, F.; Brabec, C. J.; Salleo, A.; Durrant, J. R.; McCulloch, I., High-efficiency and air-stable P3HT-based polymer solar cells with a new non-fullerene acceptor. *Nature Communications* **2016,** 7, 11585.

21. Kularatne, R. S.; Magurudeniya, H. D.; Sista, P.; Biewer, M. C.; Stefan, M. C., Donor–acceptor semiconducting polymers for organic solar cells. *Journal of Polymer Science Part A: Polymer Chemistry* **2013,** 51, (4), 743-768.

22. Liu, Y.; Chen, C.-C.; Hong, Z.; Gao, J.; Yang, Y.; Zhou, H.; Dou, L.; Li, G.; Yang, Y., Solution-processed small-molecule solar cells: breaking the 10% power conversion efficiency. *Scientific Reports* **2013,** 3, 3356.

23. Zhang, Q.; Kan, B.; Liu, F.; Long, G.; Wan, X.; Chen, X.; Zuo, Y.; Ni, W.; Zhang, H.; Li, M.; Hu, Z.; Huang, F.; Cao, Y.; Liang, Z.; Zhang, M.; Russell, T. P.; Chen, Y., Small-molecule solar cells with efficiency over 9%. *Nature Photonics* **2014,** 9, 35.

24. Troisi, A., Charge transport in high mobility molecular semiconductors: classical models and new theories. *Chemical Society Reviews* **2011,** 40, (5), 2347-2358.

25. Horowitz, G., Organic thin film transistors: From theory to real devices. *Journal of Materials Research* **2011,** 19, (7), 1946-1962.

26. Coropceanu, V.; Cornil, J.; da Silva Filho, D. A.; Olivier, Y.; Silbey, R.; Brédas, J.-L., Charge Transport in Organic Semiconductors. *Chemical Reviews* **2007,** 107, (4), 926-952.

27. Hulea, I. N.; Fratini, S.; Xie, H.; Mulder, C. L.; Iossad, N. N.; Rastelli, G.; Ciuchi, S.; Morpurgo, A. F., Tunable Fröhlich polarons in organic single-crystal transistors. *Nature Materials* **2006,** 5, 982.

28. Ding, H.; Reese, C.; Mäkinen, A. J.; Bao, Z.; Gao, Y., Band structure measurement of organic single crystal with angle-resolved photoemission. *Applied Physics Letters* **2010,** 96, (22), 222106.

29. Venkateshvaran, D.; Nikolka, M.; Sadhanala, A.; Lemaur, V.; Zelazny, M.; Kepa, M.; Hurhangee, M.; Kronemeijer, A. J.; Pecunia, V.; Nasrallah, I.; Romanov, I.; Broch, K.; McCulloch, I.; Emin, D.; Olivier, Y.; Cornil, J.; Beljonne, D.; Sirringhaus, H., Approaching disorder-free transport in high-mobility conjugated polymers. *Nature* **2014,** 515, 384.

30. Seto, J. Y. W., The electrical properties of polycrystalline silicon films. *Journal of Applied Physics* **1975,** 46, (12), 5247-5254.

31. Levinson, J.; Shepherd, F. R.; Scanlon, P. J.; Westwood, W. D.; Este, G.; Rider, M., Conductivity behavior in polycrystalline semiconductor thin film transistors. *Journal of Applied Physics* **1982,** 53, (2), 1193-1202.

32. Horowitz, G., Organic Field-Effect Transistors. *Advanced Materials* **1998,** 10, (5), 365-377.

33. Friedman, L., Transport Properties of Organic Semiconductors. *Physical Review* **1964,** 133, (6A), A1668-A1679.

34. Tsumura, A.; Koezuka, H.; Ando, T., Macromolecular electronic device: Field-effect transistor with a polythiophene thin film. *Applied Physics Letters* **1986,** 49, (18), 1210-1212.

35. Nogami, Y.; Pouget, J.-P.; Ishiguro, T., Structure of highly conducting PF6−-doped polypyrrole. *Synthetic Metals* **1994,** 62, (3), 257-263.

36. Skotheim, T. A., Reynolds, J. R, Handbook of Conducting Polymers. 3rd ed. Boca Raton, FL: CRC Press; 2007. 1680p.

37. Andrieux, C. P.; Audebert, P.; Hapiot, P.; Saveant, J. M., Identification of the first steps of the electrochemical polymerization of pyrroles by means of fast potential step techniques. *The Journal of Physical Chemistry* **1991,** 95, (24), 10158-10164.

38. Diaz, A. F.; Crowley, J.; Bargon, J.; Gardini, G. P.; Torrance, J. B., Electrooxidation of aromatic oligomers and conducting polymers. *Journal of Electroanalytical Chemistry and Interfacial Electrochemistry* **1981,** 121, 355-361.

39. Diaz, A. F., Bargon J., 1986. Handbook of Conducting Polymers, Vol 1, ed, T. A Skotheim, New York: Marcel Dekker, pp 81-115. .

40. Wei, Y.; Tian, J.; Yang, D., A new method for polymerization of pyrrole and derivatives. *Die Makromolekulare Chemie, Rapid Communications* **1991,** 12, (11), 617-623.

41. Diaz, A. F.; Kanazawa, K. K.; Gardini, G. P., Electrochemical polymerization of pyrrole. *Journal of the Chemical Society, Chemical Communications* **1979**, (14), 635-636.

42. Bocchi, V.; Gardini, G. P., Chemical synthesis of conducting polypyrrole and some composites. *Journal of the Chemical Society, Chemical Communications* **1986**, (2), 148a-148a.

43. Machida, S.; Miyata, S.; Techagumpuch, A., Chemical synthesis of highly electrically conductive polypyrrole. *Synthetic Metals* **1989,** 31, (3), 311-318.

44. Jakobs, R. C. M.; Janssen, L. J. J.; Barendrecht, E., Hydroquinone oxidation and p-benzoquinone reduction at polypyrrole and poly-*N*-methylpyrrole electrodes. *Electrochimica Acta* **1985,** 30, (10), 1313-1321.

45. Haimerl, A.; Merz, A., Catalysis of quinone-hydroguinone redox reactions at polypyrrole benzenesulphonate-coated platinum electrodes. *Journal of Electroanalytical Chemistry and Interfacial Electrochemistry* **1987,** 220, (1), 55-65.

46. Khulbe, K. C.; Mann, R. S.; Khulbe, C. P., Polymerization of pyrrole by potassium persulfate. *Journal of Polymer Science: Polymer Chemistry Edition* **1982,** 20, (4), 1089-1095.

47. Velayutham, D.; Noel, M., Effect of additives on the anodic codeposition of lead dioxide and polypyrrole. *Journal of Applied Electrochemistry* **1993,** 23, (9), 922-926.

48. Omastova, M.; Trchova, M.; Kovarova, J.; Stejskal, J., Synthesis and structural study of polypyrroles prepared in the presence of surfactants. *Synth. Met.* **2003,** 138, (3), 447-455.

49. Kudoh, Y., Properties of polypyrrole prepared by chemical polymerization using aqueous solution containing Fe2(SO4)3 and anionic surfactant. *Synthetic Metals* **1996,** 79, (1), 17-22.

50. Omastova, M.; Pionteck, J.; Trchova, M., Properties and morphology of polypyrrole containing a surfactant. *Synth. Met.* **2003,** 135-136, 437-438.

51. Lee, J. Y.; Kim, D. Y.; Kim, C. Y., Synthesis of soluble polypyrrole of the doped state in organic solvents. *Synthetic Metals* **1995,** 74, (2), 103-106.

52. Yokoyama, A.; Kato, A.; Miyakoshi, R.; Yokozawa, T., Precision Synthesis of Poly(N-hexylpyrrole) and Its Diblock Copolymer with Poly(p-phenylene) via Catalyst-Transfer Polycondensation. *Macromolecules* **2008,** 41, (20), 7271-7273.

53. Stefan, M. C.; Javier, A. E.; Osaka, I.; McCullough, R. D., Grignard Metathesis Method (GRIM): Toward a Universal Method for the Synthesis of Conjugated Polymers. *Macromolecules* **2009,** 42, (1), 30-32.

54. Lanni, E. L.; Locke, J. R.; Gleave, C. M.; McNeil, A. J., Ligand-Based Steric Effects in Ni-Catalyzed Chain-Growth Polymerizations Using Bis(dialkylphosphino)ethanes. *Macromolecules* **2011,** 44, (13), 5136-5145.

55. Merrill, B. A.; LeGoff, E., A general synthetic route to 2,2':5',2''-terpyrrole, 2,5-di(2-pyrryl)thiophene, and alkyl-substituted analogs. *The Journal of Organic Chemistry* **1990,** 55, (9), 2904-2908.

56. Wu, J.; Vetter, W.; Gribble, G. W.; Schneekloth, J. J. S.; Blank, D. H.; Görls, H., Structure and Synthesis of the Natural Heptachloro-1′-methyl-1,2′-bipyrrole (Q1). *Angewandte Chemie International Edition* **2002,** 41, (10), 1740-1743.

57. Sessler, J. L.; Cyr, M. J.; Lynch, V.; McGhee, E.; Ibers, J. A., Synthetic and structural studies of sapphyrin, a 22-.pi.-electron pentapyrrolic "expanded porphyrin". *Journal of the American Chemical Society* **1990,** 112, (7), 2810-2813.

58. Sessler, J. L.; Cyr, M.; Burrell, A. K., Sapphyrins and heterosapphyrins. *Tetrahedron* **1992,** 48, (44), 9661-9672.

59. Ikeda, H.; Sessler, J. L., Synthesis of the first .alpha.-linked quaterpyrrole. *The Journal of Organic Chemistry* **1993,** 58, (8), 2340-2342.

60. Martina, S.; Enkelmann, V.; Wegner, G.; Schlüter, A.-D., Progress toward the development of a chemical synthesis for poly(2,5-pyrrole). *Synthetic Metals* **1992,** 51, (1), 299-305.

61. Zotti, G.; Martina, S.; Wegner, G.; Schlüter, A.-D., Well-defined pyrrole oligomers: Electrochemical and UV/vis studies. *Advanced Materials* **1992,** 4, (12), 798-801.

62. Groenendaal, L.; Peerlings, H. W. I.; van Dongen, J. L. J.; Havinga, E. E.; Vekemans, J. A. J. M.; Meijer, E. W., Well-Defined Oligo(pyrrole-2,5-diyl)s by the Ullmann Reaction. *Macromolecules* **1995,** 28, (1), 116-123.

63. Andrieux, C. P.; Hapiot, P.; Audebert, P.; Guyard, L.; Dinh An, M. N.; Groenendaal, L.; Meijer, E. W., Substituent Effects on the Electrochemical Properties of Pyrroles and Small Oligopyrroles. *Chemistry of Materials* **1997,** 9, (3), 723-729.

64. Groenendaal, L.; Bruining, M. J.; Hendrickx, E. H. J.; Persoons, A.; Vekemans, J. A. J. M.; Havinga, E. E.; Meijer, E. W., Synthesis and (Non)linear Optical Properties of a Series of Donor−Oligopyrrole−Acceptor Molecules. *Chemistry of Materials* **1998,** 10, (1), 226-234.

65. Cordell, G. A., 2-Halopyrroles. Synthesis and chemistry. *The Journal of Organic Chemistry* **1975,** 40, (22), 3161-3169.

66. Gilow, H. M.; Burton, D. E., Bromination and chlorination of pyrrole and some reactive 1-substituted pyrroles. *J. Org. Chem.* **1981,** 46, (11), 2221-5.

67. De Rosa, M.; Cabrera Nieto, G., Effect of halogen on the reaction of 1-methylpyrrole with N-haloimides. *Tetrahedron Lett.* **1988,** 29, (20), 2405-8.

68. Faigl, F.; Deák, S.; Mucsi, Z.; Hergert, T.; Balázs, L.; Sándor, B.; Balázs, B.; Holczbauer, T.; Nyerges, M.; Mátravölgyi, B., A novel and convenient method for the preparation of 5-(diphenylmethylene)-1H-pyrrol-2(5H)-ones; synthesis and mechanistic study. *Tetrahedron* **2016,** 72, (35), 5444-5455.

69. Martina, S.; Enkelmann, V.; Wegner, G.; Schlüter, A.-D., N-Protected Pyrrole Derivatives Substituted for Metal-Catalyzed Cross-Coupling Reactions. *Synthesis* **1991,** 1991, (08), 613-615.

70. van Mullekom, H. A. M.; Venkemans, J. A. J. M.; Meijer, E. W., Alternating copolymer of pyrrole and 2,1,3-benzothiadiazole. *Chemical Communications* **1996**, (18), 2163-2164.

71. Edder, C.; Armstrong, P. B.; Prado, K. B.; Frechet, J. M. J., Benzothiadiazole- and pyrrole-based polymers bearing thermally cleavable solubilizing groups as precursors for low bandgap polymers. *Chemical Communications* **2006**, (18), 1965-1967.

72. Faderl, J.; Deobald, B.; Guilard, R.; Pritzkow, H.; Siebert, W., Syntheses, Structures, and Reactivity of 2,5-Diboryl-1-alkylpyrroles and Di(1-alkyl-2-pyrrolyl)boranes. *European Journal of Inorganic Chemistry* **1999,** 1999, (3), 399-404.

73. Nguyen, H. Q.; Rainbolt, E. A.; Sista, P.; Stefan, M. C., Synthesis and Polymerization of Fused-Ring Thienodipyrrole Monomers. *Macromolecular Chemistry and Physics* **2012,** 213, (4), 425-430.

74. Hendriks, K. H.; Li, W.; Wienk, M. M.; Janssen, R. A. J., Small-Bandgap Semiconducting Polymers with High Near-Infrared Photoresponse. *Journal of the American Chemical Society* **2014,** 136, (34), 12130-12136.

75. Dhanabalan, A.; van Hal, P. A.; van Duren, J. K. J.; van Dongen, J. L. J.; Janssen, R. A. J., Design and synthesis of processible functional copolymers. *Synthetic Metals* **2001,** 119, (1), 169-170.

76. Dhanabalan, A.; Knol, J.; Hummelen, J. C.; Janssen, R. A. J., Design and synthesis of new processible donor-acceptor dyad and triads. *Synthetic Metals* **2001,** 119, (1), 519-522.

77. Garcia-Amoros, J.; R. Castro, M. C.; Coelho, P.; M. Raposo, M. M.; Velasco, D., New heterocyclic systems to afford microsecond green-light isomerisable azo dyes and their use as fast molecular photochromic switches. *Chemical Communications* **2013,** 49, (97), 11427-11429.

78. Kancharla, P.; Kelly, J. X.; Reynolds, K. A., Synthesis and Structure–Activity Relationships of Tambjamines and B-Ring Functionalized Prodiginines as Potent Antimalarials. *Journal of Medicinal Chemistry* **2015,** 58, (18), 7286-7309.

79. Brodnik, H.; Pozgan, F.; Stefane, B., Synthesis of 8-heteroaryl nitroxoline analogues via one-pot sequential Pd-catalyzed coupling reactions. *Organic & Biomolecular Chemistry* **2016,** 14, (6), 1969-1981.

80. Geißler, U.; Hallensleben, M. L.; Rohde, N., Poly{arylene-alt-[bis(1-methylpyrrolylene)]}s, 1. Synthesis and electrochemical polymerization of terarenes. *Macromolecular Chemistry and Physics* **1996,** 197, (8), 2565-2576.

81. So, S.; Choi, H.; Min Ko, H.; Kim, C.; Paek, S.; Cho, N.; Song, K.; Lee, J. K.; Ko, J., Novel unsymmetrical push–pull squaraine chromophores for solution processed small molecule bulk heterojunction solar cells. *Solar Energy Materials and Solar Cells* **2012,** 98, 224-232.

82. He, L.-Y.; Urrego-Riveros, S.; Gates, P. J.; Näther, C.; Brinkmann, M.; Abetz, V.; Staubitz, A., Synthesis of poly(thiophene-alt-pyrrole) from a difunctionalized thienylpyrrole by Kumada polycondensation. *Tetrahedron* **2015,** 71, (33), 5399-5406.

83. Rieth, R. D.; Mankad, N. P.; Calimano, E.; Sadighi, J. P., Palladium-Catalyzed Cross-Coupling of Pyrrole Anions with Aryl Chlorides, Bromides, and Iodides. *Organic Letters* **2004,** 6, (22), 3981-3983.

84. Wang, X.; Lane, B. S.; Sames, D., Direct C-Arylation of Free (NH)-Indoles and Pyrroles Catalyzed by Ar−Rh(III) Complexes Assembled In Situ. *Journal of the American Chemical Society* **2005,** 127, (14), 4996-4997.

85. Fujii, M.; Nishinaga, T.; Iyoda, M., Synthesis of thiophene–pyrrole mixed oligomers end-capped with hexyl group for field-effect transistors. *Tetrahedron Letters* **2009,** 50, (5), 555-558.

86. Hemetsberger, H.; Knittel, D., Synthese und Thermolyse von α-Azidoacrylestern. *Monatshefte für Chemie / Chemical Monthly* **1972,** 103, (1), 194-204.

87. Kumagai, T.; Satake, K.; Kidoura, K.; Mukai, T., A new reaction of nitrene with 1*H*-azepine derivatives: a formation of 2,6-diazabicyclo[3.3.0]octadiene and 2,8-diazabicyclo[3.2.1]octadiene. *Tetrahedron Letters* **1983,** 24, (22), 2275-2278.

88. Kumagai, T.; Tanaka, S.; Mukai, T., Synthesis of 1,4-dihydropyrrolo[3,2-*b*]pyrrole. *Tetrahedron Letters* **1984,** 25, (49), 5669-5672.

89. Janiga, A.; Glodkowska-Mrowka, E.; Stoklosa, T.; Gryko, D. T., Synthesis and Optical Properties of Tetraaryl-1,4-dihydropyrrolo[3,2-*b*]pyrroles. *Asian Journal of Organic Chemistry* **2013,** 2, (5), 411-415.

90. Matteson, D. S.; Snyder, H. R., A Practical Synthesis of Thieno[3,2-*b*]pyrrole. *The Journal of Organic Chemistry* **1957,** 22, (11), 1500-1504.

91. Jones, C.; Boudinet, D.; Xia, Y.; Denti, M.; Das, A.; Facchetti, A.; Driver, T. G., Synthesis and Properties of Semiconducting Bispyrrolothiophenes for Organic Field-Effect Transistors. *Chemistry – A European Journal* **2014,** 20, (20), 5938-5945.

92. Berlin, A.; Pagani, G.; Zotti, G.; Schiavon, G., Electrochemical polymerization of 1*H*,7*H*-pyrrolo[2′,3′:4,5]-thieno[3,2-*b*]pyrrole and 4H-dithieno[3,2-*b*;2′,3′-*d*]pyrrole. *Die Makromolekulare Chemie* **1992,** 193, (2), 399-409.

93. Rasmussen, S. C.; Evenson, S. J., Dithieno[3,2-*b*:2′,3′-*d*]pyrrole-based materials: Synthesis and application to organic electronics. *Prog. Polym. Sci.* **2013,** 38, (12), 1773-1804.

94. Rasmussen, S. C., Ogawa K., Rothstein S. D., Synthetic approaches to band gap control in conjugated polymeric materials. In: Nalwa H. S. editor. Handbook of Organic Electronics and Photonics, vol 1. Stevenson Ranch, CA: American Scientific Publishers; 2008. p. 1-50.

95. Baumgartner, T., π-Conjugated Heterocyclic fused Bithiophene Materials. *Journal of Inorganic and Organometallic Polymers and Materials* **2005,** 15, (4), 389-409.

96. Förtsch, S.; Vogt, A.; Bäuerle, P., New methods for the synthesis of 4*H*-dithieno[3,2-*b*:2′,3′-*d*]pyrrole. *Journal of Physical Organic Chemistry* **2017,** 30, (9), 3743.

97. Liu, J.; Zhang, R.; Sauvé, G.; Kowalewski, T.; McCullough, R. D., Highly Disordered Polymer Field Effect Transistors: N-Alkyl Dithieno[3,2-*b*:2′,3′-*d*]pyrrole-Based Copolymers with Surprisingly High Charge Carrier Mobilities. *Journal of the American Chemical Society* **2008,** 130, (39), 13167-13176.

98. Zhang, W.; Li, J.; Zou, L.; Zhang, B.; Qin, J.; Lu, Z.; Poon, Y. F.; Chan-Park, M. B.; Li, C. M., Semiconductive Polymers Containing Dithieno[3,2-*b*:2′,3′-*d*]pyrrole for Organic Thin-Film Transistors. *Macromolecules* **2008,** 41, (23), 8953-8955.

99. Steckler, T. T.; Zhang, X.; Hwang, J.; Honeyager, R.; Ohira, S.; Zhang, X.-H.; Grant, A.; Ellinger, S.; Odom, S. A.; Sweat, D.; Tanner, D. B.; Rinzler, A. G.; Barlow, S.; Brédas, J.-L.; Kippelen, B.; Marder, S. R.; Reynolds, J. R., A Spray-Processable, Low Bandgap, and Ambipolar Donor−Acceptor Conjugated Polymer. *Journal of the American Chemical Society* **2009,** 131, (8), 2824-2826.

100. Zhan, X.; Tan, Z. a.; Zhou, E.; Li, Y.; Misra, R.; Grant, A.; Domercq, B.; Zhang, X.-H.; An, Z.; Zhang, X.; Barlow, S.; Kippelen, B.; Marder, S. R., Copolymers of perylene diimide with

dithienothiophene and dithienopyrrole as electron-transport materials for all-polymer solar cells and field-effect transistors. *Journal of Materials Chemistry* **2009,** 19, (32), 5794-5803.

101. Nelson, T. L.; Young, T. M.; Liu, J.; Mishra, S. P.; Belot, J. A.; Balliet, C. L.; Javier, A. E.; Kowalewski, T.; McCullough, R. D., Transistor Paint: High Mobilities in Small Bandgap Polymer Semiconductor Based on the Strong Acceptor, Diketopyrrolopyrrole and Strong Donor, Dithienopyrrole. *Advanced Materials* **2010,** 22, (41), 4617-4621.

102. Ahmed, E.; Subramaniyan, S.; Kim, F. S.; Xin, H.; Jenekhe, S. A., Benzobisthiazole-Based Donor–Acceptor Copolymer Semiconductors for Photovoltaic Cells and Highly Stable Field-Effect Transistors. *Macromolecules* **2011,** 44, (18), 7207-7219.

103. Lin, F.-J.; Lin, S.-D.; Chin, C.-H.; Chuang, W.-T.; Hsu, C.-S., Novel conjugated polymers based on bis-dithieno[3,2-*b*;2′,3′-*d*]pyrrole vinylene donor and diketopyrrolopyrrole acceptor: side chain engineering in organic field effect transistors. *Polymer Chemistry* **2018,** 9, (1), 28-37.

104. Polander, L. E.; Pandey, L.; Barlow, S.; Tiwari, S. P.; Risko, C.; Kippelen, B.; Brédas, J.-L.; Marder, S. R., Benzothiadiazole-Dithienopyrrole Donor–Acceptor–Donor and Acceptor–Donor–Acceptor Triads: Synthesis and Optical, Electrochemical, and Charge-Transport Properties. *The Journal of Physical Chemistry C* **2011,** 115, (46), 23149-23163.

105. Lin, G.; Qin, Y.; Guan, Y.-S.; Xu, H.; Xu, W.; Zhu, D., [small pi]-Conjugated dithieno[3,2-*b*:2′,3′-*d*]pyrrole (DTP) oligomers for organic thin-film transistors. *RSC Advances* **2016,** 6, (6), 4872-4876.

106. Tiwari, S. P.; Kim, J.; Knauer, K. A.; Hwang, D. K.; Polander, L. E.; Barlow, S.; Marder, S. R.; Kippelen, B., Complementary-like inverters based on an ambipolar solution-processed molecular bis(naphthalene diimide)-dithienopyrrole derivative. *Organic Electronics* **2012,** 13, (7), 1166-1170.

107. Farnier, M.; Soth, S.; Fournari, P., Recherches en série hétérocyclique. XXVII. Etude de la condensation de l'azidoacétate d'éthyle sur les thiophènedicarbaldéhydes-2,5, -2,4 et -3,4. *Canadian Journal of Chemistry* **1976,** 54, (7), 1074-1082.

108. Schiavon, G.; Zotti, G.; Berlin, A.; Pagani, G.; Sannicolo, F., Conductive materials from dihydro-benzodipyrroles. *Synth. Met.* **1989,** 28, (1-2), C199-C204.

109. Berlin, A.; Pagani, G. A.; Sannicolo, F.; Schiavon, G.; Zotti, G., Monomer tailoring to control the redox potentials of conductive polyheterocycles. *Polymer* **1991,** 32, (10), 1841-42.

110. Mitsudo, K.; Shimohara, S.; Mizoguchi, J.; Mandai, H.; Suga, S., Synthesis of Nitrogen-Bridged Terthiophenes by Tandem Buchwald–Hartwig Coupling and Their Properties. *Organic Letters* **2012,** 14, (11), 2702-2705.

111. Wetzel, C.; Mishra, A.; Mena-Osteritz, E.; Liess, A.; Stolte, M.; Würthner, F.; Bäuerle, P., Synthesis and Structural Analysis of Thiophene-Pyrrole-Based S,N-Heteroacenes. *Organic Letters* **2014,** 16, (2), 362-365.

112. Chung, C.-L.; Chen, H.-C.; Yang, Y.-S.; Tung, W.-Y.; Chen, J.-W.; Chen, W.-C.; Wu, C.-G.; Wong, K.-T., S,N-Heteroacene-Based Copolymers for Highly Efficient Organic Field Effect Transistors and Organic Solar Cells: Critical Impact of Aromatic Subunits in the Ladder π-System. *ACS Applied Materials & Interfaces* **2018,** 10, (7), 6471-6483.

113. Cho, I.; Park, S. K.; Kang, B.; Chung, J. W.; Kim, J. H.; Cho, K.; Park, S. Y., Design, Synthesis, and Versatile Processing of Indolo[3,2-*b*]indole-Based π-Conjugated Molecules for High-Performance Organic Field-Effect Transistors. *Advanced Functional Materials* **2016,** 26, (17), 2966-2973.

114. Cho, I.; Park, S. K.; Kang, B.; Chung, J. W.; Kim, J. H.; Yoon, W. S.; Cho, K.; Park, S. Y., Dicyanovinyl-substituted indolo[3,2-*b*]indole derivatives: low-band-gap π-conjugated molecules for a single-component ambipolar organic field-effect transistor. *Journal of Materials Chemistry C* **2016,** 4, (40), 9460-9468.

115. Spanggaard, H.; Krebs, F. C., A brief history of the development of organic and polymeric photovoltaics. *Solar Energy Materials and Solar Cells* **2004,** 83, (2), 125-146.

116. Huynh, W. U.; Dittmer, J. J.; Alivisatos, A. P., Hybrid Nanorod-Polymer Solar Cells. *Science* **2002,** 295, (5564), 2425.

117. Sun, B.; Marx, E.; Greenham, N. C., Photovoltaic Devices Using Blends of Branched CdSe Nanoparticles and Conjugated Polymers. *Nano Letters* **2003,** 3, (7), 961-963.

118. Skaff, H.; Sill, K.; Emrick, T., Quantum Dots Tailored with Poly(para-phenylene vinylene). *Journal of the American Chemical Society* **2004,** 126, (36), 11322-11325.

119. Yuan, J.; Gallagher, A.; Liu, Z.; Sun, Y.; Ma, W., High-efficiency polymer-PbS hybrid solar cells via molecular engineering. *Journal of Materials Chemistry A* **2015,** 3, (6), 2572-2579.

120. Sun, B.; Snaith, H. J.; Dhoot, A. S.; Westenhoff, S.; Greenham, N. C., Vertically segregated hybrid blends for photovoltaic devices with improved efficiency. *Journal of Applied Physics* **2004,** 97, (1), 014914.

121. Qian, L.; Yang, J.; Zhou, R.; Tang, A.; Zheng, Y.; Tseng, T.-K.; Bera, D.; Xue, J.; Holloway, P. H., Hybrid polymer-CdSe solar cells with a ZnO nanoparticle buffer layer for improved efficiency and lifetime. *Journal of Materials Chemistry* **2011,** 21, (11), 3814-3817.

122. Ren, S.; Chang, L.-Y.; Lim, S.-K.; Zhao, J.; Smith, M.; Zhao, N.; Bulović, V.; Bawendi, M.; Gradečak, S., Inorganic–Organic Hybrid Solar Cell: Bridging Quantum Dots to Conjugated Polymer Nanowires. *Nano Letters* **2011,** 11, (9), 3998-4002.

123. Liu, J.; Tanaka, T.; Sivula, K.; Alivisatos, A. P.; Fréchet, J. M. J., Employing End-Functional Polythiophene To Control the Morphology of Nanocrystal−Polymer Composites in Hybrid Solar Cells. *Journal of the American Chemical Society* **2004,** 126, (21), 6550-6551.

124. Palaniappan, K.; Murphy, J. W.; Khanam, N.; Horvath, J.; Alshareef, H.; Quevedo-Lopez, M.; Biewer, M. C.; Park, S. Y.; Kim, M. J.; Gnade, B. E.; Stefan, M. C., Poly(3-hexylthiophene)−CdSe Quantum Dot Bulk Heterojunction Solar Cells: Influence of the Functional End-Group of the Polymer. *Macromolecules* **2009,** 42, (12), 3845-3848.

125. Lokteva, I.; Radychev, N.; Witt, F.; Borchert, H.; Parisi, J.; Kolny-Olesiak, J., Surface Treatment of CdSe Nanoparticles for Application in Hybrid Solar Cells: The Effect of Multiple Ligand Exchange with Pyridine. *The Journal of Physical Chemistry C* **2010,** 114, (29), 12784-12791.

126. Seo, J.; Cho, M. J.; Lee, D.; Cartwright, A. N.; Prasad, P. N., Efficient Heterojunction Photovoltaic Cell Utilizing Nanocomposites of Lead Sulfide Nanocrystals and a Low-Bandgap Polymer. *Advanced Materials* **2011,** 23, (34), 3984-3988.

127. Zhou, R.; Stalder, R.; Xie, D.; Cao, W.; Zheng, Y.; Yang, Y.; Plaisant, M.; Holloway, P. H.; Schanze, K. S.; Reynolds, J. R.; Xue, J., Enhancing the Efficiency of Solution-Processed Polymer:Colloidal Nanocrystal Hybrid Photovoltaic Cells Using Ethanedithiol Treatment. *ACS Nano* **2013,** 7, (6), 4846-4854.

128. Fu, W.; Shi, Y.; Qiu, W.; Wang, L.; Nan, Y.; Shi, M.; Li, H.; Chen, H., High efficiency hybrid solar cells using post-deposition ligand exchange by monothiols. *Physical Chemistry Chemical Physics* **2012,** 14, (35), 12094-12098.

CHAPTER 2

THE EFFECT OF SINGLE ATOM REPLACEMENT ON ORGANIC FIELD TRANSISTORS: THIENO[3,2-*b*]PYRROLE VS FURO[3,2-*b*]PYRROLE

Authors – Chandima Bulumulla,[†] Ruwan Gunawardhana,[†] Cody R. Mills,[†] Ruvanthi N. Kularatne,[†] Michael C. Biewer,[†] and Mihaela C. Stefan[†*]

[†]Department of Chemistry and Biochemistry, BE26

The University of Texas at Dallas

800 West Campbell Road

Richardson, Texas 75080, USA

[*]Department of Bioengineering, BSB11

The University of Texas at Dallas

800 West Campbell Road

Richardson, Texas 75080, USA

2.1 Abstract

Despite polypyrrole having higher conductivities compared to polythiophene, pyrrole based materials are found less in organic electronics due to instability in the air. To realize stable organic semiconductors comprising of pyrrolic precursors, fused-ring systems can be employed as a unique solution. In this report, we discuss and compare the organic field effect transistor performance of the smallest *S,N*-heteroacene and *O,N*-heteroacene; thieno[3,2-*b*]pyrrole and furo[3,2-*b*]pyrrole, respectively in donor-acceptor-donor type small molecules. Since both building blocks are highly electron rich, a strong central electron withdrawing unit (thiophene flanked 5,6-difluorobenzo[*c*][1,2,5]thiadiazole) is employed. The Small molecule containing thieno[3,2-*b*]pyrrole exhibit moderate hole mobility ($\sim 10^3$ cm^2 /V s) irrespective of the annealing temperature. On the contrary, small molecule bearing furo[3,2-*b*]pyrrole is completely inactive in organic field effect transistors. The drastic difference in OFET performance created by the single heteroatom replacement is due to the molecular orientation of the two small molecules which was confirmed by grazing incidence X-ray analysis and atomic force microscopy analysis.

2.2 Introduction

Over the last few years, a tremendous amount of research has been carried out in the field of organic thin film transistors achieving high charge carrier mobilities up to 10 cm^2 /V s.[1-3] However, to realize practical OFET applications, high charge carrier mobility is not the only figure of merit that needs consideration. It is equally important to acquire low threshold voltages, low subthreshold swings and high current on-to-off ratios for fast switching processes that could trigger at low voltages.[4, 5] In order to fabricate reliable and reproducible OFETs, structural components

and self-assembling or molecular ordering, should be precise.[6, 7] Although polymeric materials exhibit promising results, they suffer from irreproducible molecular weights and uncontrollable molecular weight distributions to cause more batch-to-batch variations.[8-11] Therefore, much attention has received toward organic semiconducting small molecules or oligomers with precise molecular weights.[12-15] Out of many classes of semiconducting small molecules, linear acenes have been of great interest due to their high charge carrier mobilities and proper control over fabrication.[16-21]

Anthracene, the smallest building block in the class of acenes have utilized in single crystal thin film transistors to provide hole mobility of 0.02 cm^2 /V s.[22] By extending the conjugation using one more benzene ring; mobility was increased to 0.4 - 2.4 cm^2 /V s for tetracene.[23] Upon increasing conjugation length further with pentacene, a record high mobility of 5-40 cm^2 /V s was achieved in single crystal OFETs.[24, 25] It has been demonstrated and postulated even higher performances could be attained for unsubstituted higher acenes, but instability at ambient conditions and synthetic challenges have prevented these materials from testing.[26-29] Even though from a performance perspective unsubstituted acenes seem very promising, from an economical perspective these materials do not add significant advantages compared to conventional silicon technologies as they require high temperature and vacuum processing conditions for the fabrication. Therefore, in recent years the field has shifted to search for non-conventional materials that could mimic properties of acenes with the added advantage of solution processability to bring down the costs of manufacture. Oligothioacenes have synthesized to lower the aromaticity but charge carrier mobilities are somewhat lower compared to fused benzene rings.[30-33] Another interesting class of substituted acenes are heteroacenes.

Heteroacenes are acenes prepared by introducing heteroatoms into the acene skeleton such as chalcogenides and nitrogen. The replacement of heteroatom influences both the electronic structure and crystal packing which eventually reflects on the charge transport.[34] Unfortunately, the choice of heteroatom and impact on the charge transport has been found to be not very straightforward. In the case of chalcogen based acenes, for dinaphthochalcogen-phenochalcogenophenes,[33] circulenes,[35, 36] and diphenylbenzodichalcogenophenes,[37] selenium was found to perform similar or better than sulfur, but the trend discontinues with tellurium. However, due to the environmental toxicity caused by selenium and tellurium, we are not particularly interested in materials with either selenium or tellurium. Since nitrogen has a comparable or smaller atomic radii compared to carbon and provides a synthetic site amenable for N-alkylation reactions to control the solubility, solution processible acene derivatives could be made easily.[38-41] To tune frontier energy levels and improve intramolecular charge transfer, thiophene-pyrrole based *S,N*-heteroacenes were introduced as non-conventional building blocks.[42-44] Before synthesizing and testing a plethora of small molecular semiconductors containing higher *S,N*-heteroacenes for OFET applications, it is fundamentally important to understand the electronic characteristics by first analyzing the smallest entity of the class.

The smallest *S,N*-heteroacene, thieno[3,2-*b*]pyrrole is an interesting monomer due to the high electron density, asymmetry and easily modifiable NH group. The use of the monomer for OFETs was first reported by Driver and co-workers where authors synthesized a range of bispyrrolothiophenes with different N-alkyl groups, *N*-aryl groups, and central groups.[45] This report demonstrated the potential of the monomer when it is placed in the terminal position with central electron deficient groups to realize donor-acceptor-donor type small molecules. As a result,

we decided to explore on this building block by further reducing the electron density in the central accepting moiety by introducing fluorine atoms and extending the conjugation by having two flanking thiophene units. To expand the scope, we also selected the smallest *O,N*-heteroacene, furo[3,2-*b*]pyrrole to study the effect of the building block toward OFET properties. To the best of our knowledge, this is the first report of comparing a *S,N*-heteroacene vs *O,N*-heteroacene, and utilization of furo[3,2-*b*]pyrrole for OFETs. The chemical structures of the proposed small molecular semiconductors are shown in Figure 2.1.
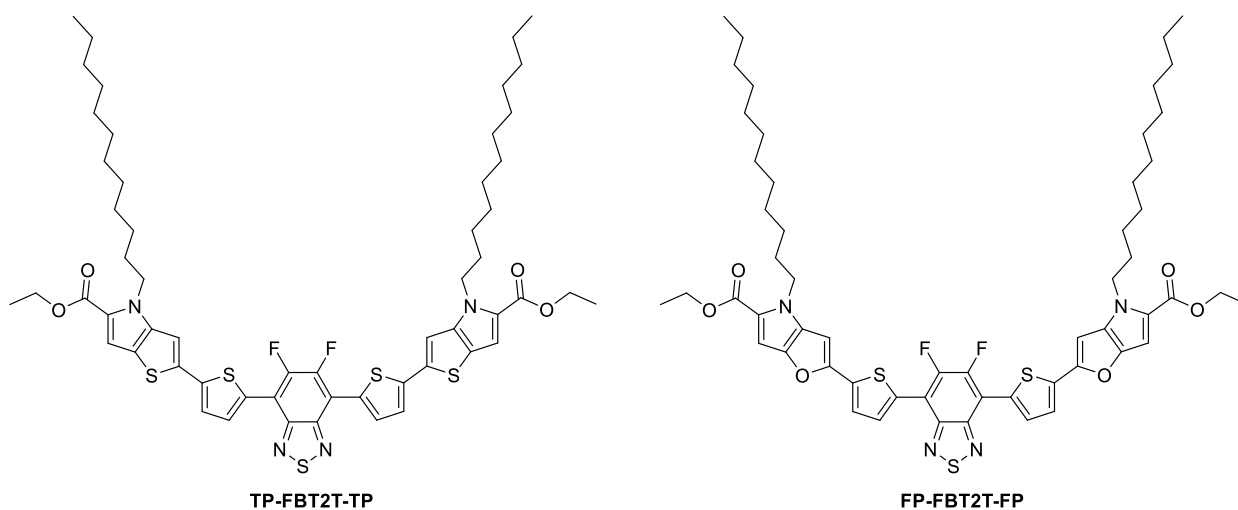
Figure 2.1 Chemical structures of TP-FBT2T-TP and FP-FBT2T-FP

2.3 Experimental

2.3.1 Materials and Methods

All commercial chemicals were purchased from Aldrich and Fisher Scientific and used without further purification unless mentioned otherwise. All reactions were performed in oven-dried

49

glassware under a nitrogen atmosphere. Tetrahydrofuran (THF) and toluene were distilled over sodium /benzophenone ketyl under nitrogen prior to use.

NMR measurements: ^{1}H and ^{13}C NMR spectra were collected on a 500 MHz Bruker AVANCE III^{TM} spectrometer using CDCl$_3$ as the solvent. Multiplicities are given as- s (singlet), d (doublet), t (triplet), q (quartet), m (multiplet).

Mass characterization: Matrix-assisted laser desorption ionization time of flight (MALDI-TOF) spectra were recorded on a Shimadzu Biotech Axima Confidence in reflectron_HiRes mode with 2,2′:5′,2′′-terthiophene as the matrix.

Optical measurements: The UV-vis absorption was measured with an Agilent 8453 UV-vis spectrometer. For solution spectra, small molecules were dissolved in chloroform, and thin films were measured by drop casting chloroform solution on to microscopic glass slides

Electrochemical measurements: Cyclic voltammetry experiments were recorded on a BAS CV-50W voltammetry analyzer. The three-electrode system; a platinum inert working electrode, platinum wire auxiliary electrode, and Ag/Ag$^+$ reference electrode was used to measure the currents. An electrolytic solution composed of 0.1 M tetrabutylammonium hexafluorophosphate in anhydrous acetonitrile was used to conduct the experiments after degassing for 15 mins under argon.

Surface Morphology characterization: Tapping mode atomic force microscopy (TMAFM) was recorded in the channel region using a Nanoscope IV Multimode Veeco equipped with a vertical engage scanner. The TMAFM images were acquired using Si cantilever with the resonance frequency of 320 kHz and spring constant of 42 N/m. AFM images with 2×2 μm scan size were recorded with a frequency of 1 Hz.

Grazing Incidence X-ray measurements: Out-of-plane measurements were carried out on a Rigaku SmartLab XRD instrument. Thin films of small molecules were deposited on OTS treated SiO_2 substrates by using the same conditions used for the OFET devices. The sample was irradiated with Cu-Kα (λ=1.54 Å) at an incident angle of 0.5° and data were recorded at 0.05° intervals from 1° to 30°.

OFET device fabrication and characterization: OFETs with common bottom-gate/bottom-contact configuration were employed to perform electrical characterizations. A highly doped n-type silicon wafer was used as the substrate with 200 nm thick thermally grown SiO_2 as the dielectric layer. First, Si/SiO_2 surface was covered with 5 nm chromium and 100 nm gold in-situ by Temescal E-beam evaporator. Cr/Au source and drain contacts were patterned using standard photolithographic techniques having different channel lengths and widths. After applying the photoresist on the electrodes, back of the silicon wafer was etched with 7:1 BOE solution from JT Baker and the gate electrode was created by deposition of 100 nm gold by an E-beam evaporator. OFET devices were sonicated for 5 mins each time using acetone, toluene, and 2-propanol. The capacitance per unit area was measured to be 17 nF cm^{-2}. The substrates were then cleaned by immersing in piranha solution (7:3 mixture of conc. sulfuric acid and 30% hydrogen peroxide) for 10 mins followed by rinsing with DI water and dried with nitrogen. An additional UV-ozone treatment was performed for 10 mins followed by washing again with DI water and dried with nitrogen. A Self-assembled monolayer (SAM) of octadecylsilane (OTS) was prepared by the base (NH_4OH) vapor-catalyzed hydrolysis of octadecyltrimethoxysilane (OTMS). Briefly, 3mM OTMS solution in trichloroethylene was added to cover the entire surface of Si/SiO_2 surface and allowed to partially assemble for 10 s and spun at 3000 rpm for 10 s. The base-catalyzed hydrolysis

was performed by placing the substrates containing thin films inside a closed container with 3 mL

of NH_4OH (28-30% NH_3 assay) in a vial for 10 h at room temperature. Substrates were rinsed with

DI water and sonicated for 10 mins in toluene and dried by nitrogen. Small molecules TP-FBT2T-

TP and FP-FBT2T-FP were dissolved in chloroform at a concentration of 5 mg/mL and 10 mg/mL,

respectively. A thin layer was deposited by spin coating at 750 rpm for 30s after covering the

device surface for 30 s and 60 s with 70 μL of TP-FBT2T-TP and FP-FBT2T-FP, respectively.

After annealing at different temperatures for 5 mins inside a nitrogen-filled glovebox electrical

measurements were performed in air at room temperature using Cascade Microtech Model Summit

Microchamber with a Keithley 4200-SCS system.

2.3.2 Synthesis of Materials

Ethyl-2-azido-3-(thiophen-2-yl)acrylate

To a 250 mL three-neck round bottomed flask was added NaOEt (3.64g, 53.50 mmol) with 48 mL

of dry ethanol under nitrogen and cooled to 0 °C. In a separate container 2-thiophenecarbaldehyde

(3.00 g, 26.75 mmol), ethyl azidoacetate (6.90 g, 53.50 mmol), and ethyl trifluoroacetate (7.52 g,

53.30 mmol) were dissolved in 10 mL of dry ethanol. The mixture was added to the sodium

ethoxide solution and reacted for 6 h at 0 °C. The reaction mixture was added to a sat. NH_4Cl

solution and extracted with Et_2O (3 × 50 mL). The combined organic extracts were washed with

deionized water, brine, and concentrated under vacuum to give a crude residue. Pure compound

was obtained as a yellow solid after purifying on column chromatography by using hexane: ethyl

acetate (9:1 v/v) as the eluent. (5.50 g, Yield = 92.3 %). ^{1}H NMR ($CDCl_3$, 500 MHz): δ_H 1.39 (t,

7.0 Hz, 3H), 4.36 (q, 7.0 Hz, 2H), 7.07 (dd, 3.5 Hz and 3.0 Hz, 1H), 7.17 (s, 1H), 7.32 (d, 3.5 Hz,

1H), 7.50 (d, 5Hz, 1H) (Figure 2.2), ^{13}C NMR (CDCl$_3$, 125 MHz); δ_C 14.39, 62.28, 119.41, 122.86, 127.19, 130.54, 132. 11, 136.77, 163.34 (Figure 2.3)
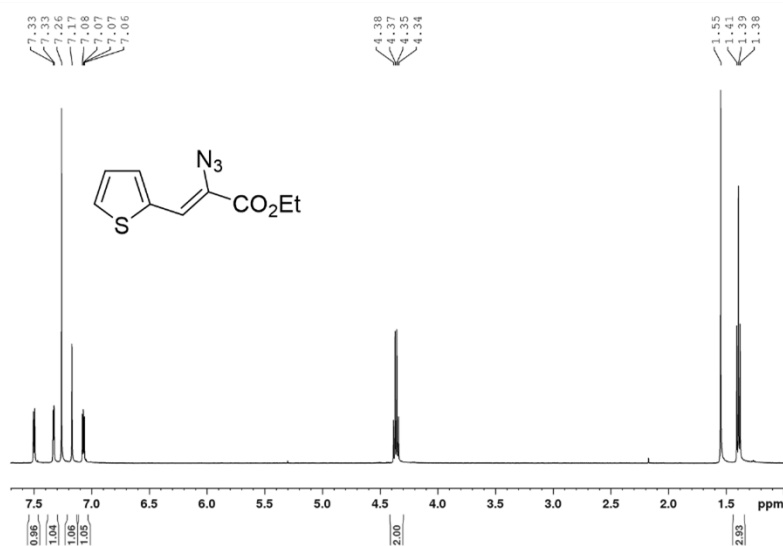
Figure 2.2 ^{1}H NMR spectrum of ethyl-2-azido-3-(thiophen-2-yl)acrylate
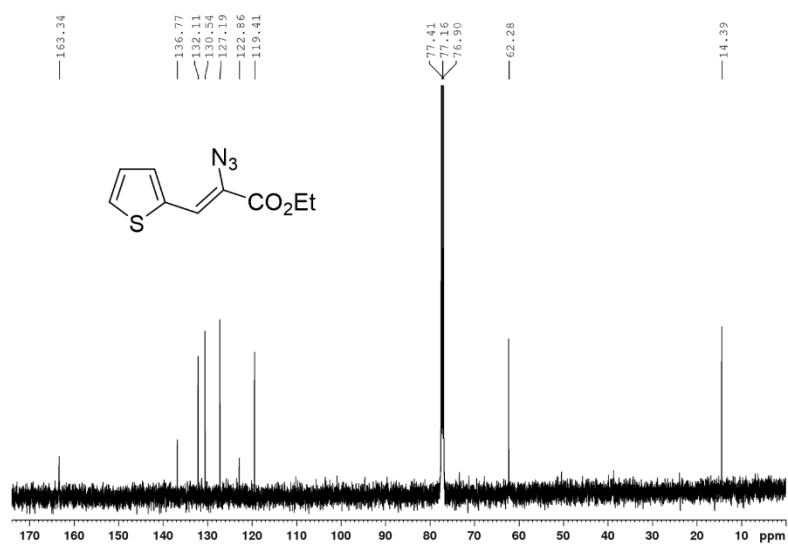
Figure 2.3 ^{13}C NMR spectrum of ethyl-2-azido-3-(thiophen-2-yl)acrylate

Ethyl-2-azido-3-(furan-2-yl)acrylate

Sodium ethoxide (3.64g, 53.50 mmol) and 48 mL of dry ethanol were added to a 250 mL three-neck round bottom flask under nitrogen and cooled to 0 °C. In a brown vial, furfural (3.00 g, 31.25 mmol), ethyl azidoacetate (7.69 g, 62.50 mmol), and ethyl trifluoroacetate (8.82 g, 62.50 mmol) were dissolved with 10 mL of dry ethanol. The mixture was slowly added to the sodium ethoxide solution and stirred for 6 h at 0 °C. The solid obtained after quenching the reaction with saturated NH$_4$Cl was filtered and dried under air to obtain the pure compound. (5.89 g, Yield = 91.2 %). ^{1}H NMR (CDCl$_3$, 500 MHz): δ_H 1.37 (t, 7.5 Hz, 3H), 4.35 (q, 7.0 Hz, 2H), 6.52 (dd, 1.5 Hz and 2.5 Hz, 1H), 6.87 (s, 1H), 7.10 (d, 3.5 Hz, 1H), 7.49 (d, 3.5Hz, 1H) (Figure 2.4), ^{13}C NMR (CDCl$_3$, 125 MHz); δ_C 14.35, 62.32, 112.73, 113.58, 115.32, 144.01, 149.69, 163.32 (Figure 2.5)
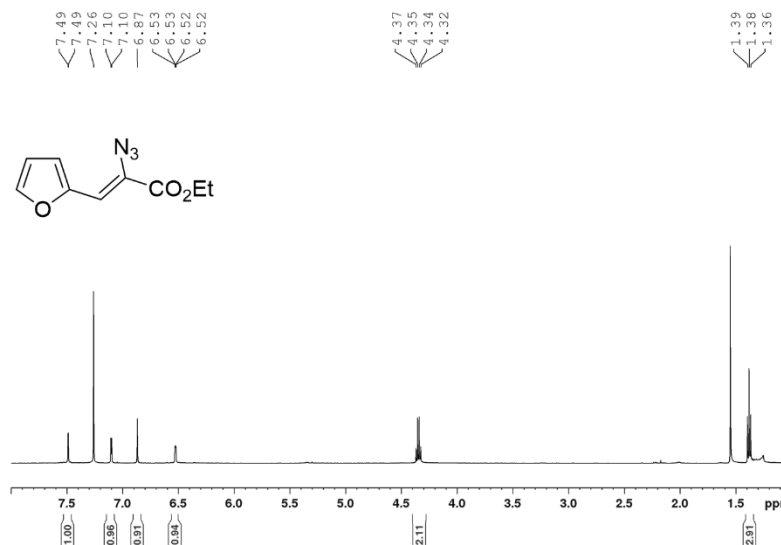
Figure 2.4 ^{1}H NMR spectrum of ethyl-2-azido-3-(furan-2-yl)acrylate
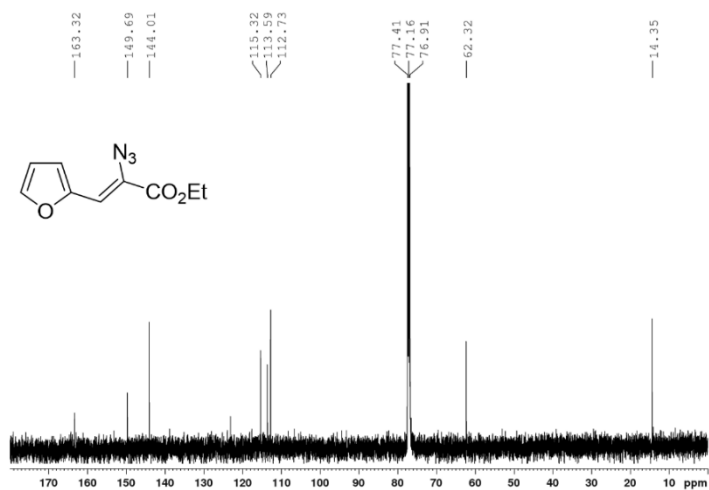
Figure 2.5 ^{13}C NMR spectrum of ethyl-2-azido-3-(furan-2-yl)acrylate

Ethyl 4H-thieno[3,2-b]pyrrole-5-carboxylate

To a 100 mL of refluxing toluene, ethyl-2-azido-3-(thiophen-2-yl)acrylate (3.60 g, 16.1 mmol) was added in portions and refluxed for 4 h. The resulting solution was cooled to room temperature and the solvent was removed under reduced pressure to obtain the pure compound. (2.67 g, Yield = 85.2 %). ^{1}H NMR (CDCl$_3$, 500 MHz): δ_H 1.39 (t, 7.0 Hz, 3H), 4.36 (q, 7.0 Hz, 2H), 6.95 (d, 5.0 Hz, 1H), 7.14 (s, 1H), 7.33 (d, 5 Hz, 1H), 9.11 (s, 1H) (Figure 2.6), ^{13}C NMR (CDCl$_3$, 125 MHz); δ_C 14.60, 60.81, 107.68, 111.19, 124.96, 127.24, 129.57, 141.33, 161.75 (Figure 2.7)
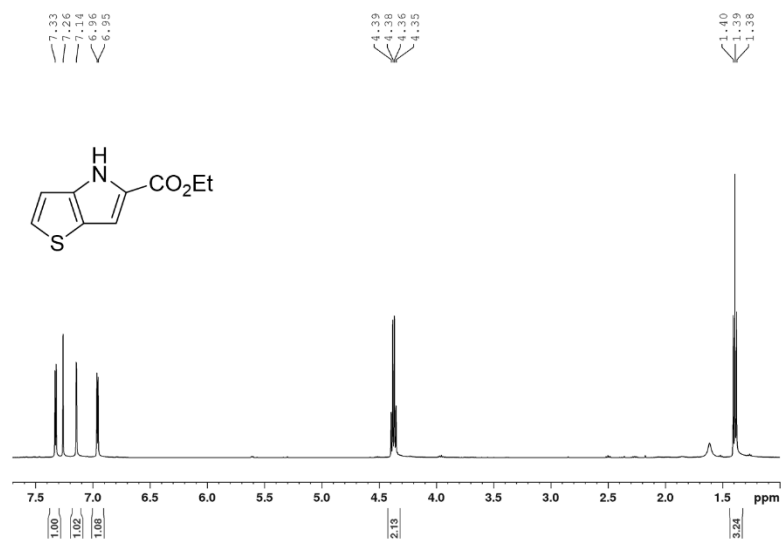
Figure 2.6 ^{1}H NMR spectrum of ethyl 4*H*-thieno[3,2-*b*]pyrrole-5-carboxylate
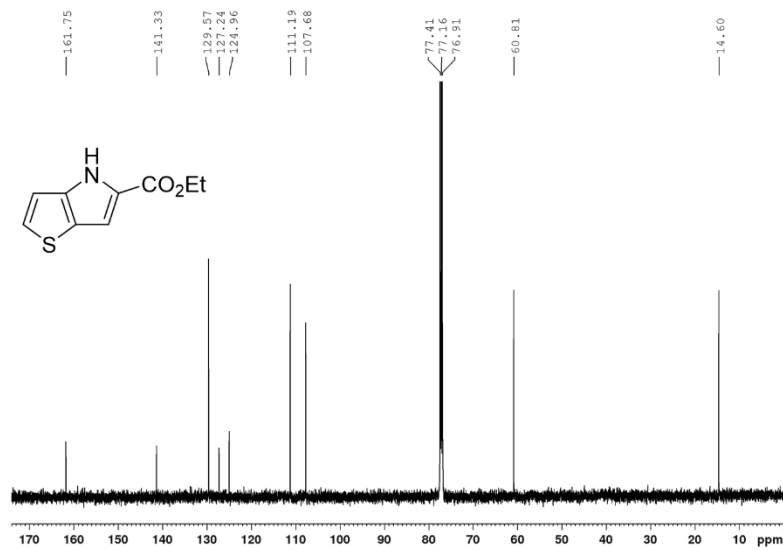
Figure 2.7 ^{13}C NMR spectrum of ethyl 4*H*-thieno[3,2-*b*]pyrrole-5-carboxylate

Ethyl 4H-furo[3,2-b]pyrrole-5-carboxylate

To 100 mL of refluxing toluene, ethyl-2-azido-3-(furan-2-yl)acrylate (3.32 g, 16.1 mmol) was added and refluxed for 4 h. The resulting solution was cooled and toluene was removed under reduced pressure to obtain the pure compound. (2.76 g, Yield = 96.0 %). ^{1}H NMR (CDCl$_3$, 500 MHz): δ_H 1.37 (t, 7.0 Hz, 3H), 4.35 (q, 7.0 Hz, 2H), 6.45 (d, 1.5 Hz, 1H), 6.80 (s, 1H), 7.51 (d, 2.0 Hz, 1H), 8.86 (s, 1H) (Figure 2.8), ^{13}C NMR (CDCl$_3$, 125 MHz); δ_C 14.61, 60.63, 96.97, 99.04, 124.39, 128.78, 148.16, 148.72, 162.28 (Figure 2.9)
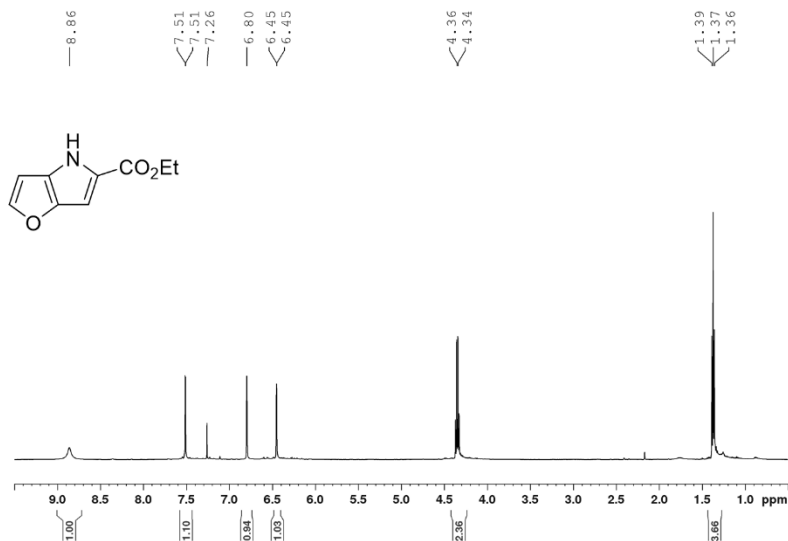
Figure 2.8 ^{1}H NMR spectrum of ethyl 4*H*-furo[3,2-*b*]pyrrole-5-carboxylate
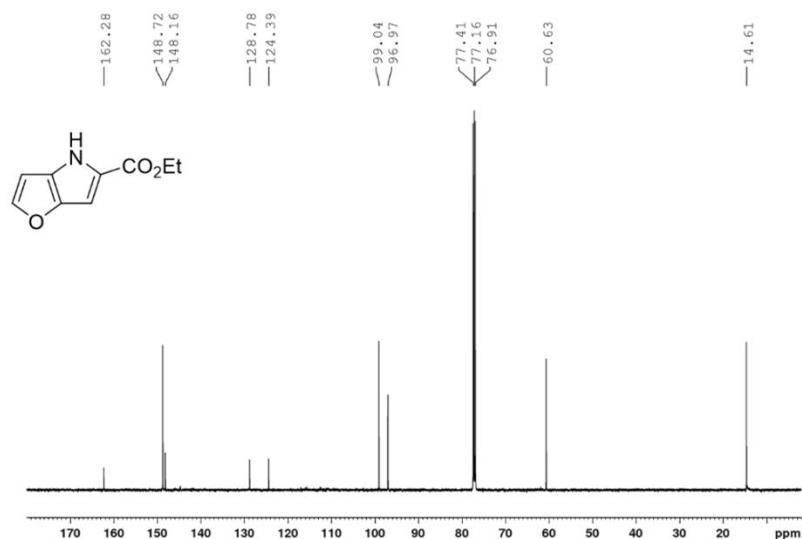
Figure 2.9 ^{13}C NMR spectrum of ethyl 4*H*-furo[3,2-*b*]pyrrole-5-carboxylate

Ethyl 4-dodecyl-4H-thieno[3,2-b]pyrrole-5-carboxylate

To a 100 mL three neck round bottom flask, ethyl 4*H*-thieno[3,2-*b*]pyrrole-5-carboxylate (2.00 g, 10.3 mmol), anhydrous K_2CO_3 (2.83 g, 21.5 mmol), 18-crown-6 ether (catalytic amount) and dry DMF (36.0 mL) were added under nitrogen. Solution was stirred at 100 °C for 2 h before adding 1-bromododecane (5.28 g, 21.5 mmol). Resulting solution was refluxed for 48h and cooled to room temperature. DI water (50 mL) was added and organic layer was extracted with ethyl acetate (3 × 30 mL). The organic layer was washed with brine, dried over anhydrous $MgSO_4$ and concentrated. The crude was purified by column chromatography using hexane: ethyl acetate (99:1 v/v) as the eluent to obtain a pale yellow color oil. (2.68 g, Yield = 71.8 %) ^{1}H NMR (CDCl$_3$, 500 MHz): δ$_H$ 0.88 (t, 6.5 Hz, 3H), 1.24–1.30 (m, 18 H), 1.38 (t, 7.0 Hz, 3H) 1.80 (t, 7.0 Hz, 2H) 4.33 (q, 7.0 Hz, 2H), 4.47 (t, 7.5 Hz, 2H), 6.92 (d, 5.0 Hz, 1H),7.19 (s, 1H), 7.30 (d, 5.5 Hz, 1H) (Figure 2.10), ^{13}C NMR (CDCl$_3$, 125 MHz); δ$_C$ 14.25, 14.56, 22.83, 27.02, 29.47, 29.67,

29.70, 29.75, 29.77, 31.28, 31.73, 32.05, 47.74, 60.15, 109.31, 110.48, 121.90, 126.32, 128.99, 145. 24, 161.65 (Figure 2.11)
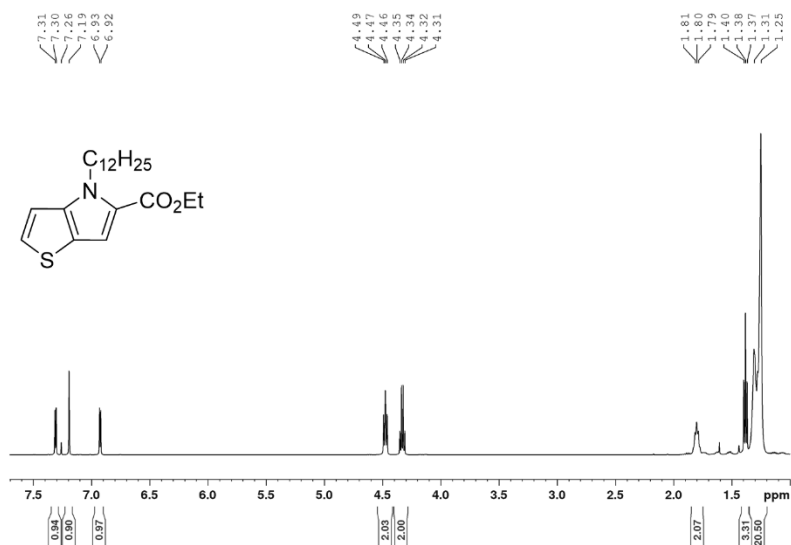
Figure 2.10 ^{1}H NMR spectrum of ethyl 4-dodecyl-4*H*-thieno[3,2-*b*]pyrrole-5-carboxylate
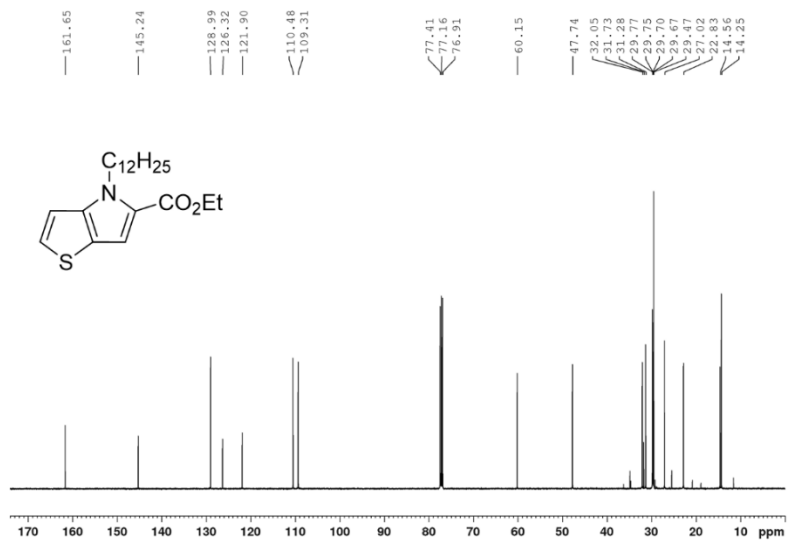
Figure 2.11 ^{13}C NMR spectrum of ethyl 4-dodecyl-4*H*-thieno[3,2-*b*]pyrrole-5-carboxylate

Ethyl 4-dodecyl-4H-furo[3,2-b]pyrrole-5-carboxylate

To a 100 mL three neck round bottom flask, ethyl 4*H*-furo[3,2-*b*]pyrrole-5-carboxylate (0.50 g, 2.79 mmol), anhydrous K_2CO_3 (1.54 g, 5.58 mmol), 18-crown-6 ether (catalytic amount) and dry DMF (20.0 mL) were added under nitrogen. Solution was stirred at 80 °C for 3 h before adding 1-bromododecane (2.08 g, 4.18 mmol) dropwise. Resulting solution was refluxed for 48 h and cooled to room temperature. DI water (50 mL) was added and neutralized using 3M HCl. The organic layer was extracted with ethyl acetate (3×20 mL). The organic layer was washed with brine, dried over anhydrous $MgSO_4$ and concentrated. The crude was purified by column chromatography using gradient elution starting from hexane: ethyl acetate: triethylamine (98:1:1 v/v) to hexane: ethyl acetate: triethylamine (94:5:1 v/v) as the eluent to obtain a pale yellow color oil. (0.97 g, Yield = 50.6 %) ^{1}H NMR (CDCl$_3$, 500 MHz): δ_H 0.88 (t, 6.5 Hz, 3H), 1.24–1.29 (m, 18 H), 1.36 (t, 7.0 Hz, 3H) 1.79 (t, 7.0 Hz, 2H) 4.29 (q, 7.0 Hz, 2H), 4.38 (t, 7.0 Hz, 2H), 6.43 (dd, 0.5 Hz and 2.0 Hz, 1H), 6.80 (d, 0.5 Hz, 1H), 7.49(d, 2.0 Hz, 1H) (Figure 2.12),^{13}C NMR (CDCl$_3$, 125 MHz); δ_C 14.26, 14.61, 22.83, 26.97, 29.45, 29.48, 29.68, 29.71, 29.76, 29.78, 31.15, 32.06, 47.81, 59.99, 98.35, 98.59, 123.47, 133.0, 145.82, 148.37, 162.14 (Figure 2.13)
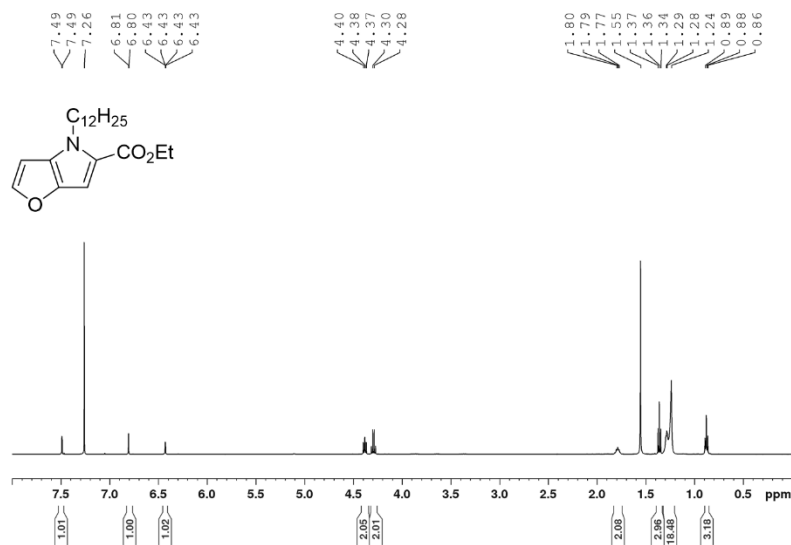
Figure 2.12 ^{1}H NMR spectrum of ethyl 4-dodecyl-4*H*-furo[3,2-*b*]pyrrole-5-carboxylate
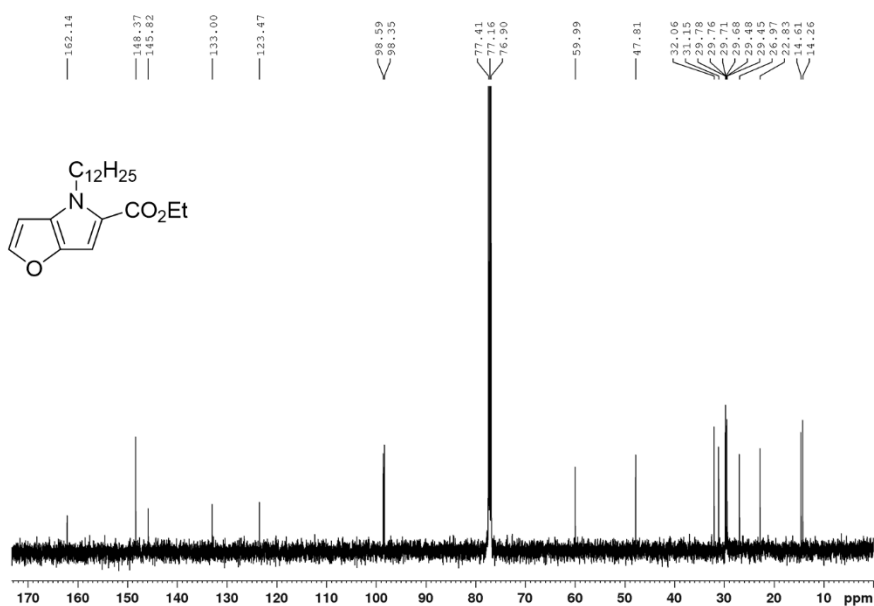
Figure 2.13 ^{13}C NMR spectrum of ethyl 4-dodecyl-4*H*-furo[3,2-*b*]pyrrole-5-carboxylate

61

Ethyl 4-dodecyl-2-(4,4,5,5-tetramethyl-1,3,2-dioxaborolan-2-yl)-4H-thieno[3,2-b]pyrrole-5-carboxylate

To a 50 mL single neck round bottom flask 4,4′-di-tert-butyl-2,2′-dipyridyl (dtbpy) (46 mg, 0.17 mmol), Ir[(μ_2-OMe)(COD)]$_2$ (57 mg, 0.086 mmol) and pinacolborane (0.3 mL) were added under nitrogen. Dry hexane (5.0 mL) and ethyl 4-dodecyl-4H-thieno[3,2-*b*]pyrrole-5-carboxylate (0.50 g, 1.72 mmol) were added to the flask and stirred for 48h at room temperature. Pure compound was obtained after performing a flash column using hexane: ethyl acetate (99:1 v/v) as the eluent. (0.83 g, Yield = 98.7 %) ^{1}H NMR (CDCl$_3$, 500 MHz): δ_H 0.87 (t, 10 Hz, 3H), 1.24–1.30 (m, 18 H), 1.36 (s, 12H), 1.38 (t, 7.0 Hz, 3H), 1.78 (t, 7.5 Hz, 2H), 4.31 (q, 5.0 Hz, 2H), 4.46 (t, 5.0 Hz, 2H), 7.17 (s, 1H), 7.45 (s, 1H) (Figure 2.14) ^{13}C NMR (CDCl$_3$, 125 MHz); δ_C 14.25, 14.52, 22.82, 24.91, 24.99, 27.03, 29.47, 29.49, 29.70, 29.74, 29.76, 31.34, 32.05, 47.76, 60.35, 75.16, 84.41, 108.99, 119.49, 127.98, 128.34, 146.44, 161.68 (Figure 2.15)
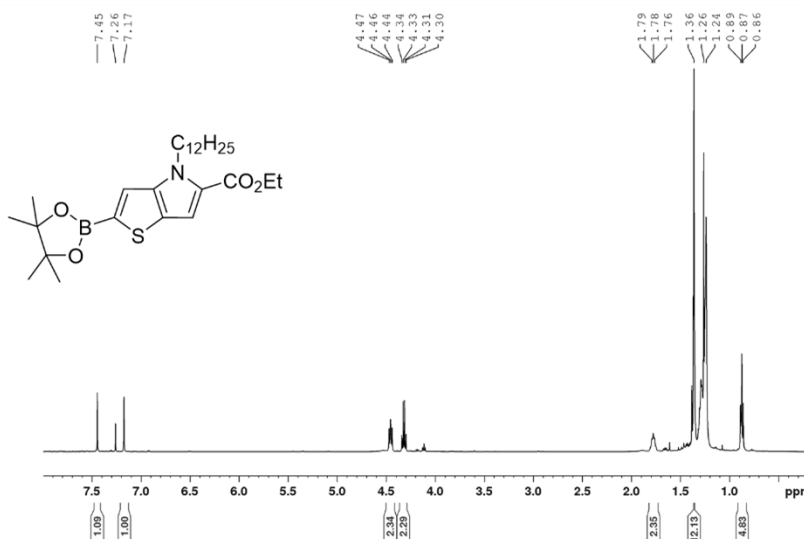
Figure 2.14 ^{1}H NMR spectrum of ethyl 4-dodecyl-2-(4,4,5,5-tetramethyl-1,3,2-dioxaborolan-2-yl)-4H-thieno[3,2-*b*]pyrrole-5-carboxylate
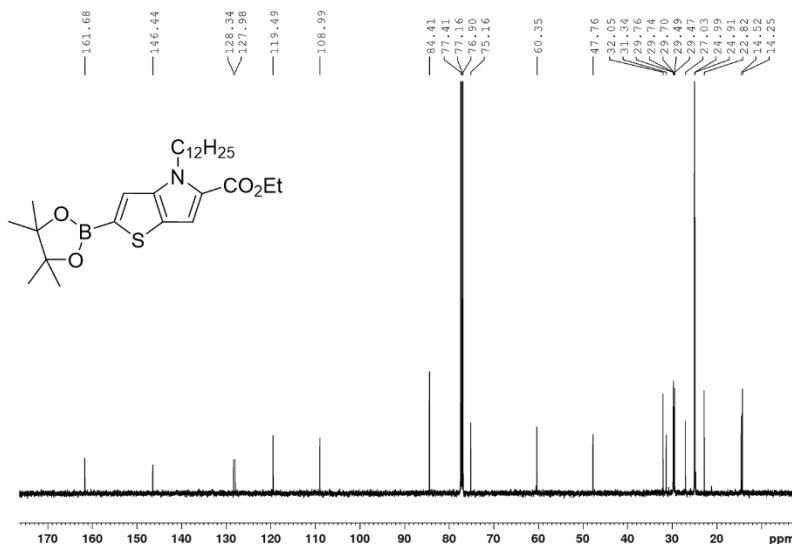
Figure 2.15 ^{13}C NMR spectrum of ethyl 4-dodecyl-2-(4,4,5,5-tetramethyl-1,3,2-dioxaborolan-2-yl)-4*H*-thieno[3,2-*b*]pyrrole-5-carboxylate

Ethyl 4-dodecyl-2-(4,4,5,5-tetramethyl-1,3,2-dioxaborolan-2-yl)-4H-furo[3,2-b]pyrrole-5-carboxylate

To a 50 mL single neck round bottom flask 4,4′-di-tert-butyl-2,2′-dipyridyl (dtbpy) (46 mg, 0.17 mmol), Ir[(μ_2-OMe)(COD)]$_2$ (57 mg, 0.086 mmol) and pinacolborane (0.3 mL) were added under nitrogen. Dry hexane (5.0 mL) and ethyl 4-dodecyl-4*H*-furo[3,2-*b*]pyrrole-5-carboxylate (0.50 g, 1.44 mmol) were added to the flask and stirred for 48h at room temperature. The crude was purified by passing through a celite pad with hexane: ethyl acetate (8:2 v/v) solvent system to afford the pure compound. (0.51 g, 75.0 %) ^{1}H NMR (CDCl$_3$, 500 MHz): δ_H 0.88 (t, 6.5 Hz, 3H), 1.23−1.30 (m, 18 H), 1.37 (b, 15H), 1.77 (t, 10 Hz, 2H), 4.30 (q, 10 Hz, 2H), 4.37 (t, 5.0 Hz, 2H), 6.74 (s, 1H), 7.04 (s, 1H) (Figure 2.16) ^{13}C NMR (CDCl$_3$, 125 MHz); δ_C 14.26, 14.58, 22.83, 24.92, 26.99, 29.46, 29.48, 29.67, 29.71, 29.76, 29.77, 31.09, 31.74, 32.06, 47.82, 60.22, 84.64, 97.99, 109.98, 126.36, 133.47, 150.09, 162.09 (Figure 2.17)

63
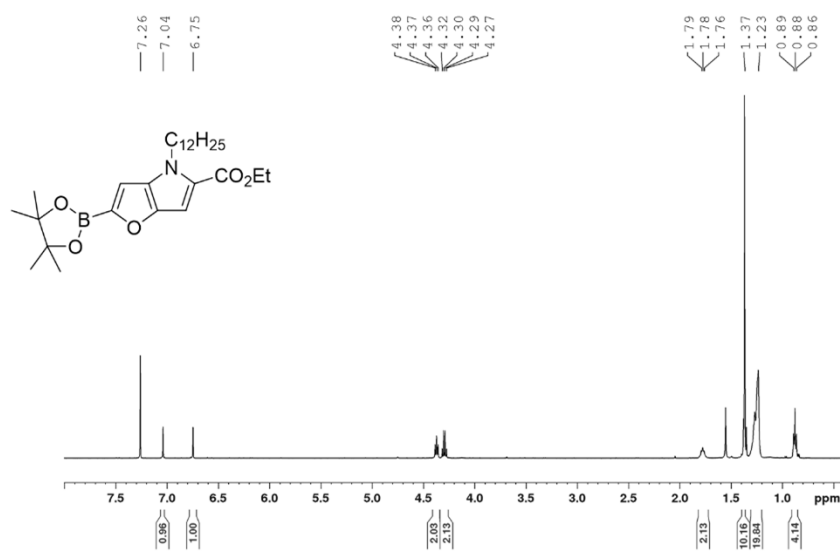
Figure 2.16 ^{1}H NMR spectrum of ethyl 4-dodecyl-2-(4,4,5,5-tetramethyl-1,3,2-dioxaborolan-2-yl)-4*H*-furo[3,2-*b*]pyrrole-5-carboxylate
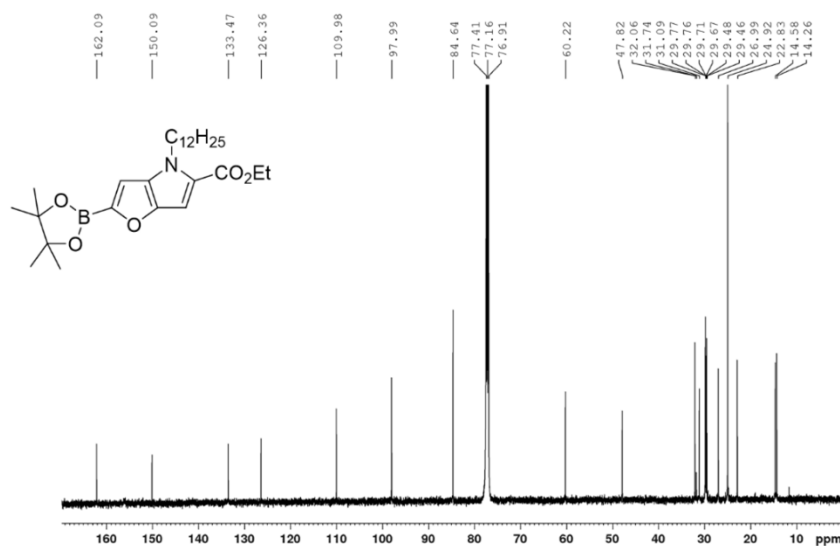
Figure 2.17 ^{13}C NMR spectrum of ethyl 4-dodecyl-2-(4,4,5,5-tetramethyl-1,3,2-dioxaborolan-2-yl)-4*H*-furo[3,2-*b*]pyrrole-5-carboxylate

TP-FBT2T-TP

To a 100 mL three neck round bottom flask, ethyl 4-dodecyl-2-(4,4,5,5-tetramethyl-1,3,2-dioxaborolan-2-yl)4*H*-thieno[3,2-*b*]pyrrole-5-carboxylate (0.83 g, 1.70 mmol), 4,7-bis(5-

bromothiophen-2-yl)-5,6-difluorobenzo[*c*][1,2,5]thiadiazole (0.33 g, 0.68 mmol) and Pd(PPh$_3$)$_4$ (196 mg, 0.17 mmol) were added under nitrogen with anhydrous THF (25.0 mL). To the solution was added 2M Na$_2$CO$_3$ (4.7 mL) and refluxed under nitrogen for 24 h. The flask was cooled to room temperature and crashed into cold methanol and resulted solid was filtered. Pure compound was obtained by column chromatography using hexane: methylene chloride 3:1 v/v as the eluent. (377.8 mg, Yield = 20.1%) ^{1}H NMR (CDCl$_3$, 500 MHz): 0.86 (t, 7.5 Hz, 3H), 1.25 (br, 18H), 1.38 (t, 5.0 Hz, 3H), 1.82 (t, 7.5 Hz, 2H), 4.31 (q, 5.0 Hz, 2H), 4.46 (t, 7.5 Hz, 2H), 7.12 (s, 1H), 7.13 (s, 1H), 7.29 (d, 5.0 Hz, 1H), 8.18 (d, 5.0 Hz, 1H) (Figure 2.18) ^{13}C NMR (CDCl$_3$, 125 MHz); δ_C 14.25, 14.57, 22.83, 27.06, 29.49, 29.53, 29.74, 29.76, 29.78, 29.81, 31.34, 32.06, 47.81, 60.31, 107.32, 109.45, 121.74, 124.25, 126.59, 130.93, 132.01, 139.59, 141.83, 145.06, 148.79, 161.29 (Figure 2.19)
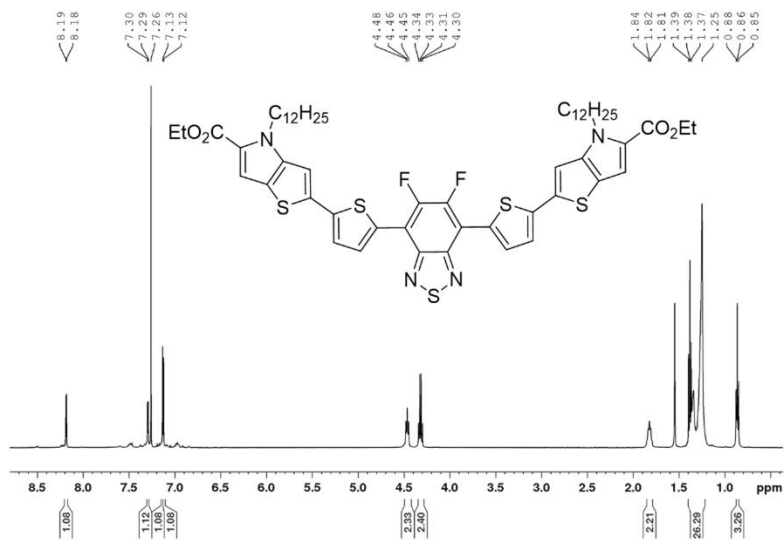
Figure 2.18 ^{1}H NMR spectrum of TP-FBT2T-TP
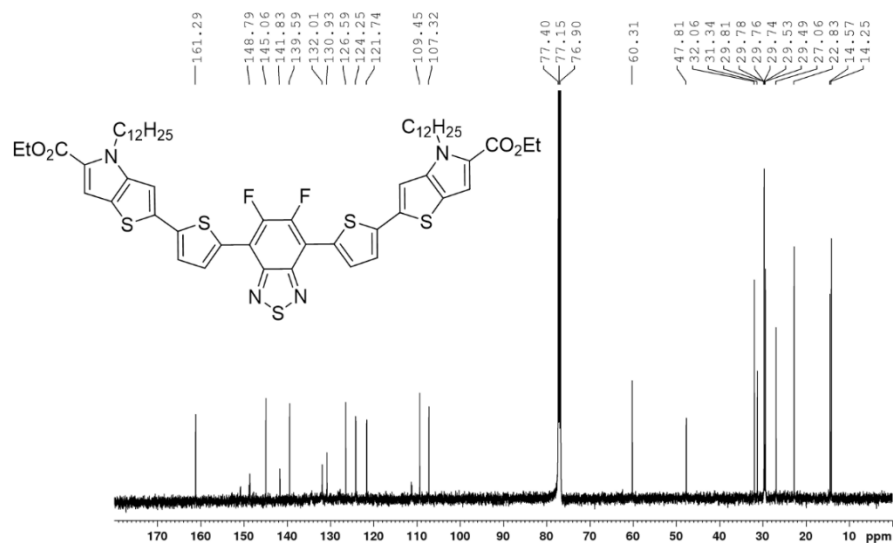
Figure 2.19 ^{13}C NMR spectrum of TP-FBT2T-TP
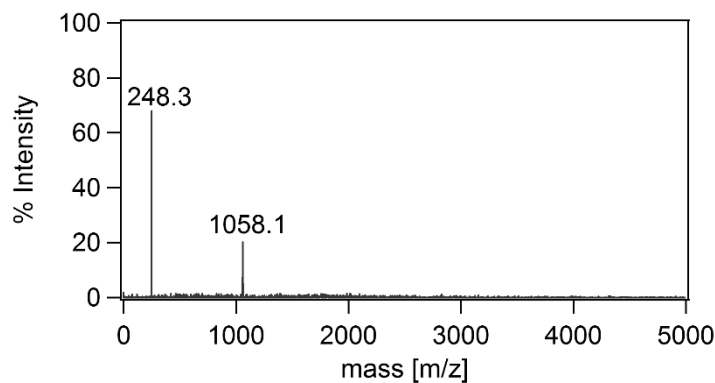
Figure 2.20 MALDI-TOF spectrum of TP-FBT2T-TP

FP-FBT2T-FP

Prepared using the same procedure as for diethyl 2,2′-((5,6-difluorobenzo[*c*][1,2,5]thiadiazole-4,7-diyl)bis(thiophene-5,2-diyl))bis(4-dodecyl-4*H*-thieno[3,2-*b*]pyrrole-5-carboxylate) with 1,4-dioxane as the solvent and K$_2$CO$_3$ as the base. Pure compound was obtained by column chromatography using hexane: methylene chloride 2:3 v/v with 1% triethylamine as the eluent.

(250.0 mg, Yield = 39.9 %) ^{1}H NMR (CDCl$_3$, 500 MHz): 0.87 (t, 7.5 Hz, 3H), 1.25 (br, 18H), 1.38 (t, 7.5 Hz, 3H), 1.83 (t, 7.5 Hz, 2H), 4.31 (q, 5.0 Hz, 2H), 4.40 (t, 7.5 Hz, 2H), 6.70 (s, 1H), 6.80 (s, 1H), 7.45 (d, 5.0 Hz, 1H), 8.26 (d, 5.0 Hz, 1H) (Figure 2.21) ^{13}C NMR (CDCl$_3$, 125 MHz); δ_C 14.27, 14.62, 22.84, 27.04, 29.50, 29.74, 29.76, 29.79, 29.81, 31.14, 32.07, 47.88, 58.07, 60.13, 94.23, 98.16, 111.46, 123.52, 124.11, 131.20, 131.85, 134.36, 137.11, 145.95, 148.69, 154.26, 161.80 (Figure 2.22)
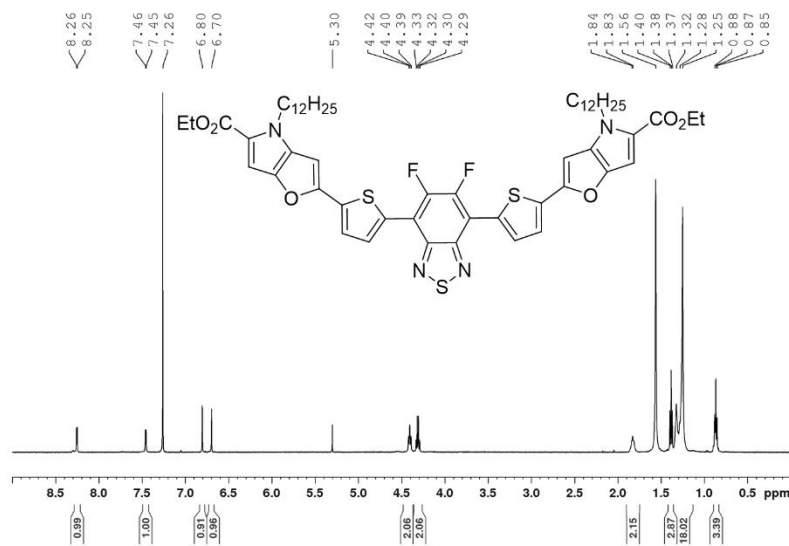
Figure 2.21 ^{1}H NMR spectrum of FP-FBT2T-FP
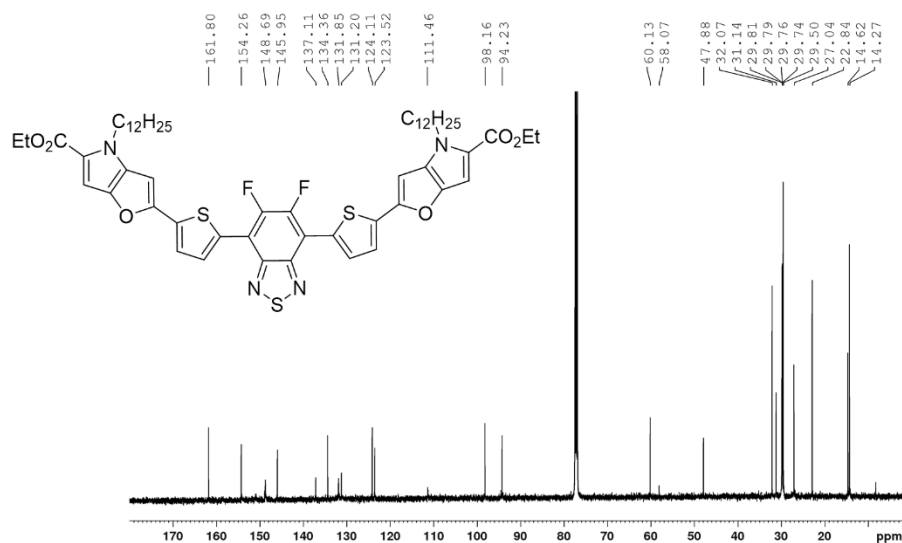
Figure 2.22 ^{13}C NMR spectrum of FP-FBT2T-FP
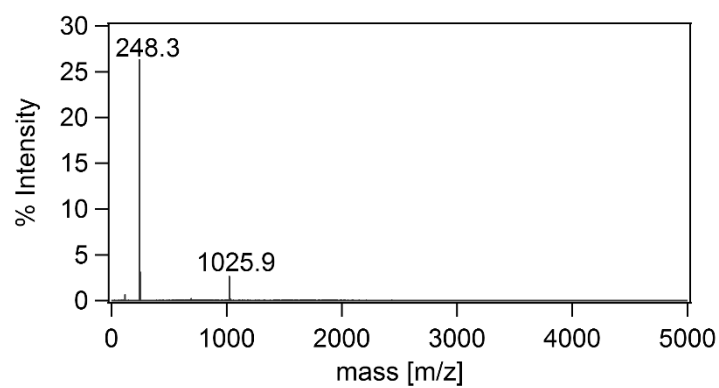
Figure 2.23 MALDI-TOF spectrum of FP-FBT2T-FP

68

2.4 Experimental

2.4.1 Synthesis and Characterization

The small molecules were synthesized according to Scheme 2.1. Commercially available 2-thiophenecarboxyaldehyde and furfural were first subjected to a Knoevenagel condensation reaction with a sacrificial electrophile (ethyl trifluoroacetate). Resulting acrylates were then cyclized by Hemetsberger cyclization. To introduce solubility for the overall compounds, N-alkylation reactions were performed by deprotonation of pyrrolic hydrogen with K_2CO_3, and with subsequent addition of 1-bromododecane. Ethyl 4-dodecyl-4*H*-thieno[3,2-*b*]pyrrole-5-carboxylate was found to be stable in air, but ethyl 4-dodecyl-4*H*-furo[3,2-*b*]pyrrole-5-carboxylate was not stable in air for more than 1.5 h. Therefore, the compound was introduced to the borylation reaction immediately after column purification. However, the compound can be stored at cold temperatures for months without detecting any degradation. Borylation reactions were performed by using pinacolborane in the presence of Ir[(μ_2-OMe)(COD)]$_2$ catalyst to obtain borylated derivatives in high yields (> 75%). Final Suzuki-Miyura coupling reactions were conducted in THF and 1,4-dioxane for TP-FBT2T-TP and FP-FBT2T-FP, respectively. Compounds were purified by column chromatography, and for the target small molecule comprising of furo[3,2-*b*]pyrrole, triethylamine (1%) was added to the eluent to stabilize the compound inside the column. Both small molecules were readily soluble in common organic solvents, and furo[3,2-*b*]pyrrole containing small molecule was more soluble. All the monomers were fully characterized by ^{1}H, and ^{13}C NMR and final organic semiconductors were characterized by MALDI-TOF spectroscopy for mass evaluation.

Scheme 2.1 Synthetic route towards TP-FBT2T-TP and FP-FBT2T-FP
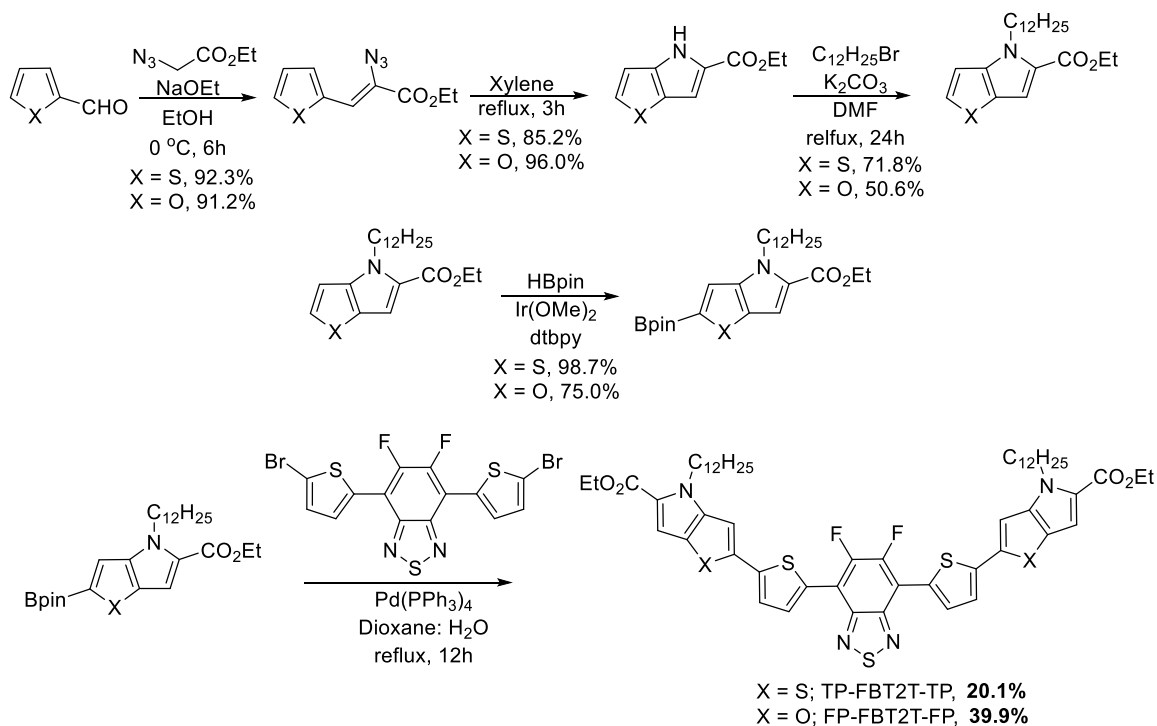
2.4.2 Theoretical Analysis

To investigate the frontier molecular orbital energy levels, density functional theory (DFT) calculations were performed using Spartan′16 at B3LYP/6-31G* level of theory. *N*-dodecane substituents were replaced with methyl groups, and ethyl groups in the ester units were replaced by methyl to simply the calculations as shown in Figure 2.24. Both molecules possess minimal torsion along the backbone to produce planar molecules. The curvature of the molecules was similar to get a close comparison to study the effect of thieno[3,2-*b*]pyrrole and furo[3,2-*b*]pyrrole building blocks. The LUMO frontier molecular orbital energy levels were somewhat different for the two building blocks although HOMO levels were comparable. FP-FBT2T-FP semiconductor

showed a low lying LUMO level compared to TP-FBT2T-TP suggesting insertion of furan units on to building blocks can effectively lower LUMO levels.
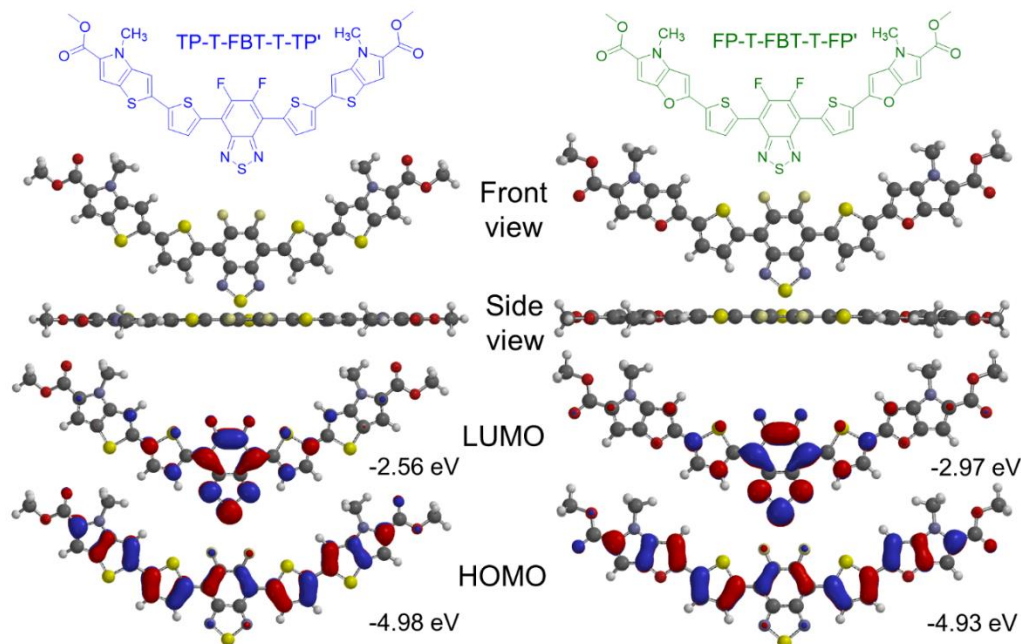
Figure 2.24 DFT calculations of TP-FBT2T-TP and FP-FBT2T-FP

2.4.3 Optical and Electrochemical Analysis

To investigate absorption profiles of TP-FBT2T-TP and FP-FBT2T-FP, UV-vis spectroscopy was used in both solution and solid state (Figure 2.25). Interestingly, both small molecules showed two equally intense bands irrespective of the state (solution or solid state). Absorption bands present at lower wavelengths (higher energies) corresponds to π-π* transitions while bands at higher wavelengths (lower energies) are due to intramolecular charge transfer which takes place from HOMO to central 5,6-difluorobenzo[*c*][1,2,5]thiadiazole localized LUMO energy level. For TP-FBT2T-TP small molecule semiconductor, a small 10 nm bathochromic shift was observed for both absorption band maxima, suggesting the arrangement of molecules in solution and solid state

are not very different. The onset of the absorption profile of TP-FBT2T-TP was estimated at 694 nm with an optical band gap of 1.79 eV. On the contrary, FP-FBT2T-FP semiconductor showed an extremely low optical band gap of 1.25 eV due to the extension of the absorption profile toward NIR II window in the solid state. Similar to TP-FBT2T-TP, 12-13 nm bathochromic shift was observed for the two absorption band maxima. Owing to the excessive electron rich nature of furo[3,2-*b*]pyrrole, thin films containing small molecule FP-FBT2T-FP showed degradation after 12 h, and therefore it was stored in nitrogen-filled glovebox for further characterization and tests.
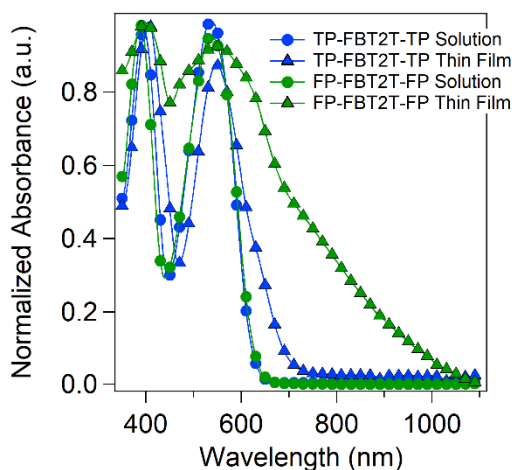
Figure 2.25 UV-vis spectra of TP-FBT2T-TP and FP-FBT2T-FP in solution and thin films

To find the electrochemical band gaps and frontier molecular orbital energy levels, cyclic voltammetry measurements of thin films of the two small molecules were performed. Both small molecules showed multiple irreversible oxidation peaks, especially for FP-FBT2T-FP with more apparent and intense peaks. Both small molecules showed two quasi-reversible reduction peaks in cyclic voltammograms as showed in Figure 2.26. The HOMO and LUMO energy levels were estimated from the onset of the first oxidation and reduction peaks. For TP-FBT2T-TP, HOMO and LUMO levels were estimated at -5.07 eV and -2.60 eV, while for FP-FBT2T-FP it was -5.05

eV and -2.07 eV, respectively. These values were well matched with our DFT calculations performed with modeled compounds. Large mismatch between the optical and electrochemical band gaps could be due to exciton binding energies which could be from 0.3 – 1.0 eV. All optical and electrochemical properties are listed in Table 2.1.
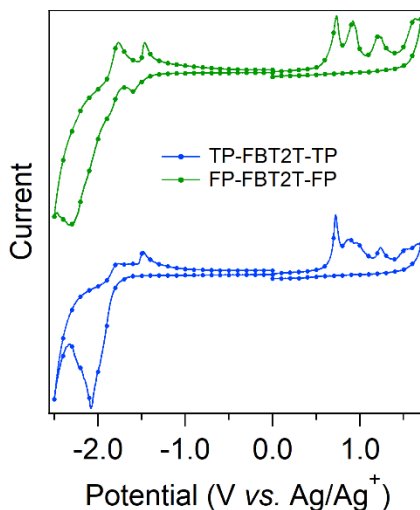
Figure 2.26 Cyclic voltammograms of TP-FBT2T-TP and FP-FBT2T-FP

Table 2.1 Optical and electrochemical properties of TP-FBT2T-TP and FP-FBT2T-FP

Small molecule	HOMO (eV)	LUMO (eV)	E_g^ec (eV)	E_g^opt (eV)	$\lambda_\text{max}^\text{sol}$ (nm)	$\lambda_\text{max}^\text{film}$ (nm)	λ_onset (nm)
TP-FBT2T-TP	-5.07	-2.60	2.47	1.79	384, 526	394, 537	694
FP-FBT2F-FP	-5.05	-2.98	2.07	1.25	388, 537	400, 550	994

2.4.4 OFET properties

The two small molecules were tested in OFETs by employing a bottom-gate/ bottom-contact (BGBC) device architecture on Si/SiO₂ substrates. Both organic semiconductors, TP-FBT2T-TP and FP-FBT2T-FP, were dissolved in chloroform at 5 mg/mL and 10 mg/mL, respectively. Without any surface modification on SiO₂, no field effect characteristics were shown irrespective

of the annealing temperatures. Therefore, Si/SiO$_2$ surface was modified to obtain a self-assembled monolayer (SAM) of octadecylsilane. After the application of the SAM, both small molecules were spun at 750 rpm inside a nitrogen-filled glovebox and subsequently, annealed at different temperatures inside the glovebox for 5 mins. Thin films of TP-FBT2T-TP and FP-FBT2T-FP on the surface treated Si/SiO$_2$ substrates disappeared when annealed at 150 °C and 120 °C, respectively. Therefore, the maximum annealing temperatures for TP-FBT2T-TP and FP-FBT2T-FP were selected as 140 °C and 100 °C, respectively.

First, TP-FBT2T-TP small molecular semiconductor was analyzed in OFETs annealed at room temperature, 80 °C, 100 °C, 120 °C and 140 °C. As expected OFETs fabricated from TP-FBT2T-TP only showed p-type OFET characteristics. No apparent changes in hole mobilities, I_{on}/I_{off}, V_T were observed when the annealing temperature was varied. All the thin films showed moderate hole mobility around 0.001 cm^2 /V s with I_{on}/I_{off} ratios ranging from 10^2 to 10^3. Threshold voltages were estimated to be around -3 V to -10 V depending on the annealing temperature. To our surprise, all the devices fabricated from TP-FBT2T-TP showed ideal transistor curves with low leakage currents and clear saturation regimes. Subthreshold swings up to 0.7 V/dec were obtained for these devices. Most of all, the $I_D^{1/2}$ vs. V_D curves were not suffered from non-linearity that generally introduce errors when extracting mobilities from transfer curves. All the transfer and output curves are shown in Figure 2.27. Summarized data for mobilities and OFET parameters can be found in Table 2.2.

Surprisingly, FP-FBT2T-FP small molecule did not show any field effect behavior irrespective of the surface treatment, processing solvent, and annealing temperature.
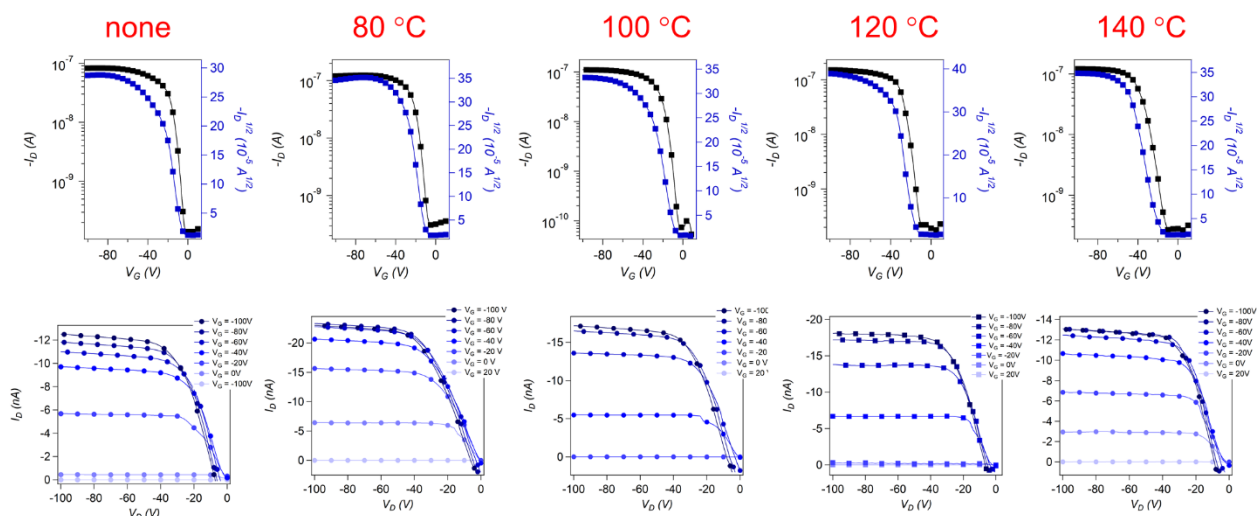
Figure 2.27 OFET performance of TP-FBT2T-TP at different annealing conditions

Table 2.2 The summary of the OFET performance of TP-FBT2T-TP

Annealing temperature	μ_{max} $(cm^2 /V\,s)$	μ_{ave} $(cm^2 /V\,s)$	V_T (V)	I_{on}/I_{off}
RT	0.93×10^{-3}	0.81×10^{-3}	-2.9 - -3.6	$>10^2$
80 °C	1.35×10^{-3}	1.29×10^{-3}	-5.7- -2.4	$>10^2$
100 °C	0.97×10^{-3}	0.82×10^{-3}	-3.7- -1.9	$>10^3$
120 °C	1.57×10^{-3}	1.39×10^{-3}	-9.6- -4.9	$>10^3$
140 °C	0.71×10^{-3}	0.58×10^{-3}	-10.4- -4.2	$>10^2$

2.4.5 Crystallinity

The complete FET inactivity of FP-FBT2T-FP prompted us to investigate the crystallinity of the

two small molecules. To probe the surface orientation with respect to the substrate, out-of-plane

grazing incidence x-ray diffraction (GIXRD) were performed on thin films of TP-FBT2T-TP and

FP-FBT2T-FP deposited on a surface treated Si/SiO$_2$ substrates. TP-FBT2T-TP showed multiple

orders of lamellar peaks when GIXRD were taken on out of plane direction suggesting π-π

stacking in the z-direction which is beneficial for transistors. For FP-FBT2T-FP, a small shoulder was observed with no evidence of sharp XRD peaks in the out of plane direction. This may be due to the face-on orientation adopted by FP-FBT2T-FP molecules. The GIXRD data are shown in Figure 2.28.
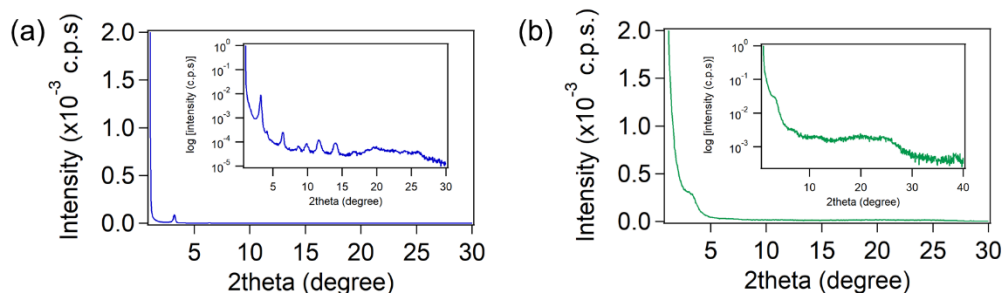
Figure 2.28 GIXRD spectra of (a) TP-FBT2T-TP and (b) FP-FBT2T-FP annealed at 120 °C and 100 °C

2.4.6 Surface Morphology

Tapping mode atomic force microscopy (TMAFM) images were recorded in the channel region to probe surface morphology. A grain-like morphology was observed for the thin films for TP-FBT2T-TP small molecules. Such morphology is considered to be highly desirable for OFETs, and many high performing small molecules resemble similar surface morphology as shown in Figure 2.29(a) and (c) for height and phase AFM images, respectively. On the other hand, TMAFM images of thin films of FP-FBT2T-FP small molecules showed smooth surfaces with RMS of 0.75 nm, and no crystallites were present in TMAFM images. Both height and phase images of the two small molecules are shown in Figure 2.29.
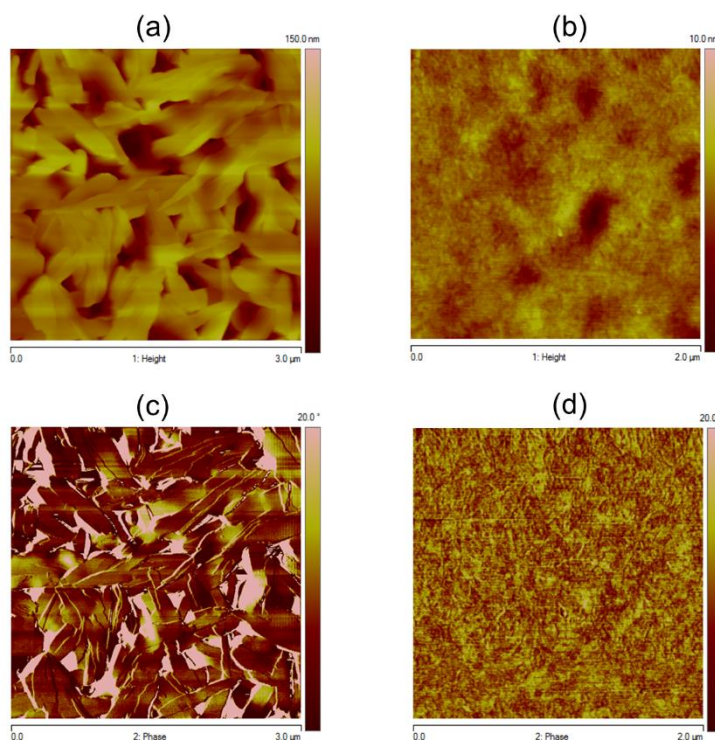
Figure 2.29 TMAFM height ((a) and (b)) and phase ((d) and (d)) images of TP-FBT2T-TP [(a) and (c)] and FP-FBT2T-FP [(b) and (d)]

2.5 Conclusions

In the quest of searching for non-conventional building blocks for organic electronics, two pyrrole containing building blocks were chosen to study. Donor-acceptor-donor type two small molecules containing terminal thieno[3,2-*b*]pyrrole and furo[3,2-*b*]pyrrole with central 5,6-difluorobenzo[*c*][1,2,5]thiadiazole were successfully synthesized and characterized. Furo[3,2-*b*]pyrrole containing small molecule showed an enhanced absorption toward NIR I and NIR II regions, but thin films were not stable in air for prolonged periods of time. Both small molecules had similar HOMO levels, but furo[3,2-*b*]pyrrole containing molecule possessed a low lying LUMO level to realize a low band-gap semiconductor. In OFETs, thieno[3,2-*b*]pyrrole containing small molecule was active toward TFTs, but furo[3,2-*b*]pyrrole containing small molecule was

77

completely inactive. The molecular orientation with respect to the substrate was orthogonal to each other causing the differences in FET activity.

2.6 Acknowledgments

2.7 References

1. Amin, A. Y.; Khassanov, A.; Reuter, K.; Meyer-Friedrichsen, T.; Halik, M., Low-Voltage Organic Field Effect Transistors with a 2-Tridecyl[1]benzothieno[3,2-*b*][1]benzothiophene Semiconductor Layer. *Journal of the American Chemical Society* **2012,** *134*, 16548-16550.

2. Minemawari, H.; Yamada, T.; Matsui, H.; Tsutsumi, J. y.; Haas, S.; Chiba, R.; Kumai, R.; Hasegawa, T., Inkjet printing of single-crystal films. *Nature* **2011,** *475*, 364.

3. Li, J.; Zhao, Y.; Tan, H. S.; Guo, Y.; Di, C.-A.; Yu, G.; Liu, Y.; Lin, M.; Lim, S. H.; Zhou, Y.; Su, H.; Ong, B. S., A stable solution-processed polymer semiconductor with record high-mobility for printed transistors. *Scientific Reports* **2012,** *2*, 754.

4. Martínez Hardigree, J. F.; Katz, H. E., Through Thick and Thin: Tuning the Threshold Voltage in Organic Field-Effect Transistors. *Accounts of Chemical Research* **2014,** *47*, 1369-1377.

5. Xiang, L.; Wang, W.; Xie, W., Achieving high mobility, low-voltage operating organic field-effect transistor nonvolatile memory by an ultraviolet-ozone treating ferroelectric terpolymer. *Scientific Reports* **2016,** *6*, 36291.

6. Mas-Torrent, M.; Rovira, C., Role of Molecular Order and Solid-State Structure in Organic Field-Effect Transistors. *Chemical Reviews* **2011,** *111*, 4833-4856.

7. Izawa, T.; Miyazaki, E.; Takimiya, K., Molecular Ordering of High-Performance Soluble Molecular Semiconductors and Re-evaluation of Their Field-Effect Transistor Characteristics. *Advanced Materials* **2008,** *20*, 3388-3392.

8. Lee, H. K. H.; Li, Z.; Constantinou, I.; So, F.; Tsang, S. W.; So, S. K., Batch-to-Batch Variation of Polymeric Photovoltaic Materials: its Origin and Impacts on Charge Carrier Transport and Device Performances. *Advanced Energy Materials* **2014,** *4*, 1400768.

9. Vangerven, T.; Verstappen, P.; Patil, N.; D'Haen, J.; Cardinaletti, I.; Benduhn, J.; Van den Brande, N.; Defour, M.; Lemaur, V.; Beljonne, D.; Lazzaroni, R.; Champagne, B.; Vandewal, K.; Andreasen, J. W.; Adriaensens, P.; Breiby, D. W.; Van Mele, B.; Vanderzande, D.; Maes, W.; Manca, J., Elucidating Batch-to-Batch Variation Caused by Homocoupled Side Products in Solution-Processable Organic Solar Cells. *Chemistry of Materials* **2016,** *28*, 9088-9098.

10. Vangerven, T.; Verstappen, P.; Drijkoningen, J.; Dierckx, W.; Himmelberger, S.; Salleo, A.; Vanderzande, D.; Maes, W.; Manca, J. V., Molar Mass versus Polymer Solar Cell Performance: Highlighting the Role of Homocouplings. *Chemistry of Materials* **2015,** *27*, 3726-3732.

11. Du, J.; Bulumulla, C.; Mejia, I.; McCandless, G. T.; Biewer, M. C.; Stefan, M. C., Evaluation of (E)-1,2-di(furan-2-yl)ethene as building unit in diketopyrrolopyrrole alternating copolymers for transistors. *Polymer Chemistry* **2017,** *8*, 6181-6187.

12. Ebata, H.; Izawa, T.; Miyazaki, E.; Takimiya, K.; Ikeda, M.; Kuwabara, H.; Yui, T., Highly Soluble [1]Benzothieno[3,2-*b*]benzothiophene (BTBT) Derivatives for High-Performance, Solution-Processed Organic Field-Effect Transistors. *Journal of the American Chemical Society* **2007,** *129*, 15732-15733.

13. Giri, G.; Verploegen, E.; Mannsfeld, S. C. B.; Atahan-Evrenk, S.; Kim, D. H.; Lee, S. Y.; Becerril, H. A.; Aspuru-Guzik, A.; Toney, M. F.; Bao, Z., Tuning charge transport in solution-sheared organic semiconductors using lattice strain. *Nature* **2011,** *480*, 504.

14. Dodabalapur, A.; Torsi, L.; Katz, H. E., Organic Transistors: Two-Dimensional Transport and Improved Electrical Characteristics. *Science* **1995,** *268*, 270.

15. Hajlaoui, R.; Horowitz, G.; Garnier, F.; Arce-Brouchet, A.; Laigre, L.; Kassmi, A. E.; Demanze, F.; Kouki, F., Improved field-effect mobility in short oligothiophenes: Quaterthiophene and quinquethiophene. *Advanced Materials* **1997,** *9*, 389-391.

16. Sakamoto, Y.; Suzuki, T.; Kobayashi, M.; Gao, Y.; Fukai, Y.; Inoue, Y.; Sato, F.; Tokito, S., Perfluoropentacene: High-Performance p−n Junctions and Complementary Circuits with Pentacene. *Journal of the American Chemical Society* **2004,** *126*, 8138-8140.

17. Singh, T. B.; Meghdadi, F.; Günes, S.; Marjanovic, N.; Horowitz, G.; Lang, P.; Bauer, S.; Sariciftci, N. S., High-Performance Ambipolar Pentacene Organic Field-Effect Transistors on Poly(vinyl alcohol) Organic Gate Dielectric. *Advanced Materials* **2005,** *17*, 2315-2320.

18. Yang, S. Y.; Shin, K.; Park, C. E., The Effect of Gate-Dielectric Surface Energy on Pentacene Morphology and Organic Field-Effect Transistor Characteristics. *Advanced Functional Materials* **2005,** *15*, 1806-1814.

19. Li, J.; Zhou, K.; Liu, J.; Zhen, Y.; Liu, L.; Zhang, J.; Dong, H.; Zhang, X.; Jiang, L.; Hu, W., Aromatic Extension at 2,6-Positions of Anthracene toward an Elegant Strategy for Organic Semiconductors with Efficient Charge Transport and Strong Solid State Emission. *Journal of the American Chemical Society* **2017,** *139*, 17261-17264.

20. He, C.; Li, A.; Yan, L.; Zhang, D.; Zhu, Y.; Chen, H.; Meng, H.; Goto, O., 2D and 3D Crystal Formation of 2,6-Bis[4-ethylphenyl]anthracene with Isotropic High Charge-Carrier Mobility. *Advanced Electronic Materials* **2017,** *3*, 1700282.

21. Lakshminarayana, A. N.; Ong, A.; Chi, C., Modification of acenes for n-channel OFET materials. *Journal of Materials Chemistry C* **2018**.

22. Aleshin, A. N.; Lee, J. Y.; Chu, S. W.; Kim, J. S.; Park, Y. W., Mobility studies of field-effect transistor structures basedon anthracene single crystals. *Applied Physics Letters* **2004,** *84*, 5383-5385.

23. Reese, C.; Chung, W.-J.; Ling, M.-m.; Roberts, M.; Bao, Z., High-performance microscale single-crystal transistors by lithography on an elastomer dielectric. *Applied Physics Letters* **2006,** *89*, 202108.

24. Jurchescu, O. D.; Popinciuc, M.; van Wees, B. J.; Palstra, T. T. M., Interface-Controlled, High-Mobility Organic Transistors. *Advanced Materials* **2007,** *19*, 688-692.

25. Takeyama, Y.; Ono, S.; Matsumoto, Y., Organic single crystal transistor characteristics of single-crystal phase pentacene grown by ionic liquid-assisted vacuum deposition. *Applied Physics Letters* **2012,** *101*, 083303.

26. Mondal, R.; Shah, B. K.; Neckers, D. C., Photogeneration of Heptacene in a Polymer Matrix. *Journal of the American Chemical Society* **2006,** *128*, 9612-9613.

27. Watanabe, M.; Chang, Y. J.; Liu, S.-W.; Chao, T.-H.; Goto, K.; Islam, M. M.; Yuan, C.-H.; Tao, Y.-T.; Shinmyozu, T.; Chow, T. J., The synthesis, crystal structure and charge-transport properties of hexacene. *Nature Chemistry* **2012,** *4*, 574.

28. Zade, S. S.; Bendikov, M., Heptacene and Beyond: The Longest Characterized Acenes. *Angewandte Chemie International Edition* **2010,** *49*, 4012-4015.

29. Tönshoff, C.; Bettinger, H. F., Photogeneration of Octacene and Nonacene. *Angewandte Chemie International Edition* **2010,** *49*, 4125-4128.

30. Xiao, K.; Liu, Y.; Qi, T.; Zhang, W.; Wang, F.; Gao, J.; Qiu, W.; Ma, Y.; Cui, G.; Chen, S.; Zhan, X.; Yu, G.; Qin, J.; Hu, W.; Zhu, D., A Highly π-Stacked Organic Semiconductor for Field-Effect Transistors Based on Linearly Condensed Pentathienoacene. *Journal of the American Chemical Society* **2005,** *127*, 13281-13286.

31. Liu, Y.; Wang, Y.; Wu, W.; Liu, Y.; Xi, H.; Wang, L.; Qiu, W.; Lu, K.; Du, C.; Yu, G., Synthesis, Characterization, and Field-Effect Transistor Performance of Thieno[3,2-*b*]thieno[2′,3′:4,5]thieno[2,3-*d*]thiophene Derivatives. *Advanced Functional Materials* **2009,** *19*, 772-778.

32. Zhang, X.; Côté, A. P.; Matzger, A. J., Synthesis and Structure of Fused α-Oligothiophenes with up to Seven Rings. *Journal of the American Chemical Society* **2005,** *127*, 10502-10503.

33. Okamoto, T.; Kudoh, K.; Wakamiya, A.; Yamaguchi, S., General Synthesis of Extended Fused Oligothiophenes Consisting of an Even Number of Thiophene Rings. *Chemistry – A European Journal* **2007,** *13*, 548-556.

34. Mei, J.; Diao, Y.; Appleton, A. L.; Fang, L.; Bao, Z., Integrated Materials Design of Organic Semiconductors for Field-Effect Transistors. *Journal of the American Chemical Society* **2013,** *135*, 6724-6746.

35. Dadvand, A.; Cicoira, F.; Chernichenko, K. Y.; Balenkova, E. S.; Osuna, R. M.; Rosei, F.; Nenajdenko, V. G.; Perepichka, D. F., Heterocirculenes as a new class of organic semiconductors. *Chemical Communications* **2008**, 5354-5356.

36. Nakano, M.; Niimi, K.; Miyazaki, E.; Osaka, I.; Takimiya, K., Isomerically Pure Anthra[2,3-*b*:6,7-*b′*]-difuran (anti-ADF), -dithiophene (anti-ADT), and -diselenophene (anti-ADS): Selective Synthesis, Electronic Structures, and Application to Organic Field-Effect Transistors. *The Journal of Organic Chemistry* **2012,** *77*, 8099-8111.

37. Takimiya, K.; Kunugi, Y.; Konda, Y.; Niihara, N.; Otsubo, T., 2,6-Diphenylbenzo[1,2-*b*:4,5-*b′*]dichalcogenophenes: A New Class of High-Performance Semiconductors for Organic Field-Effect Transistors. *Journal of the American Chemical Society* **2004,** *126*, 5084-5085.

38. Cho, I.; Park, S. K.; Kang, B.; Chung, J. W.; Kim, J. H.; Yoon, W. S.; Cho, K.; Park, S. Y., Dicyanovinyl-substituted indolo[3,2-*b*]indole derivatives: low-band-gap π-conjugated molecules for a single-component ambipolar organic field-effect transistor. *Journal of Materials Chemistry C* **2016,** *4*, 9460-9468.

39. Sim, J.; Do, K.; Song, K.; Sharma, A.; Biswas, S.; Sharma, G. D.; Ko, J., D-A-D-A-D push pull organic small molecules based on 5,10-dihydroindolo[3,2-*b*]indole (DINI) central core donor for solution processed bulk heterojunction solar cells. *Organic Electronics* **2016,** *30*, 122-130.

40. Li, Y.; Wu, Y.; Ong, B. S., Polyindolo[3,2-*b*]carbazoles: A New Class of p-Channel Semiconductor Polymers for Organic Thin-Film Transistors. *Macromolecules* **2006,** *39*, 6521-6527.

41. Boudreault, P.-L. T.; Wakim, S.; Tang, M. L.; Tao, Y.; Bao, Z.; Leclerc, M., New indolo[3,2-*b*]carbazole derivatives for field-effect transistor applications. *Journal of Materials Chemistry* **2009,** *19*, 2921-2928.

42. Wetzel, C.; Brier, E.; Vogt, A.; Mishra, A.; Mena-Osteritz, E.; Bäuerle, P., Fused Thiophene-Pyrrole-Containing Ring Systems up to a Heterodecacene. *Angewandte Chemie International Edition* **2015,** *54*, 12334-12338.

43. Arora, N.; Wetzel, C.; Dar, M. I.; Mishra, A.; Yadav, P.; Steck, C.; Zakeeruddin, S. M.; Bäuerle, P.; Grätzel, M., Donor–Acceptor-Type *S,N*-Heteroacene-Based Hole-Transporting Materials for Efficient Perovskite Solar Cells. *ACS Applied Materials & Interfaces* **2017,** *9*, 44423-44428.

44. Shim, J. Y.; Baek, J.; Kim, J.; Park, S. Y.; Kim, J.; Kim, I.; Chun, H. H.; Kim, J. Y.; Suh, H., Synthesis and properties of low band gap polymers based on thienyl thienoindole as a new electron-rich unit for organic photovoltaics. *Polymer Chemistry* **2015,** *6*, 6011-6020.

45. Jones, C.; Boudinet, D.; Xia, Y.; Denti, M.; Das, A.; Facchetti, A.; Driver, T. G., Synthesis and Properties of Semiconducting Bispyrrolothiophenes for Organic Field-Effect Transistors. *Chemistry – A European Journal* **2014,** *20*, 5938-5945.

CHAPTER 3

THIENO[3,2-*b*]PYRROLE – BENZOTHIADIAZOLE BANANA-SHAPED SMALL

MOLECULES FOR ORGANIC FIELD EFFECT TRANSISTORS

Authors – Chandima Bulumulla,[†] Ruwan Gunawardhana,[†] Ruvanthi N. Kularatne,[†]

Madison E. Hill,[†] Gregory T. McCandless,[†] Michael C. Biewer,[†]

and Mihaela C. Stefan[†*]

[†]Department of Chemistry and Biochemistry, BE26

The University of Texas at Dallas

800 West Campbell Road

Richardson, Texas 75080, USA

[*]Department of Bioengineering, BSB11

The University of Texas at Dallas

800 West Campbell Road

Richardson, Texas 75080, USA

3.1 Abstract

We report two banana-shaped organic semiconducting small molecules containing the relatively unexplored thieno[3,2-*b*]pyrrole with thiophene and furan flanked benzothiadiazole. Theoretical insights gained by DFT calculations show that furan flanked benzothiadiazole-thieno[3,2-*b*]pyrrole small molecule has a higher curvature as compared to the thiophene flanked small molecule due to the shorter bond length of C-O in furan. Despite similar optical and electrochemical properties, thiophene flanked small molecule shows high hole mobility up to 8×10^{-2} cm^2 /V s. However furan flanked small molecule performs poorly in thin film transistor devices ($\mu_h \sim 5 \times 10^{-6}$ cm^2 /V s). The drastic difference in hole mobilities was due to the annealing-induced crystallinity which was demonstrated by the out-of-plane grazing incidence X-ray diffraction and tapping mode atomic force microscopy analysis.

3.2 Introduction

Organic semiconducting materials have shown promise in the organic field effect transistor (OFET) area with performance comparable or even surpassing amorphous silicon (α-Si) (0.1-1.0 cm^2 /V s)[1-3] and approaching polycrystalline silicon (*c*-Si) FETs (>10 cm^2 /V s).[4-6] Organic semiconducting materials can be classified into two main classes: polymers and small molecules. Organic polymers have higher conjugation lengths and excellent film-forming abilities which are desirable for large area applications.[7-8] However, organic polymers often exhibit molecular weight dependence on charge carrier mobilities.[9-12] Due to the irreproducible molecular weights and relatively broad distributions of molecular weights, polymeric OFET devices display batch-to-batch variations. On the other hand, small molecules offer well-defined structures, high purities, a

high degree of ordering, and precise molecular weights, which produce less batch-to-batch variations in OFETs.[13-16] Such high performing small molecules are often vacuum deposited to eliminate the need of insulating alkyl chains which hinders the solid state packing.[17-19] Even though this method generates high-quality substrate oriented films, ultra-high vacuum processing conditions make practical applications difficult. Therefore, the challenge is to develop solution processable small molecules without compromising charge carrier mobilities.

Design strategies for high performing solution processable small molecules many times involve donor-acceptor architecture incorporating acenes or fused ring systems.[19-23] Compared to individual ring systems, fused rings provide a deep HOMO level due to the larger resonance stabilization energy and also form larger π-π overlapping areas that facilitate charge transport.[3, 7, 24] Thieno[3,2-*b*]thiophene,[3, 7-8] cyclopentadithiophene,[25-26] Dithienosilole,[16, 27] dithieno[3,2-*b*:2′,3′-*d*]pyrrole[28-29] are some of the commonly used fused ring systems in organic electronics. Although fused ring systems with different heteroatoms have a positive impact on OFETs, the structure-property relationship is not straightforward,[23, 30] leaving chemists to explore novel building blocks to improve OFET performances. Therefore, our goal is to investigate non-conventional fused ring systems that could generate high hole mobilities without compromising solubility. Relative to thiophene and furan, isoelectronic pyrrole is the most electron rich five-membered aromatic ring. Due to the high electron density, pyrrolic compounds require challenging synthesis, but nonetheless, pyrrole is an excellent building block for organic semiconductors.[31-33] Since fused rings provide stability compared to individual rings, a combination of stable thiophene and unstable pyrrole will offer a stable, strong donor.

Compared to dithieno[3,2-*b*:2′,3′-*d*]pyrrole building block, thieno[3,2-*b*]pyrrole building block has received less attention in the organic electronics community.[34]. Therefore, we have selected thieno[3,2-*b*]pyrrole as our building block of choice and benzo[*c*][1,2,5]thiadiazole as the electron withdrawing group to create π orbital overlap. To further investigate the influence of the heteroatom, we synthesized two donor-acceptor small molecules containing thiophene and furan flanked benzothiadiazole as the acceptor and thieno[3,2-*b*]pyrrole as the donor as shown in Figure 3.1.
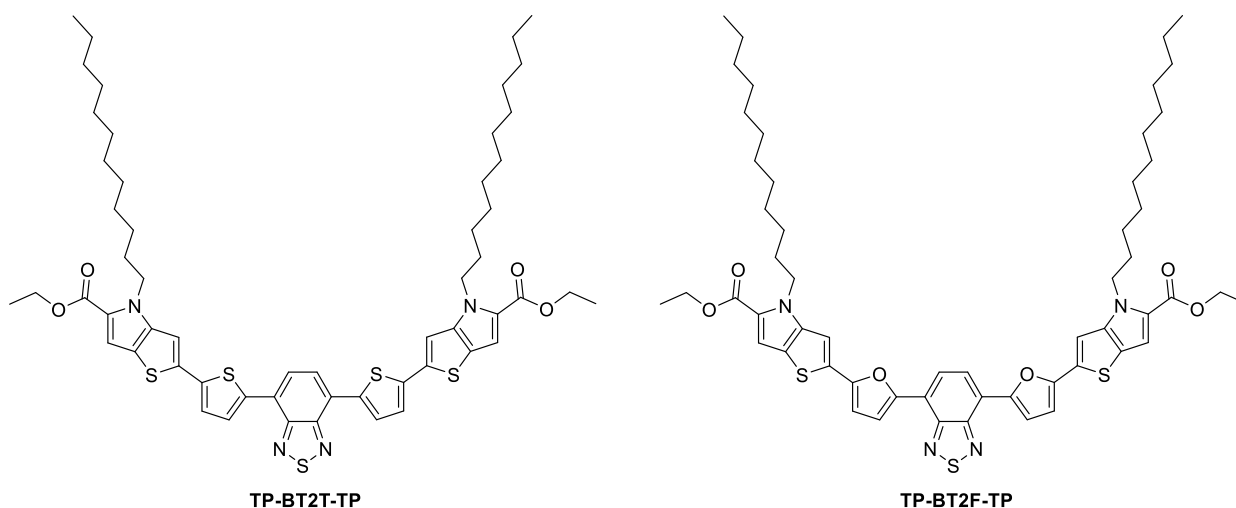
Figure 3.1 Banana-shaped molecular structures of TP-BT2T-TP and TP-BT2F-TP

It has been shown that curved backbones could lead to better charge transport by using a series of polythiophenes with varying degree of backbone curvature.[35] However, a higher degree of curvature has led to lower mobilities for polymer OFETs.[35] There have been few reports of using curved small molecules (banana shaped small molecules) for liquid crystalline applications and thin film transistors.[36-38] From the perspective of a synthetic chemist, exchange of the flanking group from thiophene to furan produces a highly coplanar structure owing to the smaller size of

oxygen atom.[39-40] Moreover, this would allow less torsion along the backbone with no effect on the backbone curvature due to non-altered bond angles. However, DFT calculations of modeled TP-BT2F-TP' shows a higher degree of curvature in the backbone due to the shorter C-O bond distance in the flanking furan. This is an interesting aspect when it comes to design and synthesize molecules with "conformational locks". Due to the effect of the heteroatom and backbone curvature, hole mobilities of the two small molecules are drastically different presenting insights for designing high performing solution processable OFET small molecules. The stark difference in hole mobilities is observed as a result of thermal annealing-induced crystallinity examined from grazing incidence X-ray diffraction (GIXRD) measurements and tapping mode atomic force microscopy (TMAFM) analysis.

3.3 Experimental

3.3.1 Materials and Methods

4,7-Dibromobenzo[*c*][1,2,5]thiadiazole,[41] 4,7-di(thiophen-2-yl)benzo[*c*][1,2,5]thiadiazole [5],[42] 2-(trimethylstannyl)furan,[43] and 4,7-bis(5-(trimethylstannyl)thiophen-2-yl)benzo[*c*][1,2,5] thiadiazole [7][44] were synthesized according to previously published procedures. The procedures for the synthesis of [2], [3], [4], 4,7-di(furan-2-yl)benzo[*c*][1,2,5]thiadiazole (BT2F) [6], 4,7-bis(5-(tributylstannyl)furan-2-yl)benzo[*c*][1,2,5]thiadiazole [8], TP-BT2T-TP, TP-BT2F-TP can be found in section 3.2.2. All commercial chemicals were purchased from Aldrich and Fisher Scientific and used without further purification unless mentioned otherwise. All reactions were performed in oven-dried glassware under a nitrogen atmosphere. Tetrahydrofuran (THF) and toluene were distilled over sodium /benzophenone ketyl under nitrogen prior to use.

NMR measurements: ^{1}H and ^{13}C NMR spectra were recorded on a 500 MHz Bruker AVANCE III^{TM} spectrometer using deuterated chloroform as the solvent. Multiplicities were given as: s (singlet), d (doublet), t (triplet), q (quartet), m (multiplet).

Mass characterization: Matrix-assisted laser desorption ionization time of flight (MALDI-TOF) spectra were obtained from Shimadzu Biotech Axima Confidence in reflectron_HiRes mode with 2,2′:5′,2″-terthiophene as the matrix.

Single crystal X-ray diffraction measurements: For BT2T and BT2F with either thiophene or furan substituents, respectively, single crystal X-ray diffraction data sets were collected at low temperature (Oxford Cryosystems cryostream, T = 100 K). The red tablet-shaped crystalline fragments used for data collection were similar in size (BT2T, ~0.16 x 0.16 x 0.06 mm^3 and BT2F, ~0.16 x 0.12 x 0.04 mm^3) and both were obtained by crystallization in ethanol using the slow solvent evaporation method. Diffraction frames were collected on a Bruker Kappa D8 Quest diffractometer equipped with Incoatec microfocus Mo Kα radiation source and Photon 100 CMOS detector. Afterward, Bruker SAINT, SADABS, and XPREP were used to integrate, scale (with multi-scan absorption correction), and evaluate space groups, respectively. Starting models were generated using SHELXT (intrinsic phasing method) and further atomic site assignments, anisotropic refinement of non-hydrogen atomic positions, and the addition of "riding" hydrogen atomic sites was completed with SHELXL2017. For the crystal structure of compound BT2T, one of the two thiophene substituents has the positional disorder (modeled with 2 possible *relative* thiophene orientations, *cis* or *trans*, with a refined percentage ratio of ~60:40).

Thermal characterization: Thermogravimetric analysis and differential scanning calorimetry (TGA and DSC, respectively) were recorded on a Mettler Toledo TGA/DSC-1 system with a heating rate of 10 °C/min and a cooling rate of -10 °C/min under nitrogen flow.

Optical measurements: The UV-vis absorption was recorded with an Agilent 8453 UV-vis spectrometer.

Electrochemical measurements: Cyclic voltammetry experiments were performed with a BAS CV-50W voltammetry analyzer. Cyclic voltammograms were recorded by using a three-electrode system; a platinum inert working electrode, platinum wire auxiliary electrode, and Ag/Ag^+ reference electrode. 0.1 M tetrabutylammonium hexafluorophosphate in anhydrous acetonitrile was used as the electrolyte.

Surface Morphology characterization: Tapping mode atomic force microscopy (TMAFM) was performed between the channel region on the OFET devices using a Nanoscope IV Multimode Veeco equipped with a vertical engage scanner. The TMAFM images were acquired using Si cantilever with the resonance frequency of 320 kHz and spring constant of 42 N/m. The images were collected in 2×2 μm scan size with a frequency of 1 Hz.

Grazing Incidence X-ray measurements: Out-of-plane GIXRD measurements were performed on a Rigaku SmartLab XRD instrument. Samples were prepared on OTS treated SiO_2 surface by using the same conditions used for the OFET devices. The sample was irradiated with Cu-Kα (λ=1.54 Å) at an incident angle of 0.5°. The data were collected at 0.05° intervals from 1° to 30°.

OFET device fabrication and characterization: Thin film transistors with common bottom-gate/bottom-contact configuration were used to fabricate OFETs. A highly doped n-type silicon wafer was used as the gate substrate and 200 nm thermally grown SiO_2 was employed as the

dielectric layer. First, SiO_2 surface was covered with 5 nm chromium and 100 nm gold in-situ by E-beam evaporator. Using standard photolithography Cr/Au source and drain contacts were patterned having different channel lengths. After applying the photoresist on the electrodes, back of the silicon wafer was etched with 7:1 BOE solution from JT Baker, followed by deposition of 100 nm gold. OFET devices were cleaned sequentially using acetone, toluene, and 2-propanol. The capacitance per unit area was measured to be 17 nF cm^{-2}. The substrates were first cleaned by immersing in piranha solution (7:3 mixture of conc. sulfuric acid and 30% hydrogen peroxide) for 10 mins followed by rinsing with copious amounts of DI water and dried with nitrogen. UV-ozone treatment was performed for 10 mins followed by washing with DI water and acetone and dried with nitrogen. A self-assembled monolayer of octadecylsilane (OTS) was prepared by base (NH_4OH) vapor-catalyzed hydrolysis of octadecyltrimethoxysilane (OTMS) according to a previously published procedure.[45] Briefly, 3mM OTMS solution in trichloroethylene was added on top of the SiO_2 surface to cover the entire surface and allowed to partially assemble for 10 s. Then the substrate was spun at 3000 rpm for 10 s. The base-catalyzed hydrolysis was performed by putting the substrates inside a closed container with 3 mL of NH_4OH (28-30% NH_3 assay) in a vial for 10 h at room temperature. Substrates were rinsed with copious amounts of DI water and sonicated in toluene for 10 mins and dried by nitrogen. Small molecules TP-BT2T-TP and TP-BT2F-TP were dissolved in chloroform at a concentration of 5 mg/mL and 10 mg/mL, respectively and stirred for 30 mins prior to spin casting. No heat was required to dissolve the small molecules. A thin layer was deposited by spin coating at 1000 rpm for 30s after covering the device surface for 30 s and 60 s with 70 μL of TP-BT2T-TP and TP-BT2F-TP respectively. Prepared devices were then annealed at different temperatures for 5 mins inside a nitrogen-filled glovebox prior to

measurements. Cascade Microtech Model Summit Microchamber with a Keithley 4200-SCS systems were used for the electrical characterization. All the measurements were conducted in air at room temperature.

3.3.2 Synthesis of Materials

Ethyl 2-azido-3-(5-bromothiophen-2-yl)acrylate [2]

Sodium metal (1.200 g, 52.34 mmol) was portionwise added to a 200% proof ethanol solution (48.0 mL) in a 250 mL single-neck round-bottomed flask under N_2. After the addition of the sodium metal, the solution was cooled to 0 °C. 5-bromothiophene-2-carboxyaldehyde (5.000 g, 26.17 mmol), ethyl azidoacetate (6.750 g, 52.34 mmol), ethyltrifluoroacetate (7.380 g, 52.34 mmol) and ethanol (10 mL) were mixed under N_2 and added to the stirring sodium ethanolate solution. After 1.5 h a yellow precipitate was formed. The precipitate containing solution was crashed in a sat. NH_4Cl solution. The yellow color needle-like precipitate was filtered under vacuum as the pure compound. (Yield = 7.240 g, 92.0 %) ^1H NMR ($CDCl_3$, 500 MHz): δ_H 1.38 (t, 7.5 Hz, 3H), 4.35 (q, 7.0 Hz, 2H), 7.10 (s, 2H), 7.03 (s, 1H) (Figure 3.2), ^{13}C NMR ($CDCl_3$, 125 MHz): δ_C 14.35, 62.39, 118.71, 123.19, 129.94, 131.80, 138.42, 163.05 (Figure 3.3)
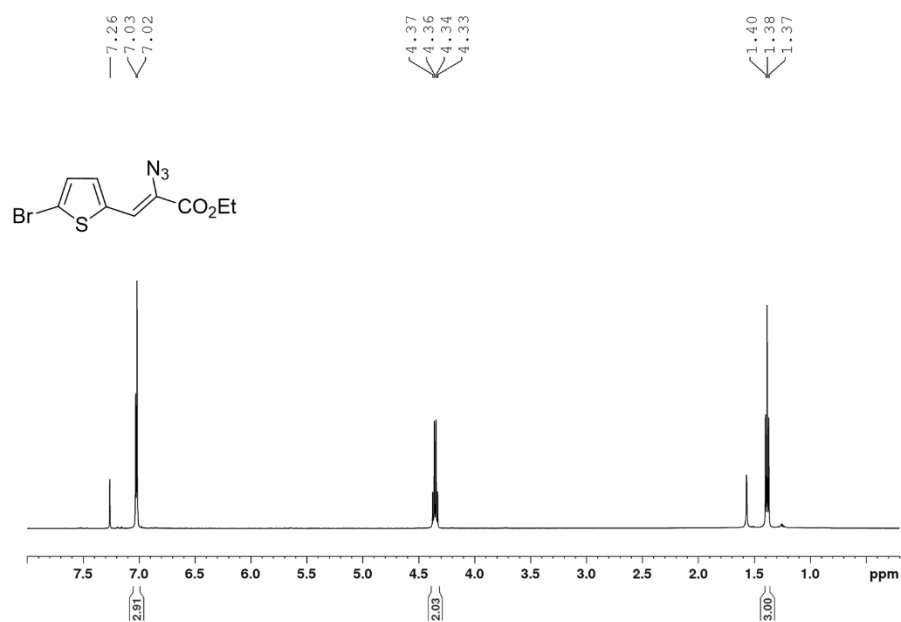
Figure 3.2 ¹H NMR spectrum of ethyl-2-azido-3-(5-bromothiophen-2-yl)acrylate
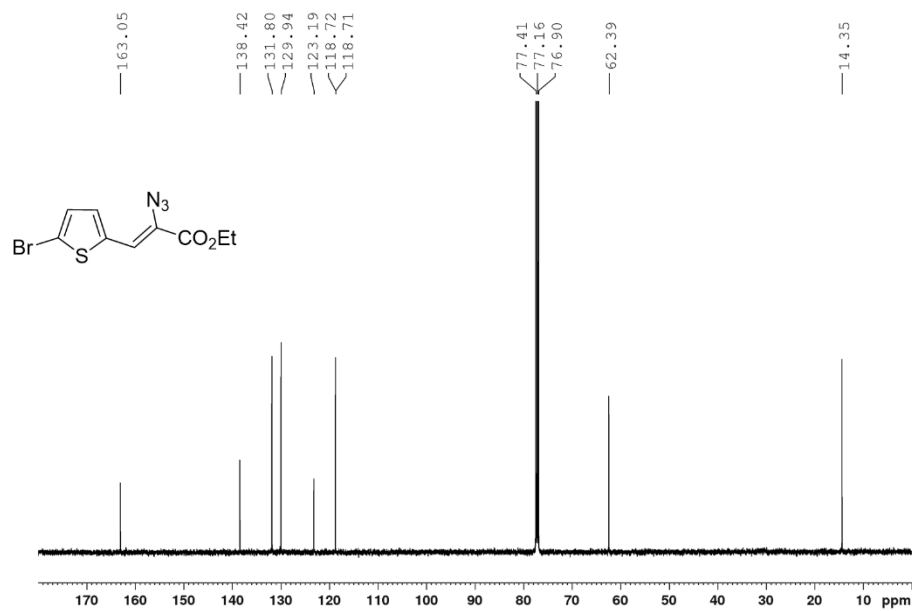
Figure 3.3 ¹³C NMR spectrum of ethyl-2-azido-3-(5-bromothiophen-2-yl)acrylate

Ethyl 2-bromo-4H-thieno[3,2-b]pyrrole-5-carboxylate [3]

Ethyl-2-azido-3-(5-bromothiophen-2-yl)acrylate (7.000 g, 23.26 mmol) was added to a refluxing toluene solution (50.0 mL) in a 250 mL single neck   round bottomed flask and refluxed for 3 h. Solution was cooled to room temperature and toluene was removed under vacuo. The brown solid formed was filtered under vacuum and washed with hexane three times to afford the pure compound. (Yield = 4.310 g, 67.9 %) ^{1}H NMR (CDCl$_3$, 500 MHz): δ_H 1.39 (t, 7.5 Hz, 3H), 4.37 (q, 7.0 Hz, 2H), 7.00 (s, 1H), 7.04 (s, 1H), 9.54 (s, 1H) (Figure 3. 4), ^{13}C NMR (CDCl$_3$, 125 MHz): δ_C 14.55, 61.01, 107.48, 114.59, 116.31, 124.91, 126.36, 139.45, 161.92 (Figure 3.5)
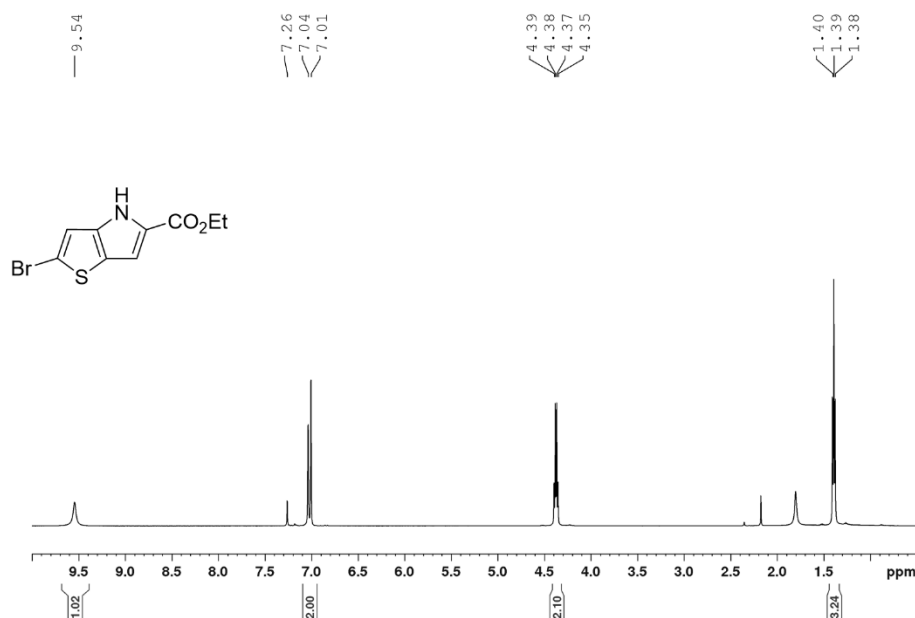
Figure 3.4 ^{1}H NMR spectrum of ethyl 2-bromo-4*H*-thieno[3,2-*b*]pyrrole-5-carboxylate
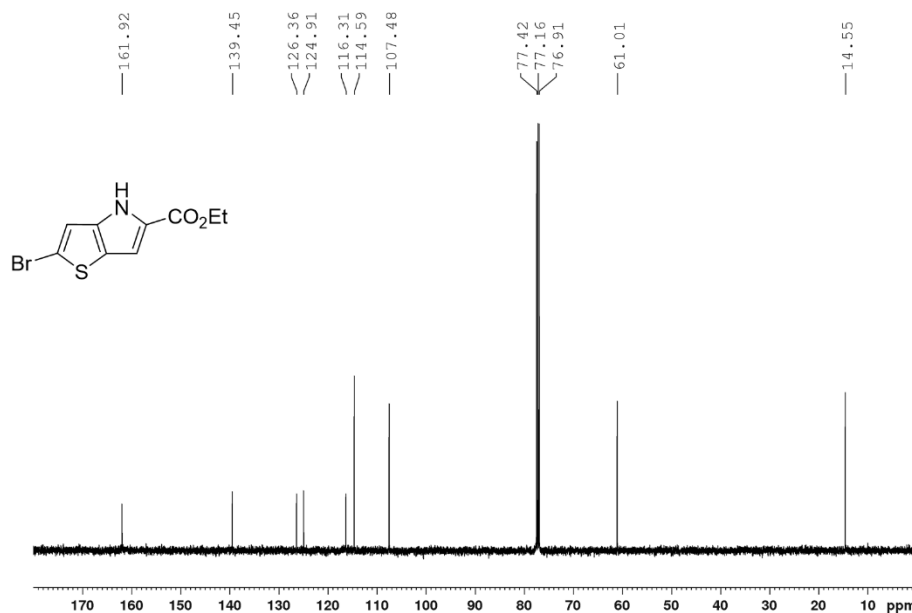
Figure 3.5 ^{13}C NMR spectrum of ethyl 2-bromo-4*H*-thieno[3,2-*b*]pyrrole-5-carboxylate

Ethyl-2-bromo-4-dodecyl-4H-thieno[3,2-b]pyrrole-5-carboxylate [4]

Ethyl 2-bromo-4*H*-thieno[3,2-*b*]pyrrole-5-carboxylate (2.000 g, 7.33 mmol), K$_2$CO$_3$ (2.010 g, 15.30 mmol) and 18-crown-6 (cat. amount) were added to a 100 mL three neck round bottomed flask under N$_2$. Distilled DMF (36.0 mL) was added and stirred at 100 °C for 2 h. 1-bromododecane (3.76 g, 15.30 mmol) was added dropwise and stirred overnight at 120 °C. The mixture was cooled and DI water (50 mL) was added. The compound was extracted with ethyl acetate and after drying with MgSO$_4$, solvent was removed under reduce pressure, pure compound was obtained by flash chromatography using hexane: ethyl acetate (99:1 v/v) as the eluent. (Yield = 2.610 g, 80.7%) ^{1}H NMR (CDCl$_3$, 500 MHz): δ_H 0.87 (t, 7.5 Hz, 3H), 1.24-1.28 (br, 18H), 1.36 (t, 7.0 Hz, 3H), 1.76 (m, 2H), 4.31 (q, 7.0 Hz, 2H), 4.41 (t, 7.5 Hz, 2H), 6.99 (s, 1H), 7.08 (s, 1H) (Figure 3.6), ^{13}C NMR

(CDCl₃, 125 MHz): δ$_C$ 14.27, 14.55, 22.84, 26.98, 29.46, 29.49, 29.67, 29.71, 29.76, 29.78, 31.23, 32.07, 47.85, 60.33, 109.13, 113.91, 115.91, 122.12, 125.12, 125.58, 142.96, 161.56 (Figure 3.7)
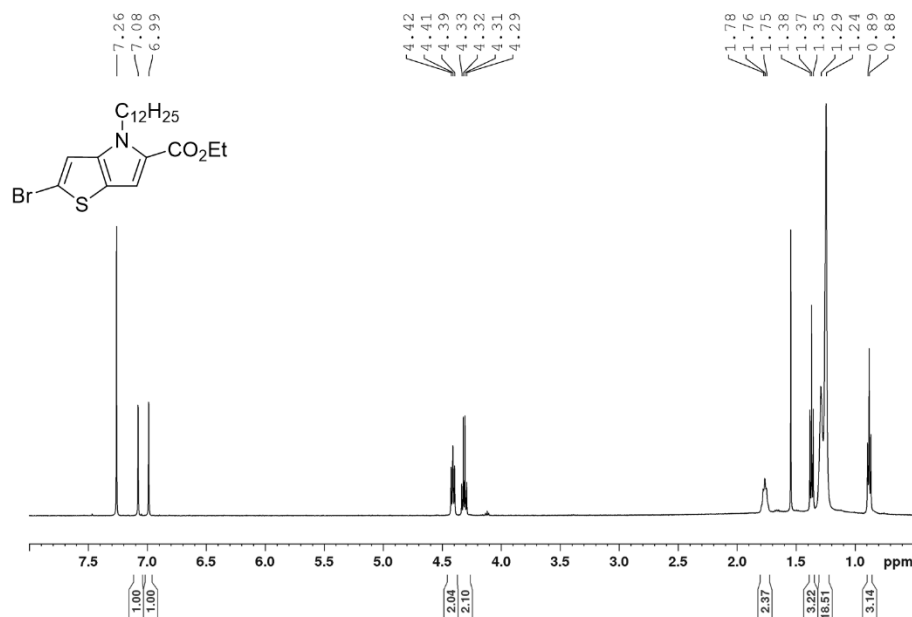
Figure 3.6 ^{1}H NMR of ethyl-2-bromo-4-dodecyl-4*H*-thieno[3,2-*b*]pyrrole-5-carboxylate
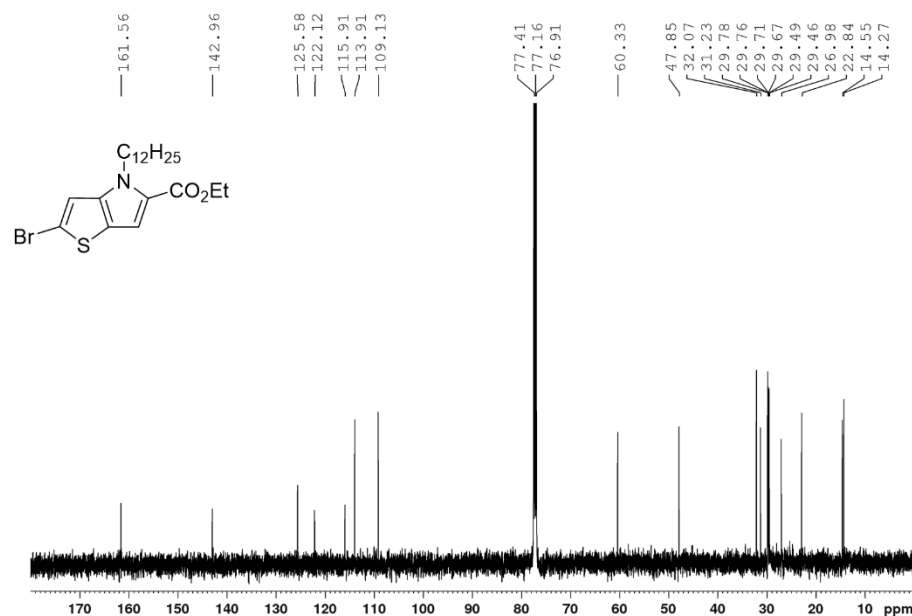
Figure 3.7 ^{13}C NMR of ethyl-2-bromo-4-dodecyl-4*H*-thieno[3,2-*b*]pyrrole-5-carboxylate

4,7-di(furan-2-yl)benzo[c][1,2,5]thiadiazole [6]

4,7-dibromobenzo[c][1,2,5]thiadiazole (0.750 g, 2.55 mmol), 2-(trimethylstannyl)furan (1.240 g, 5.37 mmol) and tetrakis(triphenylphosphine)palladium(0) (0.080 g, 0.07 mmol) were added to a 100 mL three neck round bottomed flask under nitrogen. 25 mL of anhydrous toluene was added and refluxed for 24 h. The reaction mixture was cooled to room temperature and DI water (50 mL) was added. The compound was extracted with methylene chloride (3 × 30 mL) and after drying with anhydrous MgSO4, solvent was removed under reduced pressure. The crude was purified by column chromatography using hexane: methylene chloride (1:1 v/v) as the eluent. (Yield = 0.480 g, 70.9%) ^{1}H NMR (CDCl$_3$, 500 MHz): δ_H 6.63 (q, 2.0 Hz, 1H), 7.59 (d, 1.0 Hz, 1H), 7.68 (d, 3.5 Hz, 1H), 8.05 (s, 1H) (Figure 3.8), ^{13}C NMR (CDCl$_3$, 125 MHz): δ_C 112.31, 112.64, 121.96, 123.69, 142.97, 150.31, 151.50 (Figure 3.9)
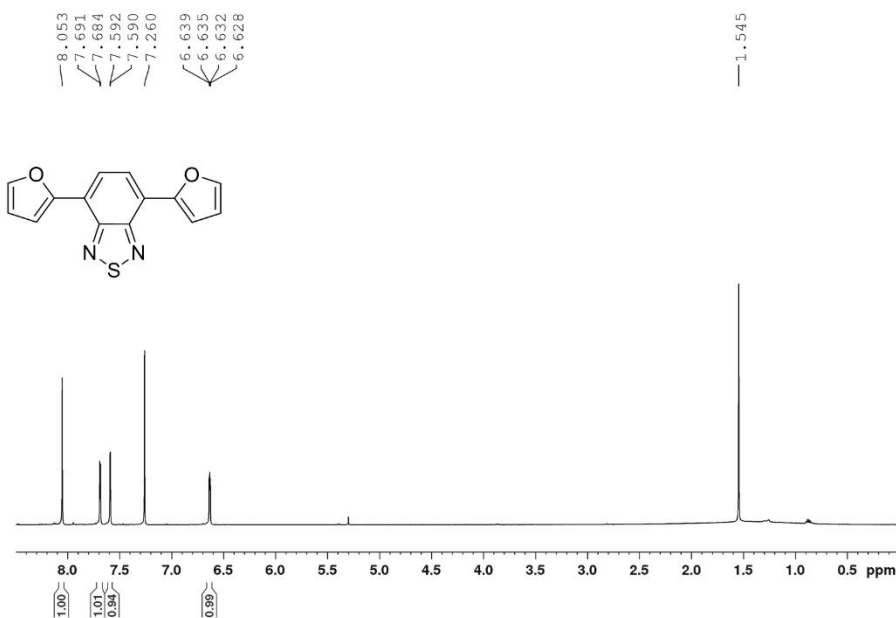
Figure 3.8 ^{1}H NMR spectrum of 4,7-di(furan-2-yl)benzo[c][1,2,5]thiadiazole
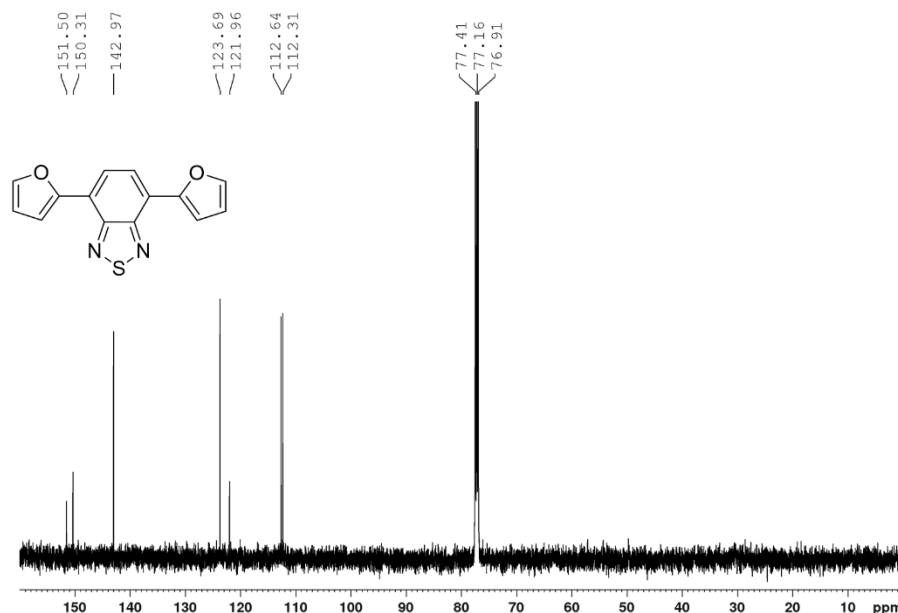
Figure 3.9 ^{13}C NMR spectrum of 4,7-di(furan-2-yl)benzo[*c*][1,2,5]thiadiazole

4,7-bis(5-(tributylstannyl)furan-2yl)benzo[c][1,2,5]thiadiazole [8]

4,7-di(furan-2-yl)benzo[*c*][1,2,5]thiadiazole (0.100 g, 0.375 mmol) and anhydrous THF (18.5 mL) were added to 100 mL three-neck round bottomed flask under nitrogen. The flask was cooled to -78 °C. After 5 mins, 2.0 M LDA (1.20 mL, 2.40 mmol) was injected dropwise (solution mixture turns to purple color) and was stirred for 2 h at -78 °C. At this time an aliquot was withdrawn from the flask, quenched into D$_2$O to check the lithiation from ^{1}H NMR analysis. Tributylstannyl chloride (0.3 mL, 1.10 mmol) was injected dropwise at -78 °C and stirred for additional 2 h. The solution mixture was allowed to warm to room temperature and added to ice-cold DI water (50 mL). After extracting with methylene chloride (3 × 30 mL), the organic phase was dried with anhydrous MgSO$_4$ and solvent was removed under reduced pressure. To remove excess tributylstannyl chloride, a small plug was used with K$_2$CO$_3$: silica (1:9 wt%) as the stationary phase and hexane: ethyl acetate (8:2 v/v) as the eluent. (Yield = 0.380 g, 78.9%) ^{1}H NMR (CDCl$_3$, 500

MHz): δ_H 0.93 (t, 5.0 Hz, 9H), 1.17 (m, 6H), 1.38 (m, 6H), 1.64 (m, 6H), 6.78 (d, 5.0 Hz, 1H),

7.70 (d, 5.0 Hz, 1H), 8.06 (s, 1H) (Figure 3.10), ^{13}C NMR (CDCl$_3$, 125 MHz): δ_C 10.48, 13.86,

27.35, 29.16, 112.15, 121.95, 123.51, 124.44, 151.51, 154.73, 162.57 (Figure 3.11)
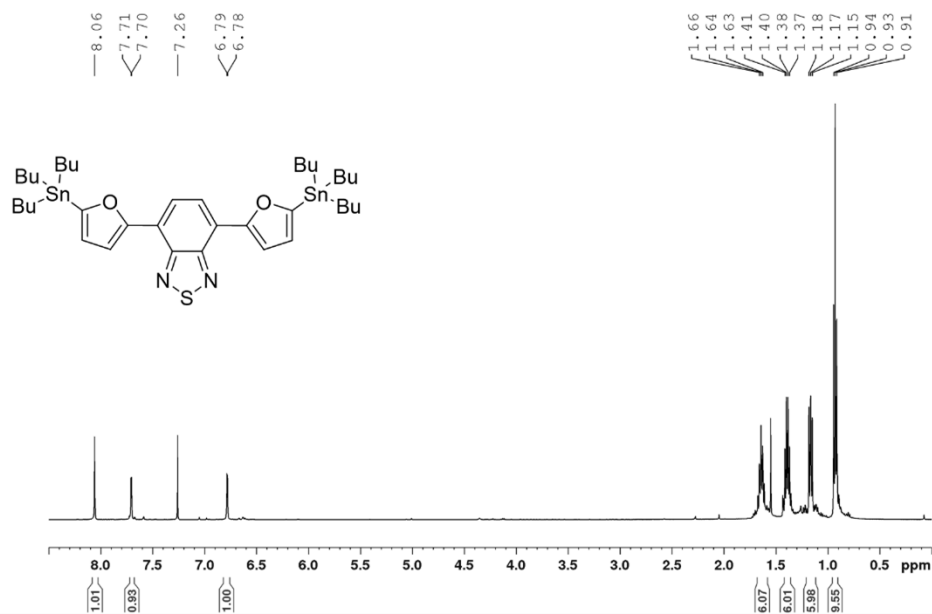
Figure 3.10 ^{1}H NMR spectrum of 4,7-bis(5-(tributylstannyl)furan-2yl)benzo[c][1,2,5]thiadiazole
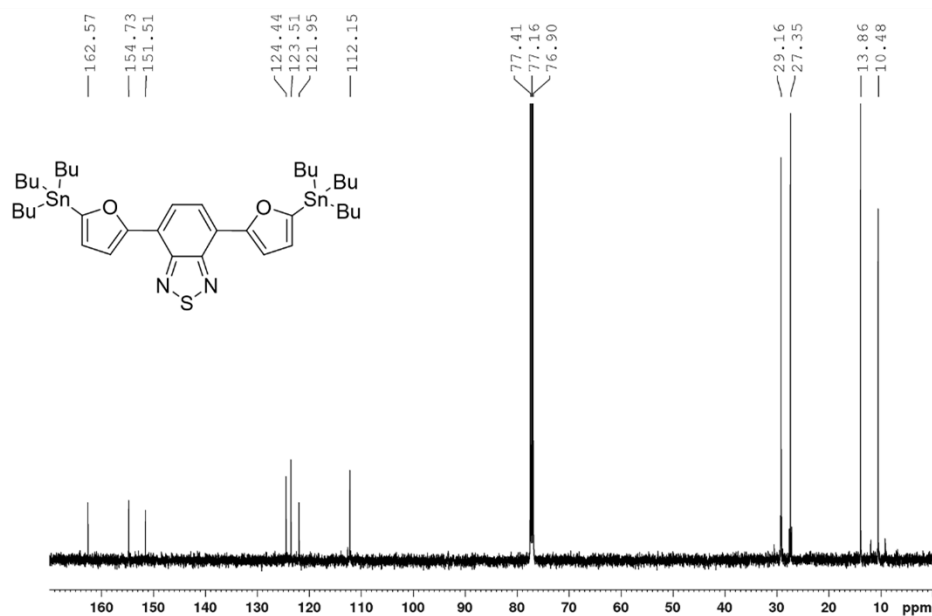
Figure 3.11 ^{13}C NMR of 4,7-bis(5-(tributylstannyl)furan-2yl)benzo[c][1,2,5]thiadiazole

98

TP-BT2T-TP

4,7-bis(5-(trimethylstannyl)thiophen-2yl)benzo[*c*][1,2,5]thiadiazole (0.110 g, 0.18 mmol), Ethyl-2-bromo-4-dodecyl-4*H*-thieno[3,2-*b*]pyrrole-5-carboxylate (0.170 mg, 0.38 mmol), tris(benzylideneacetone)dipalladium(0) (18.3 mg, 0.02 mmol,) tri(*o*-tolyl)phosphine (24.3 mg, 0.08 mmol) were added with anhydrous toluene (20 mL) to a 100 mL three neck round bottomed flask under nitrogen and refluxed for 24 h. Solution mixture was cooled down and added to a beaker containing methanol (100 mL). The precipitated solid was filtered and purified from column chromatography using hexane: methylene chloride (1:1 v/v) as the eluent. The compound was obtained as a magenta solid. (Yield = 0.134 g, 72.8%) ^{1}H NMR (CDCl$_3$, 500 MHz): δ_H 0.87 (t, 6.5 Hz, 3H), 1.25 (br, 18H), 1.38 (t, 2H), 1.81 (m, 2H), 4.31 (q, 7.0 Hz, 2H), 4.44 (t, 7.5 Hz, 2H), 7.07 (s, 1H), 7.13 (s,1H), 7.23 (d, 4.0 Hz, 1H), 7.76 (s, 1H), 7.96 (d, 4.0 Hz, 1H) (Figure 3.12) ^{13}C NMR (CDCl$_3$, 125 MHz): δ_C 14.27, 14.58, 22.84, 27.06, 29.51, 29.54, 29.75, 29.78, 29.79, 29.83, 29.85, 31.32, 32.07, 47.78, 60.27, 106.92, 109.47, 121.42, 124.71, 125.12, 125.45, 126.38, 128.24, 138.39, 139.95, 140.08, 145.09, 152.47, 161.30 (Figure 3.13)
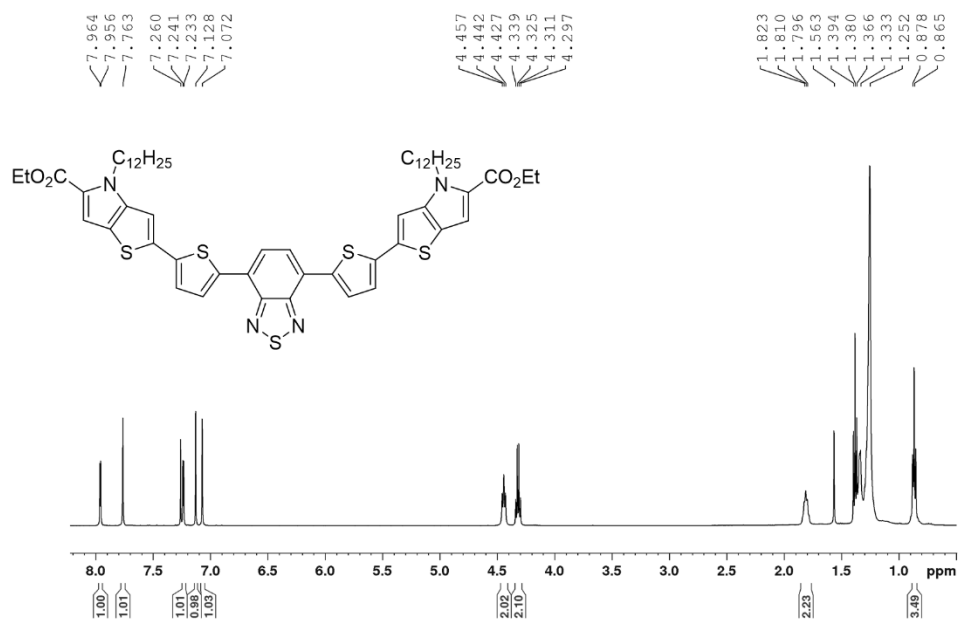
Figure 3.12 ^{1}H NMR spectrum of TP-BT2T-TP
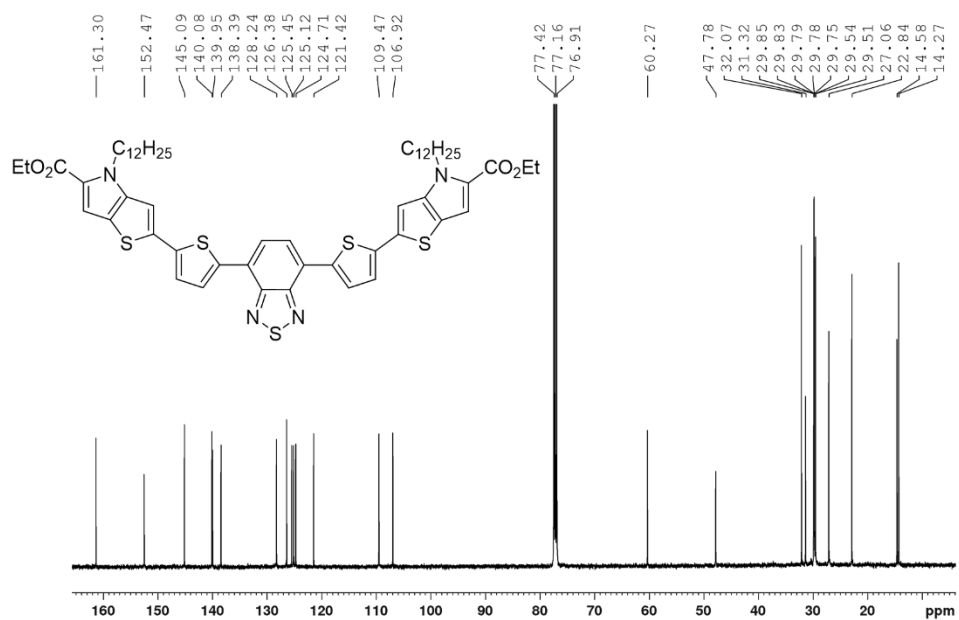
Figure 3.13 ^{13}C NMR spectrum of TP-BT2T-TP

100

TP-BT2F-TP

4,7-bis(5-(tributylstannyl)furan-2yl)benzo[*c*][1,2,5]thiadiazole (0.250 g, 0.30 mmol), Ethyl-2-bromo-4-dodecyl-4*H*-thieno[3,2-*b*]pyrrole-5-carboxylate (0.280 mg, 0.63 mmol), tris(benzylideneacetone)dipalladium(0) (27.5 mg, 0.03 mmol,) tri(*o*-tolyl)phosphine (36.5 mg, 0.12 mmol) were added with anhydrous toluene (20 mL) to a 100 mL three neck round bottomed flask under nitrogen and refluxed for 24 h. Solution mixture was cooled down and added to a beaker containing methanol (100 mL). The dark precipitate was filtered and purified from column chromatography using hexane: ethyl acetate (98:2 v/v and) as the eluent after loading the compound with a small amount of chloroform. The compound was obtained as a magenta solid. (Yield = 0.234 g, 78.8%) ^{1}H NMR (CDCl$_3$, 500 MHz): δ_H 0.85 (t, 7.0 Hz, 3H), 1.25 (br, 18H), 1.39 (t, 7.0 Hz, 2H), 1.83 (m, 2H), 4.33 (q, 7.0 Hz, 2H), 4.47 (t, 7.0 Hz, 2H), 6.74 (d, 3.5 Hz, 1H), 7.16 (s,1H), 7.72 (d, 3.5 Hz, 1H), 8.09 (s, 1H) (Figure 3.14), ^{13}C NMR (CDCl$_3$, 125 MHz): δ_C 14.25, 14.59, 22.83, 2708, 29.50, 29.55, 29.76, 29.79, 29.83, 31.34, 32.06, 47.78, 60.28, 105.90, 109.09, 109.52, 115.04, 121.08, 121.54, 123.33, 126.57, 135.88, 145.12, 149.72, 150.14, 151.41, 161.30 (Figure 3.15)
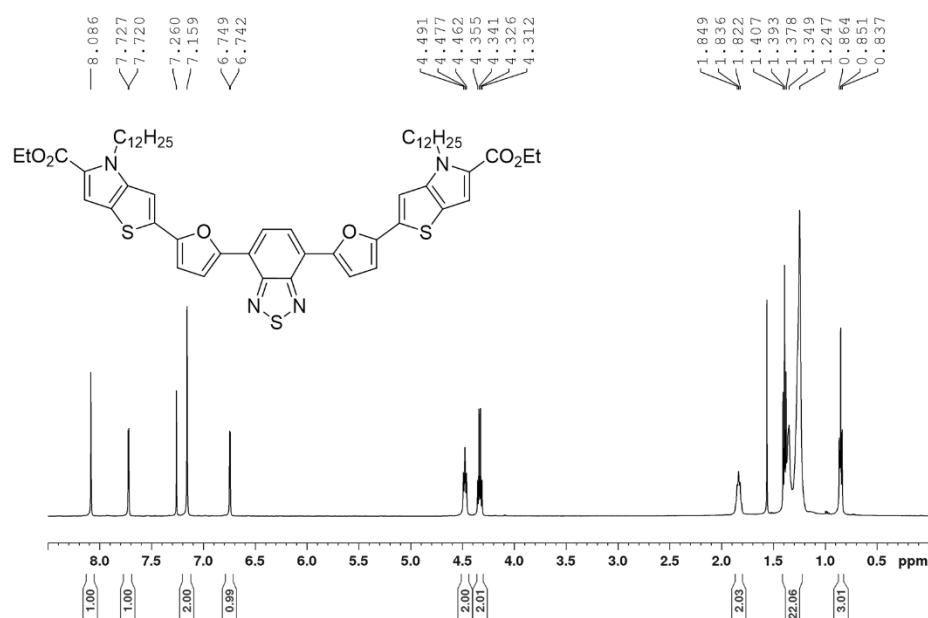
Figure 3.14 ^{1}H NMR spectrum of TP-BT2F-TP
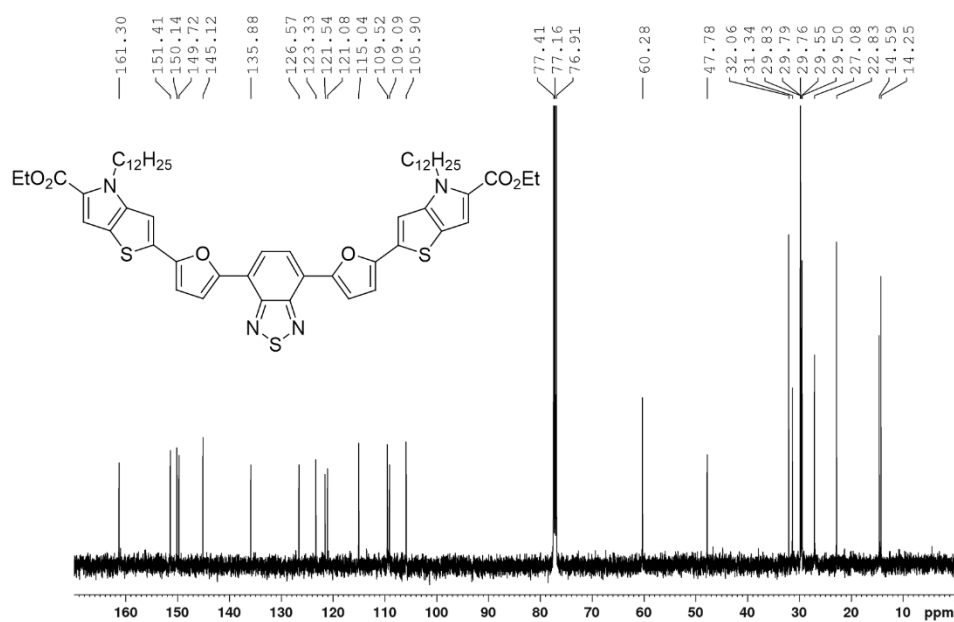
Figure 3.15 ^{13}C NMR spectrum of TP-BT2F-TP

3.4 Results and Discussion

3.4.1 Chemical Synthesis

The synthetic route for the synthesis of TP-BT2T-TP and TP-BT2F-TP is presented in Scheme 3.1. Commercially available 5-bromo-2-thiophenecarboxyaldehyde [1] was subjected to a base-promoted Knoevenagel condensation with ethyl azidoacetate in the presence of ethyl trifluoroacetate as a "sacrificial electrophile".[46] The resulting ethyl 2-azido-3-(5-bromothiophen-2-yl)acrylate [2] was converted to ethyl 2-bromo-4*H*-thieno[3,2-*b*]pyrrole-5-carboxylate [3] by a Hemetsberger cyclization. N-alkylation of [3] was performed by deprotonation of pyrrolic H with K_2CO_3 in DMF with subsequent addition of 1-bromododecane to yield ethyl 2-bromo-4-dodecyl-4*H*-thieno[3,2-*b*]pyrrole-5-carboxylate [4]. BT2T [5] and BT2F [6] were synthesized by reacting 4,7-dibromobenzo[*c*][1,2,5]thiadiazole with 2-(tributylstannyl)thiophene or 2-(trimethylstannyl)furan respectively. BT2T and BT2F were converted to the tin derivatives by reacting them with LDA at -78 °C for 2 h with subsequently quenching in trimethylstannyl chloride or tributylstannyl chloride, respectively. Small molecules TP-BT2T-TP and BT-BT2F-TP were synthesized in good yields (> 70%) by employing a Stille coupling reaction between [4] with either [7] or [8] in the presence of tris(dibenzylideneacetone)dipalladium(0) as the catalyst and tri(*o*-tolyl)phosphine as the ligand. Both small molecules were readily soluble in common organic solvents at room temperature.

Scheme 3.1 Synthetic route towards TP-BT2T-TP and TP-BT2F-TP
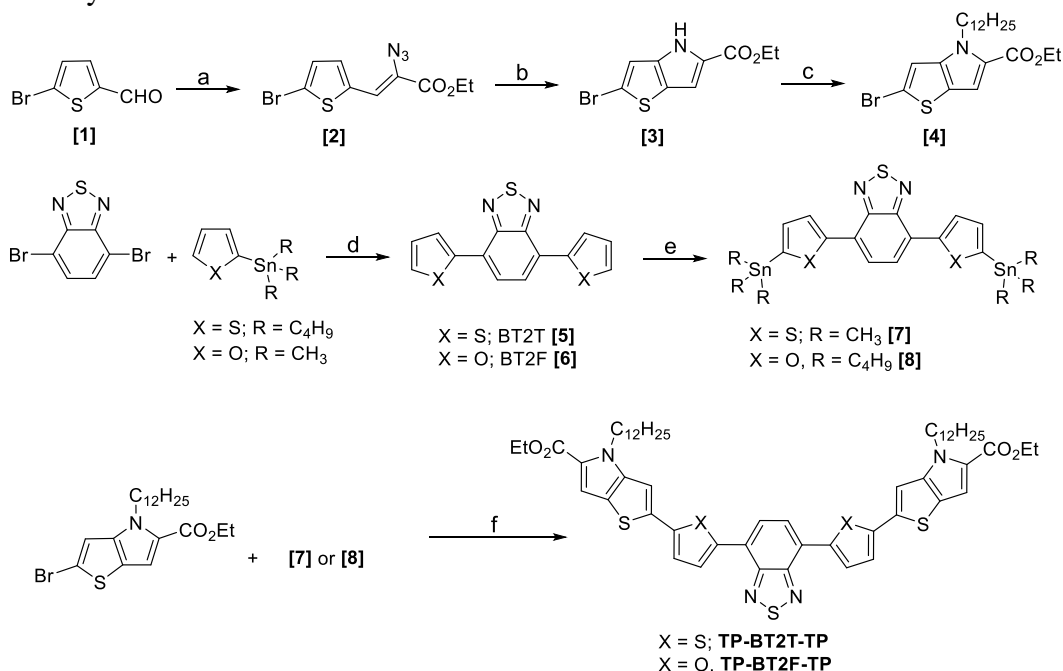
Reaction conditions: (a) ethyl azidoacetate (2 equiv), sodium metal (2 equiv), ethanol (~ 0.55 M), ethyl trifluoroacetate, 6 h, 92.0 %; (b) toluene (~ 0.15 M), reflux, 3 h, 67.9%; (c) anhydrous K_2CO_3 (2 equiv), DMF (~ 0.1 M), 100 °C, 2 h, 1-bromododecane (2 equiv), 12 h, 120 °C, 80.7%, (d) Pd(PPh$_3$)$_4$ (3 mol%), toluene (0.1 M), 12 h, for [6] 70.9%; (e) LDA (6.4 equiv, 2.0 M), THF (0.02 M), -78 °C, 2 h, tributylstannyl chloride (3.0 equiv), for [8] 78.9%; (f) Pd$_2$dba$_3$ (10 mol%), P(*o*-tol)$_3$ (30 mol%), toluene (~ 0.015 M), reflux, 24 h, TP-BT2T-TP; 72.8%, TP-BT2F-TP; 78.8%.

3.4.2 Theoretical Analysis

To gain insights with regard to the torsional effects along the backbone and distribution of HOMO and LUMO, we modeled the structures by density functional theory (DFT) with Spartan′16 at the level of B3LYP/6-31G* and are shown in Figure 3.16. To simplify the calculations, we replaced the dodecyl chains in the structure to methyl groups to get TP-BT2T-TP' and TP-BT2F-TP' (*see* Figure 3.16). According to the energy minimized structures, the dihedral angle between benzothiadiazole and thiophene was 0.66°. As expected, upon changing the flanking group to furan, dihedral angle drops to 0.01° showing minimal torsional effects. On the other hand, the

dihedral angle between thiophene and thieno[3,2-*b*]pyrrole unit is estimated to be around 2.65°, while by the inclusion of furan it drops to 0.04°. To our surprise, torsional effects were not the only changes we could observe from DFT calculations. The backbone curvature also increased from 36° to 61° with the introduction of the furan unit due to shorter C-O bond length (1.37 Å) relative to the C-S bond length in thiophene (1.76 Å). To confirm the DFT calculations, single crystal XRD data were obtained for thiophene and furan flanking benzo[*c*][1,2,5]thiadiazole (BT2T and BT2F) (*see* Figure 3.17). C-S and C-O bond distances in crystal structures were found to be 1.724 Å and 1.381 Å respectively. Due to the shorter bond length of C-O in the furan group, backbone curvature increased from 30° to 46° according to the crystal structure calculations. This observation opens up a new pathway to control the backbone curvature via bond distances rather than changing the bond geometries.[35] HOMO and LUMO are estimated to be similar irrespective of the flanking group and are shown in Figure 3.16. Both small molecules possess similar delocalized HOMO along the backbone, while LUMO is only delocalized in the central benzo[*c*][1,2,5]thiadiazole unit.
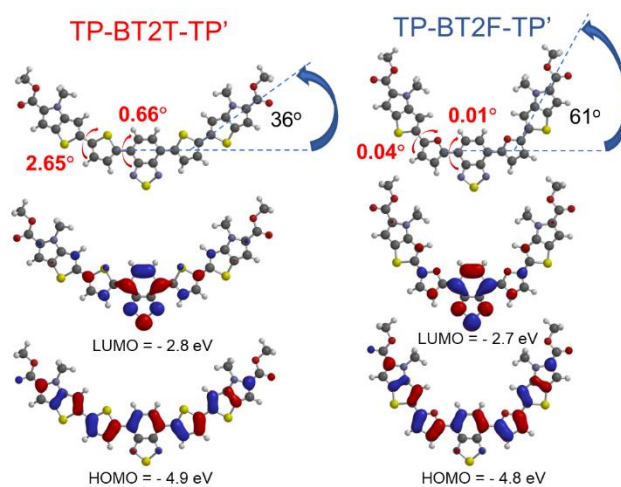
Figure 3.16 Molecular geometries and frontier energy levels calculated from Spartan′16 for TP-BT2T-TP and TP-BT2F-TP
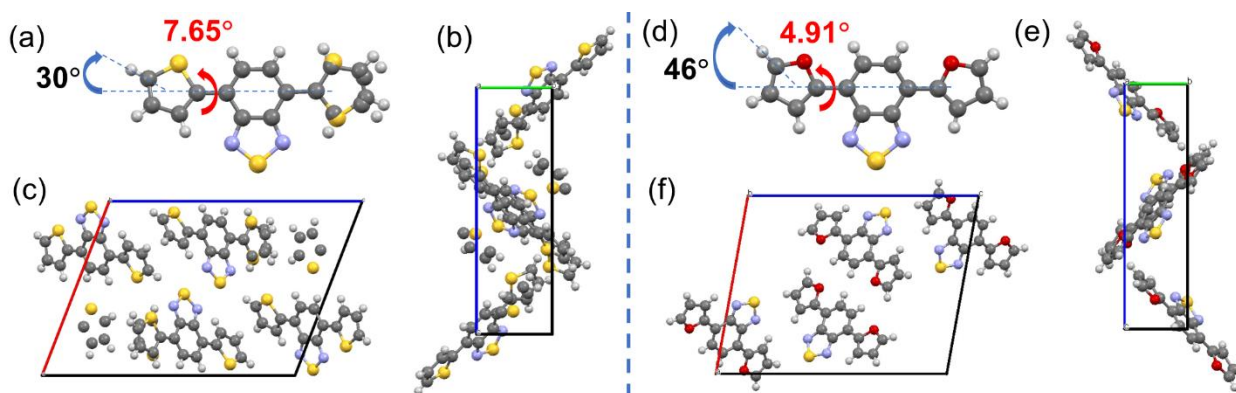
Figure 3.17 (a) Crystal structure of 4,7-di(thiophen-2-yl)benzo[*c*][1,2,5]thiadiazole (BT2T) and molecular stacking viewed along the (b) a axis, (c) b axis; (d) Crystal structure of 4,7-di(furan-2-yl)benzo[*c*][1,2,5]thiadiazole (BT2F) and molecular stacking viewed along the (e) a axis, (f) b axis. Gold ball represents sulfur atom, blue ball represents nitrogen atom, and red ball represents oxygen atom

Crystal data for BT2T (scd 1621, CCDC 1817464): $C_{14}H_8N_2S_3$, $M = 300.40$, Monoclinic, $a = 13.596$ (5) Å, $b = 5.284$ (2) Å, $c = 18.470$ (8) Å, $\beta = 111.132$ (11) °, $V = 1237.7$ (9) Å^3, $T = 100(2)$ K, space group $P2_1/n$, $Z = 4$, μ(MoKα) = 0.58 mm^{-1}, 32577 reflections measured, 2848 independent reflections ($R_{int} = 0.096$). The final R_1 values were 0.051 ($I > 2\sigma(I)$). The final $wR(F^2)$ values were

0.095 ($I > 2\sigma(I)$). The final R_1 values were 0.087 (all data). The final $wR(F^2)$ values were 0.107 (all data). The goodness of fit on F^2 was 1.06.

Crystal data for BT2F (scd 1622, CCDC 1817463): $C_{14}H_8N_2O_2S$, M = 268.28, Monoclinic, a = 14.145 (5) Å, b = 4.5741 (18) Å, c = 18.057 (7) Å, β = 100.225 (10) °, V = 1149.8 (8) Å³, T = 100(2) K, space group $P2_1/n$, Z = 4, μ(MoKα) = 0.28 mm⁻¹, 21015 reflections measured, 2623 independent reflections (R_{int} = 0.050). The final R_1 values were 0.045 ($I > 2\sigma(I)$). The final $wR(F^2)$ values were 0.093 ($I > 2\sigma(I)$). The final R_1 values were 0.066 (all data). The final $wR(F^2)$ values were 0.101 (all data). The goodness of fit on F^2 was 1.04.

3.4.3 Optical, Electrochemical and Molar Mass Analysis

The UV-vis absorption spectra of the two small molecules were measured in dilute chloroform solutions and on drop-casted thin films (Figure 3.18(a) and 3.18(b)). Both in solution and thin films, TP-BT2T-TP and TP-BT2F-TP, showed two different absorption bands which are typical for donor-acceptor small molecules and polymers. In solution, the more intense bands at higher energies (389 nm and 382 nm for TP-BT2T-TP and TP-BT2F-TP respectively) correspond to π-π* transitions, while relatively less intense bands at lower energies (541 nm and 544 nm for TP-BT2T-TP and TP-BT2F-TP respectively) originate from the intramolecular charge transfer (ICT) from delocalized HOMO to central benzo[c][1,2,5]thiadiazole localized LUMO as depicted in Figure 3.16 by DFT calculations. The hypsochromic shift observed for the furan flanked small molecule TP-BT2F-TP as compared to thiophene flanked molecule TP-BT2T-TP is due to higher LUMO level (*see* Table 3.1).[47] Thiophene flanked molecule showed an apparent redshift and broadening in both vibronic peaks (13 nm bathochromic shift for π-π* transitions and 20 nm

bathochromic shift for ICT) in the solid state as compared to solution suggesting a favorable molecular ordering when transitioning from solution to solid state. Surprisingly, TP-BT2F-TP showed a hypsochromic shift (9 nm) for π-π* transitions and a bathochromic shift (6 nm) for ICT. Optical band gaps were calculated to be 1.76 eV and 1.81 eV from the onset at 705 nm and 685 nm for TP-BT2T-TP and TP-BT2F-TP, respectively. Ionization potentials were measured from cyclic voltammetry by using Ag/Ag$^+$ as the reference electrode and tetrabutylammonium hexafluorophosphate as the electrolyte. HOMO and LUMO energy levels were calculated by the following equations: $E_{HOMO} = -(E_{ox} + 4.4)$ eV and $E_{LUMO} = -(E_{red} + 4.4)$ eV. For TP-BT2T-TP, the HOMO and LUMO energy levels are -4.76 eV and -2.86 eV resulting in an electrochemical bandgap of 1.90 eV (*see* Figure 3.19). The HOMO and LUMO energy levels for TP-BT2F-TP are -4.74 eV and -2.81 eV with an electrochemical bandgap of 1.93 eV. Minimal influence on the frontier orbital levels was observed upon changing the flanking group from thiophene to furan. The difference between optical and electrochemical bandgaps was 0.14 eV and 0.12 eV for TP-BT2T-TP and TP-BT2F-TP, respectively. To determine the molecular weights of the small molecules, MALDI-TOF MS was used (*see* Figure 3.18 c and Figure 3.18 d for TP-BT2T-TP and TP-BT2F-TP, respectively). The calculated molecular weight for TP-BT2T-TP and TP-BT2F-TP were 1022.4 g mol^{-1} and 991.3 g mol^{-1}, while MALDI-TOF measurements gave 1022.8 g mol^{-1} and 991.5 g mol^{-1}, respectively with discrepancies less than 0.04%.
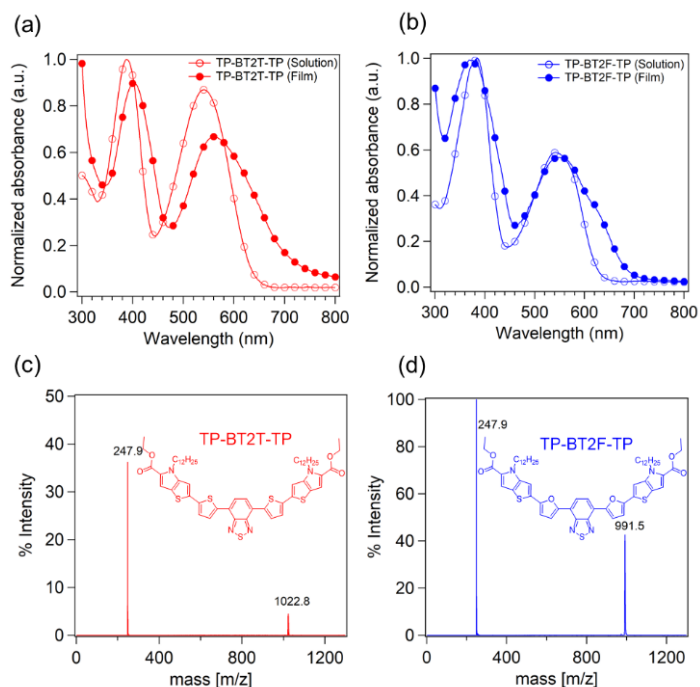
Figure 3.18 (a) UV-vis absorption spectra of TP-BT2T-TP in solution and drop casted thin films, (b) UV-vis absorption spectra of TP-BT2F-TP in solution and drop casted thin films, (c) MALDI-TOF MS spectrum of TP-BT2T-TP, and (d) MALDI-TOF MS spectrum of TP-BT2F-TP
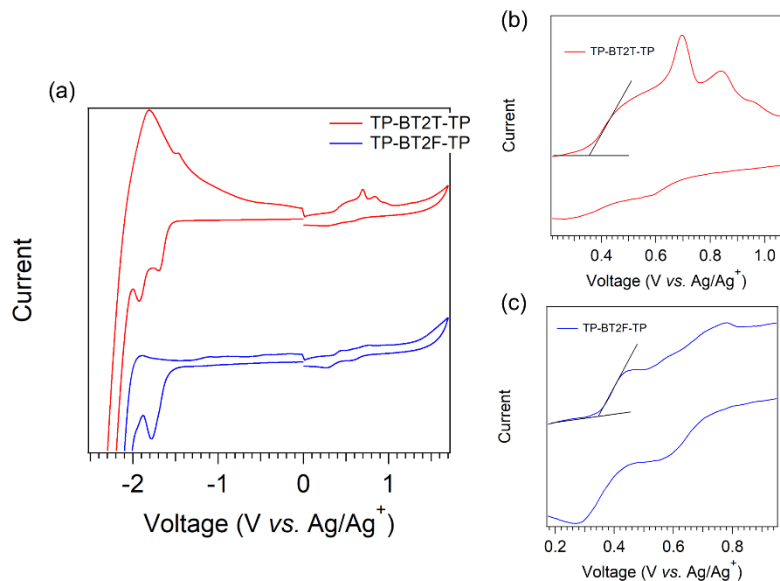
Figure 3.19 (a) Cyclic voltammograms of TP-BT2T-TP and TP-BT2F-TP, (b) Oxidation curve of TP-BT2T-TP and (c) Oxidation curve of TP-BT2F-TP

109

Table 3.1 Optical and electrochemical properties of TP-BT2T-TP and TP-BT2F-TP

Small molecule	HOMO (eV)	LUMO (eV)	E_g^{ec} (eV)	E_g^{opt} (eV)	λ_{max}^{sol} (nm)	λ_{max}^{film} (nm)	λ_{onset} (nm)
TP-BT2T-TP	-4.76	-2.86	1.90	1.76	389, 541	402, 561	705
TP-BT2F-TP	-4.74	-2.81	1.93	1.81	382, 544	373, 550	685

3.4.4 Thermal Properties

Since pyrrolic compounds are often unstable at elevated temperatures,[31-32] small molecules were tested for thermal properties. According to TGA analysis, both small molecules showed excellent thermal stability with significant degradation observed at temperatures above 400 °C (*see* Figure 3.20). Thermal decomposition temperatures (T_d, 5% weight loss) were estimated to be 385.0 °C and 369.8 °C for TP-BT2T-TP and TP-BT2F-TP, respectively. DSC experiments were conducted between 25 °C and 300 °C to gain a better understanding of the thermal properties (*see* Figure 3.21). Sharp first order transitions for melting and cold crystallization were observed for both small molecules which indicated that both molecules are crystalline. TP-BT2T-TP showed a melting point (T_m) at 160.5 °C and a cold crystallization (T_c) peak at 124.0 °C. A slightly lower T_m (158.6 °C) was measured for TP-BT2F-TP while T_c dropped to 105.5 °C from 124.0 °C with the change of the flanking group.
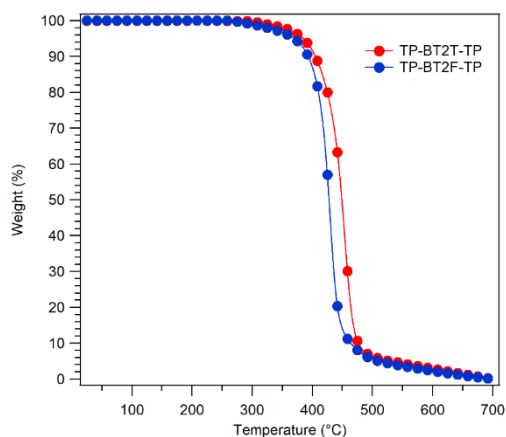
Figure 3.20 TGA thermograms of TP-BT2T-TP and TP-BT2F-TP
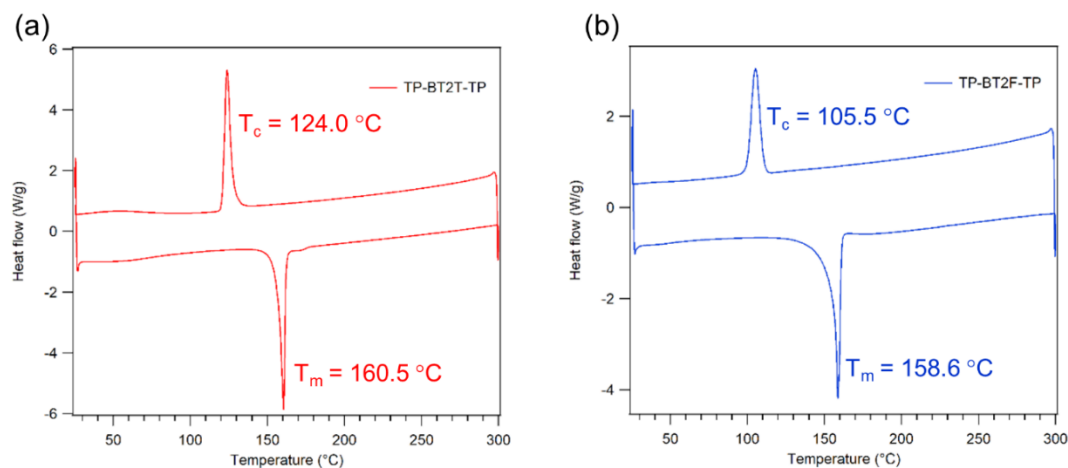
Figure 3.21 DSC thermograms of TP-BT2T-TP and TP-BT2F-TP

3.4.5 OFET Performance

Bottom-gate, bottom-contact (BGBC) field effect transistors were fabricated to probe the charge transport properties of the synthesized small molecules. A drastic difference in hole mobilities was observed for the two small molecules. Transfer curves and output characteristics are outlined for TP-BT2T-TP and TP-BT2F-TP in Figure 3.22 and Figure 3.23, respectively at different annealing conditions. All the OFET parameters are listed under Table 3.2. Without any annealing, TP-BT2T-

TP gave average hole mobility of 2.76×10^{-5} cm^2 /V s, while TP-BT2F-TP gave an average value of 3.76×10^{-6} cm^2 /V s, which is one order of magnitude lower. As shown in Figure 4, after annealing at 60 °C for 5 mins, both small molecules failed to show any improvement in charger carrier mobilities. Surprisingly, thiophene flanked small molecule TP-BT2T-TP showed an increase by three orders of magnitude in charge carrier mobility when annealed at 80 °C for 5 mins to give average hole mobility of 1.81×10^{-2} cm^2 /V s. This hole mobility was further increased up to 6.00×10^{-2} cm^2 /V s by increasing the annealing temperature to 120 °C. After increasing the annealing time to 7.5 mins maximum mobility of 8.00×10^{-2} cm^2 /V s was measured. Interestingly, when the annealing temperature was increased from 60 °C to 120 °C, for every 20 °C increment an order of magnitude change in the on-off current ratio ($I_{on/off}$) was observed. A high I_{on}/I_{off} ~ 10^5 and threshold values (V_T) as low as 4.0-6.5 V were measured for TP-BT2T-TP OFETs annealed at 120 °C. On the other hand, TP-BT2F-TP molecule did not show a significant improvement in mobility when the annealing temperature was changed and remained around 10^{-6} cm^2 /V s with $I_{on}/I_{off} \approx 10^1$ and threshold voltages ranging from -5.0 to 5.0 V until 100 °C. Thin films started to disappear at elevated temperatures (> 110 °C) leaving an OFET inactive material behind. It is noteworthy to mention most high performing polymers, and small molecules show nonlinear behavior when the square root of the drain current is plotted against the gate voltage especially in bottom gate device architectures using self-assembled monolayers to modify the SiO$_2$ gate dielectric. Such non-linear curves result in a debate on proper mobility extraction methods to compensate overestimated mobilities. However, with these two small molecules, such non-linear behavior was not observed, and only one slope was detected when the applied gate voltage was between 5V to 60V.
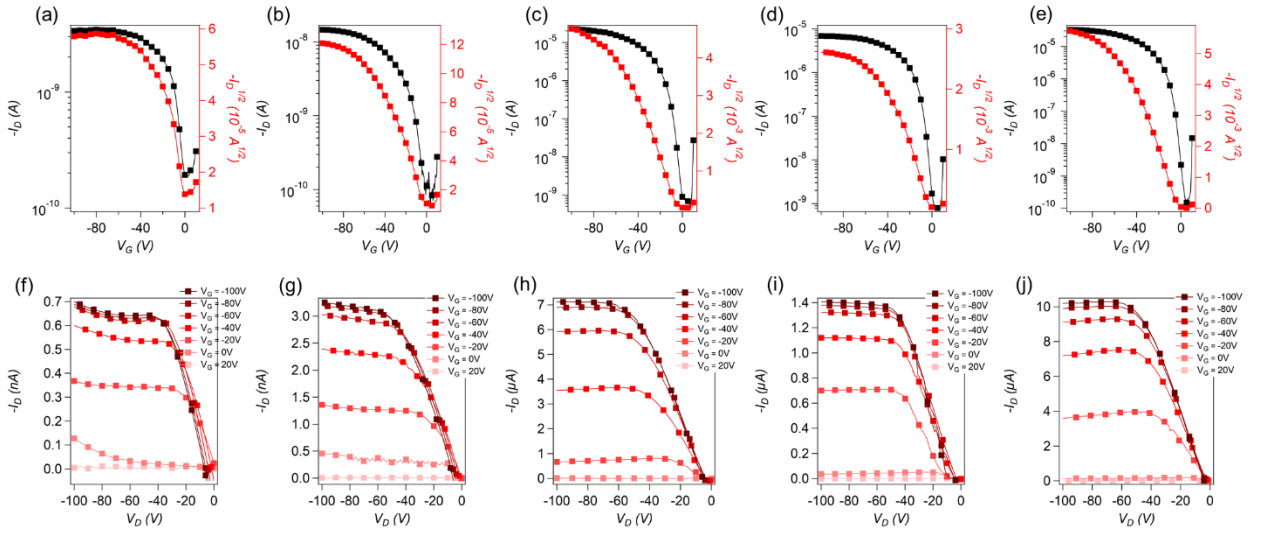
Figure 3.22 Transfer (a, b, c, d and e) and output (f, g, h, i and j) characteristics of TP-BT2T-TP with no annealing (a and f), annealed at 60 °C (b and g), 80 °C (c and h), 100 °C (d and i) and 120 °C (e and j) for 5 mins.
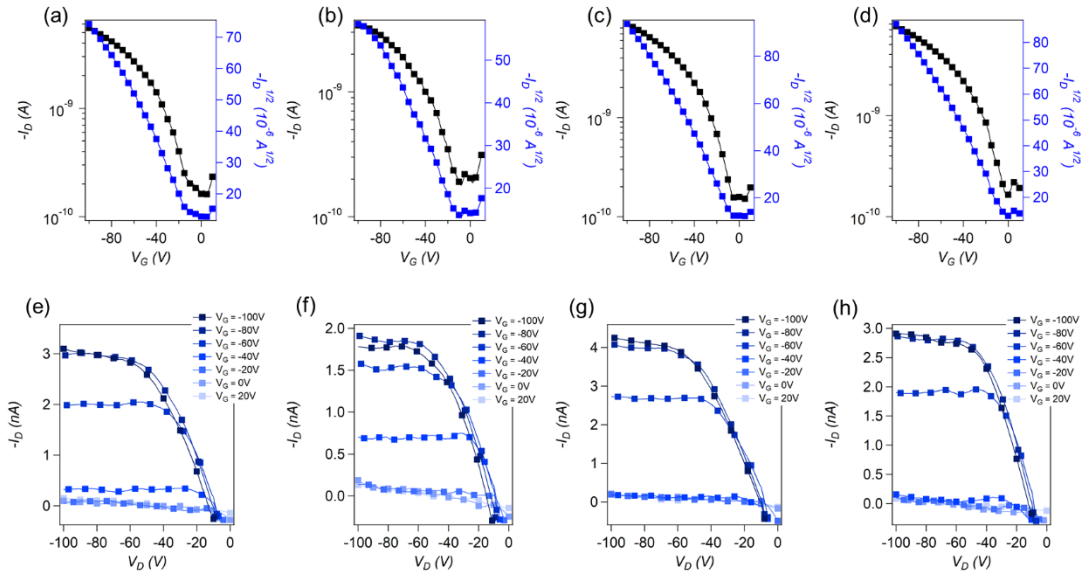
Figure 3.23 Transfer (a, b, c and d) and output (e, f, g and h) characteristics of TP-BT2F-TP with no annealing (a and e), annealed at 60 °C (b and f), 80 °C (c and g), and 100 °C (d and h) for 5 mins.

113

Table 3.2 The summary of OFET performance of TP-BT2T-TP and TP-BT2F-TP

Small molecule	Annealing temperature	μ_{max} (cm^2 /V s)	μ_{ave} (cm^2 /V s)	V_{T} (V)	$I_{\text{on}}/I_{\text{off}}$
TP-BT2T-TP	none	3.88×10^{-5}	2.76×10^{-5}	-0.5 – 0.5	$> 10^1$
	60 °C	5.98×10^{-5}	2.76×10^{-5}	-2.5 – 1.0	$> 10^2$
	80 °C	2.01×10^{-2}	1.81×10^{-2}	-5.5 – -0.5	$> 10^3$
	100 °C	4.27×10^{-2}	3.86×10^{-2}	-3.0 – -1.5	$> 10^4$
	120 °C	6.03×10^{-2}	5.75×10^{-2}	-3.0 – -1.0	$> 10^5$
TP-BT2F-TP	none	4.42×10^{-6}	3.76×10^{-6}	-15.0 – -8.5	$> 10^1$
	60 °C	3.65×10^{-6}	2.26×10^{-6}	-15.0 – -8.0	$> 10^1$
	80 °C	7.11×10^{-6}	5.36×10^{-6}	-9.0 – -5.0	$> 10^1$
	100 °C	6.87×10^{-6}	5.05×10^{-6}	-5.0 - -1.5	$> 10^1$

3.4.6 Crystallinity

Since two small molecules showed a striking difference in hole mobilities after annealing, we investigated the thin film crystallinity using out-of-plane GIXRD on the devices. Recorded GIXRD are on devices before and after annealing at 120 °C for 5 mins for TP-BT2T-TP and 100 °C for 5 mins for TP-BT2F-TP (*see* Figure 3.24). Without annealing, both small molecules did not show any diffraction suggesting no ordering in the thin films. This observation was further confirmed by very low mobilities extracted from transfer plots. Upon annealing for 120 °C for 5 mins, TP-BT2T-TP showed sharp Bragg reflection peaks (100), (200), (300) and (400) which represent highly ordered films. The thermal annealing-induced crystallinity explains the high hole mobility. Corresponding lamellar packing distance for TP-BT2T-TP is presented in Table 3.3. By contrast, TP-BT2F-TP showed minimal changes in the GIXRD pattern and stayed unordered even after thermal annealing at 100 °C for 5 mins.
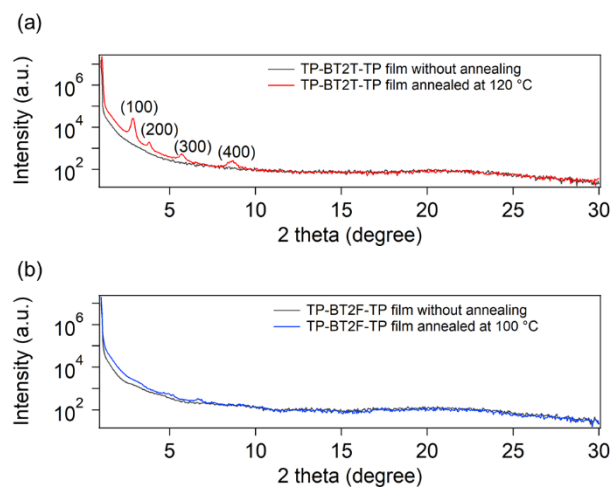
Figure 3.24 GIXRD out-of-plane measurements of thin films of (a) TP-BT2T-TP and (b) TP-BT2F-TP (b) with and without annealing prepared on OTS treated SiO_2 substrates

Table 3.3 XRD peak assignments for TP-BT2T-TP thin films

Small molecule	peaks	2θ (degrees)	d-Spacing (Å)
	(100)	2.85	30.96
TP-BT2T-TP	(200)	3.80	23.22
	(300)	5.70	15.49
	(400)	8.70	10.15

3.4.7 Surface Morphology

To probe the surface morphology in both small molecules, TMAFM images were recorded in the channel region of the OFET devices. As shown in Figure 3.25, more apparent changes in the morphology of both small molecules were observed before and after annealing. However, for TP-BT2T-TP the changes were significant (RMS value before and after annealing at 120 °C are 0.16 nm and 7.24 nm respectively) with more granular texture as compared to TP-BT2F-TP (RMS values before and after annealing at 100 °C are 1.88 nm and 3.43 nm respectively). The drastic

mobility increase for TP-BT2T-TP when the thin film was annealed from 60 °C to 80 °C could be explained by the morphological transformation observed in Figure 3.25.
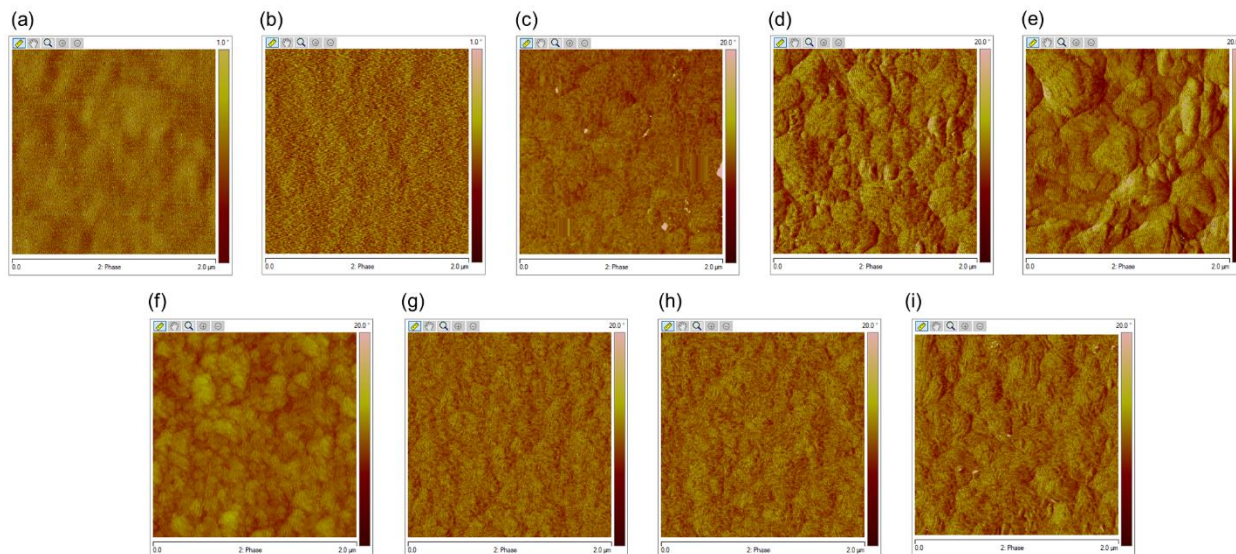
Figure 3.25 TMAFM images of TP-BT2T-TP annealed at (a) 25 °C; (b) 60 °C; (c) 80 °C, (d) 100 °C; (e) 120 °C and TP-BT2F-TP annealed at (f) 25 °C; (g) 60 °C; (h) 80 °C; (i) 100 °C for 5 mins.

3.5 Conclusions

Two solution-processable banana shaped thieno[3,2-*b*]pyrrole containing small molecules were successfully synthesized. Although both flanking groups have similar geometries, due to the shorter bond length of C-O in furan, TP-BT2F-TP molecule showed a higher degree of curvature predicted from DFT calculations. Despite similar frontier energy levels, due to both heteroatom effect and larger backbone curvature, furan containing small molecule showed poor stability and performance in OFET devices, while TP-BT2T-TP showed relatively high hole mobility of 0.08 cm^2/V s when thin films were annealed at 120 °C. The high hole mobility was achieved due to the thermal annealing-induced crystallinity in the thin film confirmed by out-of-plane GIXRD and

116

TMAFM analysis. In summary, our results show that non-conventional thieno[3,2-*b*]pyrrole building block could be used to develop high mobility p-type OFETs. Moreover, this study can be used to guide the design of semiconducting materials strategically toward high mobility solution processable small molecules. It is noteworthy to mention that the degree of curvature in organic semiconductors could also be altered without using molecules having different geometries. We believe our findings would encourage to seek more non-conventional building blocks that could be used toward high performing solution processable small molecule field effect transistors.

3.6 Acknowledgments

3.7 References

1. Mei, J.; Diao, Y.; Appleton, A. L.; Fang, L.; Bao, Z. Integrated Materials Design of Organic Semiconductors for Field-Effect Transistors. *J. Am. Chem. Soc.* **2013,** *135* (18), 6724-6746.

2. Ong, B. S.; Wu, Y.; Liu, P.; Gardner, S. High-Performance Semiconducting Polythiophenes for Organic Thin-Film Transistors. *J. Am. Chem. Soc.* **2004,** *126* (11), 3378-3379.

3. McCulloch, I.; Heeney, M.; Bailey, C.; Genevicius, K.; MacDonald, I.; Shkunov, M.; Sparrowe, D.; Tierney, S.; Wagner, R.; Zhang, W.; Chabinyc, M. L.; Kline, R. J.; McGehee, M. D.; Toney, M. F. Liquid-crystalline semiconducting polymers with high charge-carrier mobility. *Nat. Mater.* **2006,** *5*, 328.

4. Amin, A. Y.; Khassanov, A.; Reuter, K.; Meyer-Friedrichsen, T.; Halik, M. Low-Voltage Organic Field Effect Transistors with a 2-Tridecyl[1]benzothieno[3,2-*b*][1]benzothiophene Semiconductor Layer. *J. Am. Chem. Soc.* **2012,** *134* (40), 16548-16550.

5. Minemawari, H.; Yamada, T.; Matsui, H.; Tsutsumi, J. y.; Haas, S.; Chiba, R.; Kumai, R.; Hasegawa, T. Inkjet printing of single-crystal films. *Nature* **2011,** *475*, 364.

6. Li, J.; Zhao, Y.; Tan, H. S.; Guo, Y.; Di, C.-A.; Yu, G.; Liu, Y.; Lin, M.; Lim, S. H.; Zhou, Y.; Su, H.; Ong, B. S. A stable solution-processed polymer semiconductor with record high-mobility for printed transistors. *Sci. Rep.* **2012,** *2*, 754.

7. Li, Y.; Singh, S. P.; Sonar, P. A High Mobility P-Type DPP-Thieno[3,2-*b*]thiophene Copolymer for Organic Thin-Film Transistors. *Adv. Mater.* **2010,** *22* (43), 4862-4866.

8. Li, W.; Hendriks, K. H.; Roelofs, W. S. C.; Kim, Y.; Wienk, M. M.; Janssen, R. A. J. Efficient Small Bandgap Polymer Solar Cells with High Fill Factors for 300 nm Thick Films. *Adv. Mater.* **2013,** *25* (23), 3182-3186.

9. Kline, R. J.; McGehee, M. D.; Kadnikova, E. N.; Liu, J.; Fréchet, J. M. J. Controlling the Field-Effect Mobility of Regioregular Polythiophene by Changing the Molecular Weight. *Adv. Mater.* **2003,** *15* (18), 1519-1522.

10. Zen, A.; Pflaum, J.; Hirschmann, S.; Zhuang, W.; Jaiser, F.; Asawapirom, U.; Rabe, J. P.; Scherf, U.; Neher, D. Effect of Molecular Weight and Annealing of Poly(3-hexylthiophene)s on the Performance of Organic Field-Effect Transistors. *Adv. Funct. Mater.* **2004,** *14* (8), 757-764.

11. Kline, R. J.; McGehee, M. D.; Kadnikova, E. N.; Liu, J.; Fréchet, J. M. J.; Toney, M. F. Dependence of Regioregular Poly(3-hexylthiophene) Film Morphology and Field-Effect Mobility on Molecular Weight. *Macromolecules* **2005,** *38* (8), 3312-3319.

12. Zhang, R.; Li, B.; Iovu, M. C.; Jeffries-El, M.; Sauvé, G.; Cooper, J.; Jia, S.; Tristram-Nagle, S.; Smilgies, D. M.; Lambeth, D. N.; McCullough, R. D.; Kowalewski, T. Nanostructure Dependence of Field-Effect Mobility in Regioregular Poly(3-hexylthiophene) Thin Film Field Effect Transistors. *J. Am. Chem. Soc.* **2006,** *128* (11), 3480-3481.

13. Briseno, A. L.; Tseng, R. J.; Ling, M. M.; Falcao, E. H. L.; Yang, Y.; Wudl, F.; Bao, Z. High-Performance Organic Single-Crystal Transistors on Flexible Substrates. *Adv. Mater.* **2006,** *18* (17), 2320-2324.

14. Kim, Y.-H.; Yoo, B.; Anthony, J. E.; Park, S. K. Controlled Deposition of a High-Performance Small-Molecule Organic Single-Crystal Transistor Array by Direct Ink-Jet Printing. *Adv. Mater.* **2012,** *24* (4), 497-502.

15. Goto, O.; Tomiya, S.; Murakami, Y.; Shinozaki, A.; Toda, A.; Kasahara, J.; Hobara, D. Organic Single-Crystal Arrays from Solution-Phase Growth Using Micropattern with Nucleation Control Region. *Adv. Mater.* **2012,** *24* (8), 1117-1122.

16. Lim, B.; Sun, H.; Lee, J.; Noh, Y.-Y. High Performance Solution Processed Organic Field Effect Transistors with Novel Diketopyrrolopyrrole-Containing Small Molecules. *Sci. Rep.* **2017,** *7* (1), 164.

17. Afzali, A.; Dimitrakopoulos, C. D.; Breen, T. L. High-Performance, Solution-Processed Organic Thin Film Transistors from a Novel Pentacene Precursor. *J. Am. Chem. Soc.* **2002,** *124* (30), 8812-8813.

18. Meng, H.; Zheng, J.; Lovinger, A. J.; Wang, B.-C.; Van Patten, P. G.; Bao, Z. Oligofluorene−Thiophene Derivatives as High-Performance Semiconductors for Organic Thin Film Transistors. *Chem. Mater.* **2003,** *15* (9), 1778-1787.

19. Kang, M. J.; Doi, I.; Mori, H.; Miyazaki, E.; Takimiya, K.; Ikeda, M.; Kuwabara, H. Alkylated Dinaphtho[2,3-*b*:2′,3′-*f*]Thieno[3,2-*b*]Thiophenes (Cn-DNTTs): Organic Semiconductors for High-Performance Thin-Film Transistors. *Adv. Mater.* **2011,** *23* (10), 1222-1225.

20. Jurchescu, O. D.; Popinciuc, M.; van Wees, B. J.; Palstra, T. T. M. Interface-Controlled, High-Mobility Organic Transistors. *Adv. Mater.* **2007,** *19* (5), 688-692.

21. Takeyama, Y.; Ono, S.; Matsumoto, Y. Organic single crystal transistor characteristics of single-crystal phase pentacene grown by ionic liquid-assisted vacuum deposition. *Appl. Phys. Lett.* **2012,** *101* (8), 083303.

22. Nenajdenko, V. G.; Sumerin, V. V.; Chernichenko, K. Y.; Balenkova, E. S. A New Route to Annulated Oligothiophenes. *Org. Lett.* **2004,** *6* (20), 3437-3439.

23. Takimiya, K.; Kunugi, Y.; Konda, Y.; Niihara, N.; Otsubo, T. 2,6-Diphenylbenzo[1,2-b:4,5-b']dichalcogenophenes: A New Class of High-Performance Semiconductors for Organic Field-Effect Transistors. *J. Am. Chem. Soc.* **2004,** *126* (16), 5084-5085.

24. Pan, H.; Li, Y.; Wu, Y.; Liu, P.; Ong, B. S.; Zhu, S.; Xu, G. Low-Temperature, Solution-Processed, High-Mobility Polymer Semiconductors for Thin-Film Transistors. *J. Am. Chem. Soc.* **2007,** *129* (14), 4112-4113.

25. Zhang, M.; Tsao, H. N.; Pisula, W.; Yang, C.; Mishra, A. K.; Müllen, K. Field-Effect Transistors Based on a Benzothiadiazole−Cyclopentadithiophene Copolymer. *J. Am. Chem. Soc.* **2007,** *129* (12), 3472-3473.

26. Tsao, H. N.; Cho, D. M.; Park, I.; Hansen, M. R.; Mavrinskiy, A.; Yoon, D. Y.; Graf, R.; Pisula, W.; Spiess, H. W.; Müllen, K. Ultrahigh Mobility in Polymer Field-Effect Transistors by Design. *J. Am. Chem. Soc.* **2011,** *133* (8), 2605-2612.

27. Usta, H.; Lu, G.; Facchetti, A.; Marks, T. J. Dithienosilole− and Dibenzosilole−Thiophene Copolymers as Semiconductors for Organic Thin-Film Transistors. *J. Am. Chem. Soc.* **2006,** *128* (28), 9034-9035.

28. Ogawa, K.; Rasmussen, S. C. A Simple and Efficient Route to *N*-Functionalized Dithieno[3,2-*b*:2',3'-*d*]pyrroles: Fused-Ring Building Blocks for New Conjugated Polymeric Systems. *J. Org. Chem.* **2003,** *68* (7), 2921-2928.

29. Liu, J.; Zhang, R.; Sauvé, G.; Kowalewski, T.; McCullough, R. D. Highly Disordered Polymer Field Effect Transistors: N-Alkyl Dithieno[3,2-*b*:2′,3′-*d*]pyrrole-Based Copolymers with Surprisingly High Charge Carrier Mobilities. *J. Am. Chem. Soc.* **2008,** *130* (39), 13167-13176.

30. Yamamoto, T.; Takimiya, K. Facile Synthesis of Highly π-Extended Heteroarenes, Dinaphtho[2,3-*b*:2',3'-*f*]chalcogenopheno[3,2-*b*]chalcogenophenes, and Their Application to Field-Effect Transistors. *J. Am. Chem. Soc.* **2007,** *129* (8), 2224-2225.

31. Cordell, G. A. 2-Halopyrroles. Synthesis and chemistry. *J. Org. Chem.* **1975,** *40* (22), 3161-3169.

32. Nguyen, H. Q.; Rainbolt, E. A.; Sista, P.; Stefan, M. C. Synthesis and Polymerization of Fused-Ring Thienodipyrrole Monomers. *Macromol. Chem. Phys.* **2012,** *213* (4), 425-430.

33. Hendriks, K. H.; Li, W.; Wienk, M. M.; Janssen, R. A. J. Small-Bandgap Semiconducting Polymers with High Near-Infrared Photoresponse. *J. Am. Chem. Soc.* **2014,** *136* (34), 12130-12136.

34. Jones, C.; Boudinet, D.; Xia, Y.; Denti, M.; Das, A.; Facchetti, A.; Driver, T. G. Synthesis and Properties of Semiconducting Bispyrrolothiophenes for Organic Field-Effect Transistors. *Chem. E. J.* **2014,** *20* (20), 5938-5945.

35. Rieger, R.; Beckmann, D.; Mavrinskiy, A.; Kastler, M.; Müllen, K. Backbone Curvature in Polythiophenes. *Chem. Mater.* **2010,** *22* (18), 5314-5318.

36. Thisayukta, J.; Niwano, H.; Takezoe, H.; Watanabe, J. Enhancement of Twisting Power in the Chiral Nematic Phase by Introducing Achiral Banana-Shaped Molecules. *J. Am. Chem. Soc.* **2002,** *124* (13), 3354-3358.

37. Tang, Y.; Wang, Y.; Wang, G.; Wang, H.; Wang, L.; Yan, D. Vacuum-Deposited Submonolayer Thin Films of a Three-Ring Bent-Core Compound. *J. Phys. Chem. B* **2004,** *108* (34), 12921-12926.

38. Huang, C.-F.; Wu, S.-L.; Huang, Y.-F.; Chen, Y.-C.; Chang, S.-T.; Wu, T.-Y.; Wu, K.-Y.; Chuang, W.-T.; Wang, C.-L. Packing Principles for Donor–Acceptor Oligomers from Analysis of Single Crystals. *Chem. Mater.* **2016,** *28* (15), 5175-5190.

39. Du, J.; Fortney, A.; Washington, K. E.; Biewer, M. C.; Kowalewski, T.; Stefan, M. C. Benzo[1,2-*b*:4,5-*b'*]]difuran and furan substituted diketopyrrolopyrrole alternating copolymer for organic photovoltaics with high fill factor. *J. Mater. Chem. A* **2017,** *5* (30), 15591-15600.

40. Du, J.; Bulumulla, C.; Mejia, I.; McCandless, G. T.; Biewer, M. C.; Stefan, M. C. Evaluation of (E)-1,2-di(furan-2-yl)ethene as building unit in diketopyrrolopyrrole alternating copolymers for transistors. *Polym. Chem.* **2017,** *8* (39), 6181-6187.

41. Heiskanen, J. P.; Vivo, P.; Saari, N. M.; Hukka, T. I.; Kastinen, T.; Kaunisto, K.; Lemmetyinen, H. J.; Hormi, O. E. O. Synthesis of Benzothiadiazole Derivatives by Applying C–C Cross-Couplings. *J. Org. Chem.* **2016,** *81* (4), 1535-1546.

42. Mulherin, R. C.; Jung, S.; Huettner, S.; Johnson, K.; Kohn, P.; Sommer, M.; Allard, S.; Scherf, U.; Greenham, N. C. Ternary Photovoltaic Blends Incorporating an All-Conjugated Donor– Acceptor Diblock Copolymer. *Nano Lett.* **2011,** *11* (11), 4846-4851.

43. Kusuhara, N.; Sugano, Y.; Takagi, H.; Yamamura, K.; Miyake, H. A facile synthesis of β-(4-azuleno[1,2-*b*]thienyl) α,β-unsaturated ketones. *Chem. Comm.* **1997,** (20), 1951-1952.

44. Biniek, L.; Chochos, C. L.; Leclerc, N.; Boyron, O.; Fall, S.; Lévèque, P.; Heiser, T. 3,6-Dialkylthieno[3,2-*b*]thiophene moiety as a soluble and electron donating unit preserving the coplanarity of photovoltaic low band gap copolymers. *J. Polym. Sci. Part A: Polym. Chem.* **2012,** *50* (9), 1861-1868.

45. Ito, Y.; Virkar, A. A.; Mannsfeld, S.; Oh, J. H.; Toney, M.; Locklin, J.; Bao, Z. Crystalline Ultrasmooth Self-Assembled Monolayers of Alkylsilanes for Organic Field-Effect Transistors. *J. Am. Chem. Soc.* **2009,** *131* (26), 9396-9404.

46. Heaner Iv, W. L.; Gelbaum, C. S.; Gelbaum, L.; Pollet, P.; Richman, K. W.; DuBay, W.; Butler, J. D.; Wells, G.; Liotta, C. L. Indoles via Knoevenagel-Hemetsberger reaction sequence. *RSC Adv.* **2013,** *3* (32), 13232-13242.

47. Du, J.; Fortney, A.; Washington, K. E.; Bulumulla, C.; Huang, P.; Dissanayake, D.; Biewer, M. C.; Kowalewski, T.; Stefan, M. C. Systematic Investigation of Benzodithiophene-Benzothiadiazole Isomers for Organic Photovoltaics. *ACS Appl. Mater. Interfaces* **2016,** *8* (48), 33025-33033.

CHAPTER 4

INCORPORATION OF THIENO[3,2-*b*]PYRROLE INTO DIKETOPYRROLOPYRROLE-BASED COPOLYMERS FOR EFFICIENT ORGANIC FIELD EFFECT TRANSISTORS

Authors – Chandima Bulumulla,[†] Ruvanthi N. Kularatne,[†] Ruwan Gunawardhana,[†]

Hien Q. Nguyen,[†] Gregory T. McCandless,[†] Michael C. Biewer,[†]

and Mihaela C. Stefan[†*]

[†]Department of Chemistry and Biochemistry, BE26

The University of Texas at Dallas

800 West Campbell Road

Richardson, Texas 75080, USA

[*]Department of Bioengineering, BSB11

The University of Texas at Dallas

800 West Campbell Road

Richardson, Texas 75080, USA

4.1 Abstract

Recent advancements in organic field effect transistors have switched chemists focus from synthesizing libraries of organic semiconductors to a targeted approach where chemical alterations are performed on known semiconductors to further improve electrical properties. Among successful semiconducting polymer candidates, diketopyrrolopyrrole-thieno[3,2-*b*]thiophene copolymer has been subjected to receive modifications on the diketopyrrolopyrrole unit via flanking groups and side chain engineering. Thieno[3,2-*b*]thiophene moiety, however, has seen minimal modifications due to the limited number of modifying sites. Isoelectronic thieno[3,2-*b*]pyrrole could serve as an alternative since it is easily tunable via N-alkylation reactions. Therefore, for the first time, we report the replacement of the thieno[3,2-*b*]thiophene unit of with thieno[3,2-*b*]pyrrole unit and its performance on p-channel field effect transistors. The copolymer exhibits linear characteristics to obtain average hole mobility of 0.12 cm^2 /V s in bot-tom-gate/top-contact field effect transistors with threshold voltages as low as 0 V. These preliminary results highlight the potential of thieno[3,2-*b*]pyrrole monomer for utilization in organic field effect transistors.

4.2 Introduction

Over the past two decades, organic semiconducting polymers have emerged to become promising candidates for organic field effect transistors (OFETs) due to solution processability, mechanical flexibility and low manufacturing cost compared to silicon electronics.[1-5] Hole mobilities (μ_h) in OFETs have constantly improved over time mainly owing to the intensive research carried out on novel polymer backbones,[6-8] side chain engineering,[9-12] and nonsynthetic approaches.[13, 14] Out of

the above mentioned methods, developing novel polymer backbones have been the main driving force behind exceeding the performance of amorphous silicon ($\sim 0.1 - 1.0$ cm^2 /V s).

Transition from first generation homopolymers[15] to second generation copolymers consisting of fused-ring systems,[16-20] strategically paved the path toward high performing polymers for OFETs. Among many fused ring systems, thieno[3,2-*b*]thiophene (TT) is recognized as an efficient and stable building block for polymer OFETs.[21-24] Owing to the larger resonance stabilization energy of TT, the delocalization of π-electrons are less favored. Since TT possess a central cross-conjugated double bond, π orbital overlap is reduced to present more rotational freedom for the neighboring groups.[24-26] This phenomena increases the ionization potential which leads to stable material compared to first generation polythiophenes. McCullough et al. showed that the copolymer of bithiophene and thieno[3,2-*b*]thiophene (TT) could lead to hole mobilities between $0.15 - 0.6$ cm^2 /V s compared to $\sim 10^{-2} - 10^{-3}$ cm^2 /V s of conventional poly(3-hexylthiophene).[25, 27]

Third generation polymer OFETs were constructed by using a donor-acceptor (D-A) architecture.[19, 28-31] While many D-A polymer systems were studied, in recent years alternating copolymer [P(DPP-TT)] made from diketopyrrolopyrrole (DPP) and TT monomer have received significant attention due to the exceptionally high hole mobilities.[32-34] Instead of synthesizing a plethora of polymers, many scientists now try to utilize this polymer backbone as a platform to study and improve physiochemical and electronic properties in polymer OFETs. Several studies have shown the impact of side chain engineering and flanking group modifications toward FET performance.[33, 35-39] By varying chain lengths and pushing the branching point away from the polymer backbone, better electrical properties in OFETs have been observed. Interestingly, non-

synthetic approaches have also emerged to improve mobilities. An increase in hole mobilities in OFETs have achieved via the addition of an ionic additive, however this method only works best with the P(DPP-TT) system.[13] Thus, it is extremely important to understand structure-property relationships via chemical modifications. Since all the chemical modifications were executed on the DPP unit, we decided to replace the symmetric TT unit with an asymmetric, yet isoelectronic thieno[3,2-*b*]pyrrole (TP) unit. Over the past decade, regioregular polymer backbones were exclusively studied for organic electronic applications. In recent reports, however, asymmetric monomers have been employed in semiconducting polymers instead of symmetric monomers due the large interest in tuning physiochemical properties.[38, 40-43]

Compared to TT, TP is a more electron rich moiety and it is more amenable for side chain engineering via N-alkylations. Upon polymerizing highly electron rich TP with electron deficient DPP, intermolecular interactions are expected to enhance by reducing the distance between polymer chains.[32] One of the concerns of employing electron rich pyrrole monomers is the high reactivity to cause oxidization and degradation. Although pyrrole has a low ionization potential, previous reports of small molecules bearing TP have shown HOMO levels below 4.8 eV.[44] In our group, we have previously shown that TP monomer is stable enough for electronic applications and it has the potential to be one of the high performing semiconductor building block for solution processable small molecule OFETs. Small molecules were synthesized however, by intentionally functionalizing the 5 position of TP with an ester group. In this article, we report the utilization of the TP unit for semiconducting polymers by removing the ester linkage and converting to the 2,5-distannylated derivative to polymerize with 3,6-bis(5-bromothiophen-2-yl)-2,5-bis(2-octyldodecyl)pyrrolo[3,4-*c*]pyrrole-1,4(2*H*,5*H*)-dione to obtain P(DPP-TP).
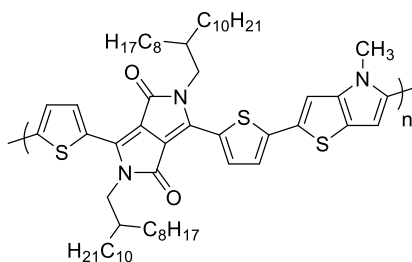
Figure 4.1 Chemical structure of P(DPP-TP)

4.3 Experimental

4.3.1 Materials and Methods

All the commercial chemicals were purchased from Fischer Scientific and Aldrich and were utilized without further purification unless otherwise noted. 3,6-Bis(5-bromothiophen-2-yl)-2,5-bis(2-octyldodecyl)-2,5-dihydropyrrolo[3,4-*c*]pyrrolo-1,4-dione were synthesized according to a previously published report.[32]

NMR experiments: A 500 MHz Bruker AVANCE III^{TM} spectrometer was used for NMR spectra with deuterated chloroform as the solvent. Multiplicities are given as: s (singlet), d (doublet), t (triplet), q (quartet), dd (doublet of a doublet) and m (multiplet).

Size Exclusion chromatography measurements: Size exclusion chromatography (SEC) data were recorded by using a Viscotek VE3580 system equipped with Viscotek columns (T6000M) connected to refractive index and UV detectors. THF (HPLC grade) was employed as the eluent with 1 mL min^{-1} rate at 30 °C with GPC$_{max}$ as the sample module. Molecular weight determination was carried out via calibration based on polystyrene standards.

UV-vis Spectroscopy measurements: The UV-vis spectra were recorded with an Agilent 8453 UV-vis spectrometer. For solution spectra, 1 cm cuvettes were used with dilute polymer solutions

in chloroform, and thin film spectra were obtained by drop-casting polymer solution on to cleaned glass substrates.

Electrochemical measurements: Cyclic voltammetry studies were performed on a BAS CV-50W voltammetric analyzer. A three electrode system: platinum working electrode, Pt wire auxiliary electrode, and a Ag/Ag^+ reference were used with 0.1 M NBu_4PF_6 in acetonitrile as the electrolyte.

Thermal characterization: TGA and DSC spectra were collected on a Mettler Toledo TGA/DSC-1 system with a heating rate of 10 °C min^{-1} and a cooling rate of -10 °C min^{-1} under nitrogen.

Atomic force microscopy measurements: TMAFM images were recorded on a Nanoscope IV Multimode Veeco equipped with a vertical engager. The images were collected in 2×2 μm scan size with a frequency of 1 Hz. (320 kHz Si cantilever; spring constant = 42 N m^{-1}).

Single crystal X-ray Diffraction measurements: Using a brown colored single crystal (size ~0.16 x 0.12 x 0.1 mm^3) selected from a batch grown via crystallization (slow evaporation method) of 2,5-distannylated thieno[3,2-*b*]pyrrole in methanol, a single crystal X-ray diffraction data set was collected. This data set was collected on a Bruker Kappa D8 Quest diffractometer with Incoatec microfocus (IμS) Mo Kα radiation source, Oxford Cryosystems cryostream (at T = 100 K), and Photon 100 CMOS detector. Within the Bruker APEX3 graphical user interface, the data set was processed (SAINT, integration; SADABS, scaling and multi-scan absorption correction) and analyzed (XPREP, space group determination) prior to generating a preliminary model (SHELXT, intrinsic phasing method). The refinement of the structural model was completed (with the anisotropic refinement of non-hydrogen atomic positions and addition of "riding" hydrogen atomic sites) with SHELXL2017.

Grazing Incidence X-Ray Diffraction Measurements: Out-of-plane GIXRD data were obtained by using a Rigaku SmartLab XRD instrument. Polymer samples were made similar to devices including surface treatment to match with OFET data. The data were collected at 0.05° intervals from 1° to 30° by irradiating with Cu-Kα ($\lambda = 1.54$ Å) at an incident angle of 0.5°.

Organic Field Effect Transistor Fabrication and Characterization: OFETs with common bottom-gate/top-contact configuration were used to fabricate devices. A highly doped n-type silicon wafer was employed as the substrate and 200 nm thermally grown SiO_2 was used as the dielectric layer. First, the photoresist was applied on the front side of the wafer before backside was etched with 7:1 BOE solution from JT Baker and 100 nm of gold was deposited as a gate. The silicon wafer was then subjected to sequential cleaning with acetone, toluene, and 2-propanol. The capacitance per unit area was measured to be 17 nF cm^{-2}. After the silicon wafer was cut into 1.5 $\times$ 1.5 cm pieces, substrates were cleaned by immersing in a hot piranha solution (7:3 mixture of conc. sulfuric acid and 30% hydrogen peroxide) for 10 mins followed by rinsing with copious amounts of DI water and dried with nitrogen. A self-assembled monolayer was prepared with octadecyltrimethoxysilane (OTMS) according to a previously published procedure.[45] P(DPP-TP) solutions (8 mg mL^{-1} in chloroform) was spin-casted on to surface treated Si/SiO$_2$ substrates at 1500 rpm for 30 s to generate thin layers with an average thickness of 60-70 nm. Prepared devices were optionally annealed at different temperatures for 5 mins inside a nitrogen-filled glovebox prior to measurements. Cascade Microtech Model Summit Microchamber with a Keithley 4200-SCS systems were used for the electrical characterization. All the measurements were conducted in air at room temperature.

4.3.2 Material Synthesis

Ethyl 4-methyl-4H-thieno[3,2-b]pyrrole-5-carboxylate

4*H*-thieno[3,2-*b*]pyrrole-5-carboxylate (1.00g, 5.13 mmol) was added to a suspension of NaH (0.20g, 7.99 mmol) in dry DMF (24.0 mL) portion wise at room temperature. After stirring for 30 mins, methyl iodide (2.20g, 15.32 mmol) was added slowly and stirred for another 1 h. The reaction mixture was poured into a saturated solution of NH₄Cl and extracted with Et₂O. The organic layer was washed with DI water (3 × 100 mL) and upon removing the solvent under vacuum pure product was obtained as the brown liquid. (Yield = 0.90g, 83.7%) ^{1}H NMR (CDCl₃, 500 MHz): δ_H 1.38 (t, J = 7.0 Hz, 3H), 4.05 (s, 3H), 4.34 (q, J = 7.0 Hz, 2H), 6.91 (d, J = 5.5 Hz, 1H),7.19 (s, 1H), 7.31 (d, J = 5.0 Hz, 1H) (Figure 4.2), ^{13}C NMR (CDCl₃, 125 MHz); δ_C 14.51, 34.62, 60.15, 108.98, 110.13, 121.75, 126.93, 129.03, 145.64, 161.85 (Figure 4.3)
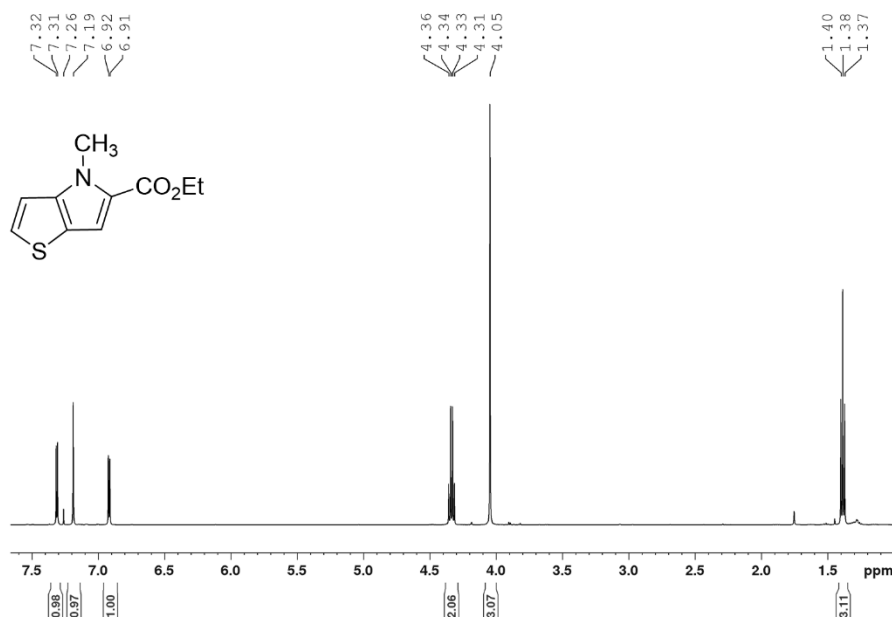
Figure 4.2 ^{1}H NMR spectrum of ethyl-4-methyl-thieno[3,2-*b*]pyrrole-5-carboxylate
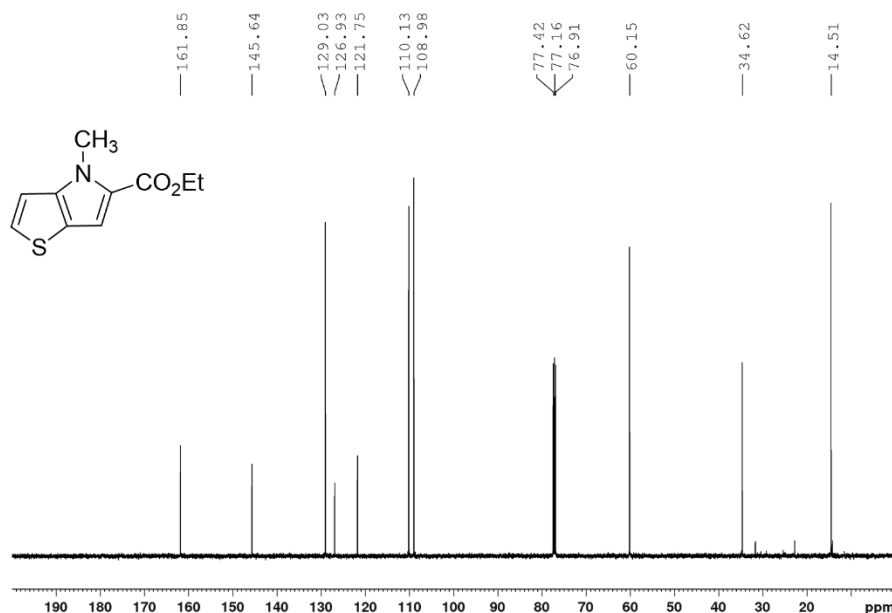
Figure 4.3 ^{13}C NMR spectrum of ethyl-4-methyl-thieno[3,2-*b*]pyrrole-5-carboxylate

4-methyl-4H-thieno[3,2-b]pyrrole-5-carboxylic acid

To a 100 mL single neck round bottomed flask ethyl 4-methyl-4*H*-thieno[3,2-*b*]pyrrole-5-carboxylate (0.90g, 4.29 mmol) was added with 200 proof ethanol (6.0 mL). A solution of LiOH (0.51g, 21.0 mmol) in DI water (6.0 mL) was added dropwise to the ethanolic solution and refluxed for 3 h. The solvent was evaporated and DI water (10.0 mL) was added. pH of the mixture was adjusted to 2, using 3M HCl and compound was extracted with ethyl acetate (3 × 30 mL). The organic layer was washed with DI water and dried over anhydrous MgSO$_4$. After removing the solvent, pure compound was obtained as a beige color solid. (Yield = 0.70g, 91.7%) ^{1}H NMR (CDCl$_3$, 500 MHz): δ$_H$ 4.07 (s, 3H), 6.95 (d, *J* = 5.5 Hz, 1H),7.34 (s, 1H), 7.39 (d, *J* = 5.0 Hz, 1H), 11.57 (br, 1H) (Figure 4.4), ^{13}C NMR (CDCl$_3$, 125 MHz); δ$_C$ 34.94, 110.21, 111.18, 122.21, 125.84, 130.45, 146.78, 166.61 (Figure 4.5)
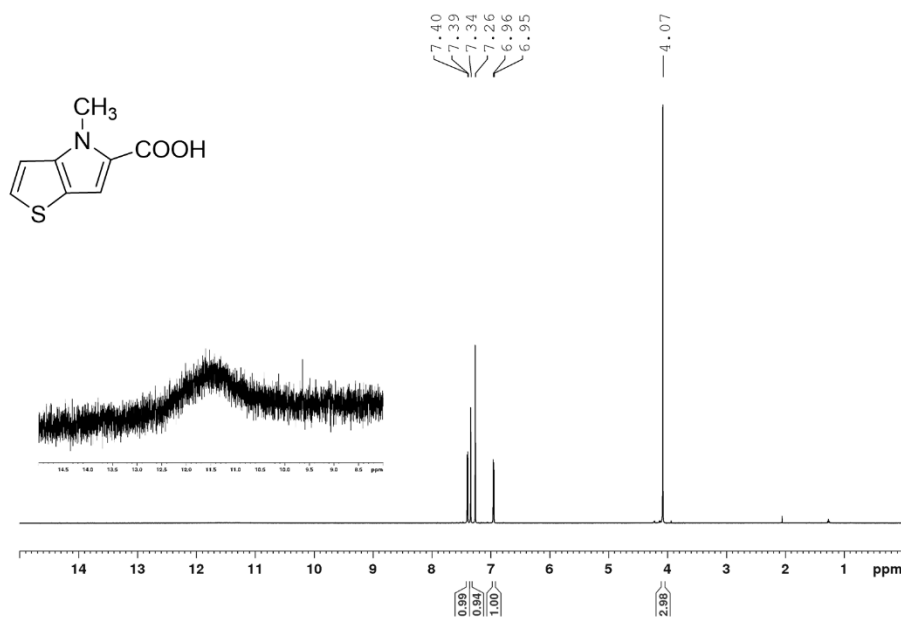
Figure 4.4 ^{1}H NMR spectrum of 4-methyl-thieno[3,2-*b*]pyrrole-5-carboxylic acid
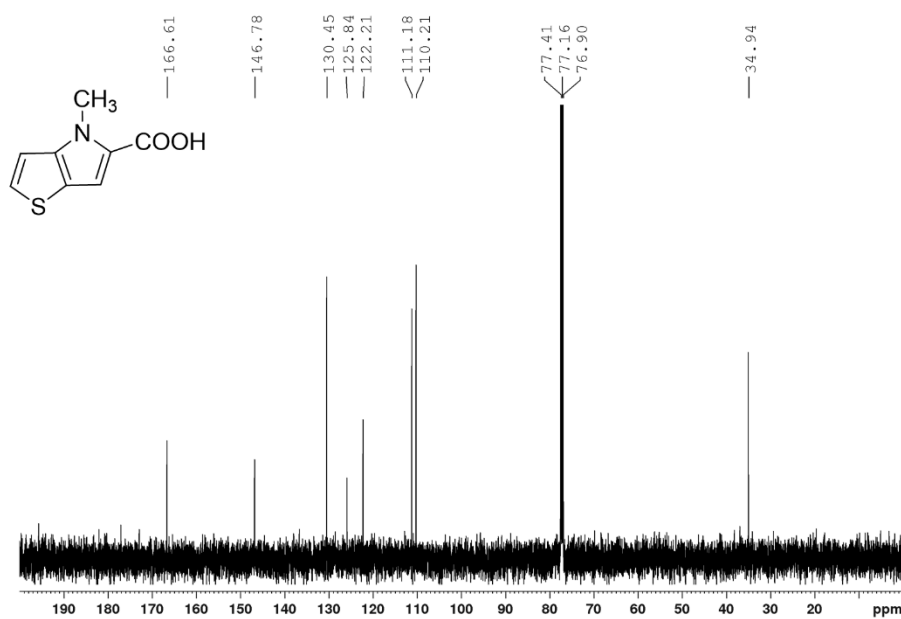
Figure 4.5 ^{13}C NMR spectrum of 4-methyl-thieno[3,2-*b*]pyrrole-5-carboxylic acid

4H-thieno[3,2-b]pyrrole

4*H*-thieno[3,2-*b*]pyrrole-5-carboxylate (1.00g, 5.13 mmol) and KOH (1.15g, 20.52 mmol) was added with anhydrous ethylene glycol (10 mL) to a 100 mL single neck round bottomed flask under nitrogen. The solution mixture was refluxed for 2 h and cooled to room temperature. Subsequently, reaction mixture was quenched with DI water and extracted with Et$_2$O (3× 50 mL). The crude did not receive any purification as it was pure enough to go to the next step. (Yield = 0.53g, 83.7%) ^{1}H NMR (CDCl$_3$, 500 MHz): δ_H 6.48 (s, 1H), 6.96 (d, *J* =5.0 Hz, 1H), 7.02 (s, 1H), 7.10 (dd, *J* = 1.0 Hz and *J* = 5.0 Hz, 1H) (Figure 4.6), ^{13}C NMR (CDCl$_3$, 125 MHz); δ_C 101.71, 111.13, 122.93, 123.97, 124.11, 138.63 (Figure 4.7)
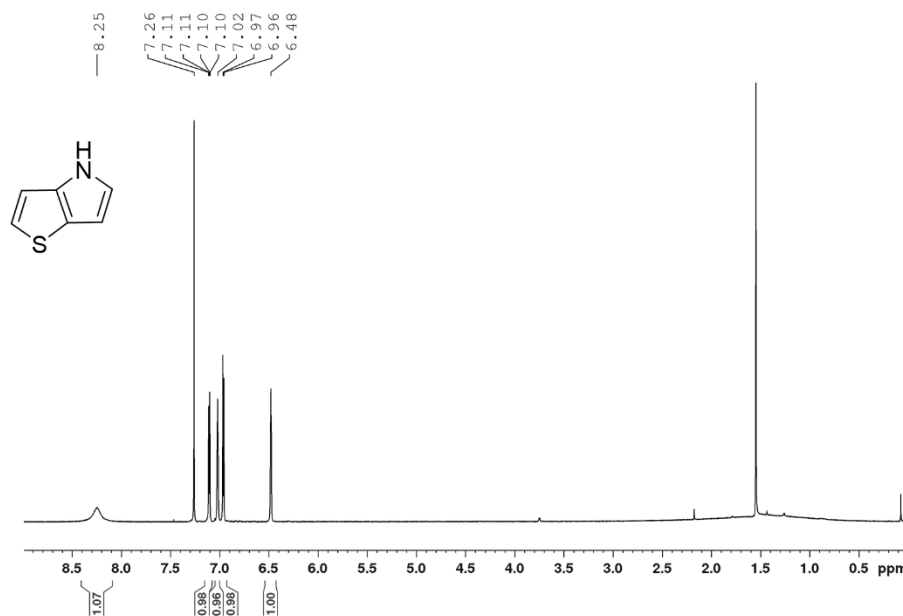
Figure 4.6 ^{1}H NMR spectrum of 4*H*-thieno[3,2-*b*]pyrrole
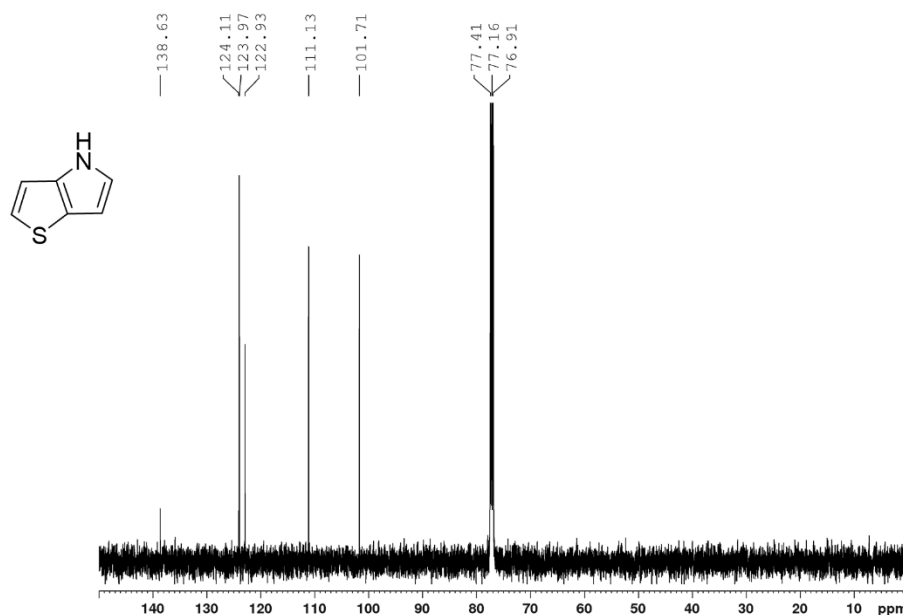
Figure 4.7 ^{13}C NMR spectrum of 4H-thieno[3,2-b]pyrrole

4-methyl-4H-thieno[3,2-b]pyrrole

Pathway II - To a 100 mL three-neck round bottomed flask 4-dodecyl-4H-thieno[3,2-b]pyrrole-5-carboxylic acid (1.75 g, 9.65 mmol) and copper chromite (barium promoted) (0.93 g, 4.0 mmol) were dissolved in quinoline (10.0 mL) under nitrogen. The mixture was heated to 200 °C for 3 h and cooled to room temperature. Ethyl acetate (50 mL) was added and filtered under gravity filtration. The filtrate was washed with 3M HCl (3 × 100 mL), DI water (3 × 50 mL) and brine. The organic layer was dried over anhydrous MgSO₄. After removing the solvent under reduced pressure, crude was purified by column chromatography using hexane: ethyl acetate: triethylamine (98:1:1 v/v) as the eluent to give a pale yellow color oil. (Yield = 0.86g, 65.1%)

133

Pathway I - NaH (0.13g, 5.33 mmol) was suspended in anhydrous DMF (5.0 mL) at room temperature in a 50 mL single neck round bottomed flask under nitrogen. A solution of 4H-thieno[3,2-b]pyrrole (0.44g, 3.55 mmol) in DMF (5.0 mL) was slowly added and stirred for 30 mins. Methyl iodide (1.53g, 10.65 mmol) was added dropwise and stirred for an additional h. The reaction mixture was quenched with DI water, and the organic layer was extracted with Et$_2$O. The solvent was removed under reduced pressure to yield the pure compound as a brown liquid. (Yield = 0.33 g, 67.3%) ^{1}H NMR (CDCl$_3$, 500 MHz): δ_H 3.78 (s, 3H), 6.37 (d, J = 3.0 Hz, 1H), 6.82 (d, J = 2.0 Hz, 1H), 6.91 (d, J = 5.5 Hz, 1H), 7.08 (d, J = 5.5 Hz, 1H) (Figure 4.8), ^{13}C NMR (CDCl$_3$, 125 MHz); δ_C 34.87, 100.37, 110.03, 123.21, 123.57, 126.87, 140.67 (Figure 4.9)
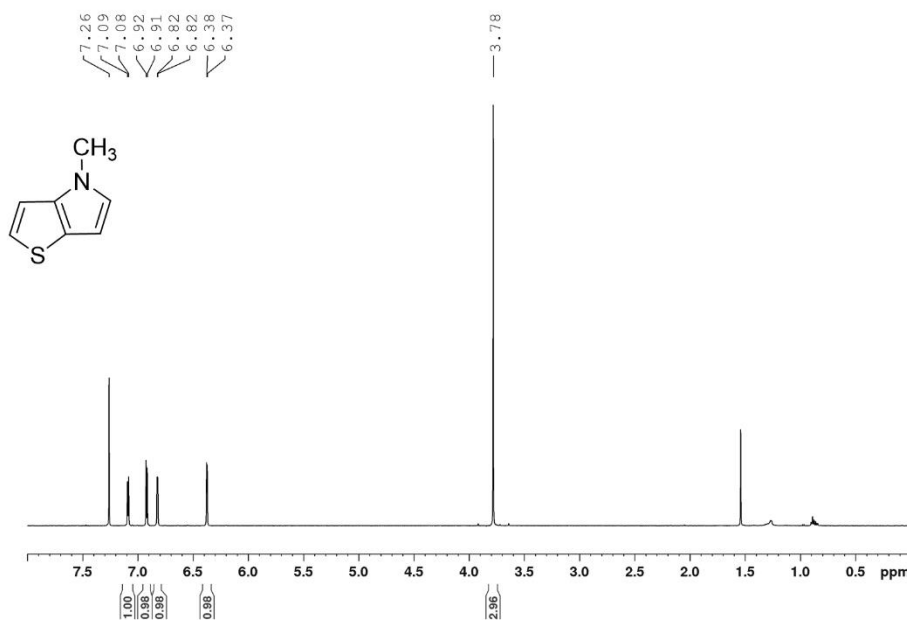
Figure 4.8 ^{1}H NMR spectrum of 4-methyl-4H-thieno[3,2-b]pyrrole
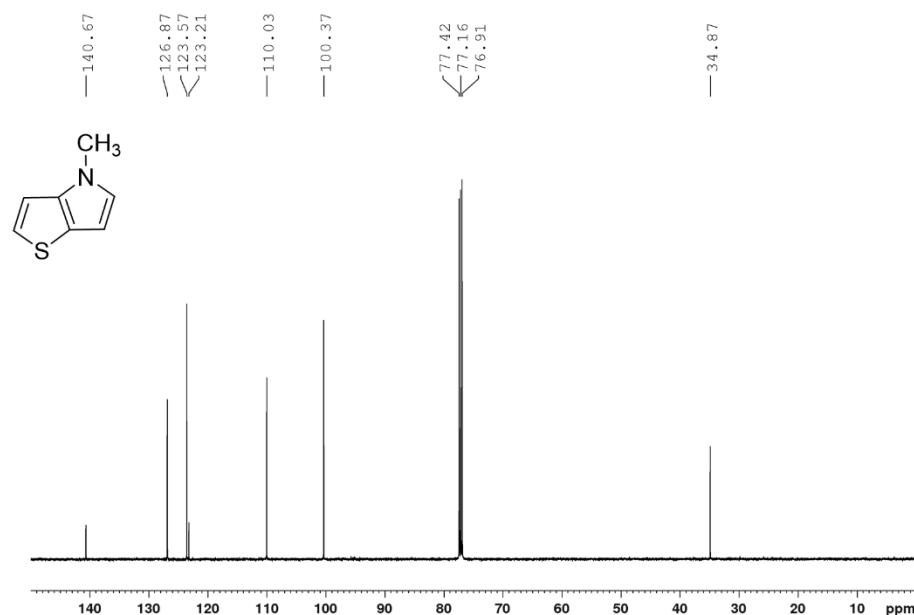
Figure 4.9 ^{13}C NMR spectrum of 4-methyl-4*H*-thieno[3,2-*b*]pyrrole

4-methyl-2,5-bis(trimethylstannyl)-4H-thieno[3,2-b]pyrrole

4-methyl-4*H*-thieno[3,2-*b*]pyrrole (78.6mg, 0.57mmol), dry hexane (5.0 mL) and TMEDA (0.17 mL, 1.14 mmol) was added to a 50 mL three neck round bottomed flask under N$_2$. 2.5 M *n*-BuLi (0.46 mL, 1.14 mmol) was added dropwise and refluxed for 1.5 h to get a bright yellow color. (lithiation completed within 1 h) Solution was cooled to room temperature and -78 °C before adding 1.0 M trimethyl tin chloride in THF (1.14 mL, 1.14 mmol). Reaction mixture was stirred in the flask for 2 h and ice-cold water (20 mL) was injected into the flask. Compound was extracted with cold Et$_2$O and dried under anhydrous MgSO$_4$. Upon removing the solvent under reduced pressure a solid was formed. Pure compound was obtained after washing the crude with cold ethanol as white crystals. (Yield = 45.0mg, 17.0%) ^{1}H NMR (CDCl$_3$, 500 MHz): δ$_H$ 0.35 (s, 9H), 0.36 (s, 9H), 3.78 (s, 3H), 6.42 (d, *J* = 0.5 Hz, 1H), 6.91 (d, *J* = 0.5 Hz, 1H) (Figure 4.10), ^{13}C

NMR (CDCl₃, 125 MHz); δ_C -8.46, -8.12, 36.30, 109.48, 116.93, 129.99, 137.09, 140.44, 147.55
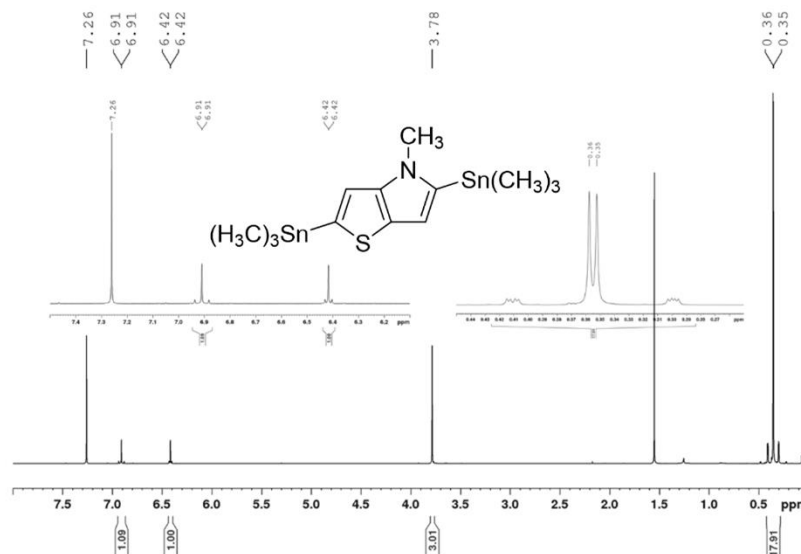
(Figure 4.11)

Figure 4.10 ¹H NMR of 4-methyl-2,5-bis(trimethylstannyl)-4*H*-thieno[3,2-*b*]pyrrole
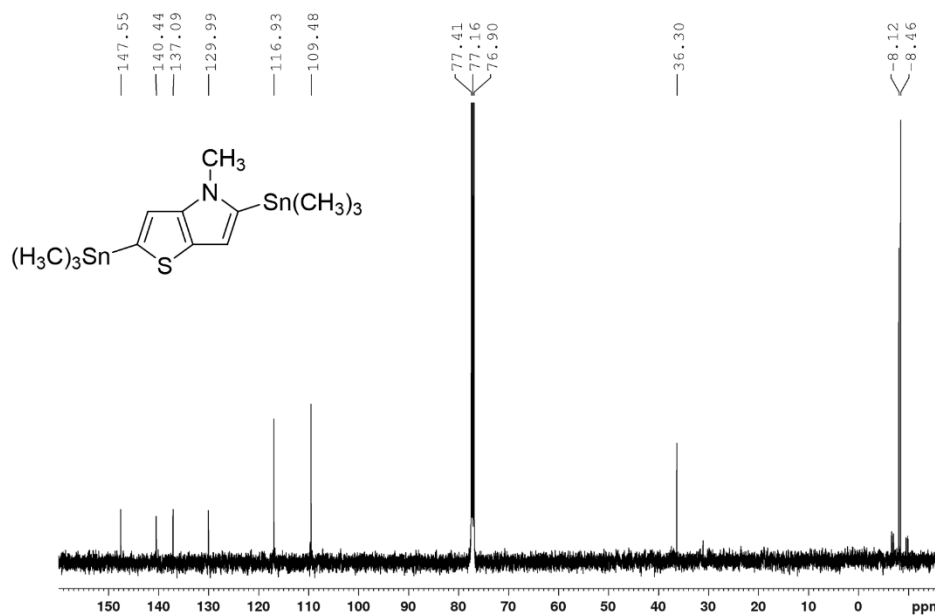
Figure 4.11 ¹³C NMR of 4-methyl-2,5-bis(trimethylstannyl)-4*H*-thieno[3,2-*b*]pyrrole

P(DPP-TP)

3,6-Bis(5-bromothiophen-2yl)-2,5-bis(2-octadecyl)-2,5-dihydropyrrolo[3,4-*c*]pyrrole-1,4-dione (101 mg, 0.1 mmol), 4-methyl-2,5-bis(trimethylstannyl)-4*H*-thieno[3,2-*b*]pyrrole (46 mg, 0.1 mmol), Pd$_2$dba$_3$ (1.8 mg, 2.0 µmmol), P(o-tol)$_3$ (2.4 mg, 8.0 µmmol) and anhydrous chlorobenzene (4 mL) were added to a 50 mL pressure flask, sealed and stirred at 130 °C for 36 h under a nitrogen atmosphere. Subsequently, the polymer was precipitated with methanol and collected in a cellulose thimble. The crude polymer was subjected to successive Soxhlet extractions with methanol, acetone, hexane (24 h each) to remove impurities and undesirable molecular weight fractions. The Final polymer was dissolved in a minimum amount of chloroform and precipitated as a dark green solid. (Yield = 65.0 mg, 65.5%) ^{1}H NMR is shown in Figure 4.12.
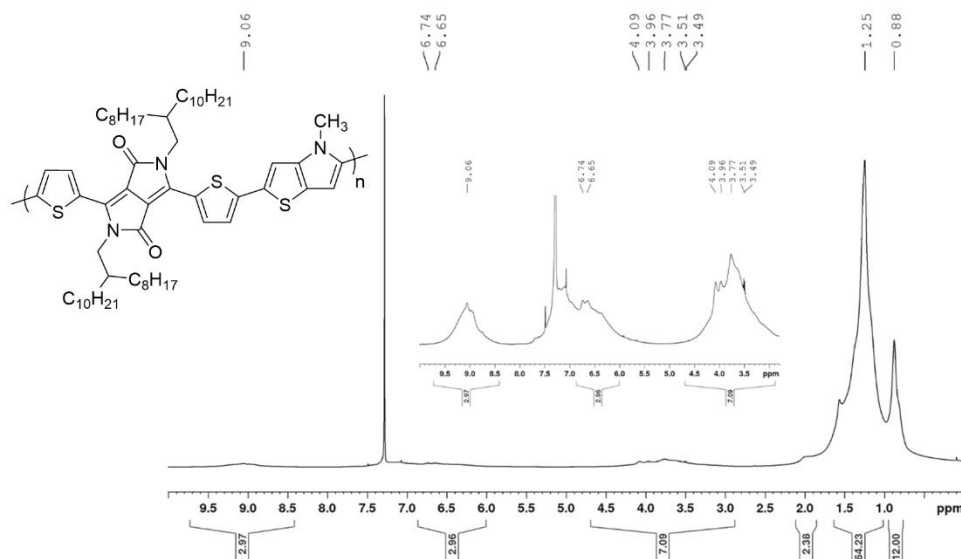
Figure 4.12 ^{1}H NMR spectrum of P(DPP-TP)

4.4 Results and Discussion

4.4.1 Synthesis and Characterization

To remove the ester group from 4*H*-thieno[3,2-*b*]pyrrole-5-carboxylate, a reduction reaction was performed by refluxing 4*H*-thieno[3,2-*b*]pyrrole-5-carboxylate with ethylene glycol in the presence of KOH for 2 h. Subsequently, a N-methylation reaction was performed at room temperature by deprotonation followed by methylation using NaH and CH_3I. The monomer could also be obtained from pathway II, although with a lower overall yield compared to pathway I as shown in Scheme 4.1.

Scheme 4.1 Synthetic routes for TP monomer and P(DPP-TP)
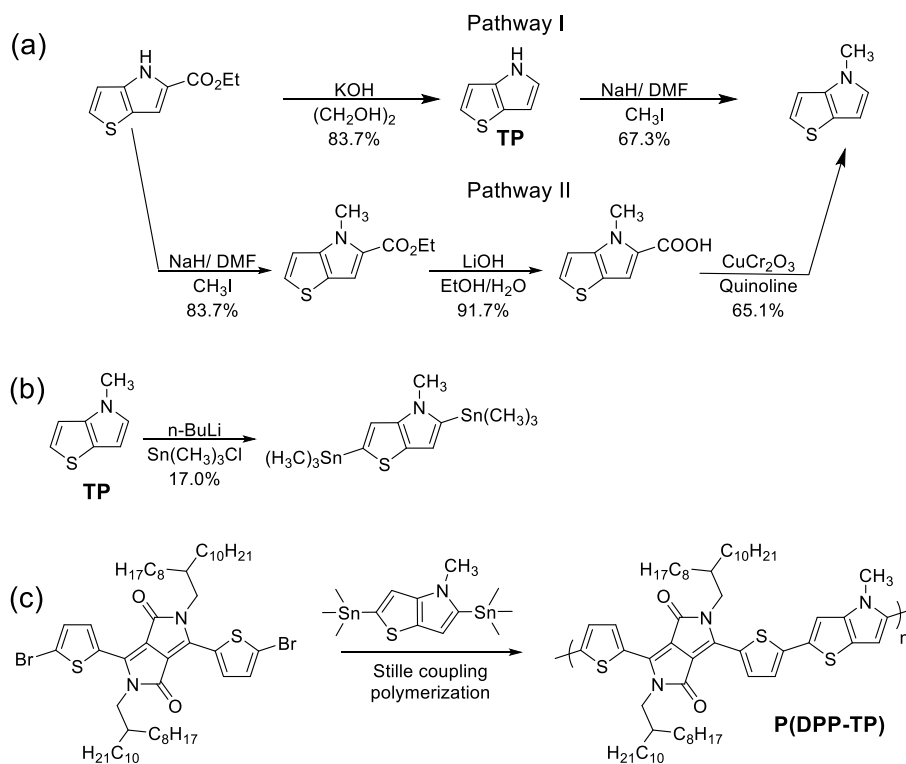
Thieno[3,2-*b*]pyrrole was surprisingly stable in air with respect to pyrrole and thieno[3,2-*b*;4,5-*b'*]dipyrrole,[46] with no signs of oxidation or self-polymerization after exposing the TP monomer to ambient conditions for over two days. Asymmetric lithiation of TP was achieved in less than 1 h when *n*-BuLi was used in the presence of N,N,N′,N′-tetramethylethylenediamine (TMEDA) at refluxing conditions (Scheme 1(b)). Immediate cooling to -78 °C with the slow addition of trimethylstannyl chloride gave the 2,5-distannyl derivative of TP. After keeping the isolated compound (in diethyl ether) under vacuum for 30 mins, colorless crystals were formed and further purified upon washing with cold ethanol and drying in a vacuum oven at 40 °C for 2 h. The thermal ellipsoid plot and packing diagram of 2,5-distannylated thieno[3,2-*b*]pyrrole are shown in Figure 4.13.
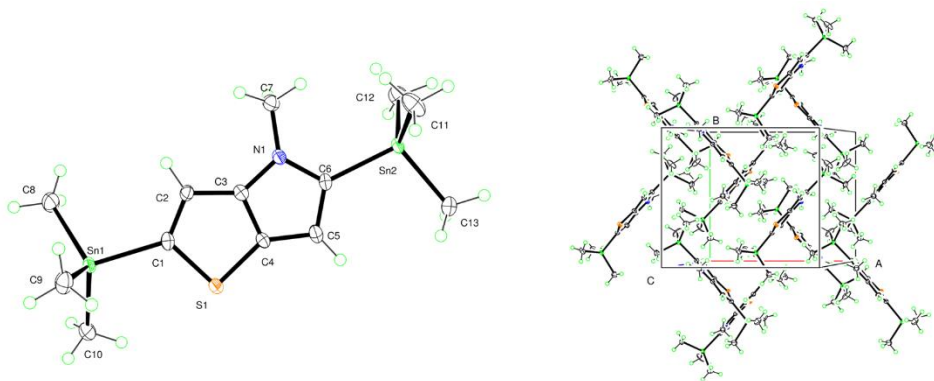
Figure 4.13 The thermal ellipsoid plot and unit cell arrangement of 2,5-distannylated thieno[3,2-*b*]pyrrole at 50% probability level

As shown in Scheme 1(c), the polymerization was carried out by a palladium catalyzed Stille coupling with 3,6-bis(5-bromo-2-thienyl)-2,5-bis(2-octyldodecyl)-2,5-dihydropyrrolo[3,4-*c*]pyrrole-1,4-dione in a pressure vessel at 110 °C for 36 h. Molecular weights were improved by screening common palladium precatalyst and ligands as shown in Table 4.1. After precipitating in

139

methanol, the dark green solid was purified by successive Soxhlet extractions in methanol, acetone, and hexane (24 h each) to remove impurities and undesired low molecular weight fractions. The polymer was recovered from chloroform. P(DPP-TP) was readily soluble in common organic solvents such as tetrahydrofuran, chloroform, and chlorobenzene.

Table 4.1 Polymerization conditions for P(DPP-TP)

Trial*	precatalyst	ligand	M_n (kDa)	M_w (kDa)	PDI
I	Pd(PPh$_3$)$_4$	-	5.2	16.6	3.20
II	Pd$_2$(PPh$_3$)$_2$Cl$_2$	P(o-tol)$_3$	9.9	22.9	2.31
III	Pd$_2$(dba)$_3$	P(o-tol)$_3$	20.8	47.2	2.27

*For each trial 2 mol% of catalyst and 8 mol% of the ligand were added with 0.1 mmol of each monomer and 4 mL of anhydrous chlorobenzene.

4.4.2 Theoretical Calculations

To gain insight on torsional effects along the polymer backbone, a dimer was modeled for density functional theory calculations using Spartan′16 at B3LYP/6-31G* level of theory. All the alkyl chains were replaced with methyl groups to simplify the calculations. As shown in Figure 4.14, the dimer has two distinct dihedral angles between adjacent thiophene and TP unit due to its asymmetric nature. When thiophene is attached to the thiophene side in TP, the dihedral angle is 11.4°, while when attached to the pyrrole side it increases to 30.7°. As a result of the large torsional angle, frontier energy orbitals are not completely delocalized along the backbone. Such rotational freedom allows polymers to adopt low lying HOMO levels, thus resistive to oxidative doping from atmospheric oxygen.
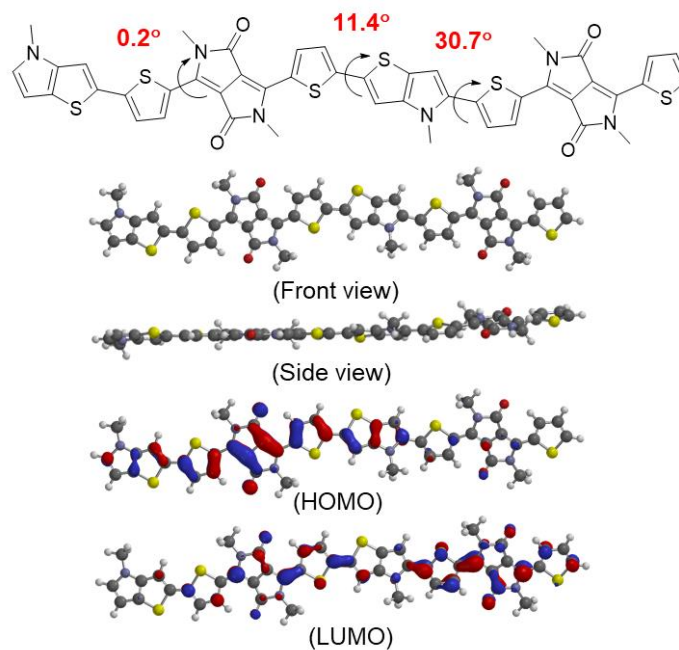
Figure 4.14 DFT calculation of the DPP-TP dimer

4.4.3 Optical and Electrochemical Analysis

Optical properties of P(DPP-TP) were investigated by UV-vis spectroscopy in dilute chloroform solutions and on drop-casted thin films (Figure 4.15 a). Two absorption bands were observed in both solution and solid state of P(DPP-TP). Peaks appeared at 393 nm for a solution, and 406 nm for thin film originated from the π-π* transitions. Peaks at 829 nm for the solution, and 893 nm for thin film correspond to intramolecular charge transfer (ICT) occurring from the HOMO level of thieno[3,2-*b*]pyrrole unit to the LUMO level of the central benzothiadiazole group. Compared to P(DPP-TT), P(DPP-TP) extends the absorption spectrum toward NIR-I region.[32] The optical band gap was calculated from the onset of the thin film absorption profile and estimated at 1.19 eV. Interestingly, P(DPP-TP) has a high absorption coefficient of 7.0×10^5 M^{-1} cm^{-1}, suggesting

P(DPP-TP) can efficiently absorb sunlight. As shown in Figure 4.15(b), the onset of oxidation and

reduction potentials (E_{ox} and E_{red}, respectively) versus F_c/F_c^+ in cyclic voltammogram was used to

measure frontier energy levels of the polymer (E_{HOMO} = -4.94 eV and E_{LUMO} = -3.05 eV) and they

were calculated from the following equations: E_{HOMO} = -(E_{ox} + 4.8 − $E_{1/2,Fc/Fc+}$)eV and E_{LUMO} = -

(E_{red} + 4.8 − $E_{1/2,Fc/Fc+}$)eV. The discrepancy between the optical and electrochemical band gaps can

be due to exciton binding energy which can be 0.4-1.0 eV.
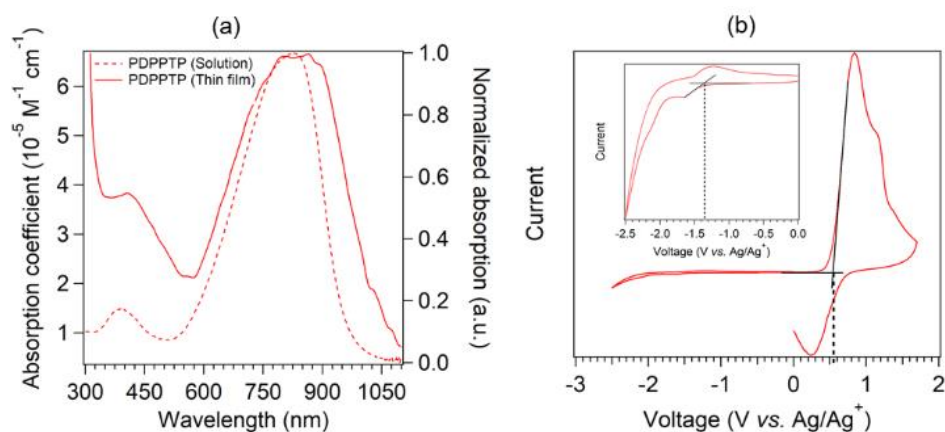
Figure 4.15 (a) UV-vis absorption spectrum of P(DPP-TP) in CHCl$_3$ solution and thin films, (b)
cyclic voltammogram of P(DPP-TP)

4.4.4 Thermal Properties

P(DPP-TP) was subjected to thermogravimetric analysis (TGA) and differential scanning

calorimetry (DSC) (*see* Figure 4.16 (a) and 4.16(b), respectively) to investigate thermal properties.

TGA analysis showed P(DPP-TP) is stable up to 300 °C with a decomposition temperature (T$_d$) of

301 °C at 5% weight loss. DSC analysis revealed a melt to isotropic phase in the heating cycle at

239 °C consistently over three cycles. However, no exotherms were observed upon cooling.
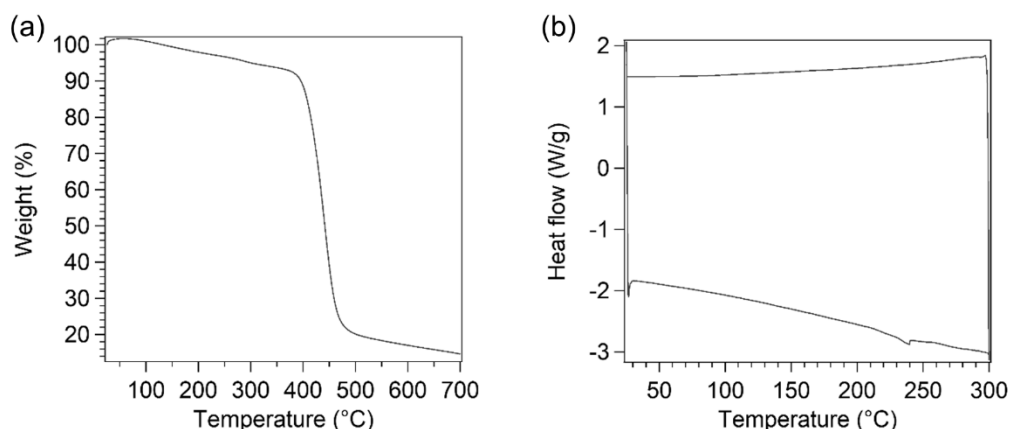
Figure 4.16 (a) TGA and, (b) DSC thermograms of P(DPP-TP)

4.4.5 OFET Characterization

OFET characteristics were explored with a bottom-gate/top-contact configuration. Heavily n-doped silicon wafer with a 200 nm thick layer of SiO_2 dielectric layer was used as the substrate for the devices. The surface was modified with octadecyltrimethoxysilane (OTMS-SAM) layer according to a previously published method.[45] A thin layer of P(DPP-TP) was spin coated on top of the surface modified silicon wafer using a polymer solution (8 mg/ mL in chloroform) at a spin rate of 1500 rpm inside a nitrogen-filled glovebox. The polymer thin films were annealed on a hot plate inside the glovebox only for 5 mins prior to thermal evaporation of gold (100 nm) as the source and drain pads under high vacuum conditions. The channel length (100 μm) and channel width (1000 μm) was defined by a shadow mask. Current-voltage characteristics of OFETs were measured at room temperature in air.

As-spun thin films of P(DPP-TP) showed typical p-type OFET characteristics with an average hole mobility of 0.0097 cm^2 /V s extracted from the transfer curve and a current on-to-off ratio (I_{on}/I_{off}) of ~550 as shown in Figure 4.17. Upon annealing at 100 °C a 5-fold increase in hole mobility was

observed to reach 0.054 cm^2 /V s , with a $I_{on}/I_{off} \sim 800$. When annealing temperature was further

increased to 150 °C, hole mobility improved to 0.099 cm^2 /V s, with a $I_{on}/I_{off} \sim 4000$. The highest

average hole mobility of 0.12 cm^2 /V s, was achieved when thin films were annealed at 200 °C,

however, I_{on}/I_{off} was decreased to ~1000. Current on-to-off ratios of P(DPP-TP) were relatively

low compared other DPP polymers, which are in the range ~10^5 -10^8.[20] For all the devices,

threshold voltages varied from 0 V to -3.5 V. The mobility extraction of semiconducting polymers

is in debate since mobilities can be extracted in two different domains due to the non-linear nature

of $I_D{}^{1/2}$ vs V_G curve.[47] While many DPP polymers have claimed to have mobilities over 1 cm^2 /V

s at lower gate voltages, mobilities extracted at higher gate voltages are believed to be closer to

the actual value. Therefore, nowadays many groups report mobilities at both lower and higher gate

voltages.[20, 48, 49] However, it is noteworthy to mention that none of the devices made from P(DPP-

TP) suffered from non-linear transfer curves unlike other polymer based bottom gate OFETs with

surface modifications performed by alkylsilanes. Such linear transfer characteristics were also

observed in TP based small molecules suggesting TP can act as an excellent building block for

OFETs. Also unlike P(DPP-TT), no weak electron transport was observed for $V_G > 0$ V suggesting

P(DPP-TP) is predominantly a hole transporter.[32] This might be attributed to the relatively high

LUMO level (-3.05 eV). The transfer and output plots are shown in Figure 4.17.

144
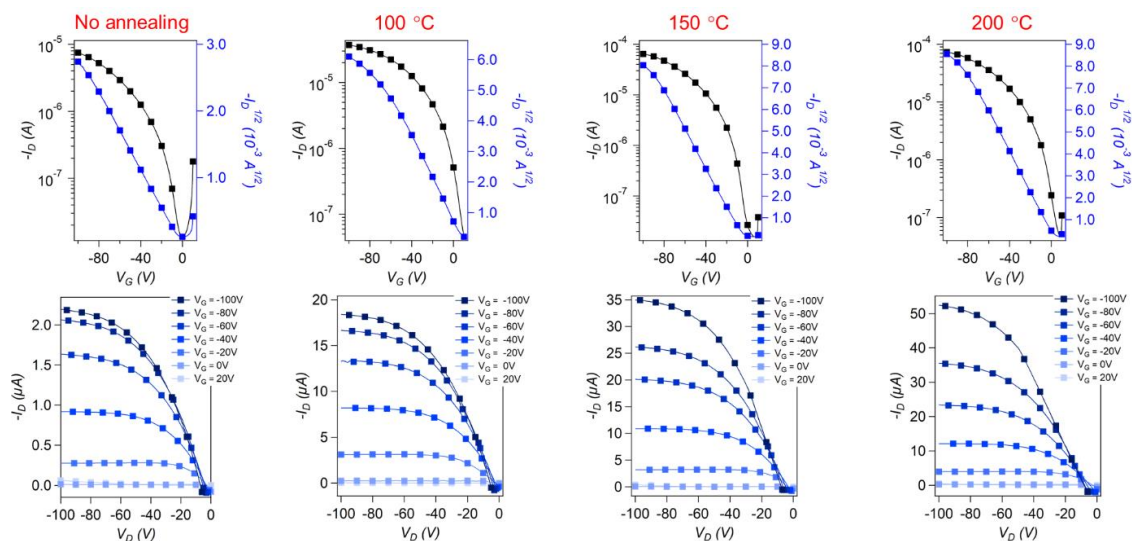
Figure 4.17 Transfer (V_D = -100 V) and output plots of P(DPP-TP) thin films annealed at different temperatures

4.4.6 Surface morphology and Crystallinity

Surface morphology of P(DPP-TP) between the channel region was investigated by tapping mode atomic force microscopy (TMAFM) (*see* Figure 4.18). Uniform intertwined fibrillar network observed for P(DPP-TT) was not observed with P(DPP-TP) thin films.[32, 34] All the images have similar features with RMS values ranging from 0.43 – 0.57 nm.

However, out-of-plane grazing incidence X-ray diffraction (GIXRD) data (Figure 4.19) showed an increase in the intensity of lamellar peaks upon annealing which explains the increase in mobility with annealing temperature. The lamellar packing distance was calculated to be 19.9 Å from the 2θ value at 4.425°. GIXRD was taken on P(DPP-TP) deposited on OTS-treated SiO_2 substrates by using the same conditions employed for the fabrication of OFETs.
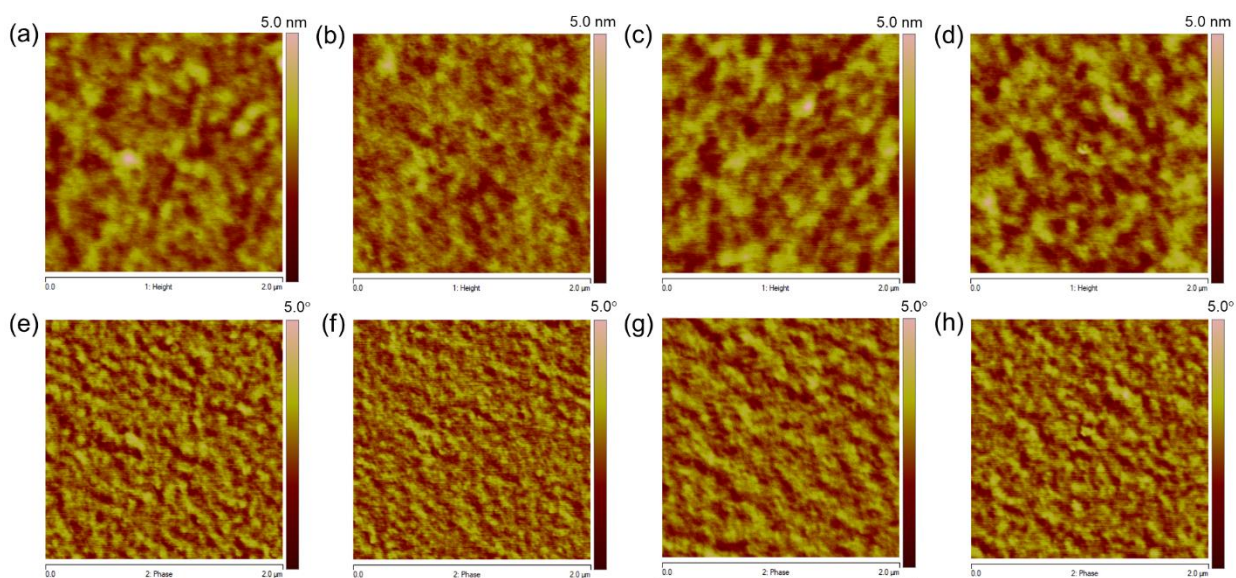
Figure 4.18 TMAFM height (a,b,c,d) and phase images (e,f,g,h) of P(DPP-TP) inside the channel region with no annealing (a & e), annealed at 100 °C (b & f), 150 °C (c & g), 200 °C (d & h) for 5.0 mins
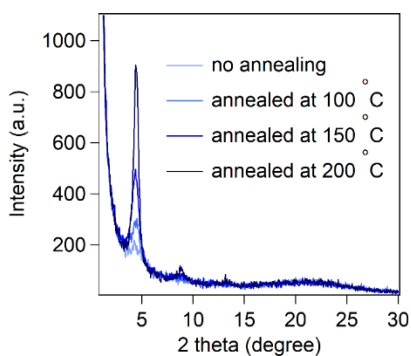
Figure 4.19 GIXRD of P(DPP-TP) thin films annealed at different temperatures

4.5 Conclusion

In conclusion, for the first time, we have demonstrated the successful synthesis of novel thieno[3,2-*b*]pyrrole monomer and the 2,5-distannylated derivative which was characterized by single crystal XRD. Preliminary results show that donor-acceptor copolymer between fused ring systems of DPP

and TP can achieve an average hole mobility of 0.12 cm^2 /V s in bottom-gate/top-contact OFET devices. We believe TP monomer is a good non-conventional building block for OFETs due to the linear curves. Also, the device performance could be further improved by increasing the molecular weight of the polymer and side chain engineering via N-alkylation.

4.6 Acknowledgements

4.7 References

1. Lu, L.; Zheng, T.; Wu, Q.; Schneider, A. M.; Zhao, D.; Yu, L., Recent Advances in Bulk Heterojunction Polymer Solar Cells. *Chemical Reviews* **2015,** *115*, 12666-12731.

2. Janssen, R. A. J.; Nelson, J., Factors Limiting Device Efficiency in Organic Photovoltaics. *Advanced Materials* **2013,** *25*, 1847-1858.

3. Heeger, A. J., 25th Anniversary Article: Bulk Heterojunction Solar Cells: Understanding the Mechanism of Operation. *Advanced Materials* **2014,** *26*, 10-28.

4. Sirringhaus, H., 25th Anniversary Article: Organic Field-Effect Transistors: The Path Beyond Amorphous Silicon. *Advanced Materials* **2014,** *26*, 1319-1335.

5. Wang, C.; Dong, H.; Hu, W.; Liu, Y.; Zhu, D., Semiconducting π-Conjugated Systems in Field-Effect Transistors: A Material Odyssey of Organic Electronics. *Chemical Reviews* **2012,** *112*, 2208-2267.

6. Tsao, H. N.; Cho, D.; Andreasen, J. W.; Rouhanipour, A.; Breiby, D. W.; Pisula, W.; Müllen, K., The Influence of Morphology on High-Performance Polymer Field-Effect Transistors. *Advanced Materials* **2009,** *21*, 209-212.

7. Rivnay, J.; Toney, M. F.; Zheng, Y.; Kauvar, I. V.; Chen, Z.; Wagner, V.; Facchetti, A.; Salleo, A., Unconventional Face-On Texture and Exceptional In-Plane Order of a High Mobility n-Type Polymer. *Advanced Materials* **2010,** *22*, 4359-4363.

8. Rasmussen, S. C.; Evenson, S. J., Dithieno[3,2-*b*:2′,3′-*d*]pyrrole-based materials: Synthesis and application to organic electronics. *Progress in Polymer Science* **2013,** *38*, 1773-1804.

9. Lei, T.; Dou, J.-H.; Pei, J., Influence of Alkyl Chain Branching Positions on the Hole Mobilities of Polymer Thin-Film Transistors. *Advanced Materials* **2012,** *24*, 6457-6461.

10. Lim, B.; Sun, H.; Lee, J.; Noh, Y.-Y., High Performance Solution Processed Organic Field Effect Transistors with Novel Diketopyrrolopyrrole-Containing Small Molecules. *Scientific Reports* **2017,** *7*, 164.

11. Lee, M.-H.; Kim, J.; Kang, M.; Kim, J.; Kang, B.; Hwang, H.; Cho, K.; Kim, D.-Y., Precise Side-Chain Engineering of Thienylenevinylene–Benzotriazole-Based Conjugated Polymers with Coplanar Backbone for Organic Field Effect Transistors and CMOS-like Inverters. *ACS Applied Materials & Interfaces* **2017,** *9*, 2758-2766.

12. Yu, H.; Park, K. H.; Song, I.; Kim, M.-J.; Kim, Y.-H.; Oh, J. H., Effect of the alkyl spacer length on the electrical performance of diketopyrrolopyrrole-thiophene vinylene thiophene polymer semiconductors. *Journal of Materials Chemistry C* **2015,** *3*, 11697-11704.

13. Luo, H.; Yu, C.; Liu, Z.; Zhang, G.; Geng, H.; Yi, Y.; Broch, K.; Hu, Y.; Sadhanala, A.; Jiang, L.; Qi, P.; Cai, Z.; Sirringhaus, H.; Zhang, D., Remarkable enhancement of charge carrier mobility of conjugated polymer field-effect transistors upon incorporating an ionic additive. *Science Advances* **2016,** *2*.

14. Liu, C.; Xu, Y.; Noh, Y.-Y., Contact engineering in organic field-effect transistors. *Materials Today* **2015,** *18*, 79-96.

15. Zhang, R.; Li, B.; Iovu, M. C.; Jeffries-El, M.; Sauvé, G.; Cooper, J.; Jia, S.; Tristram-Nagle, S.; Smilgies, D. M.; Lambeth, D. N.; McCullough, R. D.; Kowalewski, T., Nanostructure Dependence of Field-Effect Mobility in Regioregular Poly(3-hexylthiophene) Thin Film Field Effect Transistors. *Journal of the American Chemical Society* **2006,** *128*, 3480-3481.

16. Chen, W.; Xiao, M.; Han, L.; Zhang, J.; Jiang, H.; Gu, C.; Shen, W.; Yang, R., Unsubstituted Benzodithiophene-Based Conjugated Polymers for High-Performance Organic Field-Effect Transistors and Organic Solar Cells. *ACS Applied Materials & Interfaces* **2016,** *8*, 19665-19671.

17. Tiwari, S. P.; Kim, J.; Knauer, K. A.; Hwang, D. K.; Polander, L. E.; Barlow, S.; Marder, S. R.; Kippelen, B., Complementary-like inverters based on an ambipolar solution-processed molecular bis(naphthalene diimide)-dithienopyrrole derivative. *Organic Electronics* **2012,** *13*, 1166-1170.

18. Zhong, W.; Sun, S.; Ying, L.; Liu, F.; Lan, L.; Huang, F.; Cao, Y., High-Performance Organic Field-Effect Transistors Fabricated Based on a Novel Ternary π-Conjugated Copolymer. *ACS Applied Materials & Interfaces* **2017,** *9*, 7315-7321.

19. Lei, T.; Cao, Y.; Fan, Y.; Liu, C.-J.; Yuan, S.-C.; Pei, J., High-Performance Air-Stable Organic Field-Effect Transistors: Isoindigo-Based Conjugated Polymers. *Journal of the American Chemical Society* **2011,** *133*, 6099-6101.

20. Du, J.; Bulumulla, C.; Mejia, I.; McCandless, G. T.; Biewer, M. C.; Stefan, M. C., Evaluation of (E)-1,2-di(furan-2-yl)ethene as building unit in diketopyrrolopyrrole alternating copolymers for transistors. *Polymer Chemistry* **2017,** *8*, 6181-6187.

21. Li, Y.; Wu, Y.; Liu, P.; Birau, M.; Pan, H.; Ong, B. S., Poly(2,5-bis(2-thienyl)-3,6-dialkylthieno [3,2-*b*]thiophene)s—High-Mobility Semiconductors for Thin-Film Transistors. *Advanced Materials* **2006,** *18*, 3029-3032.

22. Chao, P.-Y.; Wu, H.-C.; Lu, C.; Hong, C.-W.; Chen, W.-C., Biaxially Extended Conjugated Polymers with Thieno[3,2-*b*]thiophene Building Block for High Performance Field-Effect Transistor Applications. *Macromolecules* **2015,** *48*, 5596-5604.

23. Yamamoto, T.; Nishimura, T.; Mori, T.; Miyazaki, E.; Osaka, I.; Takimiya, K., Largely π-Extended Thienoacenes with Internal Thieno[3,2-*b*]thiophene Substructures: Synthesis, Characterization, and Organic Field-Effect Transistor Applications. *Organic Letters* **2012,** *14*, 4914-4917.

24. McCulloch, I.; Heeney, M.; Chabinyc, M. L.; DeLongchamp, D.; Kline, R. J.; Cölle, M.; Duffy, W.; Fischer, D.; Gundlach, D.; Hamadani, B.; Hamilton, R.; Richter, L.; Salleo, A.; Shkunov, M.; Sparrowe, D.; Tierney, S.; Zhang, W., Semiconducting Thienothiophene Copolymers: Design, Synthesis, Morphology, and Performance in Thin-Film Organic Transistors. *Advanced Materials* **2009,** *21*, 1091-1109.

25. Heeney, M.; Bailey, C.; Genevicius, K.; Shkunov, M.; Sparrowe, D.; Tierney, S.; McCulloch, I., Stable Polythiophene Semiconductors Incorporating Thieno[2,3-*b*]thiophene. *Journal of the American Chemical Society* **2005,** *127*, 1078-1079.

26. Usta, H.; Facchetti, A., Polymeric and Small-Molecule Semiconductors for Organic Field-Effect Transistors. In *Large Area and Flexible Electronics*, Wiley-VCH Verlag GmbH & Co. KGaA2015; pp 1-100.

27. McCulloch, I.; Heeney, M.; Bailey, C.; Genevicius, K.; MacDonald, I.; Shkunov, M.; Sparrowe, D.; Tierney, S.; Wagner, R.; Zhang, W.; Chabinyc, M. L.; Kline, R. J.; McGehee, M. D.; Toney, M. F., Liquid-crystalline semiconducting polymers with high charge-carrier mobility. *Nature Materials* **2006,** *5*, 328.

28. Tsao, H. N.; Cho, D. M.; Park, I.; Hansen, M. R.; Mavrinskiy, A.; Yoon, D. Y.; Graf, R.; Pisula, W.; Spiess, H. W.; Müllen, K., Ultrahigh Mobility in Polymer Field-Effect Transistors by Design. *Journal of the American Chemical Society* **2011,** *133*, 2605-2612.

29. Lei, T.; Cao, Y.; Zhou, X.; Peng, Y.; Bian, J.; Pei, J., Systematic Investigation of Isoindigo-Based Polymeric Field-Effect Transistors: Design Strategy and Impact of Polymer Symmetry and Backbone Curvature. *Chemistry of Materials* **2012,** *24*, 1762-1770.

30. Mei, J.; Kim, D. H.; Ayzner, A. L.; Toney, M. F.; Bao, Z., Siloxane-Terminated Solubilizing Side Chains: Bringing Conjugated Polymer Backbones Closer and Boosting Hole Mobilities in Thin-Film Transistors. *Journal of the American Chemical Society* **2011,** *133*, 20130-20133.

31. Li, J.; Zhao, Y.; Tan, H. S.; Guo, Y.; Di, C.-A.; Yu, G.; Liu, Y.; Lin, M.; Lim, S. H.; Zhou, Y.; Su, H.; Ong, B. S., A stable solution-processed polymer semiconductor with record high-mobility for printed transistors. *Scientific Reports* **2012,** *2*, 754.

32. Li, Y.; Singh, S. P.; Sonar, P., A High Mobility P-Type DPP-Thieno[3,2-*b*]thiophene Copolymer for Organic Thin-Film Transistors. *Advanced Materials* **2010,** *22*, 4862-4866.

33. Bronstein, H.; Chen, Z.; Ashraf, R. S.; Zhang, W.; Du, J.; Durrant, J. R.; Shakya Tuladhar, P.; Song, K.; Watkins, S. E.; Geerts, Y.; Wienk, M. M.; Janssen, R. A. J.; Anthopoulos, T.; Sirringhaus, H.; Heeney, M.; McCulloch, I., Thieno[3,2-*b*]thiophene−Diketopyrrolopyrrole-Containing Polymers for High-Performance Organic Field-Effect Transistors and Organic Photovoltaic Devices. *Journal of the American Chemical Society* **2011,** *133*, 3272-3275.

34. Chen, Z.; Lee, M. J.; Shahid Ashraf, R.; Gu, Y.; Albert-Seifried, S.; Meedom Nielsen, M.; Schroeder, B.; Anthopoulos, T. D.; Heeney, M.; McCulloch, I.; Sirringhaus, H., High-Performance Ambipolar Diketopyrrolopyrrole-Thieno[3,2-*b*]thiophene Copolymer Field-Effect Transistors with Balanced Hole and Electron Mobilities. *Advanced Materials* **2012,** *24*, 647-652.

35. Schroeder, B. C.; Kurosawa, T.; Fu, T.; Chiu, Y.-C.; Mun, J.; Wang, G.-J. N.; Gu, X.; Shaw, L.; Kneller, J. W. E.; Kreouzis, T.; Toney, M. F.; Bao, Z., Taming Charge Transport in Semiconducting Polymers with Branched Alkyl Side Chains. *Advanced Functional Materials* **2017,** *27*, 1701973.

36. Meager, I.; Ashraf, R. S.; Mollinger, S.; Schroeder, B. C.; Bronstein, H.; Beatrup, D.; Vezie, M. S.; Kirchartz, T.; Salleo, A.; Nelson, J.; McCulloch, I., Photocurrent Enhancement from Diketopyrrolopyrrole Polymer Solar Cells through Alkyl-Chain Branching Point Manipulation. *Journal of the American Chemical Society* **2013,** *135*, 11537-11540.

37. Vezie, M. S.; Few, S.; Meager, I.; Pieridou, G.; Dörling, B.; Ashraf, R. S.; Goñi, A. R.; Bronstein, H.; McCulloch, I.; Hayes, S. C.; Campoy-Quiles, M.; Nelson, J., Exploring the origin of high optical absorption in conjugated polymers. *Nature Materials* **2016,** *15*, 746.

38. Qiu, G.; Jiang, Z.; Ni, Z.; Wang, H.; Dong, H.; Zhang, J.; Zhang, X.; Shu, Z.; Lu, K.; Zhen, Y.; Wei, Z.; Hu, W., Asymmetric thiophene/pyridine flanked diketopyrrolopyrrole polymers for high performance polymer ambipolar field-effect transistors and solar cells. *Journal of Materials Chemistry C* **2017,** *5*, 566-572.

39. Bijleveld, J. C.; Verstrijden, R. A. M.; Wienk, M. M.; Janssen, R. A. J., Copolymers of diketopyrrolopyrrole and thienothiophene for photovoltaic cells. *Journal of Materials Chemistry* **2011,** *21*, 9224-9231.

40. Yum, J.-H.; Holcombe, T. W.; Kim, Y.; Yoon, J.; Rakstys, K.; Nazeeruddin, M. K.; Gratzel, M., Towards high-performance DPP-based sensitizers for DSC applications. *Chemical Communications* **2012,** *48*, 10727-10729.

41. Yun, H.-J.; Kang, S.-J.; Xu, Y.; Kim, S. O.; Kim, Y.-H.; Noh, Y.-Y.; Kwon, S.-K., Dramatic Inversion of Charge Polarity in Diketopyrrolopyrrole-Based Organic Field-Effect Transistors via a Simple Nitrile Group Substitution. *Advanced Materials* **2014,** *26*, 7300-7307.

42. Choi, H. H.; Baek, J. Y.; Song, E.; Kang, B.; Cho, K.; Kwon, S.-K.; Kim, Y.-H., A Pseudo-Regular Alternating Conjugated Copolymer Using an Asymmetric Monomer: A High-Mobility Organic Transistor in Nonchlorinated Solvents. *Advanced Materials* **2015,** *27*, 3626-3631.

43. Ji, Y.; Xiao, C.; Wang, Q.; Zhang, J.; Li, C.; Wu, Y.; Wei, Z.; Zhan, X.; Hu, W.; Wang, Z.; Janssen, R. A. J.; Li, W., Asymmetric Diketopyrrolopyrrole Conjugated Polymers for Field-Effect Transistors and Polymer Solar Cells Processed from a Nonchlorinated Solvent. *Advanced Materials* **2016,** *28*, 943-950.

44. Jones, C.; Boudinet, D.; Xia, Y.; Denti, M.; Das, A.; Facchetti, A.; Driver, T. G., Synthesis and Properties of Semiconducting Bispyrrolothiophenes for Organic Field-Effect Transistors. *Chemistry – A European Journal* **2014,** *20*, 5938-5945.

45. Ito, Y.; Virkar, A. A.; Mannsfeld, S.; Oh, J. H.; Toney, M.; Locklin, J.; Bao, Z., Crystalline Ultrasmooth Self-Assembled Monolayers of Alkylsilanes for Organic Field-Effect Transistors. *Journal of the American Chemical Society* **2009,** *131*, 9396-9404.

46. Nguyen, H. Q.; Rainbolt, E. A.; Sista, P.; Stefan, M. C., Synthesis and Polymerization of Fused-Ring Thienodipyrrole Monomers. *Macromolecular Chemistry and Physics* **2012,** *213*, 425-430.

47. Bittle, E. G.; Basham, J. I.; Jackson, T. N.; Jurchescu, O. D.; Gundlach, D. J., Mobility overestimation due to gated contacts in organic field-effect transistors. *Nature Communications* **2016,** *7*, 10908.

48. Phan, H.; Wang, M.; Bazan, G. C.; Nguyen, T.-Q., Electrical Instability Induced by Electron Trapping in Low-Bandgap Donor–Acceptor Polymer Field-Effect Transistors. *Advanced Materials* **2015,** *27*, 7004-7009.

49. Yuan, Y.; Giri, G.; Ayzner, A. L.; Zoombelt, A. P.; Mannsfeld, S. C. B.; Chen, J.; Nordlund, D.; Toney, M. F.; Huang, J.; Bao, Z., Ultra-high mobility transparent organic thin film transistors grown by an off-centre spin-coating method. *Nature Communications* **2014,** *5*, 3005.

CHAPTER 5

INFLUENCE OF FUNCTIONALIZED SIDE CHAINS OF POLYTHIOPHENE DIBLOCK COPOLYMERS ON THE PERFORMANCE OF CdSe QUANTUM DOT HYBRID SOLAR CELLS

Authors –Chandima Bulumulla,[†] Jia Du,[†] Katherine Washington,[†] Ruvanthi N. Kularatne,[†] Hien Q. Nguyen,[†] Michael C. Biewer,[†] and Mihaela C. Stefan[†*]

[†]Department of Chemistry and Biochemistry, BE26

The University of Texas at Dallas

800 West Campbell Road

Richardson, Texas 75080, USA

[*]Department of Bioengineering, BSB11

The University of Texas at Dallas

800 West Campbell Road

Richardson, Texas 75080, USA

5.1 Abstract

The incorporation of functional groups into the side chains of polythiophenes can improve the phase separation of polymer: nanoparticle hybrid solar cells (HSCs). Our results showed that by introducing 17 mol% thiol functionality in the polymer, the J_{sc} and V_{oc} can be increased by twofold in polymer: CdSe quantum dot (QD) HSCs.

5.2 Introduction

An interpenetrated nanostructured network of organic electron-rich polymers (p-type) and electron-deficient inorganic nanoparticles (n-type) constitute a hybrid system which possess combined properties of both material classes.[1-4] Organic polymers with solution processability and good opto-electronic properties combined with inorganic semiconducting nanocrystals with tunable band gaps make a viable candidate for the next generation solar cells. Since the first hybrid solar cell (HSC) demonstrated by Alivisatos and co-workers using regioregular poly(3-hexylthiophene) (*rr*-P3HT) as the electron-rich (p-type) semiconductor and CdSe nanorods as the electron-deficient (n-type) semiconductor,[3, 5] different HSCs have been fabricated employing polythiophenes,[6-14] phenylenevinylene polymers,[15-17] and low band gap polymers.[18, 19] Among many semiconductor n-type nanocrystals, CdSe,[2, 3, 8, 9, 16 20, 21] CdTe,[22, 23] ZnO,[24] PbS,[18] CdS[25] and alloyed nanocrystals have been investigated in applications of hybrid solar cells yielding a maximum efficiency of 5.5% reported by Ma and co-workers for a poly(2,6-(*N*-(1-octylnonyl) dithieno[3,2-*b*:2′,3′-*d*]pyrrole)-alt-4,7-(2,1,3 benzothiadiazole)) blended with PbS$_x$Se$_{1-x}$ quantum dots.[19] Poor efficiencies for hybrid solar cells compared to their fullerene counterparts are most likely due to the poor nanostructured interfaces which hinders the exciton diffusion leading to

154

charge recombination pathways.[6, 9, 26] Achieving a bi-continuous network with well-defined interfaces is expected to improve charge extraction and transport.[25]

Therefore, attention is required to exploit new strategies to control the phase separation in order to improve interfacial interactions between inorganic nanocrystals and polymers. One of the key factors governing favorable three-dimensional interpenetrating network is the blending morphology. A number of methods have been utilized to obtain favorable organic-inorganic interfaces including modifications of the polymer architecture,[6] adaptation of nanocrystal surfaces via ligand exchange reactions and, in-situ polymer-nanocrystal formations.[7, 10]

Out of the aforementioned techniques, nanocrystal ligand exchange reactions and introduction of functional groups as polymer end groups have proven to be effective. Surface ligands employed in nanocrystal syntheses serves as a platform for surface passivation to generate monodispersed nanocrystals with very few surface defects. Although these ligands improve blending morphologies with polymers due to enhanced solubility in common processing solvents, they diminish photovoltaic performances by impeding charge transfer processes due to their insulating nature. Therefore, by exchanging native ligands with ligands capable of electron transfer, HSC performances can be improved. To control phase separation, Frechet and co-workers demonstrated that end functionalization of a polymer with an amine group could lead to larger interfacial areas for exciton charge separation.[6] A maximum power conversion efficiency (PCE) of 1.6% was achieved with CdSe nanorods at a 40% nanocrystal loading capacity blended with end functionalized P3HT. Later, Stefan and co-workers demonstrated a maximum efficiency of 0.90% and 0.60% of HSCs derived from H/ allyl- and H/ propylthiol terminated *rr*-P3HT blended with CdSe quantum dots, respectively.[8]

155

Moreover, PCE enhancements are achieved in HSCs by virtue of delicate ligand engineering involving thiols, amines and carboxylic acid groups. Kruger and co-workers showed through a simple hexanoic acid treatment, PCEs could increase to 2.0% for a P3HT:CdSe QD HSC.[27] The role of thiols in ligand exchange reactions were later established with the use of *tert*-butylthiols,[28] monothiols[29] and dithiols[30] with varying chain lengths. Out of the many thiols used, ethanedithiol (EDT) was found to be an interesting small molecule for post-deposition ligand exchange reactions where Xue and co-workers demonstrated the efficiency increased from 1.4% to 2.6% for P3HT: CdSe nanorod based HSCs and from 3.3% to 4.7% for PCPDTBT: CdSe nanorod based HSCs upon post deposition EDT ligand exchange reactions.[31] With the drastic differences observed using the EDT molecule, inclusion of thiols onto the side chains would be highly interesting with the intention of grafting more nanoparticles to the polymer backbone.

Here, we report two novel polythiophene block copolymers (P3 and P4) and compare their opto-electronic properties with H/Br *rr*-P3HT (P1) and allyl end capped *rr*-P3HT (2) (*see* Figure 5.1). To have a reasonable comparison of opto-electronic properties the tested H/Br P3HT, allyl-P3HT and the polythiophene copolymers have similar molecular weights.
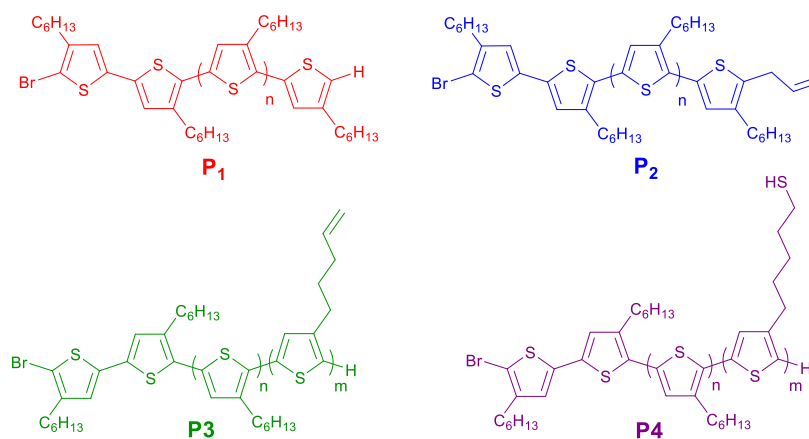
Figure 5.1 Chemical structures of P1-P4

5.3 Experimental

5.3.1 Materials and Methods

All commercial chemicals were purchased from Aldrich and Fisher chemicals and were used without further purification unless otherwise noted. All the reactions were conducted under a nitrogen atmosphere using oven-dried glassware. Tetrahydrofuran (THF) was dried over sodium/benzophenone ketyl and distilled prior to use. 2,5-dibromo-3-hexylthiophene (M1), regioregular P3HT (P1) and allyl-terminated P3HT (P2) were synthesized according to previously published procedures.[8, 33]

NMR Measurements: ^{1}H NMR spectra were recorded on a 500 MHz Bruker AVANCE III^{TM} spectrometer using deuterated chloroform as the solvent. Multiplicities were given as: s (singlet), d (doublet), t (triplet), q (quartet), br. s (broad singlet), m (multiplet).

Gas Chromatography Mass Spectrometry: GC-MS spectra were obtained on Agilent 6890-5973 GC-MS workstation. The gas chromatography column was constructed from Hewlett-Packard fused silica capillary column cross-linked with 5% phenylmethylsiloxane. He was used as the carrier gas with 1 mL/min flow rate. Temperature was ramped from 70 °C to 280 °C (10 °C/min) while injector and detector temperature was set to 250 °C.

Size Exclusion Chromatography Characterization: Size exclusion chromatography (SEC) data were obtained on a Viscotek VE3580 system equipped with viscoGEL columns (GMHHR-M) connected to a refractive index and UV detectors. HPLC grade THF was used as the eluent with 1 mL/min rate at 30 °C with GPC$_{max}$ as the sample module. Calibration based on polystyrene standards were applied to determine the molecular weights.

FT-IR Measurements: Attenuated total reflectance Fourier transform infrared (ATR-FTIR) spectroscopy was carried out using Nicolet 380 FTIR.

UV-vis Measurements: The UV-vis absorption profiles were measured with an Agilent 8453 UV-vis spectrometer. The UV-vis absorption of the molecules in chloroform was conducted in 1 cm cuvettes and the thin film were prepared by drop-casting the polymer solutions in chloroform on microscope slides.

Photoluminescence Studies: Fluorescence measurements were recorded on Perkin-Elmer LS 50 BL fluorimeter at room temperature in a 1cm quartz cuvette by dissolving a known amount of polymer in chloroform. To perform photoluminescence quenching studies, calculated amounts of CdSe QDs in chloroform were added to polymer solutions.

Electrochemical Analysis: CV studies, Ag/AgCl and platinum electrodes were used as reference and auxiliary electrodes, respectively, while a thin polymer film deposited on a platinum electrode was the working electrode. A 0.1 M solution of tetrabutylammonium hexafluorophosphate in anhydrous acetonitrile was used as the electrolyte. All the CV experiments were carried out at a scan rate of 100 mV s^{-1} under argon.

Transmission Electron Microscopy Imaging: Active layer was deposited on a PEDOT:PSS coated ITO glass and dropped into a petri dish containing DI water. Floated films were placed on a 200 mesh carbon coated copper grid and imaged from a Technai G2 Spirit TEM instrument operated at 120 keV. TEM images of QDs were obtained by drop casting toluene solutions containing QDs onto 200 mesh carbon coated copper grids.

Atomic Force Microscopy Imaging: Tapping mode atomic force microscopy (TMAFM) was performed on the active layers using a Nanoscope IV Multimode Veeco equipped with a vertical

engage scanner. The TMAFM images were recorded using a Si cantilever with a resonance frequency of 320 kHz and spring constant of 42 N/m. The images were collected in 3×3 µm scan size with a frequency of 2 Hz.

Polymer: CdSe QD hybrid photovoltaic device fabrication: Patterned ITO glasses were cleaned with DI water, acetone, toluene and isopropanol successively for 10 mins and treated in UV-ozone for 30 mins. A 30 nm thick layer of PEDOT: PSS was spin coated on the ITO glass and annealed at 150 °C for 10 mins in a nitrogen filled glovebox. The photoactive layer was spin coated (1000 rpm, 45 s) onto the PEDOT: PSS coated ITO glass. The blend film was dried for 5 s and dipped in a solution containing 0.01 M EDT in acetonitrile for 30 s followed by rinsing with pure acetonitrile. The devices were annealed at 120 °C for 10 mins and loaded to high vacuum chamber to deposit a 100 nm thick Al cathode. *J-V* testings were carried out using a Keithley 2400 interfaced with Labview software. The solar simulator used was an ORIEL 67005 equipped with a Xe lamp calibrated to 100 mW cm^{-2} with a Si photodiode purchased from PV measurements Inc.

5.3.2 Synthesis of Materials

3-Pentenylthiophene

To a clean 100 mL three neck round bottom flask was added magnesium turnings (24.0 mmol, 0.57 g) and dry diethyl ether (40 mL) under N$_2$. The solution was cooled to 0 °C while adding 5-bromo-1-pentene (23.5 mmol, 2.4 mL) dropwise with a few drops of 1,2-dibromoethane. The ice bath was removed and gently refluxed for 2 h. To a separate clean 100 mL three neck round bottom flask was added 3-bromothiophene (20.3 mmol, 1.9 mL), Ni(dppp)Cl$_2$ (0.19 mmol, 0.10 g) and dry diethyl ether (20 mL) under N$_2$. Grignard reagent was cannulated into the flask containing the

catalyst and refluxed overnight. The reaction was quenched by pouring the contents in the flask to a beaker containing ice. Crude compound was extracted with ether (3×30 mL), washed with water (3×30 mL), brine (50 mL) and dried over anhydrous $MgSO_4$ and filtered. The solvent was removed under reduced pressure and pure compound was afforded by column chromatography with hexane as the eluent (1.43 g, Yield = 47.8 %). ^{1}H NMR (500 MHz, $CDCl_3$): δ_H 1.73 (m, 2H), 2.09 (q, 7.1 Hz, 2H), 2.65 (t, 7.7 Hz, 2H), 5.00 (m, 2H), 5.83 (m, 1H), 6.94 (m, 2H), 7. 24 (dd, 4.8 Hz and 3 Hz, 1H) (Figure 5.2); EIMS (M^+) m/z calcd for $C_9H_{12}S$ 152.07, found 152.1
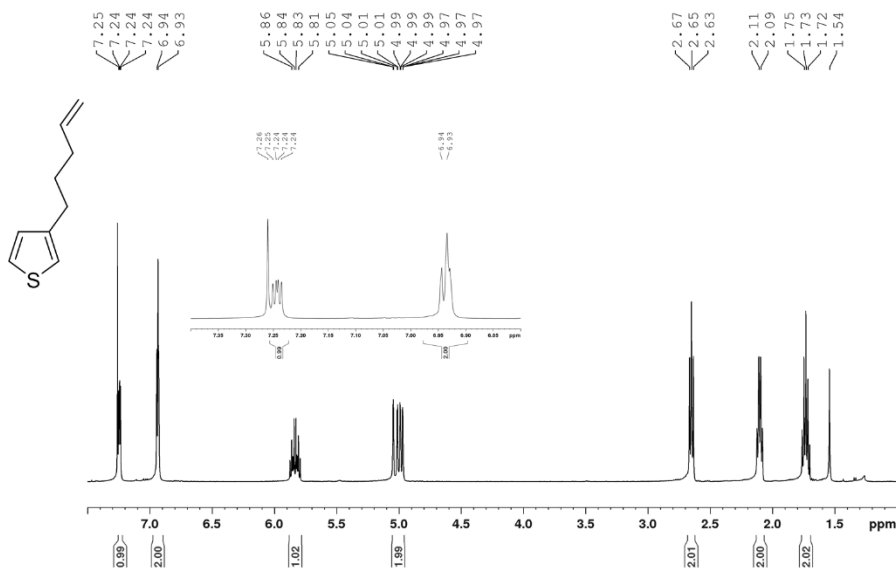
Figure 5.2 ^{1}H NMR spectrum of 3-pentenylthiophene

2-Bromo-3-pentenyl thiophene

To a clean 100 mL three neck round bottom flask was added 3-pentenylthiophene (6.57 mmol, 1.00 g) with dry THF (20 mL) under N_2. The flask was cooled to -78 °C and 2.5 M *n*-BuLi (7 mmol, 2.8 mL) was added dropwise to the solution mixture. The solution was allowed to stir at -

78 °C for 1.5 h and the temperature was raised to -40 °C. At this time, CBr$_4$ (13.79 mmol, 4.573 g) in THF (10 mL) was added in one portion and stirred for 1 h at room temperature. Reaction was quenched in ice and the organic layer was extracted with diethyl ether (3×30 mL), washed with DI water (3×30 mL), brine (50 mL) and dried over anhydrous MgSO$_4$ and filtered. The solvent was removed under reduced pressure and the pure compound was obtained by column chromatography with hexane as the eluent (0.83 g, Yield = 54.5 %). ^{1}H NMR (CDCl$_3$, 500 MHz): δ$_H$ 1.68 (m, 2H), 2.07 (q, 7.2 Hz, 2H), 2.56 (t, 7.7 Hz, 2H), 5.00 (m, 2H), 5.80 (m, 1H), 6.81 (m, 1H), 6.88 (dd, 1.5 Hz, 1H) (Figure 5.3); EIMS (M$^+$) m/z calcd for C$_9$H$_{11}$BrS 231.15, found 232.0
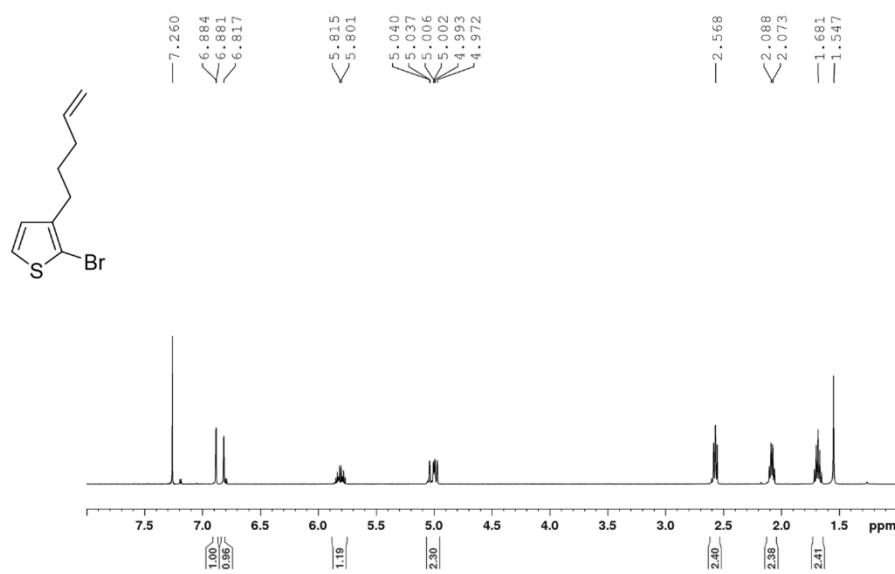
Figure 5.3 ^{1}H NMR spectrum of 2-bromo-3-pentenylthiophene

2, 5-Dibromo-3-pentenylthiophene (M2)

An oven dried 100 mL three neck round bottom flask was charged with diisopropylamine (9.48 mmol, 1.33 mL) with THF (30 mL) under N$_2$. To the flask was added 2.5 M *n*-BuLi (4.31 mmol, 1.74 mL) to generate LDA at -78 °C and stirred for 1 h. 2-Bromo-3-pentenylthiophene (4.31 mmol,

0.97 g) was added to the pot in one portion and reacted for 1 h. At this time CBr$_4$ (4.74 mmol, 1.57 g) in THF (5 mL) was injected to the flask and reacted for 1 h followed by quenching with ice. Organic layer was extracted with diethyl ether (3×30 mL), washed with DI water (3×30 mL), brine (50 mL) and dried over anhydrous MgSO$_4$ and filtered. The solvent was removed under reduced pressure and pure compound was obtained by column chromatography with hexane as the eluent (0.83 g, Yield = 54.5 %). ^{1}H NMR (500 MHz, CDCl$_3$): δ_H 1.65 (m, 2H), 2.07 (q, 7.2 Hz, 2H), 2.52 (t, 7.7 Hz, 2H), 5.00 (m, 2H), 5.80 (m, 1H), 6.78 (s, 1H) (Figure 5.4); EIMS (M$^+$) m/z calcd for C$_9$H$_{11}$BrS 310.05, found 309.9
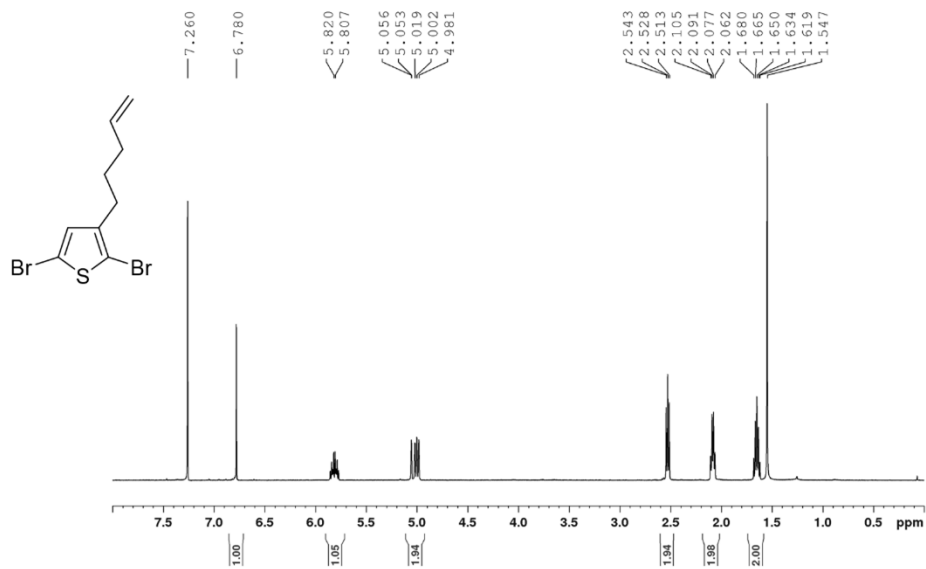
Figure 5.4 ^{1}H NMR of 2,5-dibromo-3-pentenylthiophene (M2)

Polymer P3

To a solution of 2,5-dibromo-3-hexylthiophene (M1) (9.12 mmol, 2.97 g) in THF (12.4 mL) *(Flask A)* was added *tert*-butylmagnesium chloride (9.12 mmol, 4.56 mL) under N$_2$ at room temperature. With an offset of 30 mins, to a solution of 2,5-dibromo-3-pentenylthiophene (M2) (4.51 mmol,

1.41 g) in THF (12.4 mL) *(Flask B)* was added *tert*-butylmagnesium chloride (4.51 mmol, 2.25 mL) under N$_2$ at 40 °C. After 2 h a sample was withdrawn from flask A and conversion was analyzed using GCMS. To *flask A*, Ni(dppp)Cl$_2$ (0.147 mmol, 79.5 mg) was quickly added and a sample was withdrawn and crashed in methanol to check the molecular weight. Another sample was withdrawn from *flask B* at this time to check for the conversion using GCMS. The contents of the *flask B* was cannulated to *flask A*. After stirring at 50 °C for 2 h, the mixture was cooled to room temperature and precipitated in methanol. The precipitate was filtered and washed with methanol (24 h), hexane (24 h), and extracted with chloroform (3 h) in a Soxhlet apparatus. The chloroform fraction was concentrated and dried to yield the polymer P3. ^{1}H NMR (CDCl$_3$, 500 MHz): δ_H 0.91 (t, 6.6 Hz, 3H), 1.30-1.47 (m, 6H), 1.70 (m, 2H), 1.81 (m, 2H), 2.20 (m, 2H), 2.80 (t, 7.4 Hz, 2H), 5.04 (m, 2H), 5.88 (m, 1H), 6.98 (s, 1H); (Figure 5.5) SEC: M_n = 10,094 g mol^{-1}, PDI = 1.37
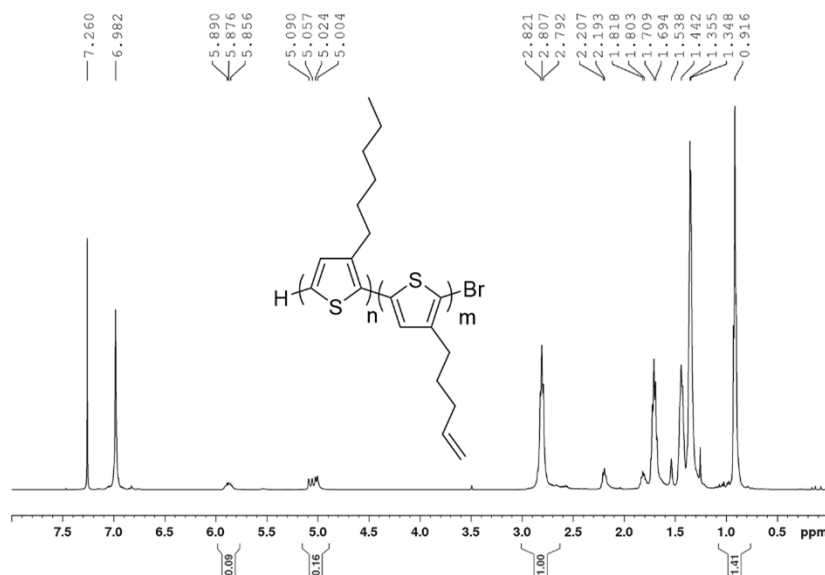
Figure 5.5 ^{1}H NMR of polymer P3

Polymer P3a

To a solution of polymer P3 (0.08 mmol, 0.80 g) dissolved in anhydrous THF (50 mL) was added 0.5 M 9-BBN solution (8 mmol, 16 mL) under N_2. The solution was stirred for 12 h at 40 °C, at which point a 6 M NaOH solution (16 mL) was added to the reaction flask followed by stirring at 40 °C for 15 mins. Flask was cooled to room temperature and 33% aqueous solution of hydrogen peroxide (16 mL) was added slowly. After heating at 40 °C for 12 h, polymer was isolated by precipitation with methanol. Precipitate was filtered and washed with methanol (24 h), hexane (24 h), and finally extracted with chloroform (3h) in a Soxhlet apparatus. The chloroform fraction was concentrated and dried to yield the polymer P3a. ^{1}H NMR (CDCl$_3$, 500 MHz): δ_H 0.91 (t, 6.6 Hz, 3H), 1.30-1.47 (m, 10H), 1.70 (m, 4H), 2.80 (t, 7.4 Hz, 4H), 3.67 (br, 2H), 6.98 (s, 2H) (Figure 5.6); SEC: M_n = 10,938 g mol^{-1}, PDI = 1.49
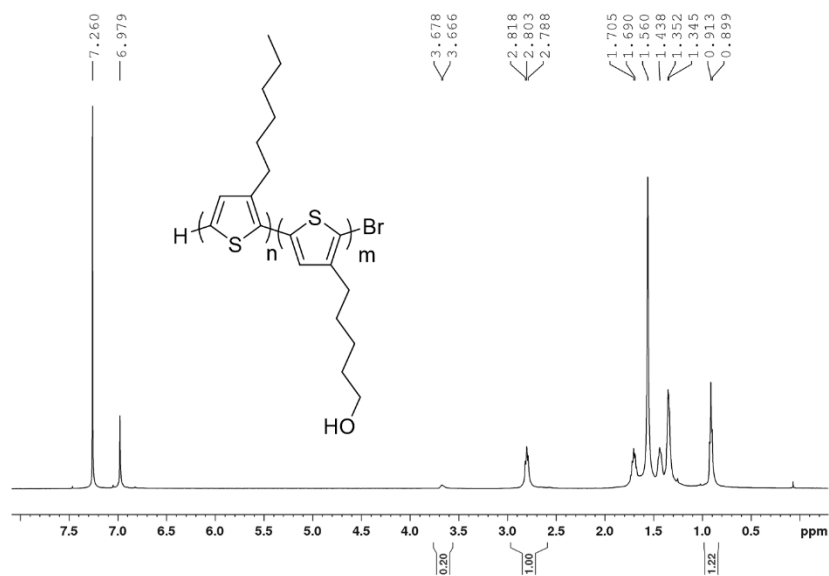
Figure 5.6 ^{1}H NMR of Polymer P3a

Polymer P3b

To a solution of triphenyl phosphine (7.5 mmol, 1.95 g) in anhydrous THF (25 mL) was added diisopropyl azodicarboxylate (DIAD) (7.5 mmol, 1.5 mL) at -30 °C under N_2. The DIAD-PPh$_3$ adduct was formed as a pale yellow precipitate after 30 mins. At this time the flask was removed from the cooling bath and allowed to warm to room temperature. To the flask was dropwise added a solution of polymer P3a (0.075 mmol, 0.75 g) and thiolacetic acid (7.5 mmol, 0.5 mL) in THF (20 mL). After heating at 40 °C for 8 h, the polymer was isolated by precipitation with methanol. Precipitate was filtered and washed with methanol (24 h), hexane (24 h), and finally extracted with chloroform (3h) in a Soxhlet apparatus. The chloroform fraction was concentrated and dried to yield the polymer P3b. ^{1}H NMR (CDCl$_3$, 500 MHz): δH 0.91 (t, 6.6 Hz, 3H), 1.30-1.47 (m, 10H), 1.70 (m, 4H), 2.31 (s, 3H), 2.80 (t, 7.4 Hz, 4H), 2.98 (t, 7.0 Hz, 2H), 6.98 (s, 2H) (Figure 5.7); SEC: M_n = 10,965 g mol^{-1}, PDI = 1.49
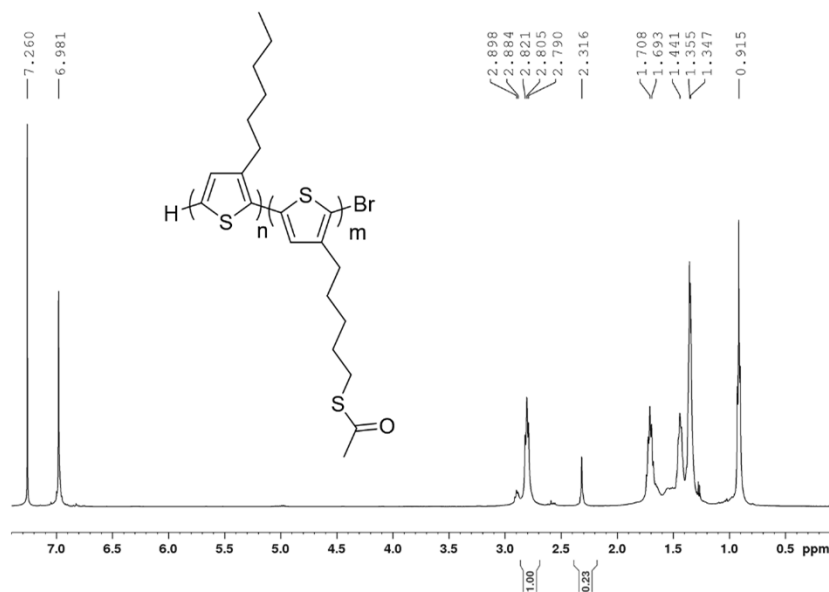
Figure 5.7 ^{1}H NMR of Polymer P3b

Polymer P4

To a solution of polymer P3b (0.06 mmol, 0.60 g) in anhydrous THF (50 mL) was added LiAlH₄ (6 mmol, 0.22 g) under N$_2$. Solution was stirred at 40 °C for 4 h followed by precipitation in methanol/ HCl (100 mL) mixture. Precipitate was filtered and washed with methanol (24 h), hexane (24 h) and finally extracted with chloroform (3h) in a soxhlet apparatus. Chloroform fraction was concentrated and dried to yield the polymer P4. ¹H NMR (CDCl$_3$, 500 MHz): δ$_H$ 0.91 (br, 3H), 1.30-1.47 (m, 12H), 1.69 (br, 4H), 2.61 (t, 10 Hz, 2H), 2.80 (br, 4H), 6.98 (s, 2H); (Figure 5.8) SEC: M_n = 10,147 g mol⁻¹, PDI = 1.49

Figure 5.8 ¹H NMR of Polymer P4
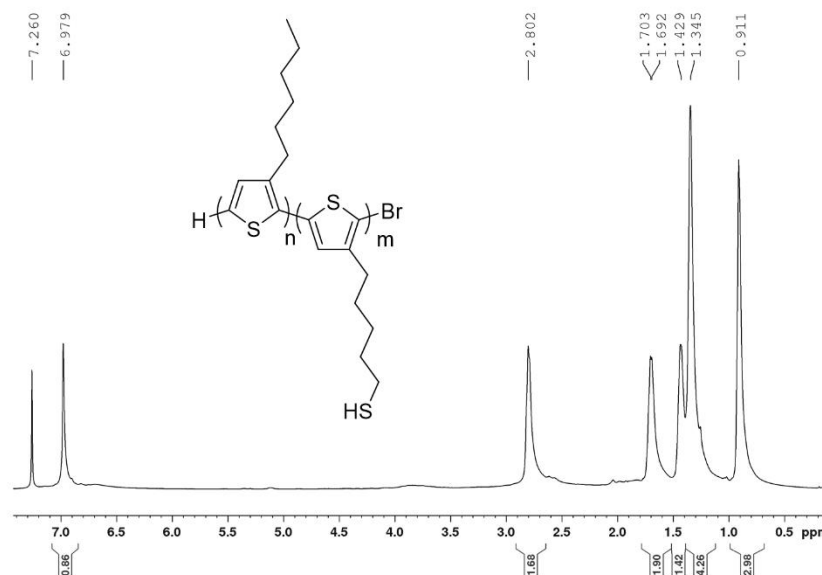
CdSe QD synthesis and colloidal ligand exchange

Nearly monodispersed nanocrystals were synthesized using a previously published procedure with slight modifications.[2] In a typical reaction, cadmium oxide (1 mmol, 128.4 mg), oleic acid (20

mmol, 5.65 g) and trioctylphosphine oxide (5 mmol, 1.93 g) were combined in a 50 mL three neck round bottom flask and degassed at 150 °C. After 1.5 h flask was purged with N_2 and heated until an optically clear solution is obtained. The temperature of the clear solution was adjusted to 250 °C and a solution of Se powder (1 mmol, 78.96 mg) in 1.33 mL of trioctylphosphine was swiftly injected to the flask. After 2 mins, the heating mantle was removed and quickly cooled to 150 °C by purging air. At 70 °C, 10 mL of toluene was added to prevent solidification of excess ligands. Nanocrystals were precipitated using methanol and collected by centrifugation followed by washing with methanol more than three times. For the ligand exchange, the precipitated CdSe QDs were dissolved in a minimum amount of toluene and refluxed with anhydrous pyridine for 24 h. Pyridine coated CdSe QDs were recovered by precipitation with excess hexane and dried by blowing N_2. For the preparation of the photoactive layer, polymers were blended with nanocrystals with a weight ratio of 1:5 in chlorobenzene/pyridine mixture (95/5 v/v) to have a total concentration of 22.5 mg/ mL.

5.4 Results and Discussion

5.4.1 Synthesis and Characterization

A facile synthetic method to generate side chain functionalized thiophene block copolymers using Grignard Metathesis (GRIM) polymerization is discussed in this paper from 3-alkenyl substituted thiophene monomer which is amenable for post-polymerization chemical modification. To gain insight on the variations in the performances with our previous results,[8] CdSe QDs are employed as the preferred inorganic nanocrystals. To generate block copolymers, 2,5-dibromo-3-

hexylthiophene (M1) and 2,5-dibromo-3-pentenylthiophene (M2) were synthesized according Scheme 5.2 and served as monomers for the synthesis of block copolymers.[32]

Scheme 5.1 Synthesis of 2,5-dibromo-3-pentenylthiophene (M2)
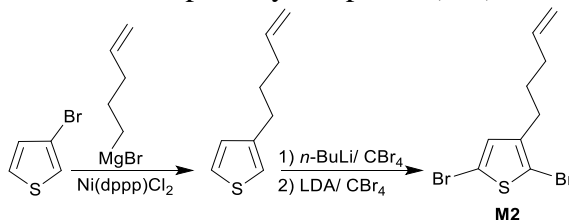
A living P3HT block with an average molecular weight of 8,000 g mol^{-1} was prepared from M1 by GRIM polymerization followed by the sequential addition of monomer M2 (*see* Figure 5.9). Due to the living nature of the Ni catalyst, the resulting monomer 2-bromo-3-pentenyl-5-thienyl magnesium chloride was injected to grow the second block. Even though the molar feed ratios of the monomers were 5:2 (M1:M2), only a 17 mol% incorporation of the second block was seen from ^{1}H NMR analysis. We speculate that the interaction between the π electrons of the alkenyl substituent and the Ni(0) in the catalytic cycle of the GRIM polymerization limits the incorporation of the poly(3-pentenylthiophene). The same reason may be attributed to the low molecular weight obtained for Poly(3-pentenylthiophene). The synthesized block copolymer (P3) was subjected to post-polymerization reactions through a hydroboration/oxidation reaction followed by a Mitsunobu reaction to generate the acetylthiol on the side chains. The subsequent reduction with LiAlH$_4$ generated the thiol containing polymer (P4). H/Br terminated P3HT (P1) and allyl/Br terminated P3HT (P2) with similar molecular weights (DP$_n$ = 60, M_n = 10,000 g mol^{-1}) were synthesized to allow for a meaningful comparison with P3 and P4 (see Table 1). Allyl/Br terminated P3HT (P2) was selected as a reference since it gave the highest efficiency in our previously published report.[8]
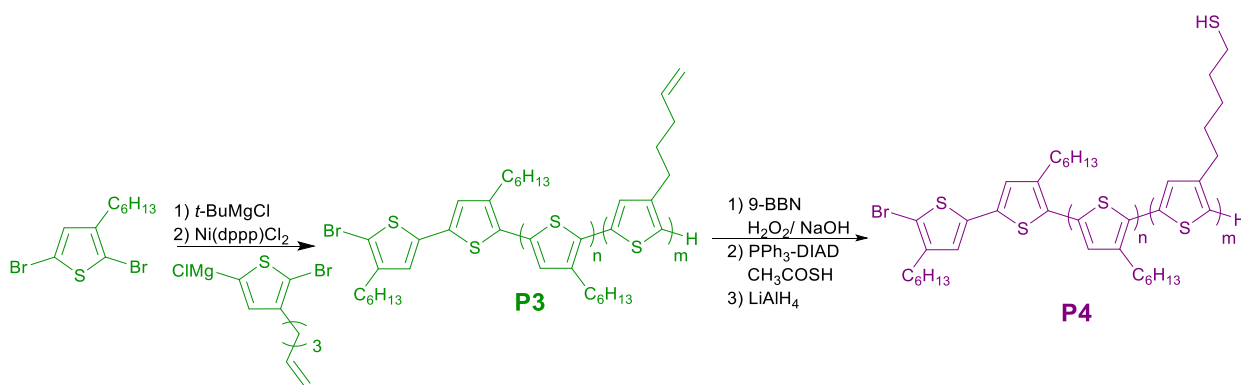
Figure 5.9 Synthesis of polymers P3 and P4

5.4.2 Optical and Electrochemical Properties

To investigate the optical and electronic properties of the four polymers, UV-vis and cyclic voltammetry (CV) studies were performed. UV-vis spectra were recorded in both solution and films with $CHCl_3$ as the solvent. For CV studies, Ag/AgCl and platinum electrodes were used as reference and auxiliary electrodes, respectively, while a thin polymer film deposited on a platinum electrode was the working electrode. A 0.1 M solution of tetrabutylammonium hexafluorophosphate in anhydrous acetonitrile was used as the electrolyte. All the CV experiments were carried out at a scan rate of 100 mV s^{-1} under argon. Based on both spectra (*see* Figure 5.10 and Table 5.1), introduction of the functional groups in the side chain doesn't affect the optical or electronic properties, which is highly desirable for this study.

169

Figure 5.10 UV-vis and CV spectra (a), (b), (c) and (d) of P1, P2, P3 and P4 respectively

Table 5.1 Optical and electrochemical properties of the synthesized polymers

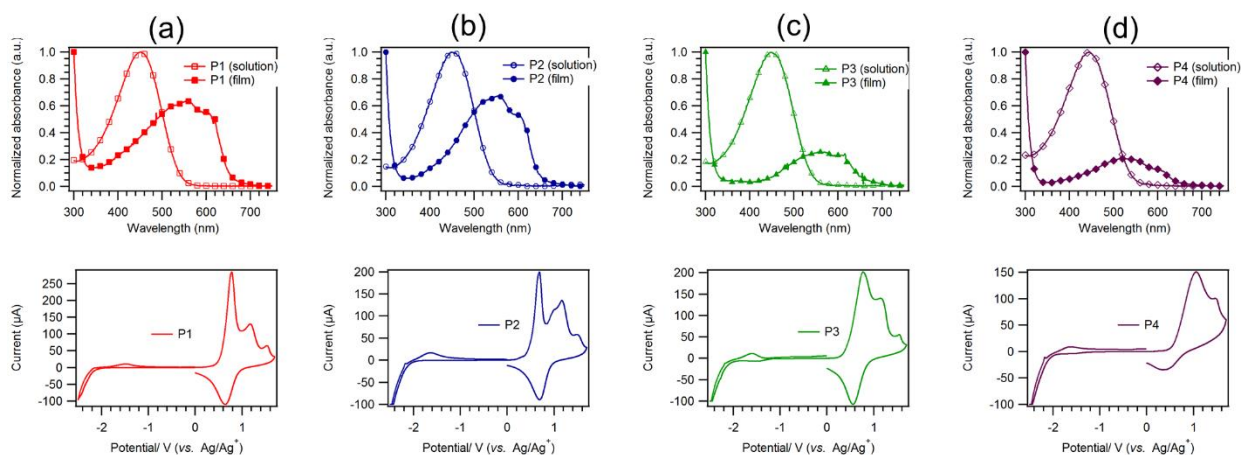| Polymer	$M_n{}^a$ (kDa)	PDI^a	$\lambda_{onset}{}^b$ (nm)	$E_g{}^b$ (eV)	HOMO^c (eV)	LUMO^c (eV)
P1	10.0	1.21	700	1.77	- 5.0	- 3.2
P2	10.0	1.22	700	1.77	- 5.0	- 3.2
P3	10.1	1.37	700	1.77	- 5.0	- 3.2
P4	10.1	1.49	700	1.77	- 5.0	- 3.2

^{a}Determined by SEC using polystyrene standards and THF as the eluent. ^{b}Estimated from the onset of the UV-vis spectra. ^{c}HOMO and LUMO levels are estimated from the onset of the oxidation and reduction peaks of cyclic voltammograms

5.4.3 CdSe QD synthesis and Ligand Exchange

The synthesis of nearly monodispersed CdSe QDs were carried out using a hot injection method performed at 250 °C. The average particle size of the QDs was around 4.0 nm, estimated by UV-vis (Figure 5.11 (a)) and confirmed by transmission electron microscopy (TEM) images (Figure 5.11(c)). Insulating ligands (oleic acid in this case) attached with the as synthesized QDs were replaced from the nanocrystal surface by pyridine molecules. The effective decrease in the inter-particle distance of the nanoparticles as seen from TEM images (*see* Figure 5.11(c) and 5.11(d)) confirms the removal of the long fatty acid chains and introduction of the smaller pyridine

molecules. TEM images were obtained by drop casting toluene solutions containing QDs onto 200

mesh carbon coated copper grids. To further confirm the removal of oleic acid ligands, FT-IR

spectra were recorded before and after the ligand exchange (*see* Figure 5.11(b)). After the ligand

replacement, optical properties of the QDs were found to be preserved by UV-vis analysis (Figure

5.11(a)).
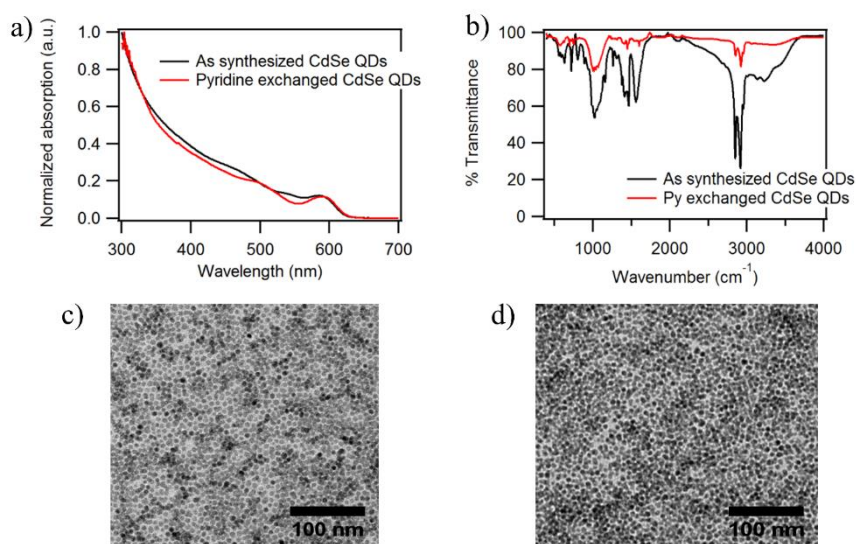
Figure 5.11 a) UV-vis and b) FTIR spectra of CdSe QDs before and after the ligand exchange
with pyridine, TEM image of CdSe QDs c) before and d) after ligand exchange with pyridine

5.4.4 Hybrid Solar Cell Performance

We studied the photovoltaic performances of the blends of block copolymers P3 and P4 and

compared them with H/Br terminated P3HT (P1) and H/allyl-terminated P3HT (P2). The optimum

weight ratios of polymer to CdSe QDs (1:5 wt%) were selected based on the photoluminescence

(PL) quenching of the polymers with CdSe QDs (*see* Figure 5.12) which were carried out in blend

solutions. P4 showed a PL quenching effect which had a normalized intensity below 0.2 when the

weight ratios were 1:5. This outcome may be attributed to the better charge transfer between the polymer and QDs when thiols are present in the polymer backbone.
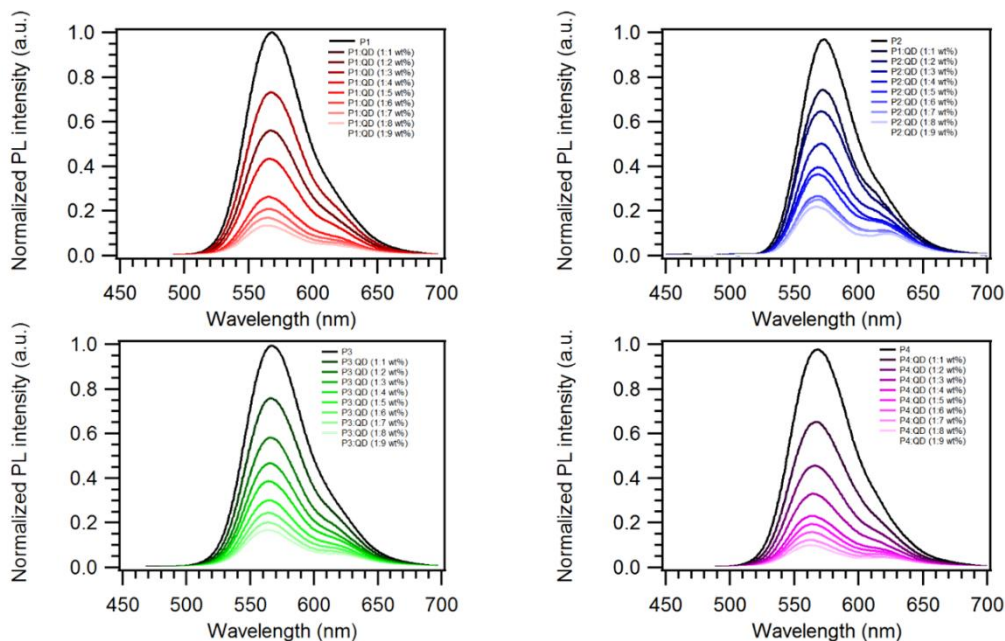
Figure 5.12 Photoluminescence quenching data for polymer: CdSe QDs blends in different weight ratios

Photovoltaic parameters were observed for the four polymer blends. Solution processed hybrid solar cell devices were fabricated with a conventional device structure of ITO/PEDOT: PSS/Polymer: CdSe QD/Al (*see* Figure 5.13 (a)). The photoactive layer was treated with 0.01 M solution of EDT in acetonitrile to improve the photovoltaic performances via a post deposition ligand exchange reaction. Among the four polymers, polymer P4 outperforms the rest with a J_{sc} and a V_{oc} almost two times greater than P1; J_{sc} from 2.01 mA cm^{-2} to 3.67 mA cm^{-2} and V_{oc} from 0.44 V to 0.70 V (*see* Table 5.2). With the introduction of olefin groups at the end of the polymer chain (P2) and side chain (P3), average device parameters increases slightly; J_{sc} from 2.17 mA cm^{-2} to 2.30 mA cm^{-2} (*see* Table 5.2). In order to investigate the effects of functionality and its position

on the device performance, external quantum efficiencies (EQE) were measured. EQE was significantly improved with a maximum value of 47% in the region of 500 nm for polymer P4, while P1 showed a maximum below 30% in the same region (Figure 5.13(b)). The calculated J_{sc} obtained by integration of the EQE curves are 2.65, 2.75, 3.00 and 4.19 mA cm^{-2} respectively for P1 through P4, which shows a 14-30% spectral mismatch compared with the values obtained from the J-V curves.
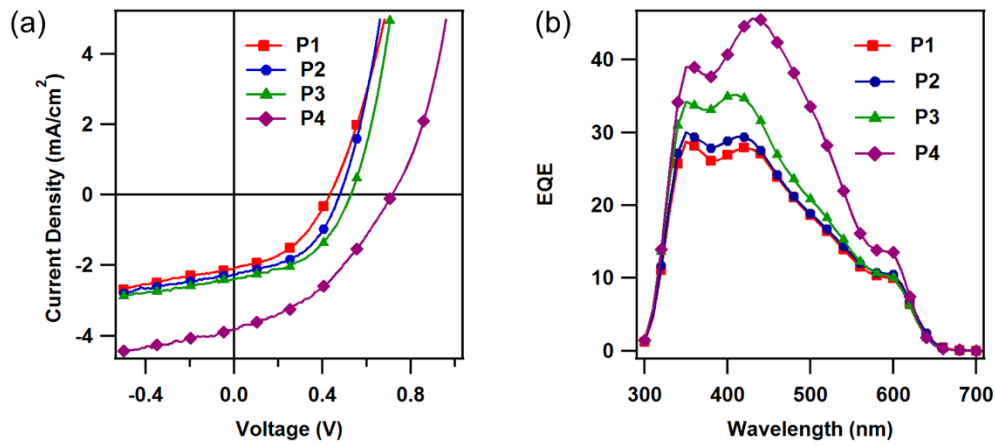
Figure 5.13 (a) J-V curves and (b) EQE curves of the polymer: CdSe QD HSCs
Summary of average photovoltaic properties of the Polymer: CdSe QD based HSCs (AM 1.5G illumination conditions)

Table 5.2 OPV performance of P1-P4

Polymer	V_{oc} (V)	J_{sc} (mA cm^{-2})	FF	PCE %	J_{sc} (mA cm^{-2})
P1	0.44 ± 0.04	2.01 ± 0.07	0.44 ± 0.02	0.39 ± 0.03 (0.42)	2.65
P2	0.50 ± 0.02	2.17 ± 0.08	0.48 ± 0.01	0.52 ± 0.03 (0.55)	2.75
P3	0.52 ± 0.02	2.30 ± 0.09	0.45 ± 0.03	0.54 ± 0.04 (0.58)	3.00
P4	0.70 ± 0.03	3.67 ± 0.08	0.40 ± 0.01	1.02 ± 0.03 (1.05)	4.19

5.4.4 Surface Morphology

The morphology of the active layer was investigated by tapping mode atomic force microscopy (TMAFM) (Figure 5.14 (A)) and TEM (Figure 5.14(B)). The root-mean square (RMS) roughness for the polymer: QD blends are 9.24 nm, 5.28 nm, 4.50 nm and 2.28 nm respectively. With the addition of the thiol groups (only 17 mol%) to the side chain of P1, a drastic decrease in the RMS is observed. By comparing TEM images of the blends films, P2 blend shows better phase separation and minimal QD aggregations compared to P1. With side chain functionalization on P3 and P4 an obvious nanoscale phase separation with a bi-continuous interpenetrating network can be clearly observed, which contributes to a higher exciton dissociation and charge transport efficiency. Therefore, the significantly improved J_{sc} observed is a function of functional group introduction and its position in the polymer.
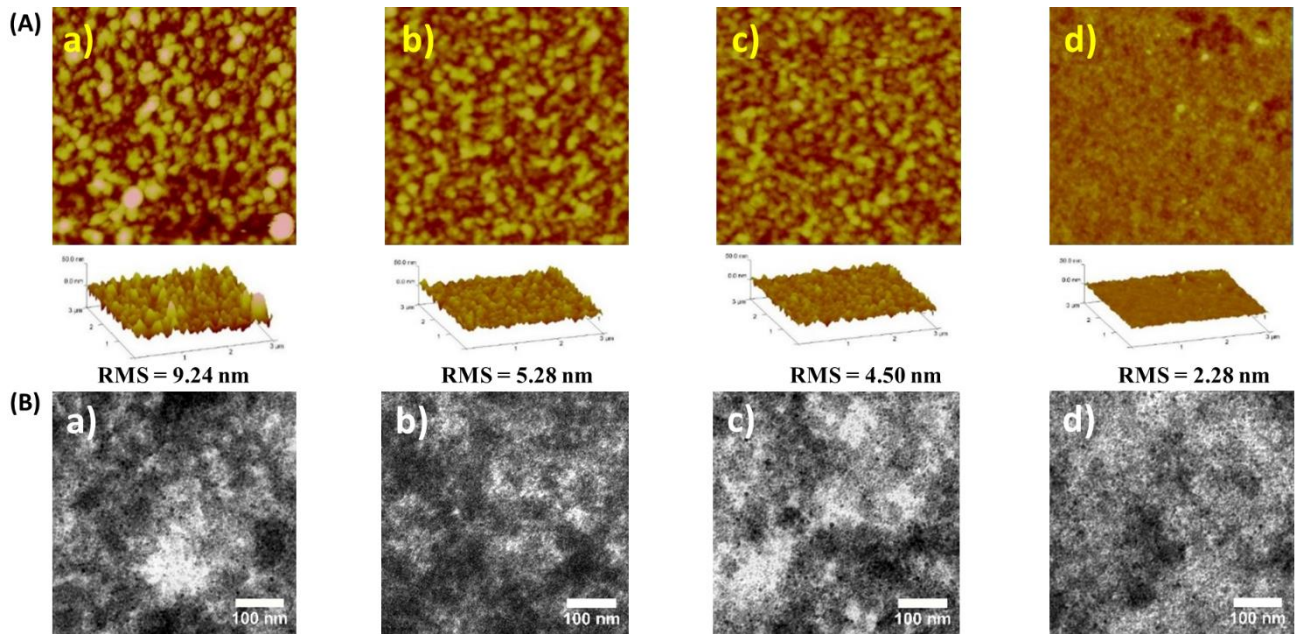

Figure 5.14 (A) Tapping mode AFM phase (3 μm × 3 μm) and height images (B) TEM images of a) P1, b) P2, c) P3 and d) P4: CdSe QD blends

5.5 Conclusion

In summary, the ability to achieve a bi-continuous interpenetrating network on HSCs via effective functionalization of the solubilizing side chains is demonstrated. When thiol functionality is introduced, PCE is nearly doubled due mostly to the observed increase in the J_{sc}. It is noteworthy that these increments were obtained with only a few thiol groups on a polymer having a medium molecular weight. We believe our findings would realize higher PCEs for HSCs on high molecular weight donor-acceptor polymers with multi armed nanoparticles having larger Bohr exciton radii. With the diversity of monomer and polymer design together with device optimizations further improvements would be expected.

5.6 Acknowledgements

5.7 References

1. Colvin, V. L.; Schlamp, M. C.; Alivisatos, A. P., Light-emitting diodes made from cadmium selenide nanocrystals and a semiconducting polymer. *Nature* **1994,** *370*, 354-357.

2. Greenham, N. C.; Peng, X.; Alivisatos, A. P., Charge separation and transport in conjugated-polymer/semiconductor-nanocrystal composites studied by photoluminescence quenching and photoconductivity. *Physical Review B* **1996,** *54*, 17628-17637.

3. Huynh, W. U.; Dittmer, J. J.; Alivisatos, A. P., Hybrid Nanorod-Polymer Solar Cells. *Science* **2002,** *295*, 2425-2427.

4. Zhao, L.; Lin, Z., Crafting Semiconductor Organic−Inorganic Nanocomposites via Placing Conjugated Polymers in Intimate Contact with Nanocrystals for Hybrid Solar Cells. *Advanced Materials* **2012,** *24*, 4353-4368.

5. Locklin, J.; Patton, D.; Deng, S.; Baba, A.; Millan, M.; Advincula, R. C., Conjugated Oligothiophene-Dendron-Capped CdSe Nanoparticles: Synthesis and Energy Transfer. *Chemistry of Materials* **2004,** *16*, 5187-5193.

6. Liu, J.; Tanaka, T.; Sivula, K.; Alivisatos, A. P.; Fréchet, J. M. J., Employing End-Functional Polythiophene To Control the Morphology of Nanocrystal−Polymer Composites in Hybrid Solar Cells. *Journal of the American Chemical Society* **2004,** *126*, 6550-6551.

7. Wang, M.; Kumar, S.; Lee, A.; Felorzabihi, N.; Shen, L.; Zhao, F.; Froimowicz, P.; Scholes, G. D.; Winnik, M. A., Nanoscale Co-organization of Quantum Dots and Conjugated Polymers Using Polymeric Micelles As Templates. *Journal of the American Chemical Society* **2008,** *130*, 9481-9491.

8. Palaniappan, K.; Murphy, J. W.; Khanam, N.; Horvath, J.; Alshareef, H.; Quevedo-Lopez, M.; Biewer, M. C.; Park, S. Y.; Kim, M. J.; Gnade, B. E.; Stefan, M. C., Poly(3-hexylthiophene)−CdSe Quantum Dot Bulk Heterojunction Solar Cells: Influence of the Functional End-Group of the Polymer. *Macromolecules* **2009,** *42*, 3845-3848.

9. Palaniappan, K.; Hundt, N.; Sista, P.; Nguyen, H.; Hao, J.; Bhatt, M. P.; Han, Y.-Y.; Schmiedel, E. A.; Sheina, E. E.; Biewer, M. C.; Stefan, M. C., Block copolymer containing poly(3-hexylthiophene) and poly(4-vinylpyridine): Synthesis and its interaction with CdSe quantum dots for hybrid organic applications. *Journal of Polymer Science Part A: Polymer Chemistry* **2011,** *49*, 1802-1808.

10. Xu, J.; Wang, J.; Mitchell, M.; Mukherjee, P.; Jeffries-El, M.; Petrich, J. W.; Lin, Z., Organic−Inorganic Nanocomposites via Directly Grafting Conjugated Polymers onto Quantum Dots. *Journal of the American Chemical Society* **2007,** *129*, 12828-12833.

11. Milliron, D. J.; Gur, I.; Alivisatos, A. P., Hybrid Organic–Nanocrystal Solar Cells. *MRS Bulletin* **2005,** *30*, 41-44.

12. Goodman, M. D.; Xu, J.; Wang, J.; Lin, Z., Semiconductor Conjugated Polymer−Quantum Dot Nanocomposites at the Air/Water Interface and Their Photovoltaic Performance. *Chemistry of Materials* **2009,** *21*, 934-938.

13. Shi, Y.; Li, F.; Tan, L.; Chen, Y., Hybrid Bulk Heterojunction Solar Cells Based on the Cooperative Interaction of Liquid Crystals within Quantum Dots and Diblock Copolymers. *ACS Applied Materials & Interfaces* **2013,** *5*, 11692-11702.

14. Yuan, K.; Li, F.; Chen, L.; Wang, H.; Chen, Y., Understanding the mechanism of poly(3-hexylthiophene)-b-poly(4-vinylpyridine) as a nanostructuring compatibilizer for improving the performance of poly(3-hexylthiophene)/ZnO-based hybrid solar cells. *Journal of Materials Chemistry A* **2013,** *1*, 10881-10888.

15. Skaff, H.; Sill, K.; Emrick, T., Quantum Dots Tailored with Poly(para-phenylene vinylene). *Journal of the American Chemical Society* **2004,** *126*, 11322-11325.

16. Sun, B.; Marx, E.; Greenham, N. C., Photovoltaic Devices Using Blends of Branched CdSe Nanoparticles and Conjugated Polymers. *Nano Letters* **2003,** *3*, 961-963.

17. Sun, B.; Snaith, H. J.; Dhoot, A. S.; Westenhoff, S.; Greenham, N. C., Vertically segregated hybrid blends for photovoltaic devices with improved efficiency. *Journal of Applied Physics* **2005,** *97*, 014914.

18. Yuan, J.; Gallagher, A.; Liu, Z.; Sun, Y.; Ma, W., High-efficiency polymer-PbS hybrid solar cells via molecular engineering. *Journal of Materials Chemistry A* **2015,** *3*, 2572-2579.

19. Liu, Z.; Sun, Y.; Yuan, J.; Wei, H.; Huang, X.; Han, L.; Wang, W.; Wang, H.; Ma, W., High-Efficiency Hybrid Solar Cells Based on Polymer/PbS_xSe_{1-x} Nanocrystals Benefiting from Vertical Phase Segregation. *Advanced Materials* **2013,** *25*, 5772-5778.

20. Greenham, N. C.; Peng, X.; Alivisatos, A. P., Charge separation and transport in conjugated polymer/cadmium selenide nanocrystal composites studied by photoluminescence quenching and photoconductivity. *Synthetic Metals* **1997,** *84*, 545-546.

21. Huynh, W. U.; Peng, X.; Alivisatos, A. P., CdSe Nanocrystal Rods/Poly(3-hexylthiophene) Composite Photovoltaic Devices. *Advanced Materials* **1999,** *11*, 923-927.

22. Chen, Z.; Zhang, H.; Du, X.; Cheng, X.; Chen, X.; Jiang, Y.; Yang, B., From planar-heterojunction to n-i structure: an efficient strategy to improve short-circuit current and power conversion efficiency of aqueous-solution-processed hybrid solar cells. *Energy & Environmental Science* **2013,** *6*, 1597-1603.

23. Jung, J.; Pang, X.; Feng, C.; Lin, Z., Semiconducting Conjugated Polymer–Inorganic Tetrapod Nanocomposites. *Langmuir* **2013,** *29*, 8086-8092.

24. Qian, L.; Yang, J.; Zhou, R.; Tang, A.; Zheng, Y.; Tseng, T.-K.; Bera, D.; Xue, J.; Holloway, P. H., Hybrid polymer-CdSe solar cells with a ZnO nanoparticle buffer layer for improved efficiency and lifetime. *Journal of Materials Chemistry* **2011,** *21*, 3814-3817.

25. Ren, S.; Chang, L.-Y.; Lim, S.-K.; Zhao, J.; Smith, M.; Zhao, N.; Bulović, V.; Bawendi, M.; Gradečak, S., Inorganic–Organic Hybrid Solar Cell: Bridging Quantum Dots to Conjugated Polymer Nanowires. *Nano Letters* **2011,** *11*, 3998-4002.

26. Milliron, D. J.; Alivisatos, A. P.; Pitois, C.; Edder, C.; Fréchet, J. M. J., Electroactive Surfactant Designed to Mediate Electron Transfer Between CdSe Nanocrystals and Organic Semiconductors. *Advanced Materials* **2003,** *15*, 58-61.

27. Zhou, Y.; Eck, M.; Veit, C.; Zimmermann, B.; Rauscher, F.; Niyamakom, P.; Yilmaz, S.; Dumsch, I.; Allard, S.; Scherf, U.; Krüger, M., Efficiency enhancement for bulk-heterojunction hybrid solar cells based on acid treated CdSe quantum dots and low bandgap polymer PCPDTBT. *Solar Energy Materials and Solar Cells* **2011,** *95*, 1232-1237.

28. Greaney, M. J.; Das, S.; Webber, D. H.; Bradforth, S. E.; Brutchey, R. L., Improving Open Circuit Potential in Hybrid P3HT:CdSe Bulk Heterojunction Solar Cells via Colloidal tert-Butylthiol Ligand Exchange. *ACS Nano* **2012,** *6*, 4222-4230.

29. Fu, W.; Shi, Y.; Qiu, W.; Wang, L.; Nan, Y.; Shi, M.; Li, H.; Chen, H., High efficiency hybrid solar cells using post-deposition ligand exchange by monothiols. *Physical Chemistry Chemical Physics* **2012,** *14*, 12094-12098.

30. Kumar, A. P.; Huy, B. T.; Kumar, B. P.; Kim, J. H.; Dao, V.-D.; Choi, H.-S.; Lee, Y.-I., Novel dithiols as capping ligands for CdSe quantum dots: optical properties and solar cell applications. *Journal of Materials Chemistry C* **2015,** *3*, 1957-1964.

31. Zhou, R.; Stalder, R.; Xie, D.; Cao, W.; Zheng, Y.; Yang, Y.; Plaisant, M.; Holloway, P. H.; Schanze, K. S.; Reynolds, J. R.; Xue, J., Enhancing the Efficiency of Solution-Processed Polymer:Colloidal Nanocrystal Hybrid Photovoltaic Cells Using Ethanedithiol Treatment. *ACS Nano* **2013,** *7*, 4846-4854.

32. Hundt, N.; Palaniappan, K.; Sista, P.; Murphy, J. W.; Hao, J.; Nguyen, H.; Stein, E.; Biewer, M. C.; Gnade, B. E.; Stefan, M. C., Synthesis and characterization of polythiophenes with alkenyl substituents. *Polymer Chemistry* **2010,** *1*, 1624-1632.

33. Iovu, M. C.; Sheina, E. E.; Gil, R. R.; McCullough, R. D., Experimental Evidence for the Quasi-"Living" Nature of the Grignard Metathesis Method for the Synthesis of Regioregular Poly(3-alkylthiophenes). *Macromolecules* **2005,** *38*, 8649-8656.

BIOGRAPHICAL SKETCH

Chandima Bulumulla was born and raised in Kandy, Sri Lanka. He received his primary, secondary and tertiary education in Trinity College, Kandy. Then he pursued his undergraduate studies at University of Peradeniya, Sri Lanka. His final year research was on conductive polymers derived from natural products under the supervision of Prof. H. M. N. Bandara and Prof. B. M. R. Bandara. He moved to Richardson, Texas in 2013 to pursue his PhD and joined Dr. Mihaela C. Stefan's group to work on synthesis and electronic characterization of non-conventional building blocks for organic electronics. After completing his PhD studies he will be joining Retina Foundation of the Southwest as a postdoctoral fellow.

Chandima Bulumulla

Address: Department of Chemistry and Biochemistry, BE 26
   The University of Texas at Dallas
   800 W Campbell Rd, Richardson, TX 75080
Email: cdb130130@utdallas.edu

Education:

The University of Texas at Dallas, Richardson, TX   Aug. 2013 - April 2018
Ph.D. candidate in Chemistry
Dissertation: 'Non-conventional Building Blocks for Organic Electronics'
Advisor: Prof. Mihaela C. Stefan

University of Peradeniya, Sri Lanka   Aug. 2008 – May 2012
B.S. in Chemistry

Graduate Research Experience:

Developed pyrrole based semiconducting materials for organic field effect transistors and side chain functionalized polythiophenes for hybrid solar cells
- Focused on synthesis, purification, and characterization of small molecules and polymers
- Studied organic electronic applications by using OFET and OPV device fabrication

Publications:

1   **Bulumulla, C.**; Kularatne, R. N.; Gunawardhana, R.; Nguyen, H. Q.; McCandless, G. T.; Biewer, M. C.; Stefan, M. C.; Thieno[3,2-*b*]pyrrole Diketopyrrolopyrrole Copolymer for Efficient Organic Field Effect Transistors, *ACS Macro Letters*, **2018**, *7*, 629-634.

2   **Bulumulla, C.**; Gunawardhana, R.; Kularatne, R. N.; Hill, M. E.; McCandless, G. T.; Biewer, M. C.; Stefan, M. C.; Thieno[3,2-*b*]pyrrole – benzothiadiazole banana-shaped small molecules for organic field effect transistors, *ACS Applied Materials & Interfaces*, **2018**, *10*, 11818-11825.

3   Kularatne, R. N.; Washington, K. E.; **Bulumulla, C.**; Calubaquib, E. L.; Biewer, M. C.; Oupicky, D.; Stefan, M. C.; Histone Deacetylase Inhibitor (HDACi) Conjugated Polycaprolactone for Combination Cancer Therapy, *Biomacromolecules*, **2018**, *19*, 1082-1089.

4   Du, J.; **Bulumulla, C.**; Meija, I.; McCandless, G. T.; Biewer, M. C.; Evaluation of (E)-1,2-di(furan-2-yl)ethene as building unit in diketopyrrolopyrrole alternative copolymers for transistors, *Polymer Chemistry*, **2017**, *8*, 6181-6187.

5   **Bulumulla, C.**; Du, J.; Washington, K.E.; Kularatne, R.N.; Nguyen, H.Q.; Biewer, M.C.; Stefan, M.C. Influence of Functionalized Side Chains of Polythiophene Diblock Copolymers on the Performance of CdSe Quantum Dot Hybrid Solar Cells. *Journal of Material Chemistry Part A*, **2017**, *5*, 2473-2477

6   Du, J.; Fortney, A.; Washington, K.E.; **Bulumulla, C.**; Huang, P.; Dissanayake, D.; Biewer, M.C.; Kowalewski, T.; Stefan, M.C. Systematic Investigation of Benzodithiophene-Benzothiadiazole Isomers for Organic Photovoltaics. *ACS Applied Materials & Interfaces*, **2016**, *8*, 33025-33033

Presentations:

1   **Bulumulla, C.**; Nguyen H.Q.; Kularatne, R.N.; Gunawardhana, R.; Du. J.; Washington, K.E.; Biewer, M.C.; Stefan, M.C. Fused ring systems containing for organic electronics, Oral Presentation at the 254th ACS National Meeting, 2017, Washington D.C.

2   **Bulumulla, C.**; Du, J.; Washington, K.E.; Mills, C.; Biewer, M.C.; Stefan, M.C. The influence of the functionalized side chains of polythiophene diblock copolymers: CdSe nanoparticle (NP) bulk heterojunction solar cells, Oral Presentation at the 251st ACS National Meeting, 2015, San Diego, CA

Posters:

1   **Bulumulla, C.**; Kularatne, R. N.; Gunawardhana, R.; Biewer, M. C.; Stefan, M. C. "Pyrrole Based Semiconductors for OFETs", 255th ACS National Meeting, 2018, New Orleans, LA